



<https://theses.gla.ac.uk/>

Theses Digitisation:

<https://www.gla.ac.uk/myglasgow/research/enlighten/theses/digitisation/>

This is a digitised version of the original print thesis.

Copyright and moral rights for this work are retained by the author

A copy can be downloaded for personal non-commercial research or study, without prior permission or charge

This work cannot be reproduced or quoted extensively from without first obtaining permission in writing from the author

The content must not be changed in any way or sold commercially in any format or medium without the formal permission of the author

When referring to this work, full bibliographic details including the author, title, awarding institution and date of the thesis must be given

Enlighten: Theses

<https://theses.gla.ac.uk/>
research-enlighten@glasgow.ac.uk

**The Development Of Confocal Laser Scanning
Methods For The Study of Vascular Structure,
Function And Receptor Distribution.**

Craig James Daly

A thesis presented for the degree of PhD (Oct. 1999).
Faculty of Medicine.
University of Glasgow.

© Copies of the thesis may be produced by photocopying.

ProQuest Number: 10391323

All rights reserved

INFORMATION TO ALL USERS

The quality of this reproduction is dependent upon the quality of the copy submitted.

In the unlikely event that the author did not send a complete manuscript and there are missing pages, these will be noted. Also, if material had to be removed, a note will indicate the deletion.



ProQuest 10391323

Published by ProQuest LLC (2017). Copyright of the Dissertation is held by the Author.

All rights reserved.

This work is protected against unauthorized copying under Title 17, United States Code
Microform Edition © ProQuest LLC.

ProQuest LLC.
789 East Eisenhower Parkway
P.O. Box 1346
Ann Arbor, MI 48106 – 1346

GLASGOW
UNIVERSITY
LIBRARY

11847

(copy 2)

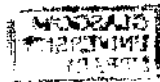
Abstract.

The work contained within this thesis describes the development of confocal laser scanning methods as applied to the study of blood vessel structure and receptor distribution. Prior to the start of the project there were no suitable techniques available for the study of 3D structure and spatial distribution of receptors which therefore necessitated the development of novel methods. The first phase of the work employed fluorescent DNA stains which provided an increased contrast and an ability to identify all cell types, number, orientation and viability within a living vascular wall. This nuclear staining method was then extended by introducing confocal analysis of myograph mounted arterial segments. The confocal method was successful in detecting areas of apparently disorganised smooth muscle cells within the wall of SHR basilar arteries. In addition, CLSM detected changes in the media of human arteries taken from cases of critical limb ischaemia and in the adventitia of mouse tail artery where the α_{1b} -adrenoceptor had been deleted.

Structural studies of the vascular wall required the use of image analysis methods for quantification and feature extraction. This required the development of novel methods specific for, CLSM-derived, 3D volumes of vascular structure. A semi-automated thresholding and segmentation algorithm (IMTS) was developed and tested. The imaging and segmentation phase of the research aided in the identification of problems associated with quantification of 3D volumetric structures.

Fluorescent-ligands can be used to identify high affinity binding sites within cells. A significant proportion of this thesis describes the development of fluorescence-binding using CLSM and image analysis. The results document the developmental work leading up to the construction of the first 'specific' binding curve to be performed on a single living cell. This paves the way for ligand-binding-type experiments on cells dissociated from biopsies or other small tissue samples.

Overall, the project has established the use of confocal microscopy for the study of blood vessel structure, function and receptor distribution. This thesis describes the key steps in the development of the techniques and hopefully serves as a guide to those interested in using confocal based methods for the study of blood vessels.



Contents.

Page No.

- I Acknowledgements
- II Declaration
- III Publications arising from the work
- IV List of abbreviations
- V List of figures
- VI Summary of results.
- VII General Introduction

Chapter I. - *The Development of Fluorescence Myography and the Use of Fluorescent Nuclear Stains.*

1- 34

Introduction.	1
<i>Blood Vessel Structure and Function</i>	1
<i>Asymmetry of responsiveness.</i>	4
<i>Wire Myography</i>	5
<i>Alpha-adrenoceptors in the vasculature</i>	6
Methods.	10
<i>Phase Contrast Studies of Vasoconstriction.</i>	10
<i>Fluorescent Staining procedures.</i>	11
<i>In-Vitro toxicity tests.</i>	11
<i>Free radical generation and cell-viability assays</i>	11
<i>Collection of Fluorescence Micrographs.</i>	12
<i>Image Analysis.</i>	12
<i>Drugs and Solutions</i>	15
Results.	16
<i>Phase Contrast</i>	16
<i>Fluorescent probes.</i>	17
<i>Hoechst 33342 & Ethidium bromide.</i>	18
<i>Extraluminal staining.</i>	18
<i>Cell Viability</i>	19
<i>Intraluminal staining.</i>	20
<i>Staining of large (thick walled) blood vessels.</i>	21
<i>Image analysis.</i>	21
Discussion.	23
<i>Phase Contrast.</i>	23
<i>Fluorescent nuclear stains</i>	25
<i>Cell viability</i>	25
<i>Image analysis.</i>	28
References.	31

Introduction.	37
<i>Principles of Confocal Microscopy.</i>	39
<i>practical uses of CLSM.</i>	41
<i>Emission attenuation with depth.</i>	42
<i>Optical aberrations in CLSM.</i>	42
<i>Bleaching and Fluorescence attenuation.</i>	45
<i>Collection of Serial Optical Sections.</i>	46
<i>Digital Images and 3-dimensional volumes.</i>	47
Methods.	49
<i>Tissue harvest.</i>	49
<i>Tissue mounting.</i>	49
<i>Tissue staining.</i>	50
<i>Fluorescent Stains.</i>	51
<i>Confocal Microscopy.</i>	52
<i>Calibration of objectives.</i>	54
<i>Image Capture.</i>	56
<i>Image Analysis and 3D processing.</i>	56
Results.	59
<i>Extracellular staining.</i>	59
<i>Cytoplasmic Staining.</i>	60
<i>Combined extracellular and nuclear staining.</i>	61
<i>BCECF stained, myograph mounted arterial segments.</i>	62
<i>Nuclear stained, myograph mounted vessels.</i>	63
<i>Agonist activation of stained pressure mounted vessels.</i>	65
<i>Vector models.</i>	66
<i>Structural studies using extracellular and nuclear stains.</i>	66
<i>Automated Analysis of 3D volumes.</i>	68
<i>Testing the IMTS segmentation method.</i>	69
Discussion.	72
<i>The Vascular Wall.</i>	72
<i>Confocal (fluorescence) microscopy.</i>	72
<i>Nuclear staining</i>	73
<i>Application of the CLSM method to studies of vascular remodelling.</i>	74
<i>Human Resistance Arteries.</i>	75
<i>Automated 3D-analysis.</i>	77
<i>Problems associated with CLSM.</i>	78
<i>Multi-level thresholding and segmentation (IMTS).</i>	80
<i>Object Classification and measurement.</i>	81
References.	84

Chapter 3. - The use of fluorescent ligands and the development of methods for fluorescent ligand-binding in isolated cells and tissues.	89-132
Introduction.	89
<i>Current Classification of α_1-adrenoceptor subtypes.</i>	91
<i>Selectivity of Antagonist drugs and new compounds.</i>	93
<i>Receptor distribution and location</i>	93
<i>History of fluorescent "drug" ligands.</i>	94
<i>Examples of fluorescent ligands for various receptors</i>	95
Methods.	98
<i>Reagents</i>	98
<i>Cell culture.</i>	98
<i>Inositol phosphate studies.</i>	98
<i>Membrane preparation.</i>	99
<i>Radioligand binding studies.</i>	99
<i>Analysis of functional antagonism by QAPB</i>	100
<i>Assessment of antagonist potency versus agonist CRCs</i>	101
<i>Confocal Microscopy.</i>	101
<i>Whole cell image analysis.</i>	102
<i>Ligand binding to tissue slices.</i>	102
<i>Iso-Surface Modelling.</i>	103
<i>Simulated Fluorescence Projection.</i>	103
Results.	104
<i>Ligand affinity.</i>	104
<i>Concentration dependent fluorescence.</i>	105
<i>Image analysis.</i>	108
<i>3-dimensional visualisation and localisation of QAPB (30nM) binding to α_{1d}-adrenoceptor transfected fibroblasts.</i>	110
<i>QAPB (0.1 μM) binding to whole tissue.</i>	111
<i>QAPB binding to transverse sections of rat mesenteric artery.</i>	112
Discussion.	113
<i>Affinity and Selectivity.</i>	114
<i>Visualisation and construction of concentration / fluorescence curves and competition binding studies on live cells.</i>	116
<i>Spatial distribution of α_1-adrenoceptor subtypes.</i>	120
<i>Iso-surface modelling.</i>	121
<i>Analysis of receptor binding intensity in thick biological specimens.</i>	122
References.	127

<u>Chapter 4 - Case Study:</u> <i>Pharmacology and Confocal Studies of Mouse Tail Artery.</i>	135-149
Introduction.	133
Methods.	137
<i>Functional Studies.</i>	137
<i>Analysis of functional data</i>	137
<i>Confocal Study of Structure</i>	138
<i>Dissociation of Smooth Muscle cells.</i>	138
<i>Drugs and Solutions</i>	139
Results.	140
<i>Antagonist profile</i>	140
<i>Agonist potency</i>	140
<i>Electrical field stimulation</i>	140
<i>Confocal analysis of structure</i>	141
<i>Fluorescent ligand binding</i>	141
Discussion.	142
<i>Antagonist potency.</i>	143
<i>Agonist potency.</i>	144
<i>Electrical field stimulation.</i>	144
<i>Confocal Studies of Structure.</i>	145
<i>α-adrenoceptor distribution.</i>	145
References.	147
General Discussion	150-154

1. Acknowledgements.

Once again I am indebted to Professor JC McGrath for giving me the freedom to follow my interests wherever they were headed. In the 19 years that I have worked in his laboratory he has been supportive in everything I have aimed for and I am grateful for his constant support and enthusiasm. Thanks.

To my old lab partner John Gordon I extend my gratitude. It was his idea to try a confocal microscope and we worked together closely on the development of the original methods. John was lucky enough to break the habit. I, on the other hand, got addicted to imaging and all things confocal and I am still feeding my habit to this day.

To my many colleagues, old and new, I offer a special thank you. It has been a great lab to work in and my confocal buddies have made it all the more enjoyable. There are too many to mention. However, special thanks go to those who have been collaborators on various confocal projects, namely, Janet, Paul, Silvia, Simon and Daisheng. There is a little of all of you within these pages.

The others who have made 440 a brighter place to work in also deserve a special mention. Jillian, Joyce, Ann, Anne, Clare, Alison and Angela. Thanks .

To my parents, a special thanks for constantly preparing me for interviews and vivas. 'So tell me again, what is it you do at your work.?' Seriously, I thank them for their love and support for much longer than the 20 years that I have been working here.

Finally, and by no means least, thanks to my wife Maureen and my children Scott and Jennifer. I learned in the course of this study that the working day finishes at 5'30pm for a reason and that is to spend time with them. There are some things more important than science and words can not express how fortunate I am to have my family around me. They know what IS important.

II. Declaration.

The work contained within this thesis is entirely my own. Some of the collaborative work has been published and is included within the references of the next section. All of the graphs are my own with the exception of;

Figure 2.15 & 2.16	Done in collaboration with Dr SM Arribas
Figure 2.17	Done in collaboration with Mr. Paul Coats
Figure 2.20	Done in Collaboration with Dr. D. Luo
Figure 3.2	Done in Collaboration with Prof G. Milligan & Dr. JF Mackenzie
Figure 3.13(h)	Done in Collaboration with Dr. JF Mackenzie
Figure 4.7	Done in Collaboration with Dr. JF Mackenzie

This work has not been presented in whole or as part of any other degree course.

III. Publications Resulting from the work in this thesis.

Chapter 1.

Daly CJ, Gordon JF, Boyle FC, Gillespie JS, McGrath JC, Moss VA & Spurway NC

(1990). Fluorescent myography: Analysis of vascular smooth muscle cells of the rat labelled with bisbenzimidazole during vasoconstriction. *J Physiol*, **429**, 11.

Gordon JF, **Daly CJ**, Boyle FC, Kusel JR, Gillespie JS & McGrath JC (1990). A

simple smooth muscle cell viability assay for use in rat blood vessels in vitro. *J Physiol*, **429**, 10.

Daly CJ, Gordon JF & McGrath JC (1991). Assessment of cell viability within the

wall of rat mesenteric arteries. *Blood Vessels*, **28**, 282.

Daly CJ, Gordon JF & McGrath JC (1991). Fluorescence image analysis methods for

the study of smooth muscle cell interaction within the vascular wall of small blood vessels. In *Resistance arteries - Structure and Function*. Eds. Mulvany MJ et al., Vol 1. Amsterdam Elsevier, 339-343.

Daly CJ, Gordon, JF & McGrath, JC (1991) Assessment of cell viability within the

wall of rat mesenteric arteries. *Blood Vessels* **28** 282.

Daly CJ, Gordon, JF, McGrath JC & Spedding M. (1991) Quantification of

experimentally induced ischaemic damage to smooth muscle cell membranes within the wall of resistance arteries. *Blood Vessels* **28** 281.

Daly CJ, Gordon JF & McGrath JC (1991) A fluorescence image analysis method for

the study of smooth muscle cell interaction within the vascular wall of small blood vessels. *Blood Vessels* **28** 281.

Daly CJ, Gordon JF & McGrath JC (1992) The use of fluorescent nuclear dyes for the study of blood vessel structure and function: novel applications of existing techniques. *J. Vasc. Res.* **29** 41-48.

Chapter 2.

Daly CJ, Gordon JF & McGrath, JC (1993) Observation of vasodilatation in small arteries with confocal microscopy. Proceedings of XXXII Congress of the International Union of Physiological Sciences, Glasgow, 1993. **73.12/O.**

Gordon JF, **Daly CJ** & McGrath JC. (1993) Analysis of rat resistance artery structure in pressurised vessels using confocal microscopy. Proceedings of XXXII Congress of the International Union of Physiological Sciences, Glasgow, 1993. **249.48/P.**

Daly CJ, Gordon JF & McGrath JC (1993) 3-Dimensional analysis of smooth muscle cell reactivity within the rat resistance artery using confocal microscopy. Proceedings of XXXII Congress of the International Union of Physiological Sciences, Glasgow, 1993. **249.47/P.**

Daly CJ, Gordon JF & McGrath JC (1994) The use of confocal microscopy for the study of resistance artery structure and function. *J. Vasc. Res.* **31** 10.

Arribas S, Gordon JF, **Daly CJ**, Davidson A, Dominiczak AF & McGrath JC (1994) Vascular smooth muscle rearrangement and impaired contractions in basilar artery of the stroke-prone spontaneously hypertensive rat. *J. Hypertension* **12** 1307-1352.

Arribas S, Gordon J, **Daly CJ**, Davidson A. Dominiczak AF & McGrath JC (1994) Smooth muscle cell rearrangement and impaired contractions basilar artery of SHRSP. *Meth. Find. Exp. Clin. Pharmacol.* **16** 47 (CO-16).

Arribas S., **Daly CJ**, Gordon JF & McGrath JC (1994) Confocal myography: applications for the study of resistance arteries. In: *The resistance arteries: integration of the regulatory pathways*. Ed. W. Halpern et al., New Jersey USA, Humana Press. pp. 259-264 [ISBN 0-8960 3-303-1]

Arribas SM, Gordon JF, **Daly CJ**, McGrath JC (1995) Confocal microscopy for structure and realtime pharmacology in blood vessels. *J. Human Hypertension* **9** 645-647.

Arribas SM, Gordon JF, **Daly CJ**, Davidson A, Dominiczak AF & McGrath JC (1995) Structural and functional alterations in the basilar artery from stroke prone spontaneously hypertensive rats. 7th European Meeting on Hypertension, Milan, June 1995, p.12, 42.

Arribas SM, Gordon JF, **Daly CJ**, Dominiczak AM & McGrath JC. (1996) Confocal microscopic characterization of a lesion in a cerebral vessel of the stroke-prone spontaneously hypertensive rat. *Stroke* **27** 1118-1123.

Luo D, Robert A, **Daly CJ**, Mackenzie JF, Arribas S, McGrory S. & McGrath JC (1997) Segmentation of laser scanning confocal microscopy images. Computers in Microscopy Meeting, Cambridge, September 1997.

Arribas SM, **Daly CJ** & McGrath JC (1999) Measurements of vascular remodeling by confocal microscopy. (ed. P.M. Conn). *Methods Enzymol.* **307** Suppl 'Confocal Microscopy' 246-273.

Chapter 3.

McGrath JC & **Daly CJ**. (1995) Viewing adrenoceptors; past, present and future; commentary and a new technique. *Pharmacol. Commun.* **6** 269-279.

- McGrath JC, Arribas S, Brown CM, **Daly CJ**, Gordon JF, Milligan G, Pediani J., Smith K. & Wilson, S.M. (1995) Real-time agonist and antagonist competition binding studies at α_1 -adrenoceptors using Bodipy FL-Prazosin; A fluorescent α_1 -adrenoceptor antagonist. *FASEB J.* **9** No3 A104.
- Daly CJ** & McGrath, JC (1997) Binding of a fluorescent quinazoline to recombinant α_1 -adrenoceptors. *J. Auton. Pharmacol.* **17** 220.
- McGrath JC, Arribas SM & **Daly CJ** (1996) Fluorescent ligands for the study of receptors. *Trends in Pharmacological. Sciences.* **17** No 11 393-399.
- Daly CJ**, de la Rue SA, Luo D. & McGrath JC (1997) 3D-distribution of α -adrenoceptors in blood vessel lack of staining on endothelial cells. *J. Vasc. Res.* **34** Suppl 1 034P.
- Daly CJ**, Mackenzie JF & McGrath JC (1997) Fluorescent ligand binding to recombinant $\alpha_{1a/d}$ -adrenoceptors. *J. Vasc. Res.* **34** Suppl 1 033P.
- Mackenzie JF, **Daly CJ** & McGrath JC (1998) Comparison and validation of human α_1 -adrenoceptor binding characteristics on live, whole cells using radioligand binding and confocal laser scanning microscopic techniques. *Naunyn-Schmiedeberg's Arch. Pharmacol.* **358** Suppl. 2 P6.45.
- Luo D, **Daly CJ**, Mackenzie JF, McGrory SP, Robert A. & McGrath JC (1998) 3D remodelling of α_1 -adrenoceptors in live cells using a fluorescent ligand, QAPB and confocal laser scanning microscopy. *Naunyn-Schmiedeberg's Arch. Pharmacol.* **358** Suppl. 2 P6.44.

- Mackenzie JF, **Daly CJ**, Luo D & McGrath JC (1998). Cellular localisation of alpha-1 adrenoceptors in native smooth muscle cells. On-line Proceedings of the 5th Internet World Congress on Biomedical Sciences '98 at McMaster University, Canada
- Daly CJ**, Milligan CM, Milligan G, Mackenzie JF & McGrath JC (1998) Cellular localisation and pharmacological characterisation of functioning α_1 -adrenoceptors by fluorescent ligand binding and image analysis reveals identical binding properties of clustered and diffuse populations of receptors. *J. Pharmacol. Exp. Ther.* **286** 984-990.
- McGrath JC, Mackenzie JF & **Daly CJ** (1999) Sub-cellular localisation of α_1 -adrenoceptors in live cells and tissues. British Pharmacological Society, Joint Spring Meeting with Portuguese Pharmacological Society, Porto, Portugal, April 1999. *Br. J. Pharmacol.* **127** 133P
- Mackenzie JF, **Daly CJ**, Luo D, & McGrath JC (1999) Cellular localisation of α_1 -adrenoceptors in human primary smooth muscle cells derived from the prostate of patients with benign prostatic hypertrophy. *Eur. Urol.* **36** Suppl 1 115.

Chapter 4.

- Daly CJ**, Cotecchia S & McGrath JC (1998) Low frequency electrical field stimulation elicits responses in segments of mouse tail artery which are slower in α_{1b} -knockout mice than in control mice. *Naunyn-Schmiedeberg's Arch. Pharmacol.* **358** Suppl. 2 P6.40.

IV. List of Abbreviations.

5,6 CF	5(6)-carboxyfluorescein mixed isomers.
AO	Acridine Orange,
BCECF AM	2',7'-bis-(2-carboxyethyl)-5-(and-6)-carboxyfluorescein, acetoxymethyl ester.
CLSM	Confocal Laser Scanning Microscopy
DHE	Dihydroethidium.
EB	Ethidium Bromide.
FITC	fluorescein isothiocyanate.
K_D	Fluorescence dissociation constant
I133342	Hoechst 33342 (bisBenzamide).
IMTS	Iterative Multi-Level Thresholding Segmentation
KCl	potassium chloride
NA	noradrenaline
pA_2	Affinity constant of an antagonist derived from Schild plot.
Phe	phenylephrine
PI	Propidium Iodide.
pK_B	Estimated affinity value for an antagonist (log)
QAPB	BODIPY FL-prazosin
SHR	Spontaneously Hypertensive Rat
TO	Thiazole Orange.
WKY	Wistar Koyoto (control for SHR)

V. List of Figures and Tables.

Chapter 1. *The development of fluorescence myography and the use of fluorescent nuclear stains.*

- Figure 1.1 Schematic diagram of the vascular wall
- Figure 1.2 In situ contraction of rat mesenteric artery
- Figure 1.3 Wire myograph mounted vessel segment
- Figure 1.4 Contraction of wire mounted vessel
- Figure 1.5 Top view; wire mounted vessel
- Figure 1.6 Cell viability; fluorescence micrographs
- Figure 1.7 Fluorescent nuclear stain of vessel segment
- Figure 1.8 H33342 & Ethidium staining of RMA
- Figure 1.9 Free radical damage of RMA segments
- Figure 1.10 In vivo staining of RMA and cerebral vessels
- Figure 1.11 Schematic of nuclear stained wire mounted vessel
- Figure 1.12 Combined brightfield and fluorescence images of RMA
- Figure 1.13 Functional toxicity test of H33342 vs RMA
- Figure 1.14 Contraction of wire mounted RMA
- Figure 1.15 Identification of nuclear group during contraction
- Figure 1.16 Analysis of movement of nuclei during contraction

Chapter 2. *Confocal Microscopy and Image analysis*

- Figure 2.1 Schematic of the confocal principal
- Figure 2.2 Extracellular (5,6 CF) staining of RMA
- Figure 2.3 Cytoplasmic staining of RMA media & adventitia
- Figure 2.4 Combined BCECF and H33342 staining in RMA
- Figure 2.5 Combined extracellular and nuclear staining of RMA
- Figure 2.6 BCECF staining of pressurised arteries
- Figure 2.7 Nuclear stained pressurised RMA segment (30mmHg)
- Figure 2.8 Nuclear stained pressurised RMA segment (80mmHg)
- Figure 2.9 Nuclear stained pressurised RMA segment (40mmHg)
- Figure 2.10 Nuclear stained WKY segment (40mmHg)
- Figure 2.11 Nuclear stained SHR segment (60mmHg)
- Figure 2.12 Nuclear stained SHR segment (120mmHg)
- Figure 2.13 KCl activated nuclear stained wire mounted RMA
- Figure 2.14 Vector models of Wistar and SHR nuclear volumes
- Figure 2.15 Vector model of KCl activated RMA segment
- Figure 2.16 Extracellular staining of WKY basilar artery segment
- Figure 2.17 Extracellular staining of SHR basilar artery segment
- Figure 2.18 Proximal and distal human cutaneous artery segment
- Figure 2.19 3D reconstruction of nuclear stained volume (RMA)
- Figure 2.20 IMTS segmentation of 3 sample volumes

- Table 2.1 List of fluorescent compounds used in the study.

Table 2.2	Average morphology of 10 randomly selected nuclei
Table 2.3	Smooth muscle cell arrangement in WKY and SPSHR rats.
Table 2.4	Analysis of human subcutaneous resistance arteries.
Table 2.5	IMTS morphometric analysis of CLSM segmented volume.

Chapter 3. *The use of fluorescent ligands and the development of the methods for fluorescent ligand binding in isolated cells and tissues.*

Figure 3.1	Chemical structure of QAPB and quinazolines
Figure 3.2	Biochemical and ligand binding assays of QAPB affinity
Figure 3.3	Functional assay of QAPB affinity in blood vessels
Figure 3.4	Functional assay of QAPB in Vas Deferens
Figure 3.5	QAPB binding to transfected fibroblasts (10-160nM)
Figure 3.6	Construction of binary masks from induced fluorescence
Figure 3.7	QAPB binding versus prazosin in transfected fibroblasts
Figure 3.8	Analysis (graph) of QAPB binding shown in figure 3.7
Figure 3.9	Displacement of QAPB with prazosin and phentolamine
Figure 3.10	QAPB binding to living and fixed cells
Figure 3.11	QAPB Saturation fluorescence curves vs competitors
Figure 3.12	QAPB binding to α_{1d} -transfected cells (0.4-10nM)
Figure 3.13	'Specific' fluorescence & radioligand binding curves
Figure 3.14	Z-sectioning of QAPB (30nM) binding in cells
Figure 3.15	Z-Sectioning showing intracellular and membrane binding
Figure 3.16	SFP and iso-surface models of membrane bound QAPB
Figure 3.17	Iso-surface models of transfected and native cells
Figure 3.18	QAPB (100nM) binding to RMA whole mount segments
Figure 3.19	Comparison of QAPB binding to mesenteric and basilar A.
Figure 3.20	QAPB binding to vascular and nonvascular smooth muscle
Figure 3.21	Schematic of method of cutting transverse vascular sections
Figure 3.22	QAPB (5-10nM) binding to TS sections of RMA
Figure 3.23	Analysis of QAPB binding to RMA transverse sections
Table 3.1	Fluorescent ligands versus radioligand. Advantages and disadvantages.
Table 3.2	Analysis of diffuse and clustered QAPB-binding
Table 3.3	List of BODIPY fluorescent linked ligands.

Chapter 4. *Case study: Pharmacology and confocal studies of mouse tail artery.*

Figure 4.1	Adrenoceptor profile of mouse isolated tail artery
Figure 4.2	Effect of CEC in wildtype and KO mouse artery
Figure 4.3	A86641 & phenylephrine vs BMY7378 in mouse tail artery
Figure 4.4	EFS responses in mouse tail artery
Figure 4.5	Adventitial structural analysis of WT and KO tail artery
Figure 4.6	3D model of pressurised tail artery segment
Figure 4.7	QAPB binding to dissociated tail artery SMC

VI. Summary of results.

Chapter 1.

1. This thesis contains the developmental work which has resulted in the group of techniques which are generally referred to as confocal myography and fluorescent ligand binding.
2. Studies of agonist induced activity in wire myograph mounted vessel segments indicated that cells were active prior to stimulation and that rhythmic activity develops from an apparently uncoordinated initial contraction
3. Hoechst 33342 provided greater contrast than cytoplasmic stains and enabled the identification of cell type, axial position, number and orientation.
4. Ethidium related dyes (i.e. bromide and homodimer) are sensitive enough to detect free radical-induced cellular damage in the vascular endothelium.
5. Nuclear stains administered in-vivo up to 30mg/kg stained vascular endothelial cell nuclei and did not cross the blood brain barrier.
6. H33342 did not alter the sensitivity of rat isolated mesenteric artery to noradrenaline.
7. NA-induced nuclei re-arrangement can be analysed, plotted and is consistent with the expected shortening (and bunching) of smooth muscle cells in a wire myograph system.

Chapter 2.

1. Confocal microscopy was evaluated as a tool for the study of vascular structure.

2. Extracellular, cytoplasmic and nuclear stains were compared. The nuclear stains appeared to be the most appropriate for confocal microscopy studies of cellular arrangement.
3. Pressure myography and CLSM was used to build 3D models of cytoplasmic and nuclear stained vessels under different transmural pressures.
4. During increases in transmural pressure the smooth muscle cell nuclei become longer and wider indicating that cells become longer and flatter.
5. WKY and SHR pressurised segments revealed the presence of significant invaginations of the internal elastic lamina which are more prominent at low (i.e. ≤ 40 mmHg) transmural pressures.
6. Vector models provided simple visualisation for 3D volumetric data of nuclei.
7. CLSM revealed regions of disorganised smooth muscle cells in basilar arteries taken from SHR but not WKY animals.
8. CLSM analysis of limb cutaneous arteries showed distal (ischaemic) arteries had fewer cells and reduced wall thickness than proximal segments.
9. A new method of segmentation, the iterative multi-level thresholding segmentation (IMTS) was found to a reliable semi-automated method of nuclei extraction which will provide a basis for further development.

Chapter 3.

1. A novel fluorescent ligand (BODIPY FL-prazosin aka QAPB) was evaluated as a possible ligand for α_1 -adrenoceptors.
2. QAPB inhibited IP_3 generation (pA_2 7.78) and $^3[H]$ -prazosin binding (pK_i 8.9) with high affinity when tested versus recombinant α_{1d} -adrenoceptors.

3. Functional studies of vascular tissues yielded pA_2 values of 8.25 (rat aorta) and 7.6 (rabbit saphenous artery).
4. QAPB (0.1 μ M) caused a rightward shift of the noradrenaline concentration response curve in the rat vas deferens. In vas, responses to acetylcholine were unaffected by QAPB. Thus, QAPB exerts its action via blockade of α_1 -adrenoceptors and is non-toxic.
5. QAPB-induced fluorescence was time- and concentration-dependent. Initial experiments revealed diffuse and clustered binding consistent with the expected distribution of receptors. QAPB binding (fluorescence) was inhibited by non-fluorescent antagonists. However, displacement of QAPB was difficult to achieve, presumably due to the high degree of intracellular binding which occurs at high (i.e. >10nM) concentrations.
6. Lowering the concentration of QAPB (0.4-10nM) and increasing the detector sensitivity enabled specific binding (K_D 3.9nM) with characteristics similar to those of radioligand binding (K_D 1.89nM). This result represents the first specific binding curve (and fluorescence K_D) to be calculated for a living cell at true equilibrium.
7. Image analysis enabled the calculation of the relative distribution of diffuse and clustered binding. Low level fluorescence (diffuse binding) accounted for 41.2% of the total whilst high intensity (clustered) binding accounted for 15.5%.
8. 3D spatial analysis of >5nM QAPB binding in live cells using a Z-section viewer showed that binding was both intracellular and membrane bound.

9. QAPB (0.1 μ M) binding to segments of blood vessels and anococcygeus muscle was inhibited in the presence of YM12617 (10 μ M) and phenoxybenzamine (10 μ M) respectively. Binding was consistent with the orientation of the smooth muscle and was both diffuse and clustered. Comparative studies of rat mesenteric and basilar arteries showed fewer QAPB binding sites in the basilar artery.
10. Staining of transverse sections of blood vessels indicated that most QAPB binding occurs in the regions of the internal and external elastic lamina.
11. In conclusion, fluorescent ligands are an ideal way of obtaining information on the spatial distribution of receptors within living tissue and isolated cells. However, issues relating to the specificity of the fluo-ligand must be resolved prior to its use for either quantitative or qualitative purposes.

Chapter 4.

1. A short case study of the mouse tail artery was undertaken to demonstrate the ways in which confocal studies can complement conventional pharmacological methods.
2. The α_2 -antagonists delequamine (pK_B 6.02) and rauwolscine (pK_B 6.33) exhibited low affinity versus noradrenaline.
3. The proposed α_{1B} -antagonist chloroethylclonidine (CEC) caused a slight rightward shift in the noradrenaline concentration response curve. In mice lacking the α_{1B} -adrenoceptor the CEC induced shift was reduced indicating only a minor role for α_{1B} -adrenoceptors.

4. The potency order of the α_1 -agonists A86441 and phenylephrine (A86441 \gg phenylephrine) and the lack of effect of BMY7378 precludes the involvement of the α_{1D} -subtype and leaves the α_{1A} -adrenoceptor subtype as the most likely subtype to be involved in the noradrenaline-induced response.
5. Electrical field stimulation indicated that the α_{1B} -subtype may initiate the initial response to adrenergic neurotransmission since responses in α_{1B} -knockout mouse were slower than those of the wild type.
6. Confocal studies of the adventitia of the wild type and knockout mouse tail artery revealed a marked reduction (59%) in the number of adventitial cells present in the adventitia of the KO mouse tail artery.
7. CLSM studies of pressurised arteries revealed a heterogeneous orientation of medial smooth muscle cells.
8. QAPB binding to mouse dissociated tail artery smooth muscle cells revealed both membrane bound and intracellular receptors. The FK_D calculated from the specific QAPB-binding to a single living cell (2nM) is constant with other values obtained for α_{1A} -adrenoceptor transfected cells in Prof. McGrath's group.
9. In conclusion, the confocal-derived data supports the pharmacological findings and gives greater confidence for the use of confocal methods in vascular research..

VII General Introduction.

Studies of vascular structure and function have yet to be unified by a single method or technique. There is no question that vascular structure is altered in many cardiovascular related diseases (such as hypertension and heart failure) and these will be discussed in the chapters that follow. There is also little doubt that a significant alteration in structure will have a subsequent impact on the normal function of the diseased vessel. Despite the intense research into vascular mechanisms worldwide, we still know very little about the structure-function relationship. Classical histological studies have not advanced our knowledge in the past twenty years. Current histology textbooks still provide only the most basic description of the vascular wall. Even if it was possible to obtain the set of cells required to build a blood vessel it would certainly not be possible to find the instructions on how to put them together. Indeed, even the placement of the first two cells is not known. Perhaps then it is not surprising that the influence that structure has on function is not yet known, except in its most basic sense (eg. a damaged endothelium may cause impaired vasodilatation).

In my previous research project (MSc) I studied the participation of α_2 -adrenoceptors in the response to sympathetic neuroeffector transmission in the rabbit isolated saphenous and plantaris veins. Briefly, it was found that α_2 -adrenoceptors can participate in the postjunctional response to neurotransmitters under certain conditions, namely in the presence of cocaine to block neuronal uptake. This raised the question of location of vascular α -adrenoceptors. Two possible conclusions were

reached from the study; i) α_2 -adrenoceptors required prolonged activation or ii) α_2 -adrenoceptors are located extrajunctionally. However, many questions were left unanswered. i) how are the adrenoceptor subtypes distributed throughout the vascular wall? ii) do smooth muscle cells express subtypes in equal quantities? iii) will noradrenaline (and other selective agonists) stimulate specific cell layers (i.e. asymmetry of responsiveness)?

For my PhD project I was given the task of determining the action of selective agonists at different depths within the vascular wall, in an attempt to answer some of the questions raised in the previous project. Fortunately, the development of wire and perfusion myographs made it possible to mount very small segments of resistance arteries. Furthermore, the design of the myograph enabled them to be used in conjunction with a microscope thus offering a view of the vessel. However, the imaging was primarily for morphometric measurement of wall thickness (wire myograph) or gross functional response (pressure myograph measure of internal and external diameter coupled with wall thickness). These technologies therefore dictated that the following study would be performed on resistance arteries. Unfortunately, this meant leaving the rabbit saphenous and plantaris veins but the questions raised with these vessels are just as relevant (and perhaps even more so) in the resistance vasculature.

With the benefit of hindsight I realise now that the task I was given was hugely complicated and it has taken my research in a direction that I could not have predicted. What started out as an adrenoceptor related pharmacological project has

required the use of fluorescence and confocal microscopy, image analysis methods, 3D modelling, cell culture and the development of novel fluorescent ligands for adrenergic receptors.

This thesis sets out to describe in detail the development of methods which have become commonly used in Professor McGrath's laboratory and is widely referred to as 'confocal myography'. Chapter 1 introduces the problems briefly outlined above and suggests a method for staining and visualising 'living' myograph mounted segments of blood vessels. In addition this chapter introduces a novel cell viability assay for blood vessels and shows that these methods can also be applied to in-vivo preparations. Chapter 2 introduces the principles of confocal microscopy and details my search for the vital stains and conditions that could be used for the study of blood vessel structure. Chapter 2 also introduces the methods of image analysis and the problems associated with 3D quantification. Chapter 3 describes the work with fluorescent ligands, which can be used with other structural stains. This chapter describes the problems of maintaining drug selectivity while at the same time obtaining good images for analysis. Chapter 3 also presents the first published 'specific' fluorescence binding curve performed on living cells. This technique will provide a means of determining receptor subtype on a single dissociated cell and will hopefully provide a direct answer to one of the questions previously raised. Chapter 4 is a case study of the mouse tail artery. This chapter shows what information can be gained using a combination of confocal microscopy and myography (confocal myography).

Chapter 1

The Development of Fluorescence Myography and the Use of
Fluorescent Nuclear Stains.

Introduction

Blood Vessel Structure and Function

Current histology texts devote very little space to the description of vascular structure. In general, the main vessels (with the exception of the capillaries) are composed of 3 'tunics'. The tunica adventitia is the outer coating of cells, comprising mainly macrophage and fibrocyte cells. The adventitia also provides support for the postganglionic sympathetic nerves that innervate some vessels and which terminate at the adventitia medial border in arteries and slightly deeper in the veins. The inner layer of endothelial cells (EC's), which form the endothelium, are generally flat cells which are in contact with the blood and are referred to as the tunica intima. Between the intima and adventitia is the tunica media. The media is composed of smooth muscle cells (SMCs), elastin and collagen fibres.

The arrangement and number of SMCs has become a focus of attention in the past 20 years, stimulated by the discovery that medial thickness (and thus wall:lumen ratio) is altered in resistance vessels of hypertensive animals. Mulvany & Halpern (1977) reported a 23% increase in wall thickness in 3rd order branches of rat mesenteric artery taken from spontaneously hypertensive rats (SHR's) compared with their normotensive Wistar Koyoto (WKY) controls. This finding has been confirmed by many workers in recent years and is reviewed in several articles by Mulvany (see most recent 1999). It is beyond the scope of this thesis to review the recent literature regarding hypertension and the reader is encouraged to read the reviews by Mulvany et al. However, in a general sense it may be worth considering the 'regular'

arrangement of vascular smooth muscle cells and the complex interactions that undoubtedly exist between the cells of the adventitia, media and intima.

Older histology texts state that the smooth muscle cells of arterioles are orientated circumferentially and spiral around the vessel lumen (Garvin 1965). Current knowledge adds nothing to this description. In a review of the fine structure of vascular walls in mammals, Rhodin (1982) writes "Generally speaking, the muscle cells are arranged in a helical fashion around the vessel". The same author estimated the angle between the helical turn and the long axis of the mouse femoral artery to be around 30°. In large 'elastic' arteries the spiralling may vary from one layer to the next (Pease & Paule 1960). Moreover, the orientation of smooth muscle cells in the rat aorta changes from oblique to radial in the lathyrin vessel (Keech 1960). Aalkjaer and Mulvany (1983) described the circumferentially orientated smooth muscle cell arrangement of resistance arteries of both rat and human.

There have been no studies which have focussed on the detailed arrangement of cells in the vascular wall. This is surprising given the intense research into the mechanisms of vascular remodelling which occurs in hypertension (Baumbach & Heistad 1989; Haegerty et al., 1993; Mulvany et al., 1996). The debate over remodelling in the literature tends to centre around the cause of the increased media thickness. However, no attempts have been made to describe the organisation of smooth muscle cells in normal vessels.

The outer coating (tunica adventitia) of most blood vessels contain post-ganglionic sympathetic nerves which release neurotransmitters (noradrenaline, ATP and

neuropeptides) which act on the vascular smooth muscle cells (VSMCs) to cause constriction of the vessel. Falck-Hillarp and Glyoxylic acid staining reveals a plexus of nerves which appears to have no real pattern or organisation. However, these nerve stains are rarely visualised in combination with stains for the VSMC or cells in the adjacent adventitia. It could be expected that the nerve plexus will be intimately linked with the underlying VSMCs upon which the neurotransmitters act. Similarly the endothelium exerts control over VSMC and the cells make individual contact yet the general relationship is not known.

In an early review of vascular structure and function Burton (1954) concentrated on the relationship of elastic fibers and SMCs and largely ignored both endothelial cells and any influence that nerves may play. In his review Burton suggested that the only important role the endothelium plays is in the closure (by nuclear swelling) of capillaries. While our knowledge of the various endothelium derived factors has been extended in recent years it is still not clear how the individual EC's relate to the adjacent SMCs.

Bozler (1941) classified smooth muscle cells into two groups. 'Multi-unit' groups are activated by motor neurones and 'visceral' smooth muscle groups are intrinsically rhythmically active. Since the vascular wall can be innervated and can exhibit rhythmic contractions the possibility exists that two (or even more) functional groups of SMCs may exist. This has yet to be established.

Figure 1.1 shows a simplified schematic of the blood vessel wall. Generally, the vascular sympathetic nerves terminate at the adventitia medial border in arteries. The

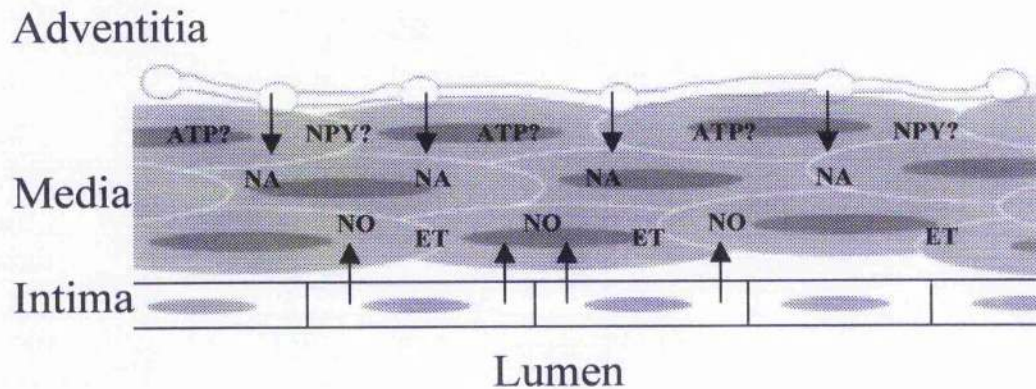


Figure 1.1. Schematic diagram of the vascular wall showing varicose sympathetic nerves terminating at the adventitia-media border. Noradrenaline (NA) and perhaps ATP & NPY are released from the varicosities to cause vasoconstriction. Nitric oxide (NO) and endothelin can be released from the endothelial cells to cause vasodilation and vasoconstriction respectively. It is not possible to represent the receptor distribution for any of these molecules on the diagram.

adrenergic nerves depicted in the diagram release NA which acts on vascular α -adrenoceptors to cause contraction. In many cases the P2x agonist ATP is a cotransmitter with NA. Neuropeptide-Y is also present in some sympathetic nerves. Nitric oxide (NO) is one of the many factors liberated by the endothelium and is presently one of the most widely studied vasodilators. The relatively unstable nature of NO and NA in the biophase might suggest that the outer layers of smooth muscle cells would be most sensitive to NA. However, this does not appear to be the case.

Asymmetry of responsiveness.

The asymmetry of responsiveness within the vascular wall is a little understood but well documented and important phenomenon. The inner layers of smooth muscle of the perfused rabbit ear artery are more sensitive to noradrenaline (NA) than the outer layers (De La Lande et al., 1967; Kalsner, 1972). Using heat damaged strips of sheep carotid artery, Graham and Keatinge (1972) showed that inner layers of SMCs were more responsive to vasoconstrictor hormones than the outer layers. The relative contraction of inner and outer smooth muscle was later assessed by measuring shortening and direction of torque produced during contraction of helical strips of sheep carotid artery (Keatinge & Torrie, 1976). Techniques using silicone grease to restrict the access of drugs to adventitia or intimal surfaces were subsequently developed and provided further evidence for asymmetry of response in strips of rabbit aorta (Pascual & Bevan, 1979; Pascual & Bevan 1980) and rings of rabbit ear artery (McCalden & Bevan, 1980). Such asymmetry has been demonstrated in isolated perfused rat mesenteric resistance arteries using on-line video analysis (Teshfariam & Halpern, 1988).

All of the above studies have concentrated on the application of the agonist to the inner (luminal) or outer (adventitial) surfaces of the preparation. Studying the activity of individual cells within the wall of a vessel requires that the tissue be visually inspected for changes in force development, circumferential length and/or resistance to flow. Present computerised techniques are capable of monitoring internal and external diameter but cannot determine how cell-cell interactions within the media brings about these changes.

A starting point for the present study was to develop a method that would enable the study of cell activation at different medial depths in response to α -adrenoceptor subtype selective and non-selective agonists.

Wire Myography

The study of small segments of resistance arteries was made possible by the development of the wire-myograph. This development was a major breakthrough and enabled the mechanical properties of vascular smooth muscle cells to be studied in-situ (Mulvany & Halpern 1976). Prior to this development smooth muscle cells were studied by visual means since it was not possible to tether individual cells between supports and transducers. One such study of the arrangement of filaments in activated SMCs (using phase contrast and birefringence) suggested that intracellular filaments are arranged in a regular 3D-pattern that reorganises on activation and in turn leads to shortening of the SMC (Fisher & Bagby 1977).

Using wire myograph mounted segments of rat mesenteric artery Mulvany and Halpern (1976) employed Nomarski interference microscopy to visualise smooth muscle cells in the media of an isolated vessel thus permitting measurement of cell length and width. The authors even report the visualisation of nuclei and mitochondria in certain cells. Apart from Mulvany's group few, if any, papers have appeared that have used the wire myograph as a tool for visualisation of contraction. Most workers have used the myograph simply to measure isometric force. In some cases morphological measurements of wall thickness have been made of mounted vessels (Mulvany & Halpern 1977).

It was therefore decided that, for the present project, wire myograph mounted segments of rat mesenteric artery would be used to study activation of cellular layers in response to α -agonists.

α -adrenoceptors in the vasculature.

Functional α -adrenoceptors (ARs) are found in most (but not all) blood vessels. α -adrenoceptors can be divided into two main classes; α and β . Circulating adrenaline can stimulate α - and β -adrenoceptors while the neurotransmitter noradrenaline (NA) activates mainly α_1 -adrenoceptors. A fuller discussion of the various α_1 -adrenoceptor subtypes is given in chapter 3 of this volume.

α_1 -ARs are 7 transmembrane domain (7TM) G-protein coupled receptors (GPCR). Activation of the receptor causes activation of the G-protein, which causes an increase

in inositol phospholipid hydrolysis. The resulting increased concentration of IP_3 triggers the release of calcium from intracellular stores. The increased $[Ca^{2+}]_i$ leads to contraction of vascular smooth muscle cells.

It has been suggested that different α_1 -subtypes utilise different pools of Ca^{2+} in effecting their response (McGrath 1982). Therefore, a vessel with a mixed population of functioning α_1 -adrenoceptors subtypes would be expected to display asymmetry of responsiveness in cases where the subtypes are distributed unevenly throughout the media. This has yet to be established conclusively.

α -adrenoceptors play a crucial role in the function of both arteries and veins. The distribution of α_1 and α_2 -adrenoceptors varies widely in the vessels of the cardiovascular system. In our own lab we have studied vessels which range from being mainly α_1 (rabbit carotid artery, M. Nahagadch PhD thesis) to mainly α_2 (rabbit ear vein, Daly et al., 1988b). Between these two anatomical locations the mix of α_1 to α_2 in individual vessels is remarkably varied (Daly et al., 1988a).

In resistance sized arteries there have been several recent studies of α -AR subtype mediated vasoconstriction. The rat mesenteric artery appears to contain α_{1A} & α_{1B} adrenoceptor subtypes (Smith & McGrath 1996) and constricts strongly to noradrenaline in-vitro and in-vivo (figure 1.2).

There are presently 4 main methods of determining degree of contraction/activation of VSMCs.

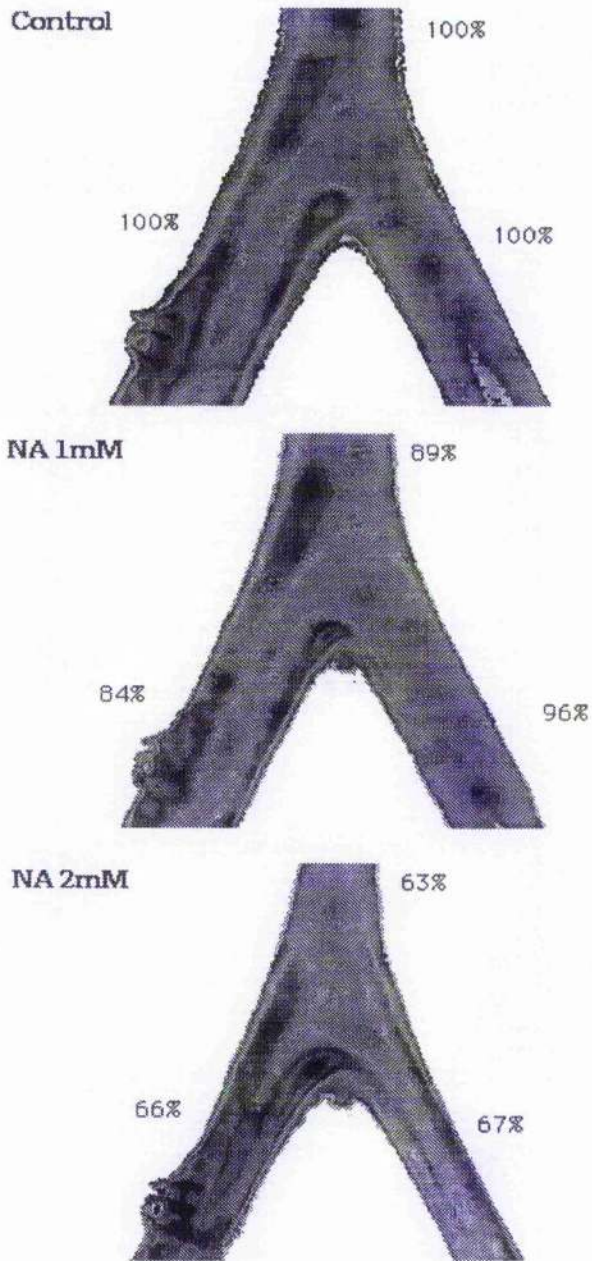


Figure 1.2. In-situ rat mesenteric artery branches contracted with exogenously applied NA. the mesenteric arcade was exposed under anaesthesia (thiopentone Na) and immersed in Krebs solution. A standard monochrome camera was used to image the bifurcation prior to and during exposure to topical application of 1 & 2mM noradrenaline.

- i) Biochemical; Tissue levels of G-protein, IP3 etc. can be measured at set times during incubation with activators.
- ii) Fluorimetry; Ca^{2+} indicators can be used to report $[\text{Ca}^{2+}]_i$ in cells in the presence of activators. The signal can be detected by PMT devices or CCD cameras.
- iii) Physiological; Isolated cells or tissue segments can be studied for their electrophysiological or mechanical response to activators.
- iv) Molecular; Recent developments have enabled the measurement of DNA and RNA synthesis in homogenised tissues. The amount of mRNA can be an indicator of receptor synthesis which in turn may be linked to degree of cellular activation.

Unfortunately, there is no recognised method for studying cellular activation at different depths within thick 'living' biological specimens. Ideally, a combination of methods ii & iii would have the potential to answer questions regarding the asymmetric action of certain agonists.

The eventual goal of the current research project is to establish a collection of methods that together will be able to report on the actions of agonists from a 3-dimensional perspective.

The experiments in this chapter detail the search for a method of staining cells and detecting movement in response to pharmacological stimuli. An interesting use of cell-viability assays was also investigated. A significant portion of this chapter has been published in the *Journal of Vascular Research* (Daly et al., 1992) and was presented in both poster and oral form at the International Symposium on Resistance Arteries (ISRA3, Rebild, Denmark, 1991).

Methods.

Male Wistar rats (250-300g) were killed by stunning followed by exsanguination. Branches of rat mesenteric artery (RMA; 3rd order) and segments of rat aorta were isolated and cleared of connective tissue for subsequent in-vitro staining. Male Wistar rats were prepared for *in-vivo* study as described below.

Phase Contrast Studies of Vasoconstriction.

Segments of RMA were mounted on a wire myograph and normalised at $L_1=0.9L_{100}$ (Mulvany & Halpern 1977). Using a x40 Zeiss water immersion objective the wall of the vessel (including the supporting 40 μ m wire) was brought into focus. The vessel was then stretched by 20 μ m to observe the change in wall morphology. After an initial 'sighting concentration' (noradrenaline 10 μ M followed by washing) a variety of known vasoconstrictors were added to the bath (KCl 30mM; NA 1 μ M; α , β , mA TP 3 μ M).

In a separate series of experiments the centre of the vessel (top surface) was focused. Phase contrast optics permitted the discrimination of adventitia and smooth muscle. Therefore, it was possible to focus past the adventitia and into the media. The movement of the cells was video taped prior to and during application of NA (1 μ M) to initiate rhythmic activity. In some experiments prazosin (10nM) was used to block rhythmic activity.

Fluorescent Staining procedures.

The use of fluorescent markers was investigated with the purpose of providing a greater degree of contrast between cellular structures and extracellular matrix. The dyes used were Hoescht 33342 (Bisbenzimidazole) 5ug/ml (Sigma) , Ethidium Bromide 5ug/ml (Sigma) and Ethidium Homodimer 4µM (Molecular Probes).

Two methods of staining were used. a) Extraluminally (in-vitro); Isolated tissues were incubated in Krebs' solution containing dyes for 20-30 minutes at room temperature or 15 minutes at 37°C. b) Intraluminally (in-vivo); Wistar rats were anaesthetised (i.p. injection) with Thiopentone Na (120mg/kg). Dyes were then administered via a cannula in the left jugular vein. After 15-45 minutes (depending on the amount of staining required) the animals were sacrificed and the tissues (vessels) of interest were quickly removed and placed in fresh Krebs solution.

In-Vitro toxicity tests.

To identify any toxic effects of H33342 in RMA, cumulative concentration response curves (CCRC) to NA (10nM - 10uM) were performed in the presence and absence of H33342 (5ug/ml). After an initial sighting concentration to NA (10uM), a CCRC to NA was constructed. After washing RMA segments were incubated with H33342 for 45 minutes prior to construction of a second CCRC to NA.

Free radical generation and cell-viability assays

Segments of rat mesenteric artery were used to determine the sensitivity of the cell-viability assay. Segments were subjected to incubation with hypoxanthine (1mM; HO) and xanthine oxidase (0.025 units specific activity/ml; XO) along with the nuclear

stains H33342 and ethidium homodimer for 45 minutes. These experiments were performed in 1ml aliquot vials. Following incubation, vessel segments were removed to fresh Krebs's for immediate viewing (unfixed) under fluorescence.

Collection of Fluorescence Micrographs.

Stained vessels were mounted (unfixed) on glass microscope slides. A central square well was created on the slide using thin streaks of silicone grease. The vessel segment was placed in the well and covered with fresh Krebs solution. A number 1 coverslip was then placed over the vessel and was gently pressed down to hold the sample in position.

A Zeiss Axiophot fitted with a 35mm camera was used to photograph the vessels under different excitation wavelengths. Filter blocks for UV (Ex. 364nm; LP >400nm), Fluoresceine (Ex. 488nm; LP >515nm) and rhodamine (Ex. 529nm; LP 610nm) were used to image Hoechst 33342, Calceine and Ethidium respectively. Exposure time was determined automatically by the camera system.

Image Analysis.

A standard Zeiss microscope fitted with an Hg light source and epi-fluorescence assembly was used with filter sets for Hoechst (Zeiss filter set 2, Excitation 365nm, Beam splitter 395nm, Long pass filter 420nm) and Rhodamine (Zeiss filter set 15, Excitation 546nm, Beam splitter 580nm, Long pass filter 590nm). The microscope was also fitted with a Panasonic camera (type WV CD 20).

Branches of rat mesenteric artery were mounted on a wire myograph and normalised at $L_1=0.9L_{100}$ (Mulvany & Halpern 1977). Tissues were then stained extraluminally

before the whole myograph was placed on the stage of the microscope. A water immersion objective (x40/0.75) was used to focus discrete layers of cells within the upper wall of the vessel (see figure 1.11). Images obtained on the microscope were simultaneously captured on video tape and computer. The video recorder was a Pal u-matic model CR 606OE. The computer was a colour Macintosh Ilex with 8Mb of on board RAM fitted with an analog-digital 'Data capture' board. The 'public domain' software for thresholding and imaging was 'Image v1.16'. This software reports the cartesian coordinates in pixels of any selected object (nucleus) on the screen. For each nucleus the x-y coordinates were recorded during movement on a frame by frame basis. This particular system does not provide an automated means of identifying the centre of a nucleus (more advanced object analysis routines are described in Chapter 2). For my initial experiments I was only concerned with the principle of the technique and therefore I estimated the centre of the nuclei, based primarily on pixel intensity, before and after contraction. Clearly this manual method introduces a degree of error which was reduced by further developments outlined at the end of chapter 2 of this thesis.

The way in which vessels are mounted on an isometric wire myograph causes accumulation of tissue between the wires during contraction of sufficient force (see discussion). I have concentrated not on the overall movement of nuclei along the circular axis but on the average spacing of a group of cells (defined by their nuclei positions) relative to each other along the circular and longitudinal axis. I also calculated the average diagonal spacing between the nuclei of the selected group. To measure the change in nuclei spacing during contraction the method employed was as follows.

a) The video camera is oriented to show the vessel segment as it is on the myograph, with the circular smooth muscle running horizontally and the longitudinal axes of the vessel (lumen) running vertically. The computer will therefore display smooth muscle cell nuclei oriented along the computer screen x-axis.

b) A group of nuclei were selected for analysis prior to contraction. The arrangement of smooth muscle is such that groups of nuclei will generally be arranged in a roughly diagonal distribution. The nucleus nearest the bottom of the screen is designated number 1 the next nearest in the longitudinal axis being number 2 and so on until all nuclei within the group are numbered. These numbers are not used in any calculation and are for reference only.

c) The centre of each nucleus is estimated and a pointing device (mouse) used to label the centre and obtain screen coordinates in pixels. The positions of nuclei in the group were thus obtained and logged.

d) The average of spacing of the group of nuclei, ordered in this way, was then calculated as follows;

(i) Circular Spacing

The difference in the x-axis coordinates between nucleus 1&2, 2&3, 3&4 etc. was calculated by subtraction to give the circular spacing between each pair. The average circular spacing was thus calculated.

(ii) Longitudinal Spacing

The difference in the y-axis coordinates between nucleus 1&2 , 2&3, 3&4 etc. is calculated by subtraction to give the longitudinal spacing between each pair. The average longitudinal spacing was thus calculated.

(iii) Diagonal Spacing

By constructing right angled triangles between nucleus 1&2, 2&3, 3&4 etc. the hypotenuse can be calculated from the known opposite and adjacent (x and y spacings) to give the diagonal spacing between each pair. The average diagonal spacing was thus calculated.

Points c and d are then repeated after contraction has reached a plateau and the two data sets are compared.

A fully automated system would ideally perform steps c and d continuously and in real time. .

Drugs and Solutions.

The composition of the Krebs-Henseleit solution was (mM): NaCl 118, KCl 4.7, CaCl₂ 2.5, MgSO₄·7H₂O 1.2, NaHCO₃ 24.9, KH₂PO₄ 1.2, and glucose 11.1. The substances used were: Hoechst 33342 (Ex. 343nm, Em. 483nm) (Sigma), ethidium bromide (Ex. 482, Em. 616) (Sigma), ethidium homodimer (Ex. 492, Em. 627) (Molecular Probes Inc.), noradrenaline (NA) (Sigma) & acetylcholine (ACh) (Sigma).

Results.

Phase Contrast.

After mounting on the wire myograph (figure 1.3a & 1.3b) a x40 water immersion objective was used to focus the wall of the vessel (figure 1.3c). The supporting wire, media and adventitia can be clearly discriminated. On activation with noradrenaline (NA; 1 μ M) the tissue becomes compressed causing thinning of the wall on the wire and also causing increased folding of the internal elastic lamina (figure 1.3d).

On all of the arteries studied the media appeared to contain an area of high contrast which appears as a thin black line running down the centre of the media. Alteration in brightness and contrast were moderately successful at enhancing this feature (figure 1.4).

KCl 50mM caused a visible thinning of the vessel wall (figure 1.4a).

NA 1 μ M caused a visible thinning of the wall and disappearance of the central line of contrasting material (figure 1.4b).

α , β , mATP 3 μ M also caused a significant thinning of the wall which equated to 300mg of force generation as measured on the wire myograph (figure 1.4c).

These experiments show that the wire myograph is not 100% isometric and that contraction of vascular smooth muscle can be visualised.

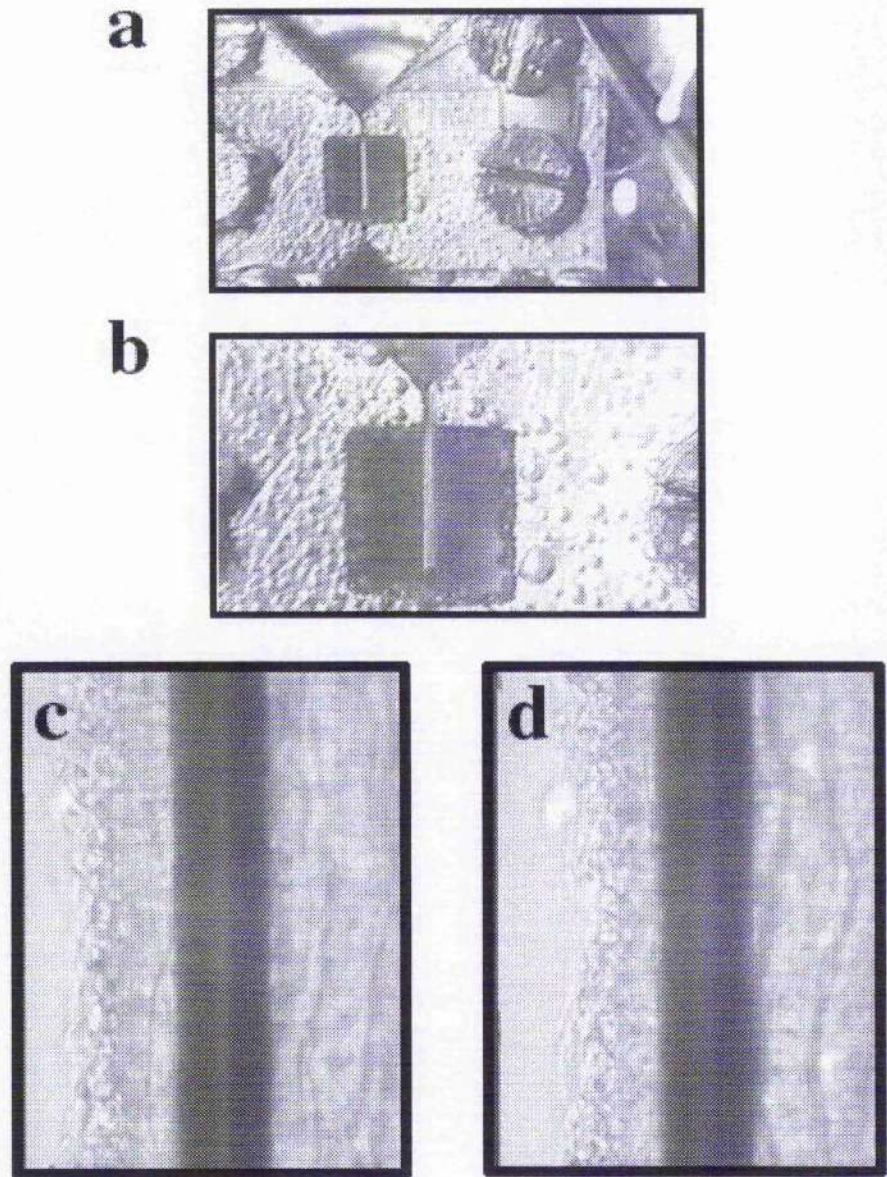


Figure 1.3. Rat mesenteric artery segment mounted on a wire myograph. a) low magnification image showing the supporting wires and vessel segment in the space between the adjacent heads. b) Higher magnification showing only the vessel segment. c) Using a water (x40 NA 0.75) immersion objective the supporting (left hand wire) and wall thickness can be imaged. d) The vessel region shown in c) during contraction to 1 μ M noradrenaline.

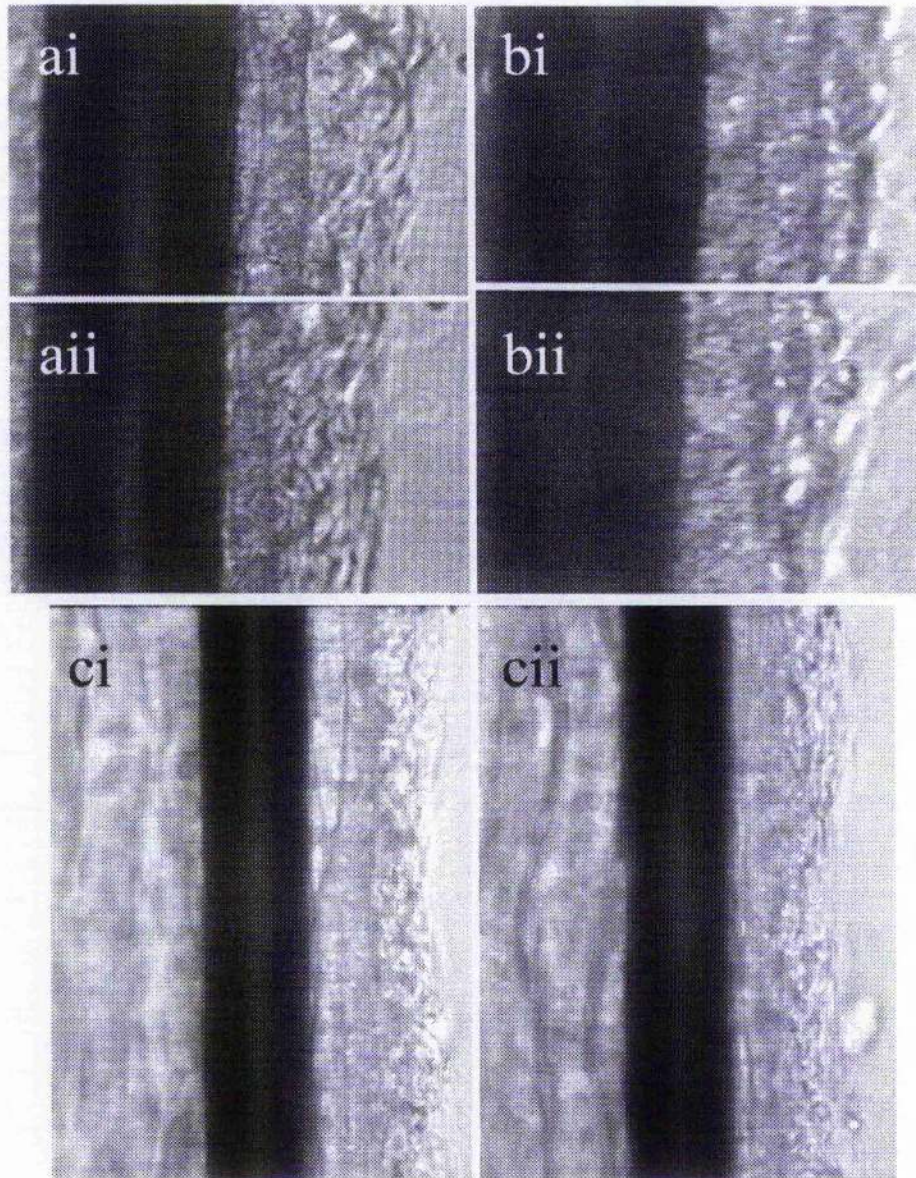


Figure 1.4. The effect of contractile agents on wall thickness of wire mounted segments of rat mesenteric artery. ai), bi) & ci) show arteries at rest. aii), bii) & cii) show arteries contracted with 50mM KCl, 1 μ M NA & 3 μ M α,β , mATP repectively.

NA caused rhythmic activity to develop in certain arteries. Figure 1.5 shows one such example. The central point on the top surface of the mounted segment is brought into focus (x40 w/0.75). Prior to contraction, very slight vasomotion was observed under no active tone. As phasic activity continues the artery oscillates between two general arrangements (figure 1.5c&d). The smooth muscle cells (SMCs) appear to be arranged circumferentially around the artery. Focussing into deeper medial layers did not enable visualisation of inner layers of SMCs (figure 1.5b). During contraction to NA (1uM) rhythmic activity developed and the folds of the internal elastic lamina became clearly defined. The lowest (figure 1.5c) and highest (figure 1.5d) forces of rhythmic contraction are shown.

Regardless of the focal position, degree of stretch or activator used, it was not possible to achieve sufficient contrast to identify individual cells or cell layers. Therefore, a series of fluorescent vital stains were tested.

Fluorescent probes.

The molecular probes cell viability kit contains Calceine AM and ethidium bromide. Live cells will take up calceine AM after which esterase activity will cleave the AM to produce green fluorescence in the healthy cells. Ethidium bromide is a red nuclear stain which is excluded from live cells and will stain only the nuclei of permeabilised cells. Figure 1.6 shows a representative example of a series of experiments. The artery was lifted in the middle using forceps prior to being incubated in EB & calceinAM. Subsequent analysis revealed the damaged areas adjacent to the live (green) cells (figure 1.6a). Unfortunately, calceine fluorescence bleached quickly

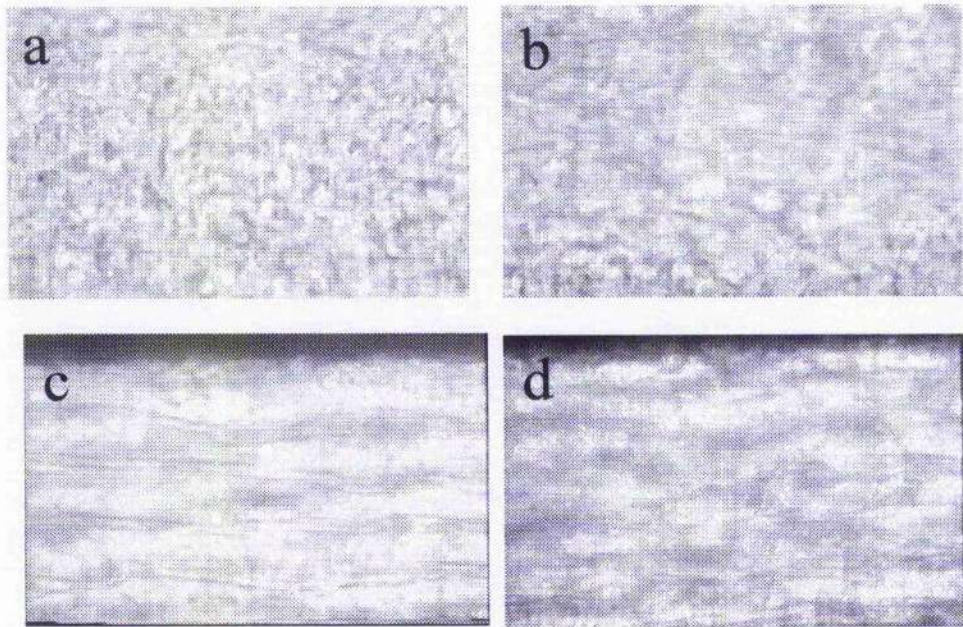
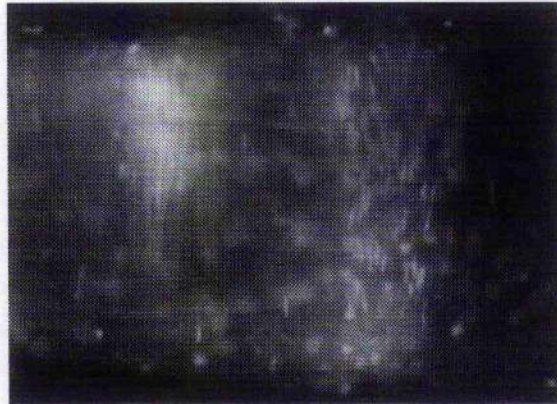
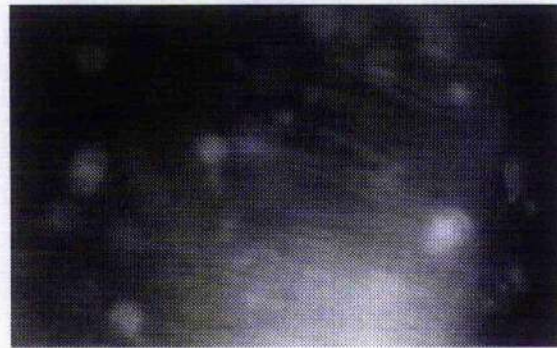


Figure 1.5. All four plates show a wire mounted segment of rat resistance artery viewed under bright field illumination. a) Immediately under the adventitia, smooth muscle cells are arranged circularly (top to bottom on the plate). b) focussing deeper into the media results in a loss of definition of cellular structure. c) Focussing in the lumen reveals the folds of the internal elastic lamina. d) During contraction distance between the folds decreases as the tissue becomes compressed.

a



b



c

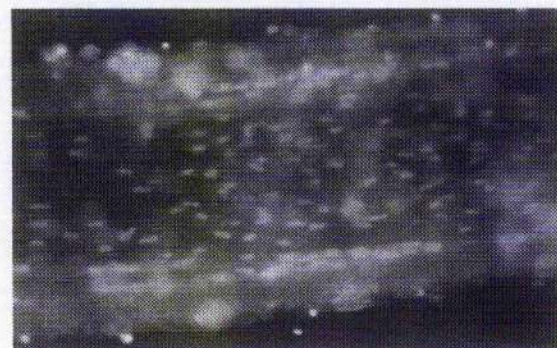


Figure 1.6. Results obtained using a standard cell viability assay on segments of rat isolated mesenteric arteries. Calceine AM is a vital stain which is taken up into living cells where esterases render it fluorescent producing green fluorescence in the cytoplasm. Ethidium Bromide is a nuclear stain which is cell impermeant and therefore will only stain nuclei of non-viable cells. a) Shows an area of live (green) cells alongside an area of forcep damaged (orange nuclei) cells. b) Shows a high magnification view of 'live' cells. c) A vessel with healthy media and damaged endothelial cell nuclei (see text for details)

making prolonged study impossible. The contrast even in healthy cells was often not sufficient to resolve cell boundaries. Cells in inner layers of the media could not be visualised (figure 1.6b). Figure 1.6c shows the healthy (green) media and damaged (orange nuclei) of a free radical treated vessel (described later).

Hoechst 33342 & Ethidium bromide.

H33342 is a lipophilic vital stain for DNA. Together with EB this combination should be able to distinguish viable from non-viable cells. H33342 will label ALL cell nuclei while other stains can be used which target specific cells/nuclei. Image subtraction can then be used to determine nuclear differences.

Extraluminal staining.

Branches of rat mesenteric artery were stained extraluminally with Hoechst 33342 (5µg/ml) and ethidium bromide (5µg/ml) for 15minutes at 37°C. Under fluorescence using the Hoescht filter set only the nuclei of the various cells are visible (figure 1.7). When the focus is only on the adventitia the cell nuclei are irregular or roughly round in shape (figure 1.7a), this is consistent with the known shape of macrophage and fibroblast cells, which are the main cell types of the adventitial coat. We have observed that a proportion of the outermost cells take up ethidium and are presumably damaged during dissection. If the focus is set on the outermost smooth muscle the adventitial nuclei fall out of focus but can still be identified (figure 1.7b). The smooth muscle cell nuclei however can be sharply focused (figure 1.7b) and these are distinguished by their elongated shape. When the plane of focus is set on the luminal surface the endothelial cells are sharply focused and the smooth muscle cell nuclei fall



Figure 1.7. Fluorescent nuclear staining of rat mesenteric artery. The top panel (a) shows the image obtained when the focal plane is set within the adventitia. The lower panel (b) shows the smooth muscle cell nuclei of those cells immediately under the adventitia.

out of focus, the adventitial cell nuclei cannot be distinguished. The use of objectives $\times 25$ with a numerical aperture of 0.75-1.00 does not permit simultaneous viewing of the adventitia, smooth muscle and endothelium. Thus focal plane and nuclear shape can be used to identify cell types and focal depth and therefore allow identification of discrete cell layers.

Cell Viability

Segments of RMA were incubated in H333342 & EB and visualised at $\times 10$ to show the general structure of the vessel (figure 1.8a&b) or the wall thickness and lumen diameter (figure 1.8d)

There appears to be no damage to smooth muscle cells during careful dissection of most blood vessels (figure 1.8a). If, however, forceps are used to hold the vessel, the area under the compression can be severely damaged (figure 1.8b&c). This technique is sensitive enough to show damage caused by less invasive methods, e.g. infusion of air (figure 1.8e), 'gentle intimal rubbing' (not shown) and exposure to free radicals (figure 1.9).

In a brief study of rat aorta it was found that the aortic wall is too thick to permit visualisation of the endothelial cell layer through the adventitial surface. Therefore, rings of aorta were cut open to permit viewing from the luminal surface (figure 1.8f). this technique is particularly well suited for studying endothelial cell arrangement.

Figure 1.9 demonstrates the greater selectivity (brightness relative to background) of ethidium homodimer (figure 1.9 b, c & d) compared with ethidium bromide (figure

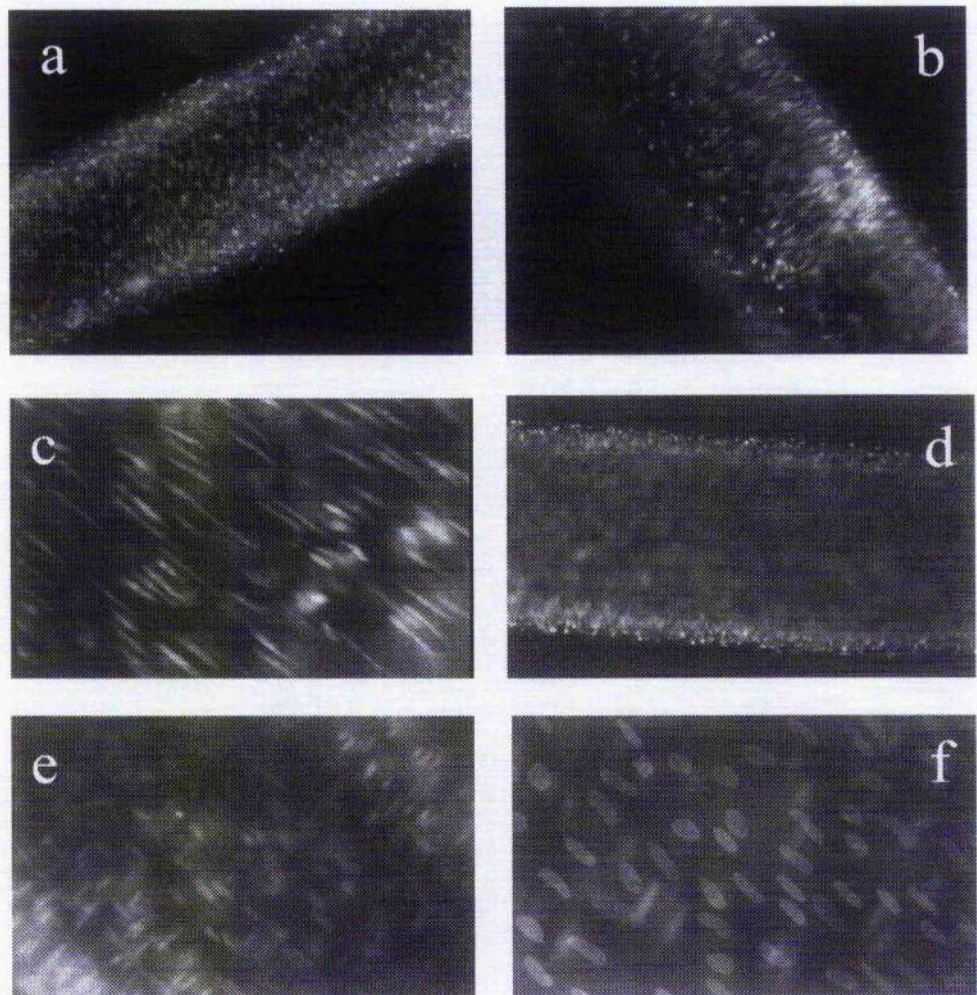


Figure 1.8. Segments of rat isolated rat mesenteric artery (RMA; a-e) and rat aorta (f) stained with Hoechst 33342 in combination with ethidium bromide. a) RMA showing damage (orange nuclei) in only the outermost cells of the adventitia. b) RMA showing damage of smooth muscle cells in the media following compression with forceps. c) High magnification view of forcep damage to the medial smooth muscle. d) Focussing through to the lumen provides good enough contrast to measure wall thickness and lumen diameter. e) The passage of air through the lumen causes damage to the endothelial cells, indicated by the orange nuclei. f) Endothelial cell nuclei of the rat aorta

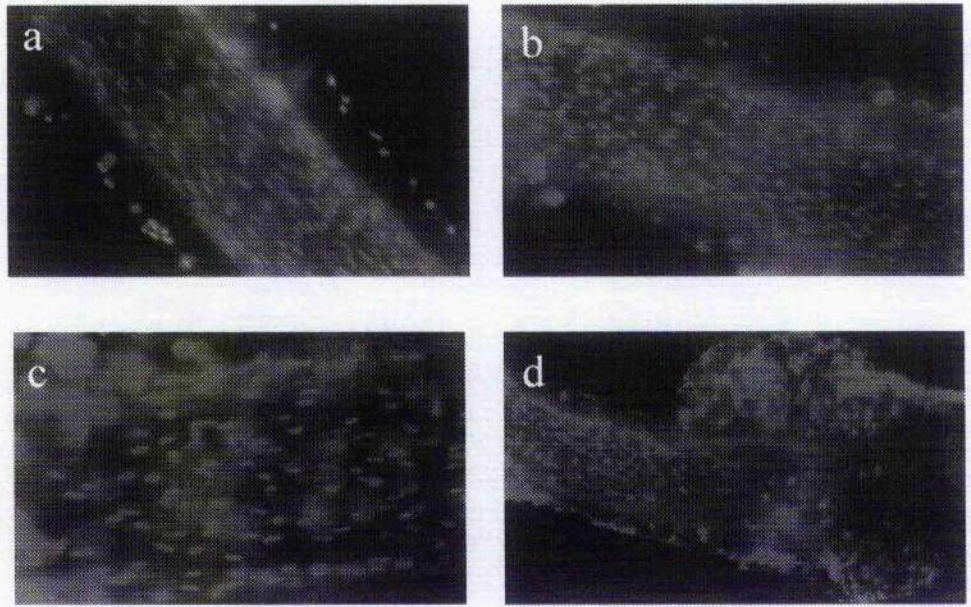


Figure 1.9 Free radical damage in four segments (a-d) of rat mesenteric artery. The images are from 4 different vessels. Nuclei of damaged cells are stained with (red) stain ethidium homodimer.

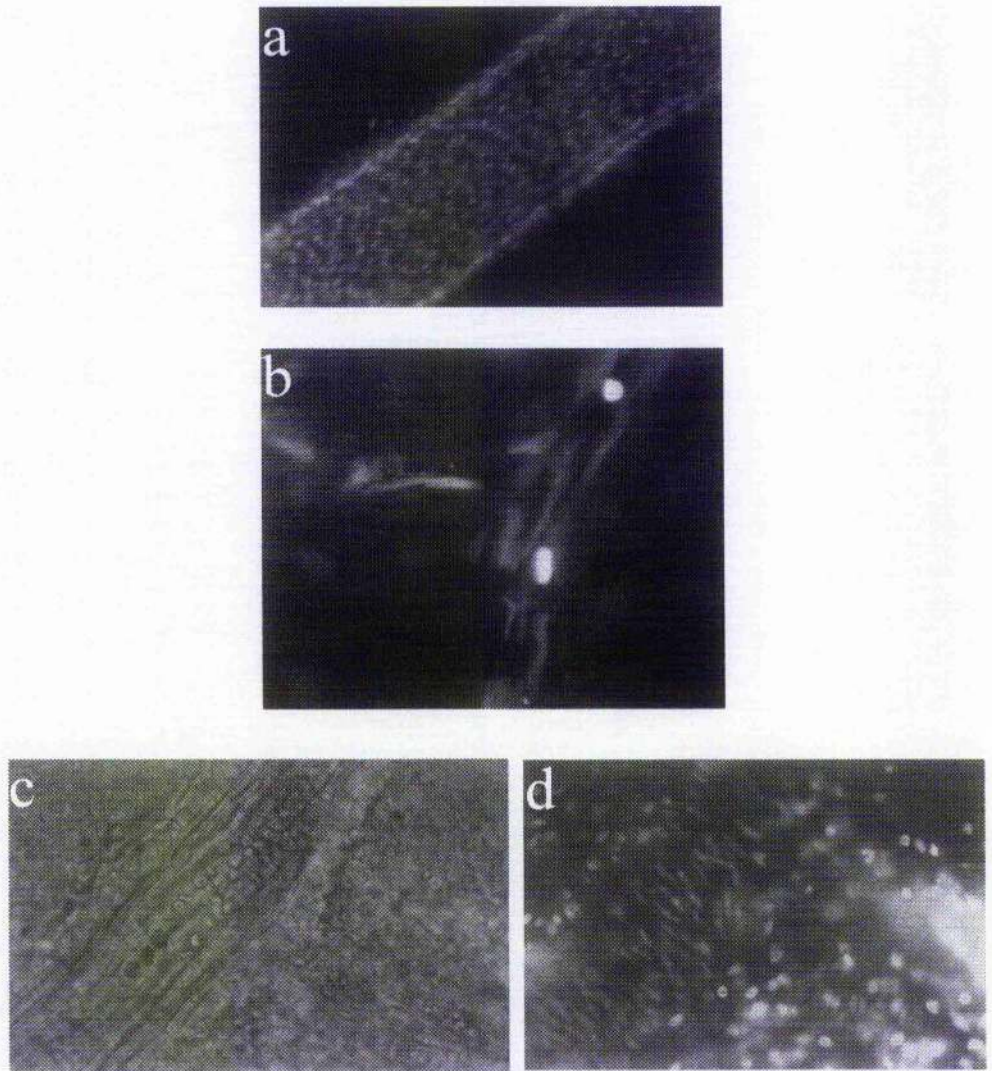


Figure 1.10. In-vivo staining using 30mg/Kg Hoechst 33342 (intravenously). a) Examination of the rat mesenteric arteries revealed good staining of the endothelial cell nuclei. b) Inspection of capillaries in the brain revealed much poorer staining although white blood cells were clearly visible within the lumen. c) Bright-field imaging of larger cerebral arteries showed the presence of red blood cells in the artery and its branches. d) Fluorescence microscopy showed good staining of the main arterial smooth muscle nuclei but an absence of stain in the branch.

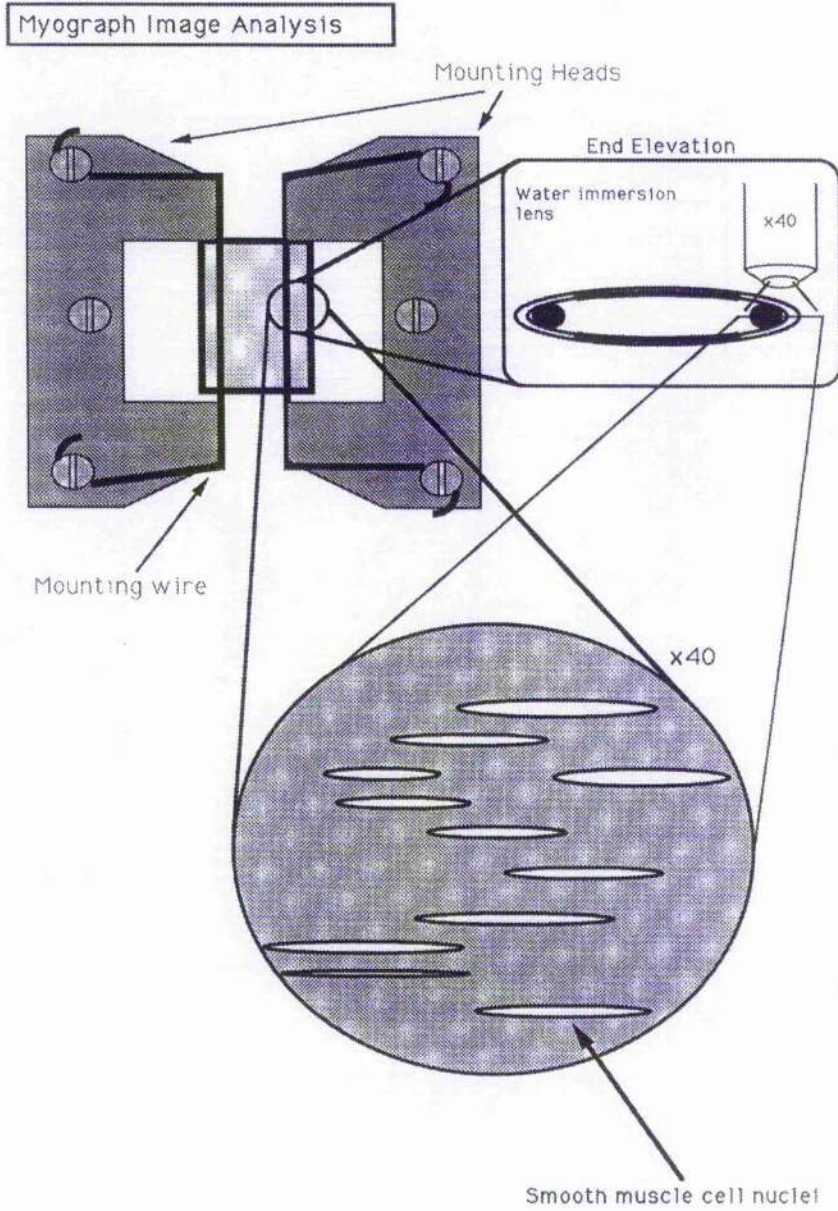


Figure 1.11. Schematic diagram of a nuclear stained segment of rat mesenteric artery mounted for visualisation on a wire myograph.

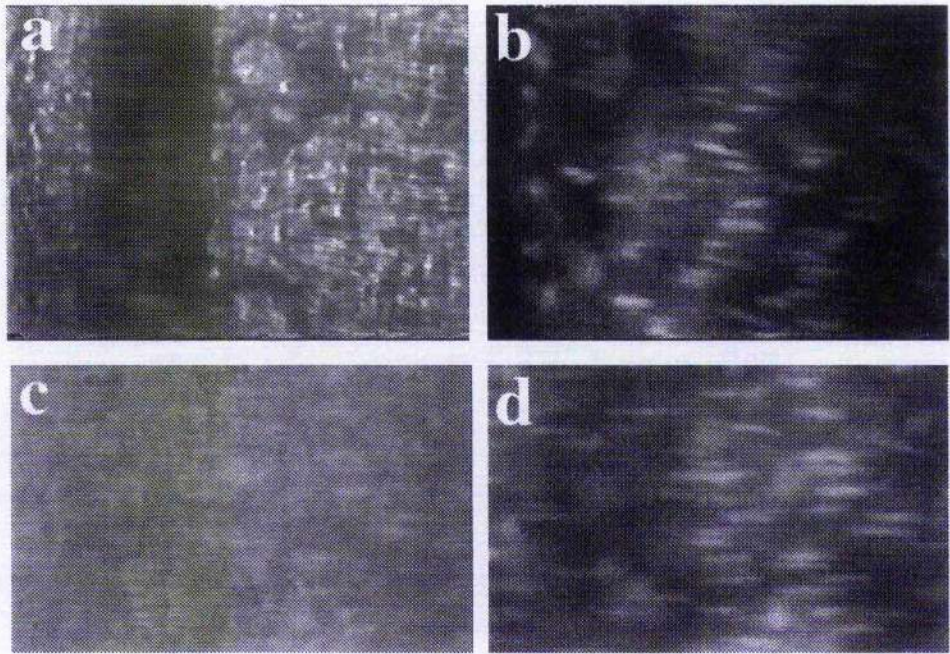


Figure 1.12. Combination of brightfield images (a&c) and fluorescence images (H33342; b&d). a) shows the brightfield image obtained when focussed near the lumen where the supporting wire is clearly visible. The fluorescence image at the same plane of focus (b) shows the arrangement of smooth muscle cells at this depth. c) the brightfield image shows the general direction of smooth muscle in the layer immediately below the adventitia. The fluorescence image at this depth reveals a different smooth muscle cell layer. (40x water objective, NA 0.75).

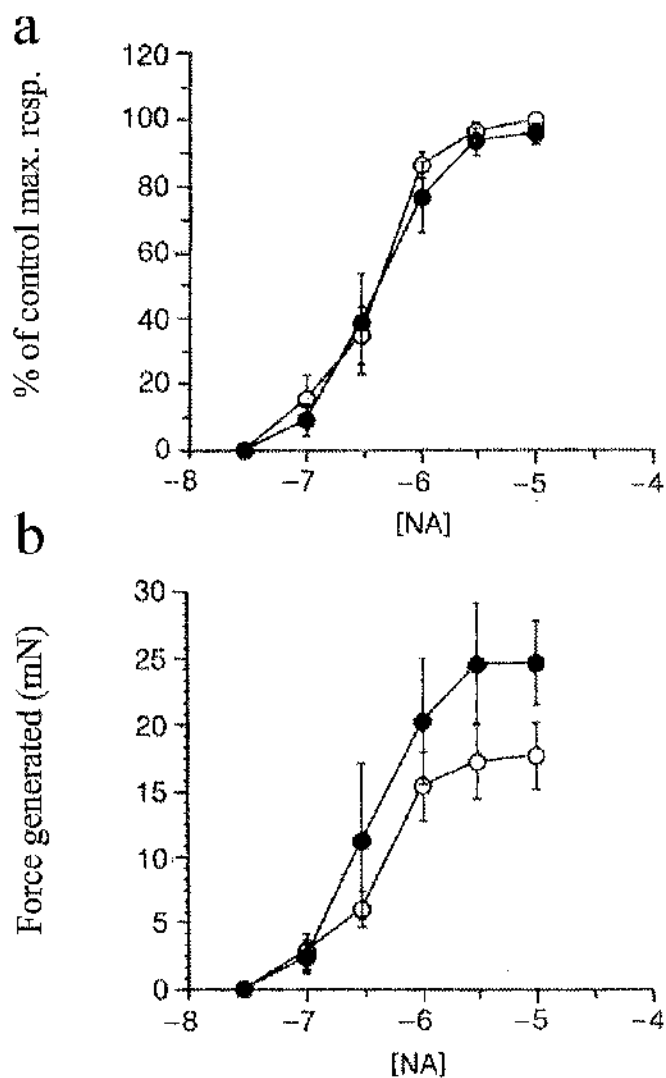


Figure 1.13. The effect of H33342 on responses to noradrenaline in isolated segments of wire myograph mounted rat mesenteric artery. Filled symbols represent responses in the presence of H33342. a) responses expressed as a percent of control (unfilled symbols) maximum. b) results expressed in mN force generated. Data points represent the mean \pm s.e.m of 4 experiments. there was no significant difference between stained and unstained tissues.

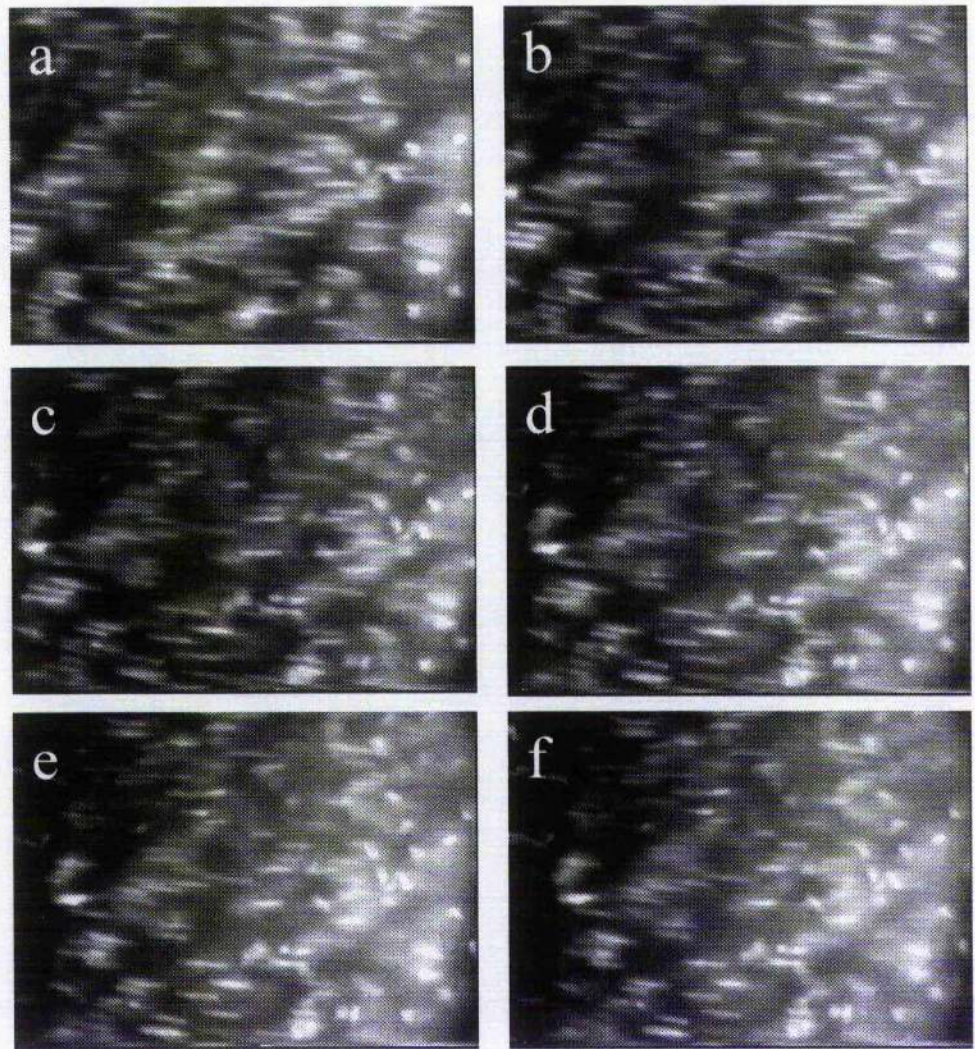


Figure 1.14. The plate shows the position of the outer layer of smooth muscle cells prior to (a) and during (b-f) contraction to $1\mu\text{M}$ noradrenaline. The last image (f) required refocusing to show the nuclei which had fallen out of focus as a result of tissue bunching. The contraction lasts only a few seconds and images b-f are at different time points (chosen for clarity rather than being equally spaced in time). The entire sequence shows the movement of tissue towards the center (left - right) of the segment. (x40 water objective, NA 0.75).

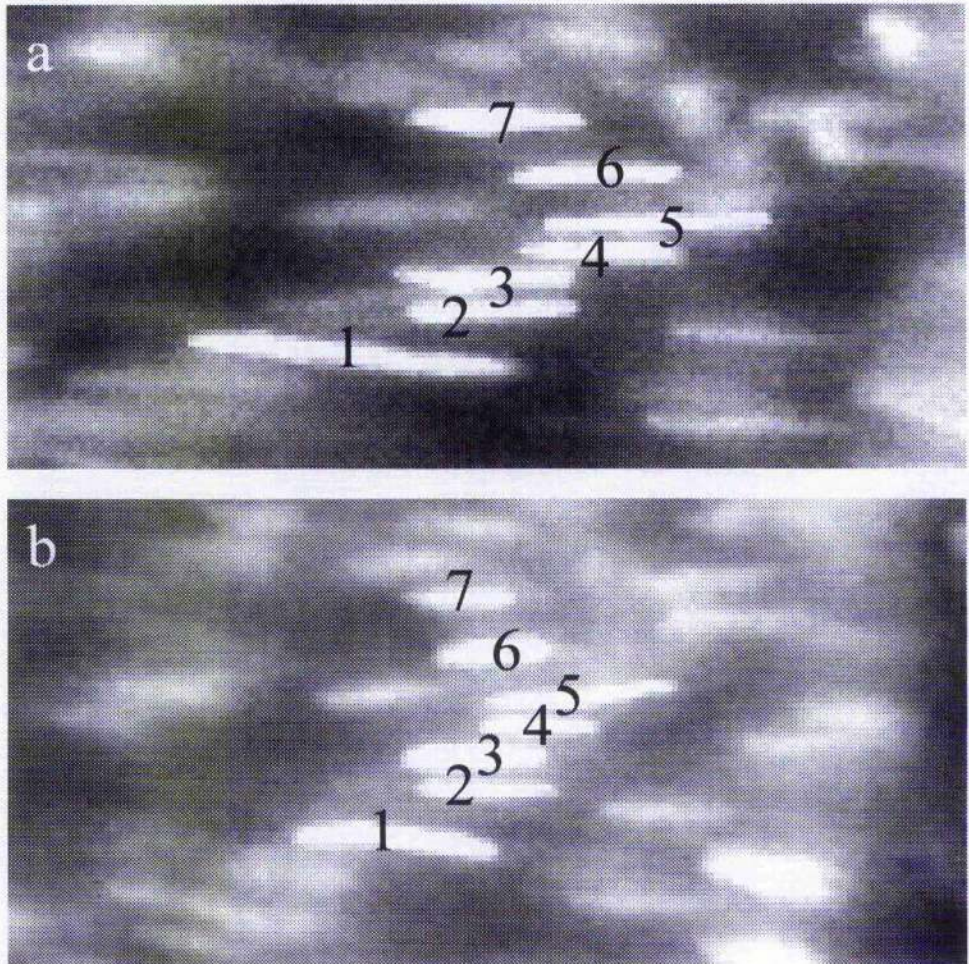


Figure 1.15. The position of 7 nuclei identified from the previous figure. The upper panel shows nuclei position at rest. The lower panel shows the result of contraction to $1\mu\text{M}$ noradrenaline. The average circular, longitudinal and diagonal spacing were calculated as described (in methods page 15) and results are shown in the following figure.

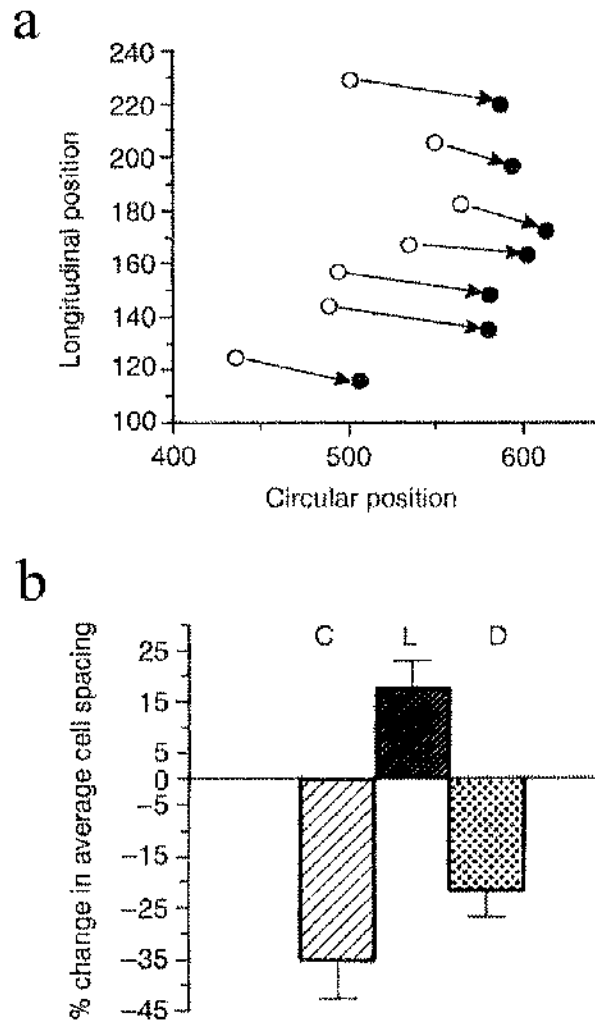


Figure 1.16. Shows the analysis of cellular movement shown in figures 14 & 15. The top graph (a) shows the change in xy position of 7 cell nuclei from resting (open circles) to contracted positions (closed symbols). The lower graph (b) shows an analysis of the relative changes in circular (C) longitudinal (L) and diagonal (D) spacing. see methods section for a full description of the analysis method used.

1.9a). Rat mesenteric arteries were bathed in Krebs containing ethidium homodimer ($4\mu\text{M}$), hypoxanthine (HO, 1mM) and xanthine oxidase (XO, 0.025 units specific activity/ml) for 45 minutes. This combination of HO and XO has been shown to produce free oxygen radicals (Ytrehus et al., 1986) Examination under fluorescence of vessels treated in this way showed that ethidium homodimer stained the nuclei of only the outermost adventitial cells and the endothelium, giving it the appearance of an 'inner-tube'. The absence of any stain in the media suggests that the free radical treatment has selectively permeabilised the endothelium. The cells of the adventitia are damaged due to dissection. Furthermore, damage was not observed in 1st order branches of the superior mesenteric artery, suggesting that ECs may be a heterogeneous population in the vasculature.

Intraluminal staining.

Rats were prepared as described above. Bolus injections of Hoechst 33342 (10mg/kg) had no effect on either blood pressure or heart rate. Bolus injections of 30mg/kg , however, were observed to cause accumulation of fluid in the trachea. Rats were therefore injected with $3 \times 10\text{mg/kg}$ doses of Hoechst 33342 at 5 minute intervals which eliminated this. The rats were killed by exsanguination 5-40 minutes after the third injection. Subsequent inspection, under fluorescence, of branches of rat mesenteric artery revealed a selective staining of the endothelium (Figure 10a). Further experiments have shown the staining to be both time and concentration dependent. If the animals are killed 60 minutes after injection 3 substantial staining of the media is observed. If this time period is increased to two hours all cells within the vessel are well stained.

Analysis of a variety of blood vessels showed that 33342 accumulated in the lungs, probably due to the i.v. route delivering the stain to the lungs first. Interestingly, capillaries in brain slices of cortex showed much lighter staining compared with RMA from the same animal. Indeed, white blood cells stained much brighter than the endothelial cells in brain capillaries (figure 1.10).

Staining of large (thick walled) blood vessels.

Experiments were performed to investigate the effect of free radical generation on responses to exogenously applied NA and endothelium derived vasodilation in isolated rings (3-4mm in length) of rat aorta. At the end of the experiment the rings were incubated in Krebs' containing Hoechst 33342 (5 μ g/ml) for 45 minutes at 37°C. After washing in fresh Krebs' the rings were cut open and placed endothelial side up on slides. Under fluorescence the endothelial cell nuclei can be distinguished by their oval shape, their positions relative to the overlying smooth muscle and their focal position (i.e. on top) (Figure 1.8f). After exposure to hypoxanthine (HO, 1mM) and xanthine oxidase (XO, 0.025 units specific activity/ml) for 45 minutes, causing the formation of free radicals, endothelial cell number is reduced (see Daly et al., 1992 for full details).

Image analysis.

Nuclear staining facilitates tracking of cell positions during vasomotion and the dyes themselves do not interfere with contraction (figure 1.11 & 1.13). Light and electron microscopy studies have confirmed the assumption that the nucleus remains central within the cell during contraction (Lance 1965; Gabella 1976). Therefore the

assumption is that the nucleus position is a reliable indicator of the cell position within the wall. Rings of rat mesenteric artery ($149 \pm 10 \mu\text{m}$ normalised diameter) were mounted on a wire myograph and a layer of cells within the media was selected (figure 1.12 & 1.14). The artery was then challenged with NA ($1 \mu\text{M}$) and the average spacings (circular, longitudinal and diagonal) of the 7 nuclei before and during contraction were compared. Figure 1.15 shows the positions of the 7 nuclei during force development of 13.3mN. The positions of the nuclei before and during contraction can be plotted on a graph (figure 1.16a). During contraction circular and diagonal spacing between nuclei is decreased whereas longitudinal spacing is increased (figure 1.16b), as expected from a shortening and widening of the circular helically arranged smooth muscle cells.

Discussion.

Phase Contrast.

Vessels mounted on the wire myograph can be imaged using conventional 'white light' (bright field). Use of phase contrast optics provides further contrast and enables the identification of smooth muscle cell orientation. Image quality is similar to that obtained using the Nomarski interference method (Mulvany & Halpern., 1976). However, unlike the Nomarski method it was not possible to resolve intracellular organelles including nuclei or mitochondria in any of the vessels studied. It should be noted that the Nomarski method does not enable detection of the organelles of all cells.

Using bright field illumination (phase contrast) it is possible to make morphological measurements of wall thickness. It is possible to distinguish adventitia from media using this approach although determination of intimal thickness is difficult. Initial experiments showed that wall thickness could be measured before and during contraction with KCl and the agonists NA and α , β , mA TP. All three agents caused a significant thinning of the wall adjacent to the wires and presumably bunching of the tissue in the centre of the vessel. The three vasoconstrictors appeared to cause a uniform thinning of the wall and showed no 'visual' evidence of asymmetric agonism. Since it was not possible to distinguish individual cells in the wall surrounding the wires, even after image processing it was decided to study the vessel between the wires from the top surface where the cells are presented for viewing as essentially a flat sheet.

An unexpected property of the vessel wall was observed when viewing from the top. After normalisation and under no active tension visible vasomotion was observed. The movement of VSM was very subtle, detectable, but did not cause a measurable degree of isometric force. Although no further investigation was made of this phenomenon this spontaneous activity may be the basis on which the greater rhythmic activity observed in response to 1 μ M of NA is based. If this is the case dihydropyridine drugs may be expected to block this, Ca²⁺ channel, activity. Whatever the mechanism this phenomenon may be worthy of further study.

The tunica adventitia can easily be distinguished from the tunica media using phase contrast. The adventitia has a very disorganised 'swirly' appearance. Focusing through the adventitia reveals the media as an almost 'striated' layer of tissues. Unfortunately, contrast is not sufficient to permit identification of individual cells. The response to application of 1 μ M NA was fast and powerful. The vessel appears to twist on the wires in what seems to be an uncoordinated fashion which eventually gives way to rhythmical contractions. The most notable feature of rhythmic activity is the folding of the internal elastic lamina which can be clearly seen in figure 5. Interestingly, prazosin (0.1 μ M) effectively abolished the rhythmic contractions within 2 minutes (not shown). This raises some interesting questions regarding the optimum incubation time required for such antagonists to reach equilibrium within a tissue and to produce a maximum effect.

Overall, the results of these preliminary experiments proved that it is possible to image vasoconstrictor response to various agonists in myograph mounted segments of arteries. While these studies revealed many interesting properties of the wall it was

not possible to determine which (if any) cells were more sensitive to agonists or were responsible for the onset of rhythmic/phasic activity (i.e. pacemakers). Therefore, a search for non-toxic, vital stains was undertaken in the hope of finding a suitable, contrast enhancing, stain that could be used on living myograph mounted vessels.

Fluorescent nuclear stains

Nuclear fluorescent dyes have been used routinely by cell biologists for many years to quantify cell numbers and screen out non-viable cells (i.e. those which would not survive in culture medium). The range of application of these dyes outwith cell culture has not been appreciated. This chapter describes preliminary experiments which indicate that these dyes can be applied successfully to the study of cell viability within blood vessels *in vitro* and *in vivo*. Standard histological techniques depend primarily on labelling the cell nuclei to facilitate identification of tissue type and any abnormalities associated with pathology. Similarly vital fluorescent nuclear dyes provide information by outlining the position and distribution of cells via their nuclei. However their use confers significant advantages. Since fixation and sectioning is not necessary the labelling procedure is simpler and more flexible. This lack of a fixation requirement allows dynamic events such as cell movement to be monitored, vital characteristics such as viability to be measured and labelling of living tissue *in vivo* and *in vitro* to be achieved.

Cell viability

I define cell viability as being the ability of a cell to survive in a normal culture medium, such as DMEM, which mimics extracellular fluid. Cell survival is wholly dependent on the maintenance of ionic gradients across the plasma membrane. Loss

of such gradients allows passage of Ethidium Homodimer and labelling of the nuclei. I would draw a distinction between cell viability and cell function since permeabilised cells retain some intracellular functions such as enzymatic activity. I have previously investigated this distinction in saponin skinned/permeabilised blood vessels (not work for this thesis). In skinned preparations, of rat mesenteric artery, esterase activity was present and was indicated by the ability of the smooth muscle cells to hydrolyse Calcein AM to the fluorescent product Calcein. In addition, the contractile apparatus can function if the intracellular fluid is mimicked. However, the smooth muscle cells also label with Ethidium Homodimer indicating their non-viability in the long term in extracellular conditions. This was supported by the loss of contractile function in normal Krebs'.

The results of this chapter have shown this method to be sensitive enough to show damage to blood vessels which have been manipulated with forceps, damaged during dissection, exposed to free radicals and other mechanisms such as intimal rubbing (not shown).

The experiments with free radicals highlights the two ways in which hydrophilic and lipophilic dyes can be used. In figure 1.9 there is significant ethidium staining in the lumen of a vessel exposed to free radicals. This is not surprising as it is widely accepted that free radicals can cause lipid peroxidation (Wrens & Lucchesi 1990). The results show that in rat mesenteric artery it is the endothelial cells which are most sensitive to the effects of free radicals. If this vessel was stained with Hoechst 33342 it would be possible to quantify the ratio of viable and non-viable cells (Daly et al., 1991a). However the purpose of figure 1.9 is to show that ethidium is sensitive

enough to show localised biochemical injury. Therefore, lipophilic dyes can be used to obtain information about cell arrangement and density. Hydrophilic dyes can be used to identify permeabilised cells. Labelling with both dyes simultaneously, therefore, provides a convenient cell viability assay for isolated blood vessels.

Experiments using segments of blood vessels are sometimes ended when the tissue has lost its responsiveness. This is often attributed to desensitisation of membrane receptors or second messenger systems. Alternatively a loss of responsiveness may be blamed on the combination of pharmacological antagonists or physiological interventions which the tissue has been exposed to. The double labelling techniques described here can be used to demonstrate any damaging effects of a particular protocol, which results in permeabilisation of the membrane and loss of viability.

Studies on cell viability are not limited to isolated blood vessels. These dyes can be given intravenously to anaesthetised animals and are not toxic with the protocol used. Intra-venous injections of 30mg/kg Iloescht 33342 causes staining of the endothelium after as little as 15 minutes. If the dyes are left to circulate for 1-2 hours examination of any blood vessel (except those of the brain, figure 1.10) will show staining of the media as well as the intima and adventitia. Preliminary experiments have shown that the dyes do not cross the blood brain barrier. All other organs and tissue types will stain well if given sufficient time. This creates a great number of possibilities for investigations of pathological conditions. Animals could be subjected to an experimental protocol and then injected with a dye combination for cell viability. Any blood vessel or tissue bed could then be inspected for cell death.

Endothelial cell nuclei can be stained selectively by intravenous application of the dyes for a short time period (15 minutes, figure 1.10a). This has now been done in Professor McGrath's laboratory using a perfusion myograph where the amount of staining can be monitored and therefore optimised for any given vessel type.

Nuclear dyes can be used in many areas of physiology and pharmacology. The most immediate uses may be for morphological studies. Normally this is done by histology or electron microscopy and requires reconstruction of several sections. Using fluorescent dyes, morphological studies (e.g. smooth muscle cell density, arrangement, viability, etc.) can be done by non-microscopists either before or after experimentation.

Image analysis

I draw a distinction between the lateral movement of a nucleus and the spacing between groups of nuclei. Cell movement refers to the displacement of a single cell within the overall dimensions of the vessel. This displacement occurs along the circular (x) axis of the vessel. All of the nuclei in figure 1.15 move from left to right towards the central axis of the section of the wall running between the supporting wires during contraction. This lateral movement is ignored to concentrate on the change in average nuclei spacing (see methods) during contraction.

Overall the results have highlighted advantages and disadvantages of the isometric wire myograph. If cell movement is to be analysed then clearly a truly isometric system is not suitable. However, the wire myograph is not truly isometric partly due

to elasticity within the tissue and a little compliance within the mounting wires. To generate sufficient measurable change in nuclear spacing the vessel segment was challenged with 1 μ M noradrenaline. This concentration normally produces 80% of the maximum contraction. It is not surprising therefore that at this degree of contraction some nuclei will twist or fold and thus increase their fluorescence. This does not present much of a problem since nuclear spacing is measured and not lateral movement or length. What is perhaps surprising is that it is possible to make any kind of quantitative analysis of change in cell spacing on an isometric myograph. Thus it is difficult to make any suggestions about the physiological relevance of the measurements made other than they are consistent with the expected shortening and widening of vascular smooth muscle cells during contraction. What is important in the context of this chapter is that the techniques developed make it possible to monitor cell rearrangement within the wall of a small artery during contraction.

Clearly the wire myograph is limited as a tool for image analysis of cellular rearrangement, although the flat surface of the stretched vessel may be useful for Ca²⁺ studies where the cellular movement must be kept to a minimum if ratiometric Ca²⁺ indicators are not used. The next logical step for the current technique, is to move to an isotonic or perfusion myograph where greater rearrangement for a given agonist concentration may be observed. The ability to make measurements up to at least 80% of the maximum contraction means that it should be possible to construct concentration response curves for change in nuclear spacing. Exactly what physiological information on vascular mechanics this will provide remains to be seen.

While asymmetry of responsiveness has been clearly demonstrated in a number of preparations, the various investigators have concentrated on the route of drug administration and have measured the response of the whole tissue. The work of Tesfamariam, and Halpern (1988) concentrated on visualising a perfused microvessel to show asymmetry. However, this method is unable to distinguish movement within discrete layers of cells. Nomarski interference microscopy has been used to obtain a general outline of smooth muscle cells, some of which have visible nuclei and mitochondria (Mulvany & Halpern 1976). Nuclear fluorescent dyes provide significant advantages: a) the position of all cells is clearly marked; b) the contrast for image analysis is significantly enhanced; c) the transparency of the cytoplasm, under fluorescence, allows discrimination of layers at depth within the media and d) cell viability can be assessed in parallel.

Clearly much more work needs to be done on the basic mechanics of blood vessel contraction. It is not clear how much independence of movement a given layer of smooth muscle cells has. This is fundamental information which will be required before making any assessment of the sensitivity of different layers of cells to selective and non-selective agonists. To this end comparisons of responses obtained on isometric, isotonic, isobaric and perfusion systems will be invaluable.

In conclusion, nuclear fluorescent dyes can be used to assess cell viability in a number of tissue types but is particularly well suited to blood vessels. The dyes can be used to enhance current diametric image analysis methods and can be used to enable the study of cell rearrangement within the wall of myograph mounted vessels.

References.

- Aalkjaer C. and Mulvany M.J. (1983) Human and rat resistance vessels: A comparison of their morphological and pharmacological characteristics. *Gen. Pharmac.* Vol. **14**, 85-87.
- Baumbach, G.L. & Heistad, D.D. (1989) Remodelling of cerebral arterioles in chronic hypertension. *Hypertension*, Vol **13**, 968-972
- Bozler E. (1941) Action potentials and conduction of excitation in muscle. *Biol. Rev.* **3**: 95-110
- Burton A.C. (1954). Relation of Structure to Function of the Tissues of the Wall of Blood Vessels. *Physiological Reviews*. Vol **34**. No.4; 619-642.
- Daly C.J., McGrath J.C. & Wilson V.G. (1988a) An examination of the post-junctional α -adrenoceptor subtypes for (-)-noradrenaline in several isolated blood vessels from the rabbit. *Br. J. Pharmacol.* **95** 473-484.
- Daly, C.J., McGrath, J.C. & Wilson, V.G. (1988b) Evidence that population of post-junctional adrenoceptors mediating contraction of smooth muscle in the rabbit isolated ear vein is predominantly α_2 . *Br. J. Pharmacol.* **94** 1085-1090.
- Daly C.J., Gordon J.F. & McGrath J.C. (1991). Assessment of cell viability within the wall of rat mesenteric arteries. *Blood Vessels*, **28**, 282.
- Daly C.J., Gordon J.F. & McGrath J.C. (1992) The use of fluorescent nuclear dyes for the study of blood vessel structure and function: novel applications of existing techniques. *J. Vasc. Res.* **29** 41-48.
- De La Lande I.S., Frewin D. & Waterson J.G. (1967). The influence of sympathetic innervation on vascular sensitivity to noradrenaline. *Br J Pharmacol*, **31**, 82-93.

- Fisher B.A., Bagby R.M. (1977). Reorientation of myofilaments during contraction of a vertebrate smooth muscle. *Am J Physiol* Jan; **232**(1) :C5-14
- Gabella G. (1976). Structural changes in smooth muscle cells during isotonic contraction. *Cell Tissue Res*, **170**, 187-201.
- Garvin, H.S.D. (1965). A Student's histology (2nd Edition). Pub. E & S Livingstone Ltd.
- Gordon J.F., Daly C.J., Boyle F.C., Kusel J.R., Gillespie J.S. & McGrath J.C. (1990). A simple smooth muscle cell viability assay for use in rat blood vessels in vitro. *J Physiol*, **429**, 10.
- Graham J.M. & Keatinge W.R. (1972). Differences in sensitivity to vasoconstrictor drugs within the wall of the sheep carotid artery. *J. Physiol*, **221**, 477-492.
- Haegerty, A.M., Aalkjaer, C. Bund, S.J., Korsgaard, N & Mulvany, M.J. (1993) Small artery structure in hypertension: dual process of remodeling and growth. *Hypertension* Vol **21**, 391-397,.
- Haugland R.P. (1989-1991). Nuclear stains. in Handbook of fluorescent probes and research chemicals. Eugene, Molecular Probes.
- Kalsner S (1972). Differential activation of the inner and outer cell layers of the rabbit ear artery. *Eur J Pharmacol*, **20**, 122-124.
- Keatinge W.R. & Torrie C. (1976). Action of sympathetic nerves on inner and outer muscle of sheep carotid artery, and the effect of pressure on nerve distribution. *J Physiol.*, **257**, 699-712.
- Keech, M.K.(1960) Electron microscopy study of the lathyrin rat aorta. *J. Biophys. Biochem. Cytol.* Vol **7**, 539.

- Lance B.P. (1965). Alterations in the cytologic detail of intestinal smooth muscle cells in various stages of contraction. *J Cell Biol*, **27**, 199-213.
- McCadden T.A. & Bevan J.A. (1980). Asymmetry of the contractile response of the rabbit ear artery to exogenous amines. *Am J Physiol*, **238**, H618-H624.
- McGrath J.C. (1982) Commentary: Evidence for more than one type of post-junctional α -adrenoceptor. *Biochem. Pharmacol.* **31** 467-484.
- Mulvany MJ & Halpern W (1976). Mechanical properties of vascular smooth muscle cells in-situ. *Nature*, **260**, 617-619.
- Mulvany MJ & Halpern W (1977). Contractile properties of small arterial resistance vessels in spontaneously hypertensive and normotensive rats. *Circ Res*, **41**, 19-26
- Mulvany, M.J., Baumbach, G.L., Aalkjaer, C. & Heagerty, A.M. (1996) Vascular remodelling. *Hypertension*, Vol **28**, 505-506.
- Mulvany MJ. (1999) Vascular remodelling of resistance vessels: can we define this? *Cardiovascular Research* **41**, 9-13.
- Pascual R & Bevan JA (1979). Variation in contractile response characteristics of rabbit aorta strips with surface of drug entry. *J Pharmacol Exp Ther*, **210**, 51-55.
- Pascual R & Bevan JA (1980). Asymmetry of consequence of drug disposition mechanisms in the wall of the rabbit aorta. *Circ Res*, **46**, 22-28.
- Pease, D.C. & Paule, W.J. (1960) Electron microscopy of elastic arteries; the thoracic aorta of the rat. *J. Ultrastruc. Res.* Vol 3, 469,

- Rhodin (1982). Fine Structure of the Vascular Wall in mammals. In. *'Vascular smooth muscle : metabolic, ionic, and contractile mechanisms'*. ed. by M.F. Crass and C.D. Barnes Pub. New York London : Academic Press, 1982
- Smith, K.M. & McGrath, J.C. (1996) Investigation of developmental changes in α_1 -adrenoceptor subtypes in rat mesenteric resistance arteries. *Br. J. Pharmacol.* **119** 340P.
- Tesfamariam B & Halpern W (1988). Asymmetry of responses to norepinephrine in perfused resistance arteries. *Eur J Pharmacol*, **152**, 167-170.
- Werns SW & Lucchesi R (1990). Free radicals and ischemic tissue injury. *TIPS*, **11**, 161-166
- Ytrehus K, Myklebust R & Mjos R (1986). Influence of oxygen radicals generated by xanthine oxidase in the isolated perfused rat heart. *Cardiovasc Res*, **20**, 597-603.

Chapter 2

Confocal Microscopy and Image Analysis

Introduction

In the previous chapter a method for studying cellular distribution and activation was developed. It was found that nuclear fluorescent stains could be used to assess cell viability and identify cell type, number and orientation by nuclear morphology alone (Daly et al., 1992). Using conventional wide field fluorescence microscopy it was possible to image nuclei of cells at varying depths within the blood vessel wall. In some cases, depending on wall thickness, it was even possible to determine endothelial cell nuclei morphology and number. Unfortunately, computer analysis of digitised images of nuclei was severely hampered by out-of-focus glare from nuclei above and below the plane of focus. In particular, it was almost impossible to obtain images of cell cytoplasm at sufficiently high resolution to determine cell size. Following on from this it can be postulated that measures of cell volume would not be practicable using conventional epi-fluorescence.

Nevertheless, the data from the previous chapter provided an insight into the kind of methodology that would have to be adopted and the kind of problems that would have to be addressed in order to achieve the goal of studying the activation of individual cells within the wall of a living resistance artery. The first major problem to overcome concerned the loss of resolution (contrast) in images deep within a relatively thick biological specimen. The second major problem was that of quantification. During a visit to our laboratory by Dr. John Russ (author of the internationally renowned Handbook of Image Processing) he correctly pointed out that '...an image may well be worth a thousand words but a *number* is worth a thousand

pictures'. I was soon to discover how true this is when presenting image data to the physiological and pharmacological community.

A colleague, Dr. John Gordon, suggested that Laser Scanning Confocal Microscopy (CLSM) may offer some solutions to the problems outlined above. CLSM provides thin 'optical sections' of thick biological specimens that are relatively free from out-of-focus glare emanating from structures above and below the plane of focus. The laser illumination source can be tuned to excite specific fluorescent markers and the resulting images are digitised and stored (as numbers) in the memory of a computer. It therefore would seem to be an ideal tool for the study of vascular structure and function, assuming that suitable non-toxic dyes can be found and also that methods of quantification can be adapted or developed.

In the summer of 1990 I travelled through to Edinburgh to examine some slide mounted nuclear stained vessels on a Leica CLSM system. The results were (at that time) astonishing and proved without doubt that confocal microscopy could be used to obtain 'quality' images (optical slices) of nuclei from the adventitia through to the endothelium. I realised that if this technique could be combined with wire or even perfusion myography it would create the potential to study many features of vascular mechanics that previously had not been studied due to technical limitations. Fortunately, the Edinburgh data was collected in time to be presented at the forthcoming Physiological Society meeting being held in The Institute of Physiology, University of Glasgow (1990). At the meeting I demonstrated the method of Fluorescence Myography (Chapter 1) and introduced the idea of using Confocal Microscopy (Daly et al., 1990).

From 1990 to 1992 I studied the use of nuclear dyes and evaluated methods of tracking the movement of nuclei using freely available Macintosh imaging software (e.g. Vision, NIH Image etc.). Following the publication of the studies with nuclear stains (Daly et al., 1990, 1991a, 1991b & 1992) and based on the preliminary confocal and imaging data, Prof. J.C. McGrath secured funding for a NORAN Odyssey CLSM system. The system was evaluated during August 1992 and was installed soon after. There followed a period of intense research into the possibilities for the use of confocal microscopy in studying vascular structure.

The following sections describe the results obtained using various fluorescent stains, the study of normotensive and hypertensive resistance arteries, 2D methods of quantification, 3D modelling and the problems associated with developing a fully automated algorithm for the quantification of segmented objects within digital volumes.

Principles of Confocal Microscopy.

The patent which describes the illumination path of the confocal system was registered by Marvin Minsky in 1957. In his patent he describes both transmitted and epi-illumination pathways. The essential components of the system are the pinholes (or slits) through which the excitation and emission light sources must pass. In the transmitted light path the excitation light source passes through a pinhole and is focussed by a condenser onto a specimen. The transmitted light is then focussed by an objective and passes through a second pinhole which is positioned at an equal distance from the point of focus in the specimen. The two equidistant pinholes are said to be

'confocal' to one another. The more common epi-illumination light path is shown in Figure 2.1. The resulting image is a sharply focussed point of light which is relatively free from out-of-focus glare. Therefore the sample (stage) must be moved in order to build up a picture of the complete focal plane. More modern systems move (scan) the beam rather than the stage. The beam scan is typically performed using a galvanometer or, in the case of the NORAN Odyssey, an acousto optical deflector (AOD). The patented Noran AOD provides a scan speed of 25 frames per second (video rate Odyssey) and 250 fps in the new Oz systems.

The advantages of using confocal over conventional fluorescence are as follows;

- i) Reduced blurring of images
- ii) Increased effective resolution
- iii) Improved signal to noise ratio
- iv) Axial (z-axis) scans are possible
- v) Serial axial scans can be combined
- vi) Digital images are produced
- vii) Living (i.e. unfixed) tissue can be studied
- viii) Numerous fluorescent stains are available

Points vi-viii are now generally applicable to many epi-fluorescence (imaging) systems.

Although the confocal principle was first published in 1957 it was not until the mid 1980's that commercial instruments (using lasers) became widely available. The biological applications of such techniques were quickly realised (Carlsson et al. 1985; Amos et al., 1987 & White et al., 1987).

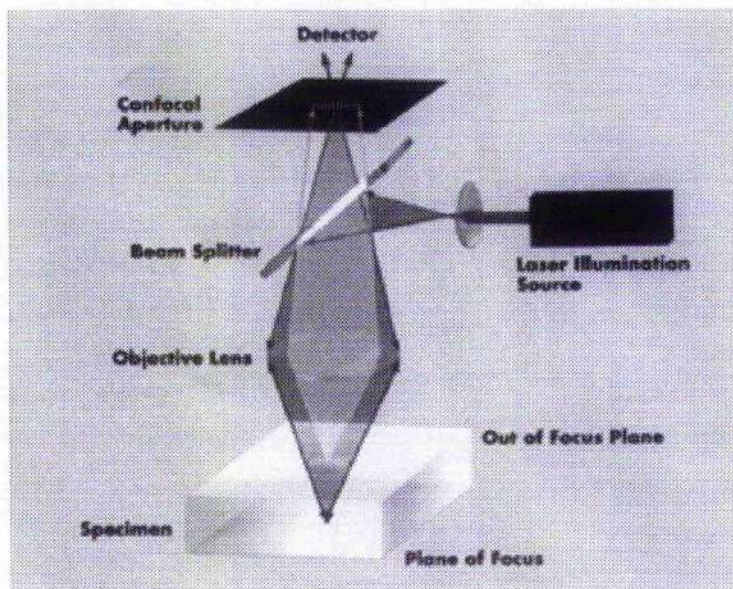


Figure 2.1. Schematic diagram of the confocal light path. The yellow coloured block represents the biological specimen. The light from the laser illumination source is reflected off the beam splitter and down to the tissue. Reflected light of a longer wavelength passes back along the same light path and passes through the dichroic mirror (beam splitter) and then through the pinhole to reach the detector (PMT). Light from above the point of focus (green light path) is focussed behind the pinhole and is therefore rejected. Light below the plane of focus (not shown) would focus in front of the pinhole. Diagram reproduced from the NORAN Odyssey sales material (1991).

practical uses of CLSM.

Confocal systems can use reflective surfaces to form an image. This property has been exploited in the imaging of silicon chips and in other metallurgic applications. However, apart from the autofluorescent properties of elastin and other biological molecules, it is generally necessary to use a fluorescent stain to 'label' a structure of interest. Fortunately, there are stains and antibodies for practically every cellular component from the nucleus to the plasma membrane bound proteins. The major drawback of using fluorescent stains is the phenomenon known as photobleaching.

Definition: An excited fluorophore is raised to a singlet state and decays back to ground state in a variety of ways. The most common way is emission of a photon which generates a fluorescent signal. Powerful, excitation can raise the fluorophore to a triplet state which can react with molecular oxygen to generate a non-fluorescent molecule. Thus fluorescence is lost and addition of free radical scavengers (anti-fade agents) can reduce the rate of photobleaching.

Effect: Significant photobleaching will cause a fluorescent sample to fade rapidly.

Photobleaching is a significant problem for both wide field and confocal microscopy. If we consider that a thick sample like a blood vessel wall is to be scanned 60 to 80 times during the collection of a 3D volume of data, it might be expected that photobleaching could be a significant problem to be overcome. Therefore, it is important to balance illumination intensity (laser power) with photomultiplier gain and photon averaging in order to minimise bleaching and still maintain adequate signal/noise ratio. Unfortunately, each stain on each sample will require different parameters. It is not simply a matter of preparing the slide and turning on the scanner.

Emission attenuation with depth.

In an ideal situation where dye loading is even throughout the sample and photobleaching is minimal, focal planes deep within the specimen will be dimmer due to light diffraction and absorption. While there are routines for correcting this it remains a significant disadvantage of studying thick specimens.

Optical aberrations in CLSM.

Confocal laser scanning microscopy has been shown to be a powerful technique for the 3 dimensional imaging of relatively thick living biological specimens (Brackenhoff et al., 1989). These authors calculated that lateral resolution is more affected by pinhole diameter than is axial resolution. This feature of the confocal system is important when faint staining is required to be imaged and excessive bleaching requires that the pinhole aperture be opened. This feature of a CLSM system is exploited in Chapter 3 of this volume.

Given that relatively thick specimens will be studied on a CLSM system, one should consider the nature of any optical aberrations that may exist when light may be passing through air (objective), oil (immersion media), glass (cover slip) and tissue components.

In a study of thick (up to 300um) uniform samples (a volume of water), Carlsson (1991) noted that axial/lateral resolution ratio is reduced by a factor of 3 as scanning depth increases from zero to 300um. Carlsson suggests that for thick specimens it may be necessary to increase the sampling distance in the axial plane. These

measurements were made using reflected light. In confocal fluorescence microscopy the axial resolution could deteriorate by a factor of eight where refractive indices (RI) are mismatched. Therefore, specimen RI can seriously affect the resolution of thick tissues. Even high NA objectives are subject to the same limitations and it is suggested by Carlsson that dependent upon the actual sample it may be advisable to use a low NA objective.

Chen et al., (1991) developed a correction factor for the refraction of light passing through a blood vessel wall which they quote has an RI of 1.523. However, this value (taken from Gahm & Witte, 1986) appears to be derived from a sample of rat mesentery comprising mainly "hyaluronic acid, elastin, collagen fibrils and connective tissue cells". Gahm & Witte make no mention of blood vessels in their paper. It is not clear therefore how accurate this value is with respect to the vascular wall. It has been reported by others that embryonic cytoplasm has an RI of 1.5.

Chen et al., go on to suggest that internal diameter measurement of vessels mounted in a Halpern style myograph (Halpern et al., 1984) should be corrected since the water solution has an RI of 1.33 compared with the blood vessel wall RI of 1.523.

Further studies cast doubt on the published data of measured volumes imaged by confocal microscopy. Visser et al., (1992) point to the inaccuracy of depth measurements made of watery samples using high NA oil immersion objectives. These authors examined the lateral aberrations caused by RI mismatch using fluorescent beads and a Biorad CLSM. The data show that RI of sample and

mounting/immersion media must be matched in order to maintain lateral/axial resolution ratio at 1.

Further aberrations in CLSM systems caused by RI mismatch were considered by Hell et al., (1993). These authors state that "provided that immersion liquids of correct Refractive Index are used, aberrations can be neglected". Hell et al., provide descriptions and quantification of the point spread functions at different depths within a watery sample using an oil immersion objective. The full width half maximum (FWHM; measure of axial resolution) is reduced from 0.53 μ m (plane zero) to 0.68 μ m (5 μ m in) to 0.9 μ m (10 μ m in) to 1.23 μ m (20 μ m in). This and other data provided by Hell et al., explained the physical properties which are responsible for the main aberrations caused by RI mismatch in CLSM systems namely: 1) loss of resolution as axial focal position increases; 2) signal attenuation as axial position increases; 3) elongation of the sample as axial position increases.

Increasing detector pinhole increases the affect of aberrations. High NA oil immersion objective measurements of biological specimens are more susceptible to aberration than are low NA (less than 1) objectives. Overall the published literature would suggest that if myograph blood vessels are to be studied the best conditions would be to use a water immersion objective. The choice of NA would appear to be of less importance given the relatively thick nature of the sample and the expected axial resolution.

In the present study three objectives were used: for slide mounted samples an X60 oil immersion (NA 1.1); for myograph mounted vessels an X40 water immersion objective (NA 0.75) and X40 water immersion objective (NA 1.13, UV corrected.)

Bleaching and Fluorescence attenuation.

Bleaching and attenuation with depth is a common problem in both conventional and confocal fluorescence microscopy. Since confocal microscopy encourages the use of thick specimens it is important to consider the implications such physical effects will have on any attempts to quantify amounts of fluorescence in a 3D volume of confocal derived data.

Using thick (50um) slices of nuclear stained rat liver Rigaut & Vassy (1991) quantified the amount of photobleaching and attenuation caused by confocal scanning. The method of staining used by these authors allowed penetration of dye from both sides of the tissue block thus ensuring equal staining. Using axial step sizes of 1um they concluded that at depths up to 50ums there was no attenuation of excitation through the sample. However, attenuation of emission was observed. With regards to photobleaching Rigaut & Vassey observed uniform bleaching that was independent of depth.

For the present study of isolated perfused blood vessels it seemed appropriate to use a luminal and extra-luminal staining protocol to ensure equilibrium. Furthermore, since the vascular wall thickness of (200 - 300um i.d.) resistance arteries would be expected to be in the region of 50 - 70 um axial step sizes of 1um appear to be acceptable.

Collection of Serial Optical Sections.

As stated above CLSM provides a means of capturing optical sections of a living specimen. In order to construct a 3D volume it is necessary to optically section the sample at fixed distances along the optical axis of the imaging system. This raises the question of what is the correct sampling distance (Z). Unfortunately, there is not one answer to this as the optimal value of Z will be determined by tissue/imaging conditions and by investigator requirements. There is though one school of thought which states that Z -sampling distance should equal twice the spatial resolution. This is known as the Nyquist theorem and in practical terms demands that Z -sampling should be no greater than $0.3\mu\text{m}$. The rule applies particularly where quantification of 3D volumes is to be relied on. In many cases it will simply be spatial information that is required (i.e. how many cells of a particular shape are present at a specific depth). It appears to be left to the individual to justify their chosen parameters.

In their review of digital 3D imaging Chen et al., (1995) described the variety of protocols used in their studies. For studies of living embryos they prefer to use Z steps of 0.5 to $1\mu\text{m}$ in combination with X60 (1.4) or X40 (1.3) objectives respectively.

When photobleaching is problematic, or even where intensity is to be measured within a volume, it is advisable to take a reverse stack of images. This requires that the focal plane be set at the maximum depth within the specimen and the focus direction is moved step-wise towards the surface. This will minimise the deleterious effect of light in the converging and diverging cones of the excitation beam.

Digital Images and 3-dimensional volumes.

The Human eye and brain together form an unparalleled imaging system which is able to recognise millions of colours, shapes and forms almost instantaneously. Computers and cameras (or photomultipliers) by comparison are really very poor and while cameras may be capable of capturing images at high resolution, once digitised the image will be typically reduced to 256 colours or grey levels for the purpose of image processing. All of the images contained within this thesis are 8 bit and fall into this category. High end systems now work with 24 bit images and in time this will improve further. For the purpose of this thesis though we will consider only 8 bit images.

An 8 bit digital image comprises a 2D array (in this case 512 x 512) of picture elements (pixels). These are small squares that have an intensity value of between 0 (black) and 255 (white). Values between 0 and 255 are usually assigned shades of grey or colours (pseudocolour). The mapping of a colour to a particular intensity is done by a look up table (LUT or palette). Different palettes can be assigned to an image and these can be user defined. Palette editing can be useful in assigning a particular colour to a range of intensities which may define a specific feature.

The digital (numeric) nature of the captured image is such that numeric algorithms can be applied to alter selected values in order to remove or enhance certain features. This would be commonly known as *image processing*. Once images have been processed measurements can be made in order to quantify the data (*image analysis*). These are general definitions that will be adopted for the discussion and description of work in this thesis. A comprehensive review of current methods and theories of digital

imaging is far beyond the scope of this thesis and the reader is referred to the several good texts that are available (e.g. 'Handbook of Image Processing' by Dr. John Russ).

The experiments in this chapter detail the search for appropriate fluorescent probes that can be used for the study of vascular structure using confocal microscopy and small vessel myography. In addition, the transferral of the techniques developed in Chapter 1 to CLSM, the analysis of diseased vessels and the first steps towards a semi-automated analysis method are detailed.

Methods.

Tissue harvest.

Male wistar, WKY and SPSHR rats were obtained from either Biological Services (Internally bred colonies of wistar) or from Dr. A. Dominiczak (WKY & SPSHR) at the Department of Medicine and Therapeutics, University of Glasgow. The SPSHR are a genetically modified strain of (stroke prone) spontaneously hypertensive rat. The WKY rats serve as controls and are sex and age matched in all experiments. The SPSHR & WKY rats have been bred in the department since 1991. Wistar rats were generally killed by stunning followed by exsanguination. WKY & SHR were killed by inhalation of halothane (4%) in oxygen. All rats weighed between 250 and 300g.

Branches off the superior mesenteric artery (3rd order) were excised and cleaned of surrounding fat and connective tissue before being placed in fresh PSS solution (at room temperature). Cerebral vessels were obtained from whole brains (ex vivo) which were dissected in cooled PSS (i.e. on ice). Branches of posterior cerebral artery or the complete basilar artery were removed from the brain and cleaned of connective tissue. Samples of human subcutaneous (limb) resistance arteries were obtained from amputated limbs following critical limb ischaemia. One segment of rat pulmonary artery was also used. Vessels to be kept for later study were refrigerated at 4°C.

Tissue Mounting.

Vessel segments were visualised mounted on a perfusion myograph or on glass slides. Slide Mounting: Standard glass slides and coverslips (No. 1) were used throughout. A well was created on the slide using high vacuum grease. The grease is applied using a

long needle. The streaks of grease resemble a noughts and crosses grid on the slide. The central portion of the grid is filled with PSS into which is placed the vessel segment. A coverslip is then placed over the grid and gently pressed taking care not to compress the tissue. The slide is then ready for viewing. Nuclear stained sample such as these can be kept refrigerated for up to two days with no discernible loss in tissue integrity or staining.

Myograph Mounting: The model used was a Halpern Pressure Myograph system (Living Instruments, Burlington, Vermont). Segments of artery are cannulated between two micro pipettes and tied in position using fine ligatures. Warmed PSS is allowed to flow through the system prior to mounting to remove any air bubbles and to flush out any cleaning solution or water in the system. Once the vessel is mounted the pipette at one end is blocked by closing its associated three-way tap. By use of a servo-pump the pressure can be increased from 0 to 199mmHg. Pressures of between 40 and 60mmHg were chosen for WKY arteries and in some cases 120mmHg for SHR arteries. The choice of 40-60mmHg was based on the observed values for $0.9I_{100}$ obtained in normalisation of wire mounted vessels.

Tissue Staining.

A variety of staining protocols was employed depending on the requirements of the stain and thickness of the preparation. All of the stains used require either, fixed tissue, unfixed tissue and/or staining at 37°C.

Fixed Tissue: Vessel segments are fixed in formalin, in aliquots, and left to equilibrate in nuclear stains overnight in a fridge (4°C). Before visualisation fixed segments are rinsed in fresh PSS to remove any unbound stain.

Living Tissue (room temperature): Vessel segments are incubated in aliquots with either nuclear or extracellular stains. Aliquots are either wrapped in foil or stored in a cupboard to prevent any degradation of the fluorophores by bright laboratory lighting.

Living Tissue (37°C): Many AM ester dyes require to undergo esterase activity within a cell before the fluorescent molecule is activated/released. To enable staining at 37°C two methods were used. For myograph mounted vessels the dye was simply applied to the bathing chamber once the gassing conditions (pH) and temperature were at the desired level. For vessels stained in aliquots it was first necessary to vigorously oxygenate the PSS to stop the precipitation of calcium. Vessel segments were then incubated in sealed, 'full' aliquots of gassed PSS containing the stain. The aliquots were then floated in a water bath (37°C) using plastic aliquot racks. After staining tissues are rinsed with fresh PSS and visualised immediately.

Fluorescent Stains.

All stains were purchased from Molecular Probes inc (Eugene, Oregon or Leiden Netherlands). Table 1 shows the full list of fluorescent compounds tested in this thesis along with their solubility, fluorescent characteristics and sites of action.

Table 2.1. Fluorescent Stains used in this study. Excitation and Emission wavelengths are those used and do not necessarily reflect the maxima reported for each compound. Confocal microscopy is often limited by the available laser lines and long pass filters.

Stain Name	Solubility of stock soln.	Conc.	Site Stained	Ex. (nm)	Em (nm)	Comments
FITC-albumin	water	1mg/ml	extracellular	488	515	effective for elastin, collagen and lamella
5,6 CF	water	1mg/ml	extracellular	488	515	fills extracellular space, excluded from living cells
BCECF AM	DMSO	5uM	cytoplasmic	488	515	pH indicator, stain at 37oC
DHE	DMSO	1uM	DNA	529	610	requires esterase activity, poor shelf life, red stain-'live' cells
PI	water	10ug/ml	DNA	529	610	red stain for fixed/damaged cells. Stable under LSCM
H33342	water	10ug/ml	DNA	364	400	excellent, stable, UV stain
AO	water	10ug/ml	DNA+RNA	488	515	shows DNA in green; RNA in orange
TO	water	10ug/ml	RNA	488	515	toxic in blood vessels
EB	water	10ug/ml	DNA	529	610	good red stain for dead cells
Phalloidin	DMSO		F-actin	488	515	requires fixation and long incubation period
Rhodamine 123	DMSO		mitochondria	529	610	gave poor results in blood vessels good results in cells
QAPB	DMSO	0.4-100nM	α -receptors	488	515	interference from autofluorescence in blood vessels (Ch.3)

FITC: fluorescein isothiocyanate.

5,6 CF: 5(6)-carboxyfluorescein mixed isomers.

BCECF AM: 2',7'-bis-(2-carboxyethyl)-5-(and-6)-carboxyfluorescein, acetoxymethyl ester.

DHE: Dihydroethidium., PI: Propidium Iodide. AO: Acridine Orange. TO: Thiazole Orange. EB: Ethidium Bromide.

H33342: Hoechst 33342 (bisBenzamide).

QAPB: BODIPY FL-prazosin (see chapter 3 for full details)

Confocal Microscopy.

Two NORAN odyssey confocal laser scanning microscope were used in the course of this project. The vessel work was performed on an upright (Nikon Optiphot) configuration and the single cell work of chapter 3 was performed on an inverted configuration (Nikon Diaphot). The NORAN odyssey CLSM is a slit scanning system that runs at video rate (25 frames per second). The raw video rate signal can be captured directly to video tape. Alternatively, the signal can be output to a computer via an analogue (Matrox) frame grabber board. This is the preferred option if frame averaging is required or if there is no need to run at the top speed. The Odyssey uses point illumination and slit detection and as such sits between point scanners and slit scanners in terms of design. The xy scan is performed by a galvanometer (y-scan) and an acousto-optical deflector (AOD; x-scan). The AOD controls the horizontal sweep and the diffraction efficiency, which in simple terms means that the laser intensity can be software controlled. Therefore if the laser power entering the system is set to 50%, the AOD can be tuned to deliver 0 - 100% of that incoming laser intensity. The Odyssey is a two channel fluorescence system which uses a primary and secondary photomultiplier (PMT) for detection

UV CLSM system: The upright microscope is fitted with a mixed gas UV laser (Coherent) and can deliver lines of 364nm, 488nm and 525nm. The laser is water cooled and is remote from the scan module due to its large size. The laser is delivered to the scan module via an optical cable. The scan module offers barrier filters of 400nm, 515nm and 529nm. This system is optically best suited for UV stains and green fluorescent stains. However, the power of this laser enables excitation of red

stains such as PI and EB (see table 1 for spectral information). The system is physically best suited for myograph mounted vessels and fixed cell work.

Argon Ion CLSM system: The inverted system is fitted with a single argon ion laser (OmniChrome) capable of delivering lines of 454nm, 488nm and 529nm. The laser is cooled by a motorised fan and is housed within the scan module. Available barrier filters are 515nm, 550nm and 610nm. This system is optically best suited to dual fluorescence work using green and red stains (i.e. fluorescein and rhodamine type stains). The system is physically best suited to work with single cells mounted on a specialised flow chamber (see chapter 3).

Control software for the CLSM system was used to set the following parameters to ensure that similar or identical parameters can be set when comparing different specimens.

- i) Brightness (PMT offset)
- ii) Contrast (PMT gain)
- iii) Laser intensity (AOD power)
- iv) Pan and Zoom (Illumination area and size)
- v) Excitation wavelength (depending on the stain)
- vi) Emission wavelength (barrier/long pass filter)
- vii) Slit size (the size of the detection aperture)
- viii) Frame averaging (2-256)

The above parameters (together with axial step size and lateral resolution) are the settings that are recorded and stored with each image or stack. These settings are

important for purposes of 3D reconstruction and psf calculations required for deconvolution algorithms.

Calibration of objectives.

Objectives: The main objectives used in this study were; Nikon x60 oil (NA 1.3); Nikon x40 water (NA 1.13); Zeiss x40 water (NA 0.75). These objectives produce final images which are 70, 100 & 102 μm square respectively.

For each objective used it is important to know the calibration in microns. This requires that the pixel per micron scaling is determined at each excitation wavelength and at each optical zoom. In addition, if dual excitation is required it is important that the two excitation beams are aligned and that 'image shift' is minimised. It is also useful to know the psf of the optical system for any combination of excitation wavelength and objective. This can be determined using sub-resolution *point speck-beads*. The final important calibration is the determination of axial resolution of a given objective.

Distance calibrations: A slide which has vertical lines etched 10 μm apart was imaged under a given combination of objective and illumination (no slit for detection was used). The line tool of MetaMorph (see below) was used to draw a line parallel to the y-axis and joining the right hand side of one etched line to the right hand side of the next. The number of pixels was recorded and used to determine pixels per micron. This process was repeated for all objectives at all wavelengths.

Laser alignment: Focal check beads (15 μ m diameter) were obtained from Molecular probes. These beads have a coating of one fluorescent dye and a core of a different dye (i.e. blue (UV) core, green (fluorescein) surface. This enabled the 364, 488 and 525 nm beams of the upright CLSM to be aligned. The 488 and 529nm beams of the inverted CLSM were aligned in the same way.

psf determination: As mentioned in the introduction the point spread function (psf) is an important determinant of the axial resolution and can be calculated if a sub-resolution point of light can be imaged. Point speck beads (0.15 μ m diameter) were purchased from molecular probes and mounted on slides using non-fluorescent mounting media. A point of light was located using a high NA objective ($\times 40$ water NA 1.13) and a confocal volume ($z = 0.1\mu$ m) was collected. The data set was then processed by HuginsII software (Bitplane AG) to measure the psf of the system. This calibration was only performed for the 364nm line of the upright CLSM system since this is the microscope used for thick (i.e. blood vessel) specimens.

Axial resolution: A mirrored slide is used to measure the reflected fluorescent light. As the focal plane moved towards the mirror the intensity at the PMT is plotted. This results in a transient peak which generally displays a tail on its trailing edge. The width of the peak at the point of 50% maximum intensity is referred to as the full width half maximum (FWHM) and is a measure of axial resolution. This calibration was performed by a NORAN engineer at the time of installation.

Image Capture.

MetaMorph (v2.5) image processing software (described below) was used to control the microscope and to acquire images. A special drop down menu contains all of the functions required to control the scan and capture systems. A general running average of 16 frames was used. This enables the live monitor to be used as a reasonable 'real time' display. The actual scan speed 33.33msec per frame (30Hz) but some time must be given for the hardware to perform the frame averaging. Nevertheless, averaging at 16 frames gave a good response time for general use. Depending on the signal quality and bleach rate a frame average of between 16 and 256 was chosen (64 being the norm and producing an image in just over two seconds).

A stack of images was collected by selecting a start plane within the specimen, setting the stepper motor interval (z) and specifying the number of planes required. The motor can be set to travel in a positive or negative direction. After each plane (optical section) is scanned the shutter is closed (to preserve the sample) and the resulting image is stored in the computer memory. This process is repeated for each plane until the required volume has been scanned. The resulting stack of optical sections can then be inspected before being saved or deleted to make way for a new stack with different settings of brightness, contrast, AOD intensity or frame averaging as required.

Image Analysis and 3D processing.

The upright CLSM system was originally used in conjunction with the IMAGE1 image processing package (Universal Imaging Corporation). This software eventually became MetaMorph (MM) and is currently at version 4 which is windows95

compliant. The versions used for this study were v2.5 for Image Capture and v2.76 for off-line analysis of 2D images. For 3D visualisation a combination of Imaris (Bitplane AG, Switzerland) and Microvision (Fairfield Imaging, England) software packages were used.

Extended Focus Models: EF models were constructed using MMs 3D-reconstruction option. The models are built using all of the slices in a volume and using a maximum intensity projection. The models are rotated around a central x-axis in steps of 10° and an animation is created to help perspective viewing of the volume. For myograph mounted vessels where 1 μm steps in z were used a pixel distance of 3 was used (without interpolation) to introduce artificial space into the model.

Rendered Models: More realistic alpha blended or back to front (BTF) rendering was performed on SiliconGraphics workstations using Imaris and Microvision respectively. The rendering algorithms work with the parameters listed in the previous section (confocal microscopy) to interpolate between the collected slices.

Limited image processing was employed prior to the building of EF models. In some cases a low pass or median (3 x 3) smoothing filter may have been used to reduce noise in images with low frame averaging.

Measurements of angles: For the comparison of basilar arteries taken from WKY and SPSHR rats the measure angle tool of MetaMorph was used. Full details are given in (Arribas et al., 1996). Briefly, the direction of flow was established by visualising the direction of the longest axis of the endothelial cells or by detecting the folded internal

lamina of vessels under low pressure. The axis of flow is set and the angle of the longest axis of individual smooth muscle cells is measured relative to the axis of flow.

Results.

Extracellular staining.

Slide mounted, isolated segments of 3rd order rat mesenteric artery (RMA) branches were incubated in 1mg/ml 5,6 carboxyfluorecein for 20 minutes prior to visualisation under excitation of 488nm (em 515nm) using a x60 oil immersion objective (NA 1.3). No washing was performed prior to visualisation. 5,6 CF produced a very bright 'green' fluorescence which under non-confocal (slit = none) conditions did not provide images of extracellular space due to out-of-focus glare. Reducing the slit width to 15µm enabled resolution of cell boundaries within the media of the arteries (Figure 2.2a & 2.2b). The images in figure 2.2 show the high degree of fluorescence in the lumen and around the outside of the vessel. Live cells were shown to exclude 5,6 CF producing a cell profile or negative image of cell cytoplasm.

By combining the 'red' nuclear stain dihydroethidium (DHE, 1µM) with 5,6 CF it was possible to image the cell nuclei and cell profiles independently. The images can then be combined to show the nuclear position in each cell. As expected, not all cells have nuclei due to the optical sectioning and plane of section (Figure 2.2c & 2.2d). Figure 2.2e shows a vessel similar to those of 2.2a-d but under a x2 zoom. Figure 2.2f shows another view of a dual stained vessel observed from the top surface of the vessel, just under the adventitia. The longitudinal profiles can be seen along with the nuclei of a few smooth muscle cells as they wrap around the wall.

Using a water immersion (x40, NA 0.75) objective it was not possible to obtain comparable images of myograph mounted vessels due to the amount of fluorescence in solution. Unfortunately, a short working distance high NA objective (as used for

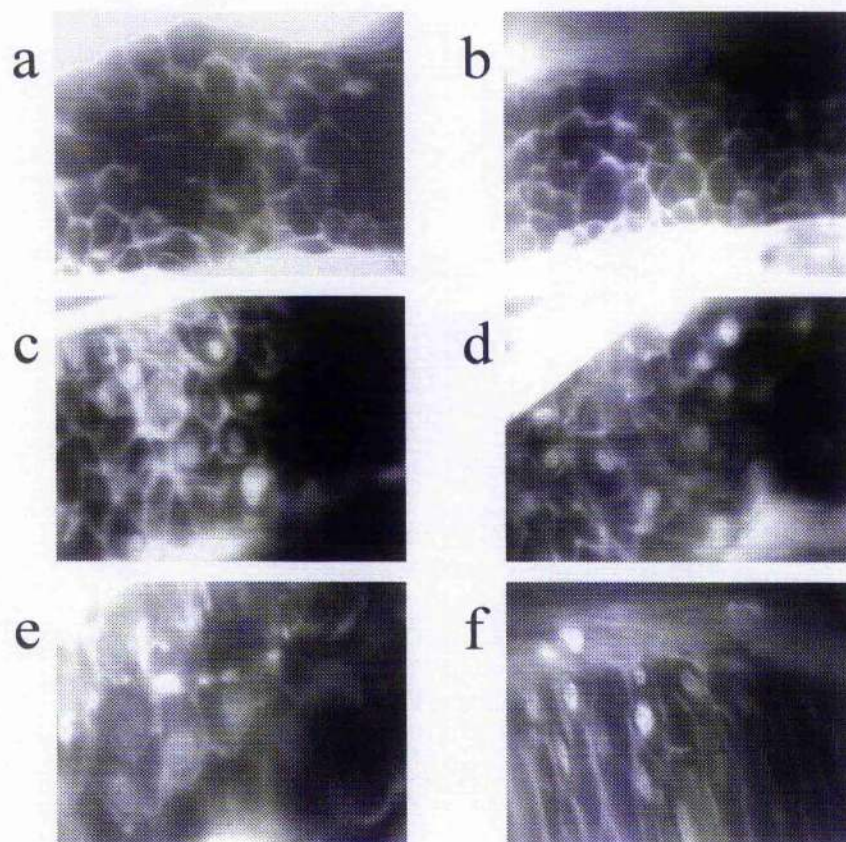


Figure 2.2. Combination staining of 5,6 carboxyfluoresceine and DHE showing cell profiles in the media of isolated segments of rat mesenteric artery (60x oil immersion NA 1.3).

the human studies at the end of this chapter (figure 2.18) was not available at the time these experiments were performed.

Cytoplasmic Staining.

The use of Calcein AM as a cytoplasmic stain for live cells was described in chapter 1. Under confocal excitation this stain was found to be extremely unstable and bleached too quickly to be of any use. Another stain had to be found.

BCECF is a commonly used fluorescent pH indicator and as such has been shown to be non-toxic (see discussion). It was therefore of interest to examine the distribution of this stain throughout the media and to determine its usefulness as a cytoplasmic stain. Segments of RMA were incubated in 5 μ M BCECF in PSS for 15 minutes at 37°C. Vessels were then removed, rinsed and incubated for a second time for 15 minutes at 37°C. This double staining protocol was found to give optimal loading of the dye. Vessel segments were then rinsed in fresh PSS and slide mounted for visualisation using an x60 oil immersion objective (NA 1.3). By balancing laser (AOD) and contrast (PMT sensitivity) it was possible to reduce bleaching rate to enable 64 frame averaging and scanning times of several seconds. The adventitial cells loaded BCECF in apparently equal amounts to the SMCs of the media. Figure 2.3a shows at least 3 different structures in the adventitia which have loaded BCECF. The smooth muscle cells directly below this area of adventitia are shown in figure 2.3b. It was not possible to resolve SMC in deeper layers of the media. Therefore, BCECF may be of use for imaging studies only of outer layers of smooth muscle or of arterioles. Smaller cerebral arteries are particularly well suited for study using this stain (see figure 2.6). An extended focus view of a different vessel segment to that shown in figure 2.3a&b suggests that certain adventitial structures stained by BCECF

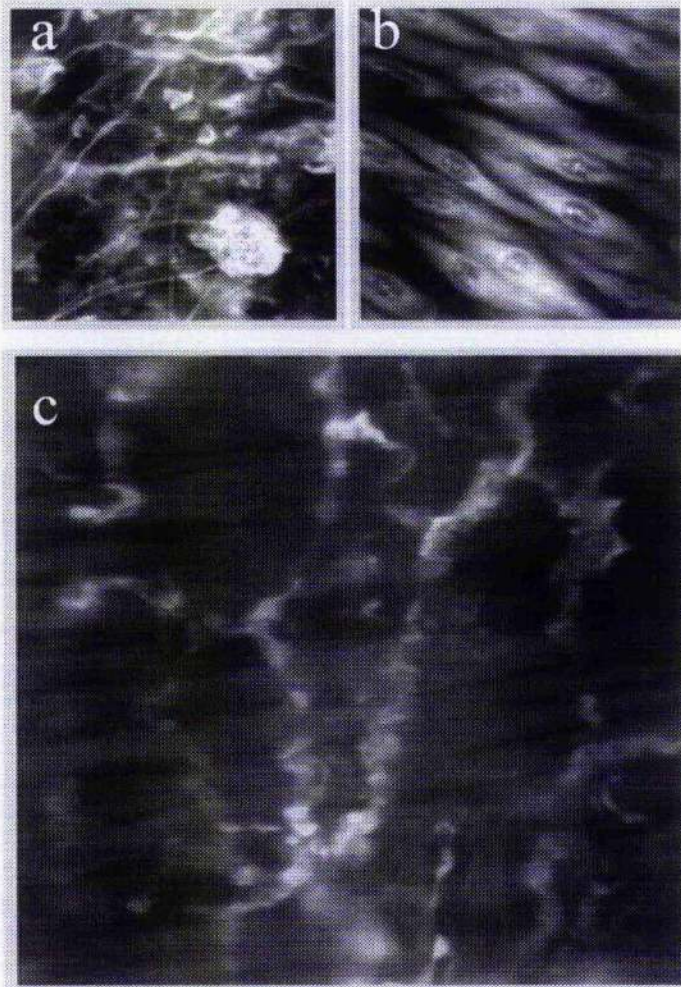


Figure 2.3. Rat mesenteric artery stained with BCECF (5uM). a) adventitia showing several cellular structures. b) smooth muscle within the media immediately below the adventitial region shown in a). c) The overlay shows possible nerves (at the adventitia/media border) and the underlying smooth muscle cells. All images were collected from slide mounted vessels using a x60 oil immersion objective. Ex. & Em. as shown in table 2.1.

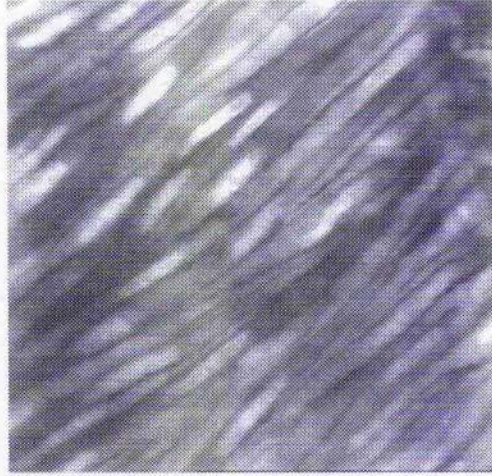
may be nerves (Figure 2.3c). The nerve-like structures shown in figure 2.3c resemble similar structures found in the adventitia following staining with glyoxylic acid, rhodamine 123 and phalloiden (not shown).

By combining BCECF with DHE (as above with 5,6 CF) it was possible to image both cell cytoplasm and nuclei position in isolated segments of slide mounted RMA (Figure 2.4a&b). These studies confirmed that the nucleus is indeed generally confined to the central part of the cell (as suggested in chapter 1). Although this methodology can provide beautiful images of cell cytoplasm and thus shape, it is not possible to resolve the tips (ends) of the cells. Furthermore, the amount of fluorescence (due to the relative lack of extracellular space) makes it difficult to analyse 3D volumes of cytoplasmic staining. Preliminary studies of volumetric analysis were largely unsuccessful but provided valuable information on the limitations of 3D-image analysis (see figure 2.19 & 2.20 and discussion).

Combined extracellular and nuclear staining.

Figure 2.5 shows the results obtained from imaging RMA segments stained with both DHE and FITC-albumen. The combination of these two stains enables visualisation of both stains together when using 529nm excitation (610nm emission). Figure 2.5 shows images from both slide mounted (2.5a) and pressure myograph mounted (2.5b-d) RMA segments. Figure 2.5a provides an excellent example of the confocality of the instrument when using the x60 oil objective. Figure 2.5ai shows adventitial cell nuclei and elastin fibrils. Focusing towards the media shows the adventitial nuclei falling out of focus and new elastin fibres become visible (Figure 2.5aii). Increasing the plane depth brings the external elastic lamina into focus (figure 2.5aiii) and just

a



b

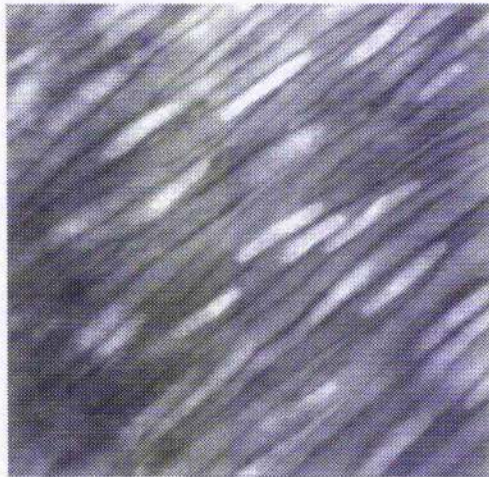


Figure 2.4. Rat mesenteric artery stained with a combination of BCECF and DHE. The plates (a&b) show medial smooth muscle of unfixed (slide mounted) tissue.

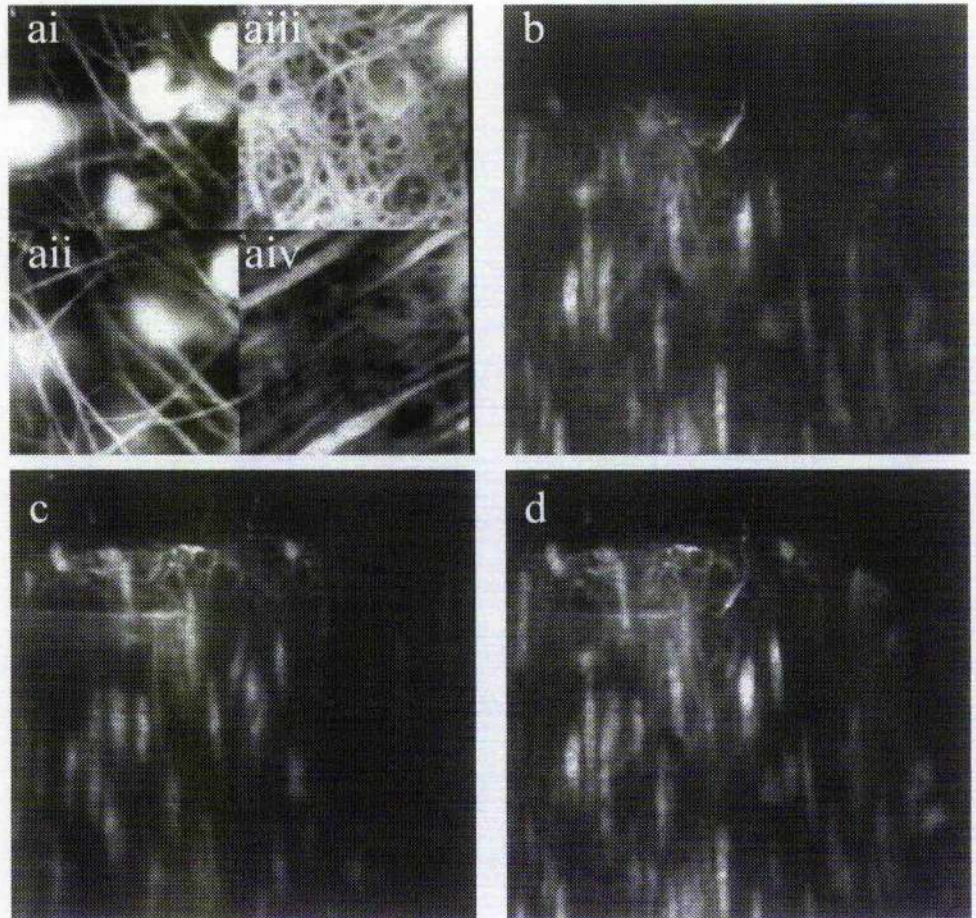


Figure 2.5. Combination of FITC-albumin and DHE. Rat mesenteric artery segment mounted on slide ai-aiv or pressure mounted at 60mmHg b-d. ai) adventitial nuclei and elastin fibers on the outermost surface of the vessel. aii) a deeper adventitial section showing fibres immediately under the cells shown in ai. aiii) the external lamina. aiv) Smooth muscle cell nuclei immediately below the external lamina (x60 oil immersion objective NA 1.3). b) outer layers of smooth muscle cell nuclei and external lamina. c) inner layers of smooth muscle also showing internal elastic lamina. d) extended focus model of all optical slices from b&c (water immersion x40 NA 0.75).

under the external lamina the first layers of smooth muscle cell nuclei can be clearly resolved (Figure 2.5iv).

Figures 2.5b-d show different optical sections of a pressure mounted (60mmHg) RMA segment visualised with an x40 water immersion objective (NA 0.75). The external lamina can be seen in addition to the underlying smooth muscle cell nuclei. The low NA of the x40 water objective provides a thicker optical section (i.e. focal depth). A diagonal (helical) arrangement of smooth muscle cells is suggested from the image. Focusing down to the inner layers (just above the internal lamina) shows a different layer and arrangement of cells (Figure 2.5c). An extended focus view of all of the optical sections in the volume produces the image shown in Figure 2.5d.

BCECF stained, myograph mounted arterial segments.

Vessel segments of RMA and rat posterior cerebral artery (PCA) were stained with BCECF as described above prior to mounting on a pressure myograph. Both segments were pressurised to 40mmHg and imaged under 488nm excitation using the x40 water objective. Optical sections were collected at 1µm steps along the optical axis and extended focus models were constructed from the resulting stack of images. Figure 2.6a and 2.6b show RMA and PCA respectively. The lack of substantial adventitia on the PCA vessel makes it easier to visualise the smooth muscle cell cytoplasm. By rotating the EF models by 30° around a central y-axis, the images shown in figures 2.6c & 2.6d are obtained. Visualisation of the animated model shows how surprisingly thin the wall is when pressurised and suggest that these 200µm i.d. vessels have no more than two layers of smooth muscle when under pressure.

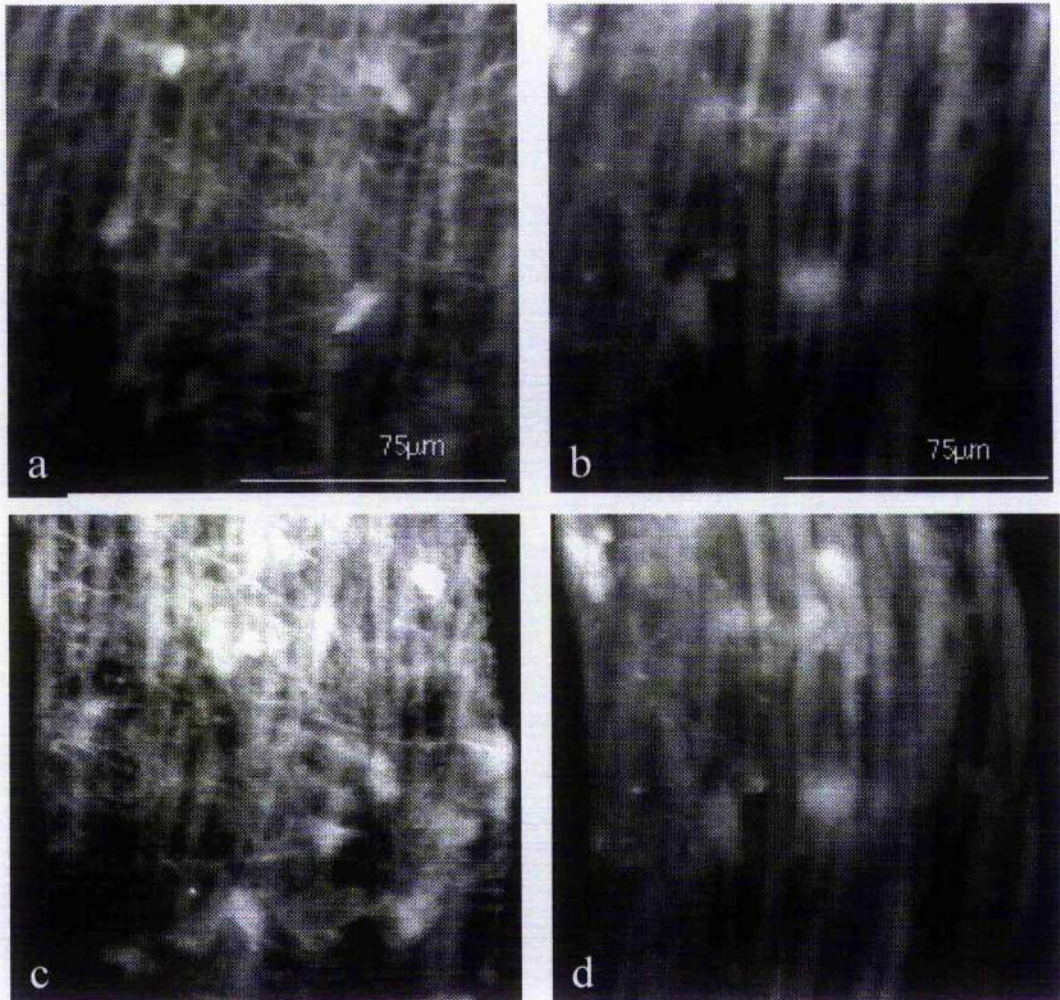


Figure 2.6. BCECF staining of pressure mounted segments of rat mesenteric artery (a&c) and rat basilar artery (b&d). All plates show extended focus models of the complete 'confocal' stack. The model can be rotated for viewing at different angles. The 0° view is shown in a&b. The view at 30° rotation is shown in c&d. Both vessels were held at 60mmHg and viewed with x40 water objective (NA 0.75).

The combination of FITC-albumen and DHE proved to be a very useful combination providing images of nuclei and extracellular matrix under a single wavelength excitation (488nm; the most widely used CLSM laser line). Figure 2.5 shows that this combination of dyes can be used with both high NA (figure 2.5a) and low NA (figure 2.5b-d) objectives. Figure 2.5 also shows images of a pressurised vessel. This is a significant improvement on the techniques developed in chapter 1. The vessel is now under the physical forces that would be experienced in-vivo and therefore the cells have their natural arrangement. This provides a very interesting platform for further study of vascular function. A similar method using BCECF stained vessel produced good images but the general arrangement of cells is difficult to determine when there are no cellular markers other than the homogeneous staining of the cytoplasm. These experiments did however highlight the optical clarity of cerebral vessels compared with the mesentery, due mainly to the virtual lack of adventitia (Figure 2.6).

Nuclear stained, myograph mounted vessels.

DHE (1 μ M) stained vessels were mounted on a pressure myograph and pressurised to 30mmHg. Full z-sections from adventitia through to endothelium were obtained and archived. When the extended focus model of the vessel shown in figure 2.7 was constructed (without adventitial layers), two distinct arrangements of circularly arranged smooth muscle cells were observed. In addition to the expected diagonal arrangement there was an apparent region of cells arranged in a ring. This does not appear to be associated with a branch point since no leak was detected in the vessel. If the servo was constantly re-inflating the vessel due to a leak it would not have been possible to collect the sharp z-series of images since movement artefacts would have

severely blurred the image. It is tempting to speculate that this group of cells may represent a functional unit. Figure 2.7 shows 4 orientations (0,40,60 & 90°) of the EF model. Figure 2.7d gives an indication of the curvature of the vessel under the loading pressure. Increasing the holding pressure to 80mmHg caused the vessel to lengthen, thus changing the lateral position of the 'ring' of nuclei (Figure 2.8a). The nuclear spacings did not appear to be altered dramatically by this increase of 50mmHg. However, the nuclei became 13.7% longer and 11.4% broader as a result of the pressure increase. This suggests that the smooth muscle cells become longer and flatter (as opposed to thinner). As the wall thins and cells compress during pressurisation it is reasonable to assume that the cells will get flatter. However, analysis of full 3-dimensional volumes would be the only way to verify this assumption.

Figure 2.9a-d shows a different segment of rat mesenteric artery stained (DHE 1µM) and pressurised to 40mmHg. The plates show different views of the full EF model (0,40,60 & 90°). The SMCs are all orientated circumferentially and are perpendicular to the axis of flow indicated by the endothelial cell nuclei which are aligned from left to right on the image. The endothelial cells line the grooves in the internal elastic lamina (IEL) which form invaginations at this transmural pressure. This gives the impression that the endothelial cells are arranged in horizontal lines. A roughly helical (zig-zag) arrangement of SMC nuclei can also be seen. The adventitial cells do not appear to be ordered in any particular fashion.

Segments of WKY mesenteric artery show structurally similar features to the Wistar mesenteric arteries. Figure 2.10 a-d shows a segment of WKY RMA stained (DHE

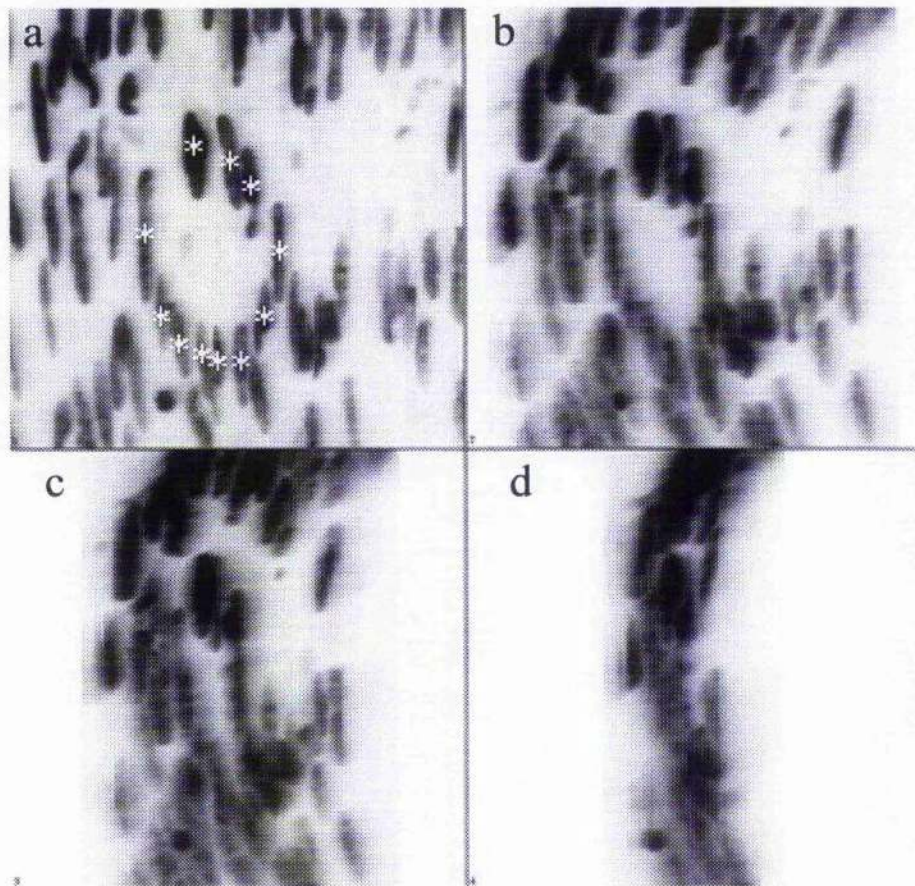


Figure 2.7. A pressure mounted segment of DHE stained rat mesenteric artery showing only the media. The holding pressure was set to 30mmHg. Extended focus views are shown for different rotations. a) 0°, b) 40°, c) 60° & d) 80°. The asterisks in panel (a) shows those nuclei chosen for analysis as detailed in the results section. Images were collected using a x40 water immersion objective (NA 0.75).

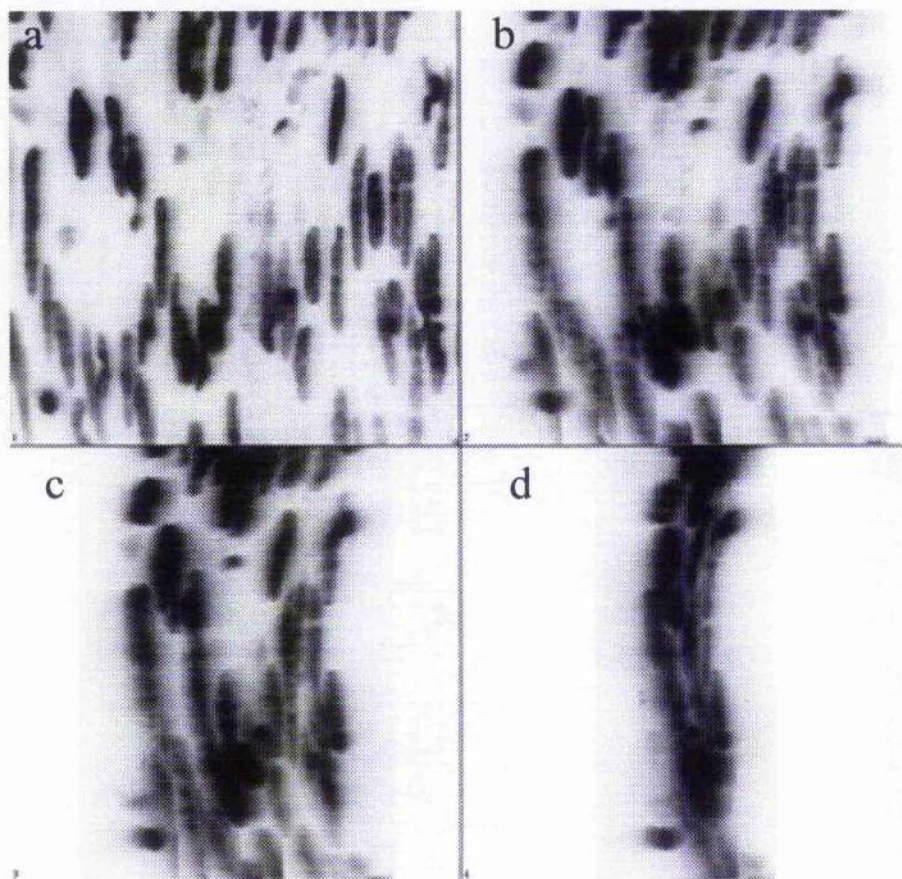


Figure 2.8. A pressure mounted segment of rat mesenteric artery (as shown in figure 2.7). The holding pressure was set to 80mmHg. Extended focus views are shown for different rotations. a) 0°, b) 40°, c) 60° & d) 80°. The same nuclei as those shown in figure 2.7 were selected for analysis.

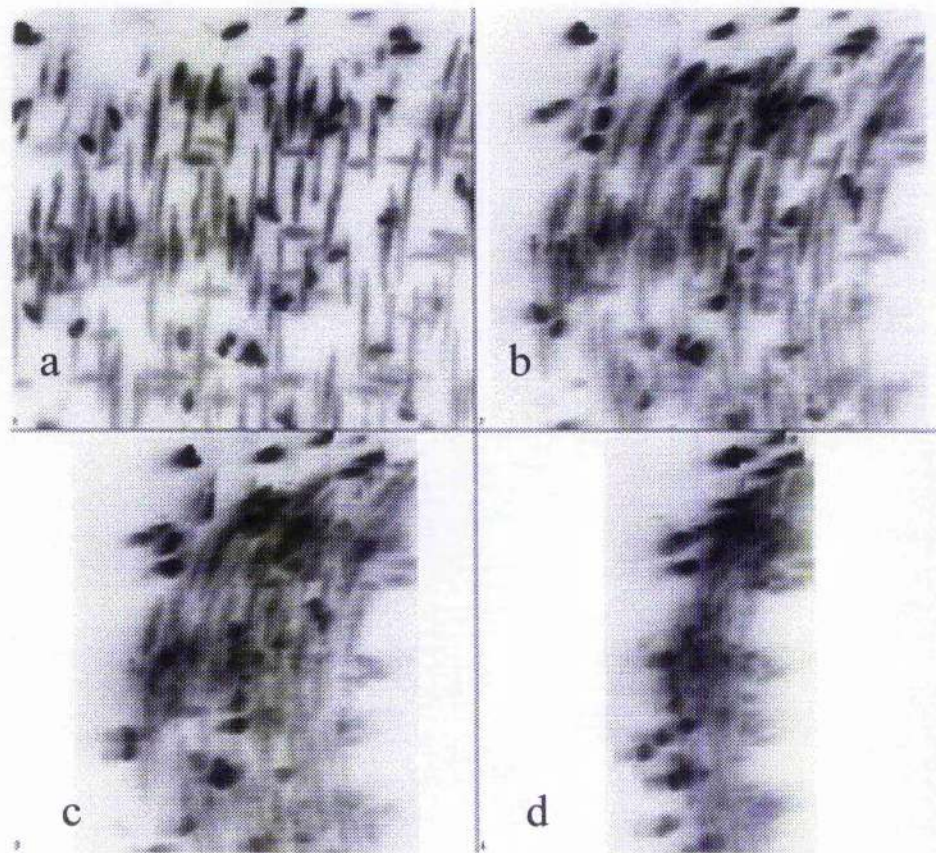


Figure 2.9. A segment of DHE stained rat mesenteric artery pressure mounted at 40mmHg showing the full depth of the vascular wall. Round nuclei represent adventitial cells. Elongated nuclei running from top to bottom represent smooth muscle cells of the media. Elongated nuclei running left to right represent the endothelial cell nuclei. Extended focus views are shown for different rotations. a) 0°, b) 40°, c) 60° & d) 80°. Images were collected using a x40 water immersion objective (NA 0.75).

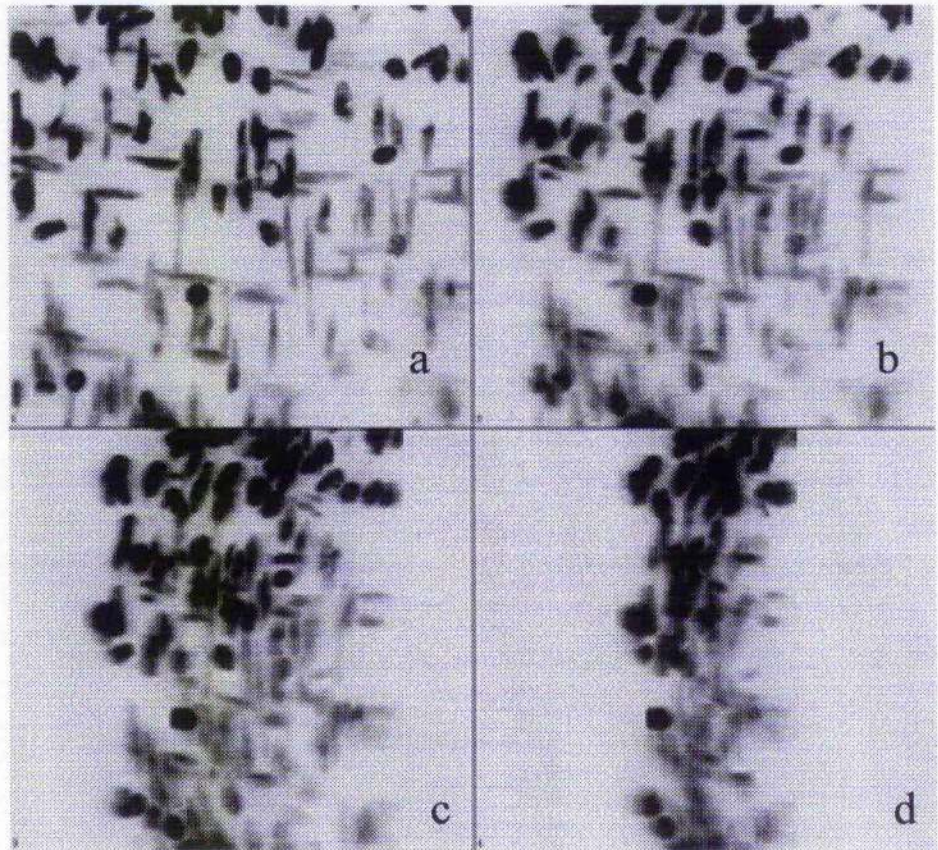


Figure 2.10. A segment of DHE stained WKY rat mesenteric artery pressure mounted at 40mmHg showing the full depth of the vascular wall. Round nuclei represent adventitial cells. Elongated nuclei running from top to bottom represent smooth muscle cells of the media. Elongated nuclei running left to right represent the endothelial cell nuclei. Extended focus views are shown for different rotations. a) 0°, b) 40°, c) 60° & d) 80°. Images were collected using a x40 water immersion objective (NA 0.75).

1 μ M) and pressurised to 40mmHg. The plates show different views of the full EF model (0,40,60 & 90 $^{\circ}$). Like the Wistar RMA the SMCs are arranged perpendicular to the endothelial cells, which again appear to run in lines due to folding of the IEL. Comparing figure 2.10a with 2.9a suggests that the WKY may have a lower density of SMCs per unit area.

Figure 2.11a-d shows a segment of SHR RMA stained (DHE 1 μ M) and pressurised to 60mmHg. The plates show different views of the full EF model (0,40,60 & 90 $^{\circ}$). In this particular vessel there appears to be more deviation of SMCs from the circular axis perpendicular to the endothelial cells (i.e. axis of flow). A striking increase in the density of adventitial cells was observed in this sample. Increasing the transmural pressure to 120mmHg caused no significant change in length (figure 2.12).

Agonist activation of stained pressure-mounted vessels.

A DHE stained vessel was mounted on a perfusion myograph and maintained at 40mmHg (figure 2.13a). An series of optical sections through the media of the vessel was captured before and after the application of 50mM KCl to cause a graded contraction. During contraction all nuclei appeared to move as a unit (figure 2.13b). Analysis of 10 nuclei picked at random from control (figure 2.13a) and contracted (figure 2.13b) showed no difference in shape, length breadth or orientation.

Table 2.2 shows the average morphology of 10 randomly selected nuclei shown in figure 2.13

	Length	Breadth	Shape	Orientation
Control	89.0 +/- 4.9	22.67 +/- 1.16	0.4 +/- 0.02	84.9 +/- 0.8
Contracted	90.8 +/- 4.85	22.67 +/- 1.26	0.42 +/- 0.03	84.85 +/- 0.64

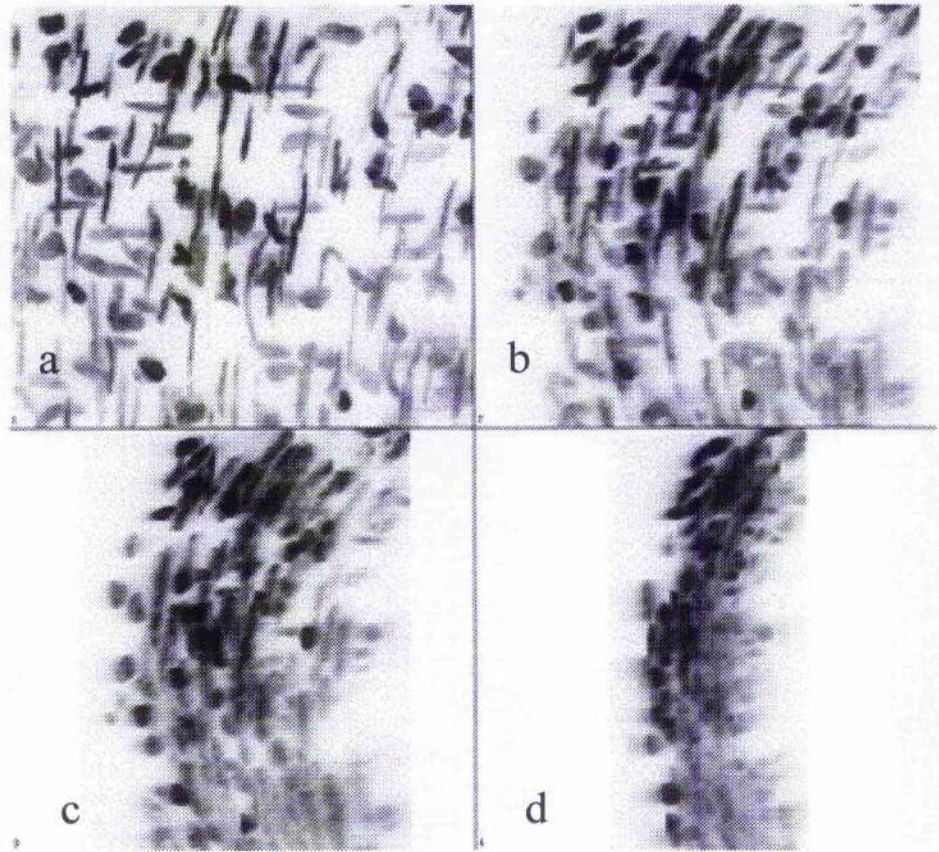


Figure 2.11. A segment of DHE stained SHR rat mesenteric artery pressure mounted at 60mmHg showing the full depth of the vascular wall. Round nuclei represent adventitial cells. Elongated nuclei running from top to bottom represent smooth muscle cells of the media. Elongated nuclei running left to right represent the endothelial cell nuclei. Extended focus views are shown for different rotations. a) 0°, b) 40°, c) 60° & d) 80°. Images were collected using a x40 water immersion objective (NA 0.75).

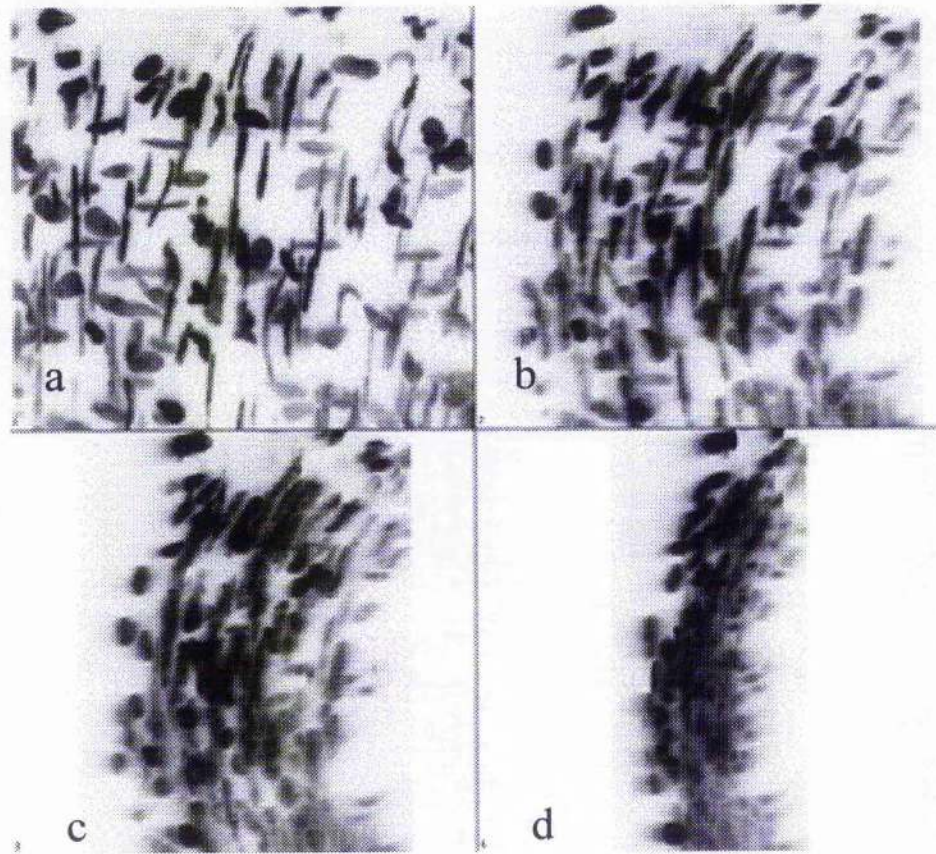


Figure 2.12. The segment of DHE stained SHR rat mesenteric artery (shown in figure 2.11) pressurised to 120mmHg showing the full depth of the vascular wall. Round nuclei represent adventitial cells. Elongated nuclei running from top to bottom represent smooth muscle cells of the media. Elongated nuclei running left to right represent the endothelial cell nuclei. Extended focus views are shown for different rotations. a) 0°, b) 40°, c) 60° & d) 80°. Images were collected using a x40 water immersion objective (NA 0.75).

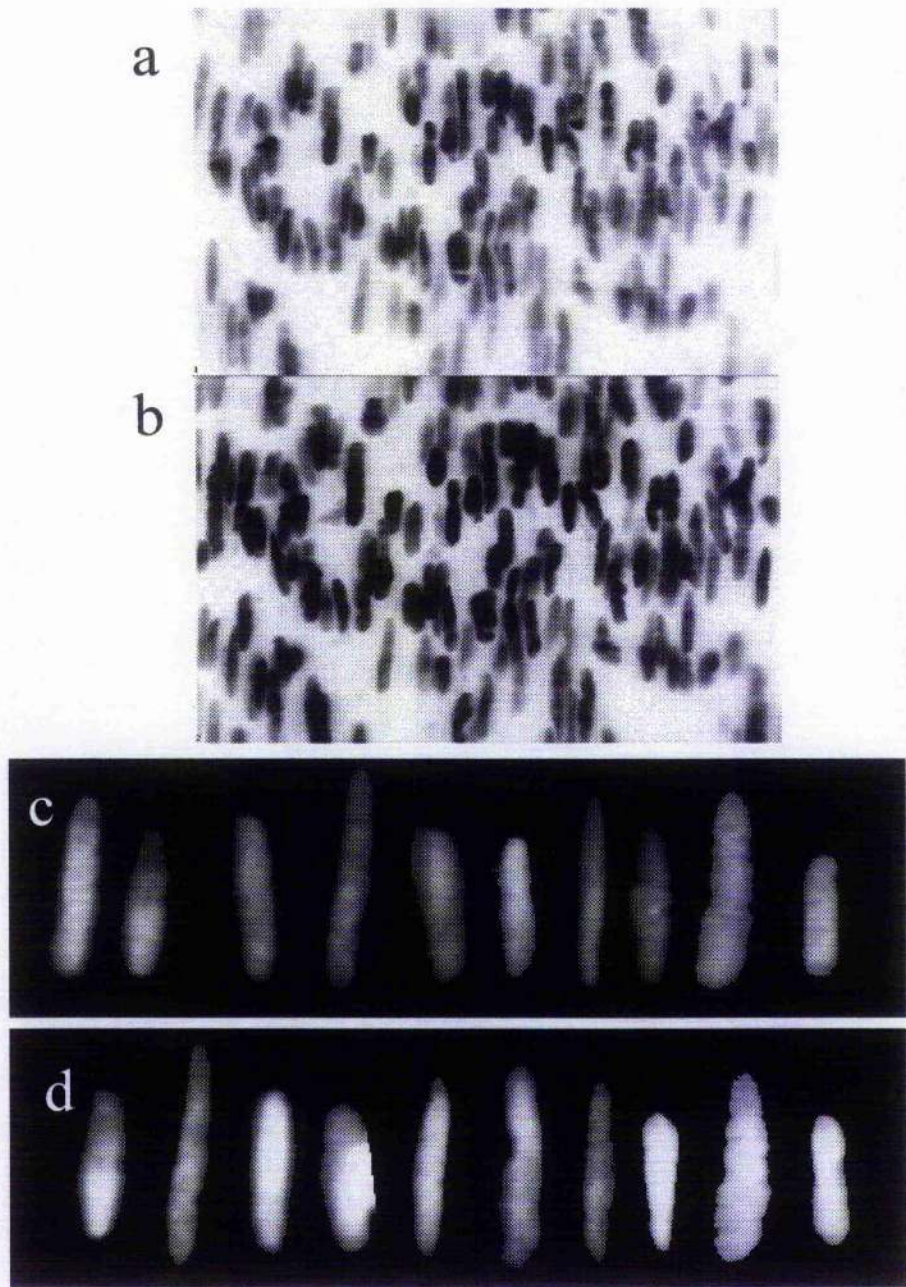


Figure 2.13 . The effect of KCl on the arrangement of vascular smooth muscle cells within the media of a wire myograph mounted segment of rat mesenteric artery. a) Extended focus view of the media prior to contraction. b) Extended focus view of the media during contraction to KCl. c) 10 nuclei selected from view (a). d) 10 nuclei selected from view (b).

Vector models.

The first attempt to visualise data sets in 3D involved reducing all nuclei down to their longest cord (vector) which would describe the position and orientation in 3D space. A freeware software package (3Dvicut) was used for visualisation on the vector fields. Figure 2.14 shows an example of vector maps of the real data sets shown in figure 2.9 (mapped in fig 2.14 a&b) and figure 2.12 (mapped in fig 2.14 c&d). This approach was then applied to the data sets shown in figure 2.13 (KCl contraction data). The resulting vector maps (figure 2.15) aid the visualisation of the effects of contracting a pressurised vessel with KCl.

Structural studies using extracellular and nuclear stains.

The data thus far suggested that interesting observations could be made of smooth muscle cell organisation in pressurised arteries. Therefore a more detailed structural and functional study of basilar arteries isolated from WKY and SPSHR animals was undertaken in collaboration with Dr. Silvia Arribas. The results given in this section are confined to the confocal-derived data since the full study (including functional data) has already been published (Arribas et. al., 1996).

Isolated segments of basilar artery were stained with 5,6 carboxyfluoresceine as described above. Full z-series stacks ($z=1\mu\text{m}$) were obtained for both WKY (Figure 2.16) and SPSHR (Figure 2.17) arteries. The axis of flow was determined by focusing the IEL and drawing a line parallel to the long axis of the endothelial cells. The long axis of the SMCs in three distinct layers (outer, middle and inner) was then identified

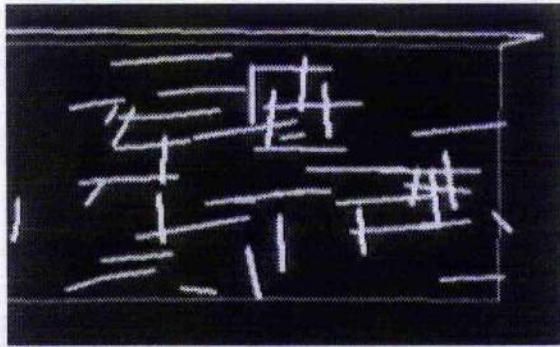
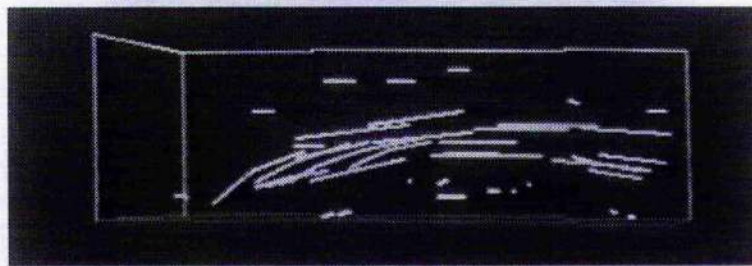
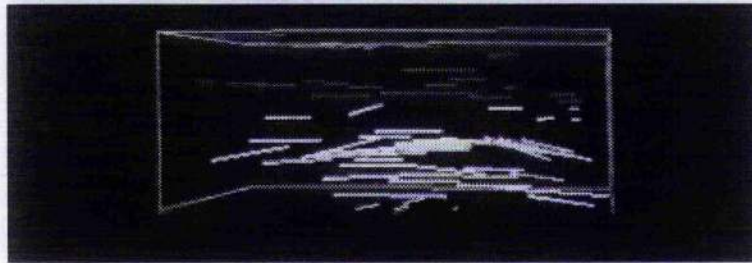
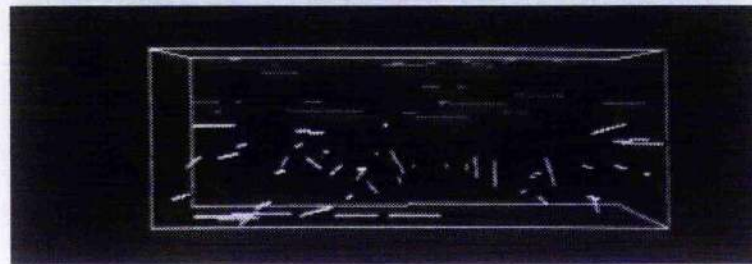
a**b****c****d**

Figure 2.14. The plate shows vector models of a wistar (a&b) and SHR (c&d) segment of RMA pressure mounted and stained with DHE. Rotation of the models permits visualisation of the orientation and arrangement of the smooth muscle cell nuclei. a&b represent data taken from the RMA segment shown in figure 2.9. c&d represent data taken from the SHR RMA segment shown in figure 2.11. Yellow/green vectors represent smooth muscle cell nuclei.

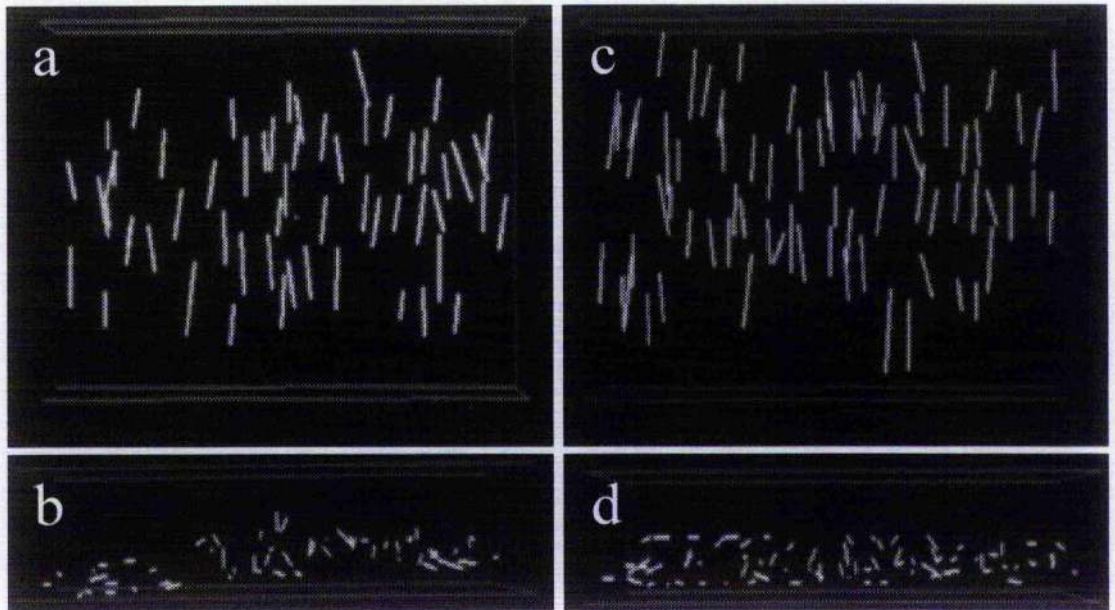


Figure 2.15. Vector diagrams of the data shown in figure 2.13. The left hand panels show views of the smooth muscle cell nuclei at rest in a pressurised RMA. The adventitial and endothelial cells have not been plotted. a) top view (i.e. looking down on the vessel). b) end elevation view. c) & d) show identical views during contraction with KCl.

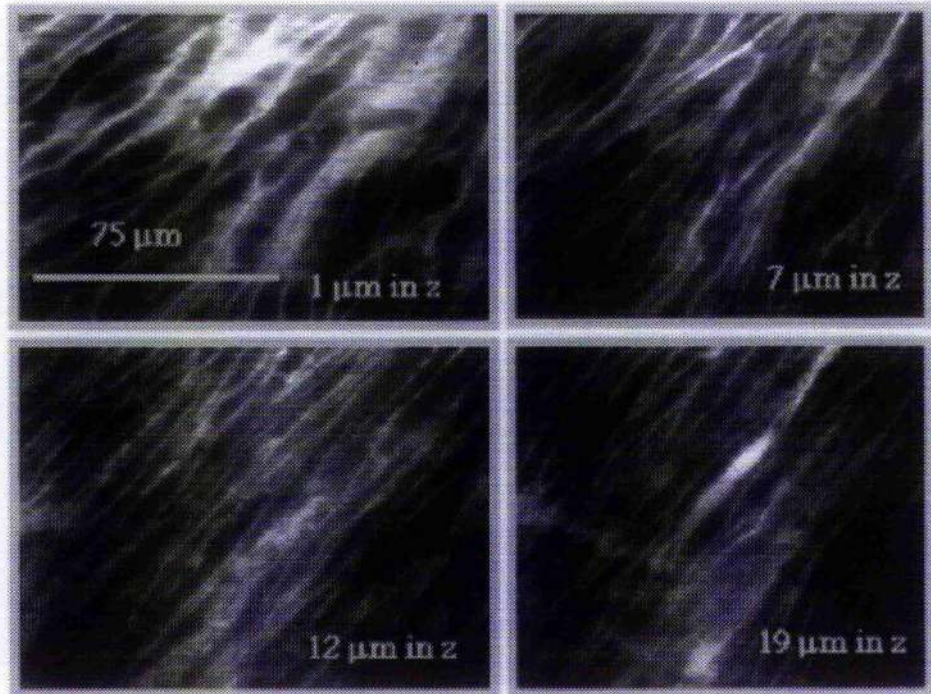


Figure 2.16 . Basilar artery from WKY stained with 5,6-CF. The figure shows selected images from the full stack of optical slices, collected at 1 μm intervals along the axial plane. 5,6 CF is excluded from live cells which appear as 'empty' cells in these images. The extracellular space is clearly visible and the orientation of the cells in each plane can be easily distinguished. Images are of slide mounted vessel segments visualised with a x40 water immersion objective (NA 0.75).

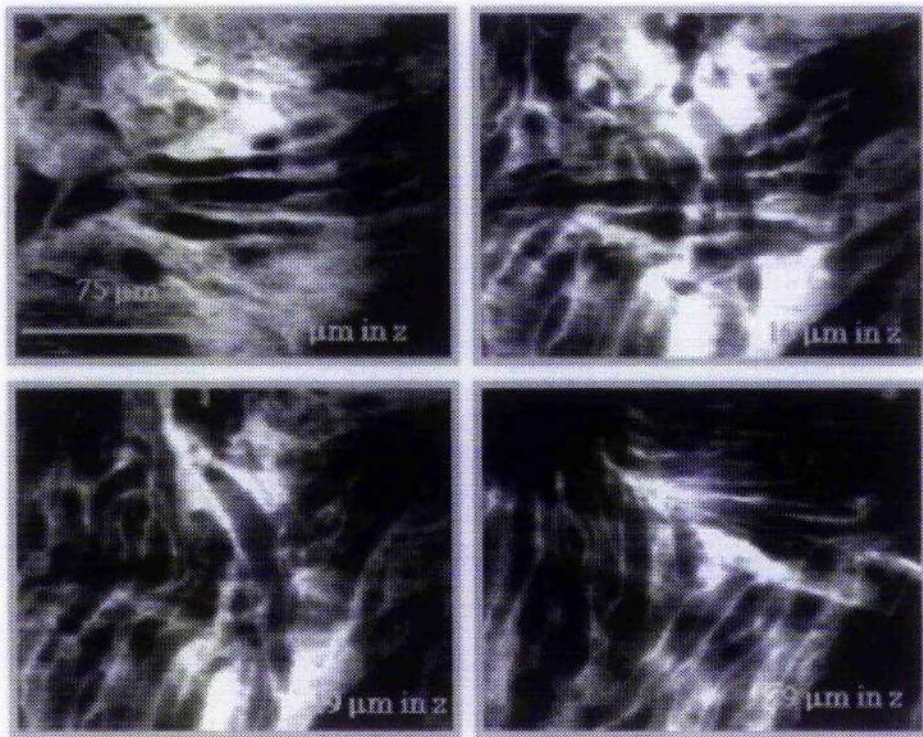


Figure 2.17 . Basilar artery from SHR stained with 5,6-CF. The figure shows selected images from the full stack of optical slices, collected at 1 μm intervals along the axial plane. 5,6 CF is excluded from live cells which appear as 'empty' cells in these images. The extracellular space is clearly visible and the orientation of the cells in each plane can be easily distinguished. Images are of slide mounted vessel segments visualised with a x40 water immersion objective (NA 0.75).

for each cell and this angle was expressed as a deviation from 90° to the axis of flow.

The results are summarised in table 2.3.

Table 2.3 The average deviation from 90° of the long axis of smooth muscle cells in comparable layers of WKY and SHR basilar arteries. Number in parentheses represents number of cells measured from 6-9 different animals. Measurements were made according to the description of angle measurements given in the methods section.

Data taken from: Arribas S, Gordon J, Daly CJ, Davidson A, Dominiczak AF & McGrath JC. (1994). Smooth muscle cell rearrangement and impaired contractions in basilar artery of SHRSP. *Methods & Findings in Experimental & Clinical Pharmacology*, 16, p47

Strain	Layer 1	Layer 2	Layer 3	KCl	5HT
WKY	7.2±0.2 (45)	6.4±0.7 (46)	5.5±0.6 (46)	235 ± 37	256 ± 30
SHR	25.0±2.0 (57) **	9.1 ± 1 (65)	11.6±2.0 (65)*	77 ± 19**	98 ± 25**

A brief study of human cutaneous resistance vessels was conducted as part of a Wellcome Trust funded project grant to study the structure of vessels taken from critical limb ischaemic patients. Vessels were mounted in a pressure myograph as previously described and inflated to 80mmHg. Preliminary observations showed that at 40mmHg tissue compression (or folding) within the wall severely limited the ability to obtain good quality optical sections. Increasing the pressure to 80mmHg provided much clearer images. The reasons for this observation require further study. Figure 2.18 shows examples of both proximal (i.d. 186 µm) and distal (i.d. 174 µm) vessels taken from ischaemic limbs. Overall the distal portion of the artery had fewer smooth muscle cells and a thinner wall. The data is summarised below.

Table 2.4. Analysis of the z-series collected of H33342 stained pressurised (80mmHg) segments of human subcutaneous resistance arteries taken from proximal and distal regions of amputated ischaemic limb.

	Wall thickness	Cell No. (Adv.)	Cell. No. (SMC)	Cell No. (EC)	W:L ratio	Media (% of wall)
Proximal	41µm	14	49	14	22.2%	56.3%
Distal	25µm	8	23	15	14.8	47.1%

It is interesting that hypotension, as a result of the blockage, appears to cause remodelling in the opposite direction to that observed in cases of increased pressure.

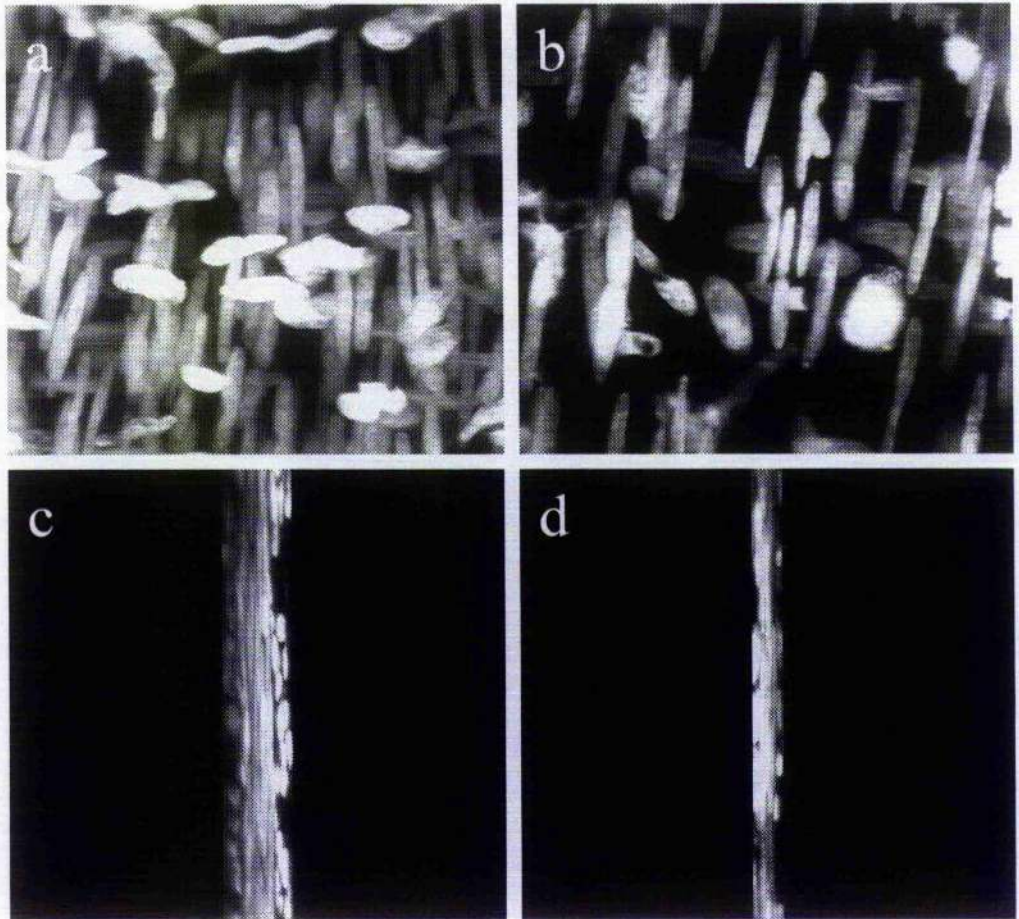


Figure 2.18. Comparison of proximal and distal subcutaneous resistance arteries taken from a human lower limb. Amputation was the result of critical limb ischaemia. a) Extended focus model of a pressurised proximal artery at 80mmHg. b) Extended focus model of a distal segment of artery pressurised at 80mmHg. c) a 90o rotation of the proximal EF model. Wall thickness measured at 41um. d) a 90o rotation of the distal EF model. Wall thickness measured at 25um. Field size 102um square.

In any case the CLSM method is shown to be sensitive enough to detect the differences in cellular composition of the two arterial segments.

Automated Analysis of 3D volumes.

Several methods of 3D rendering were investigated. The extended focus visualisation method is adequate for displaying general cellular arrangement. However, the EF is not a true 3D volume where the slices would be blended together and the space between the slices would be interpolated to produce a solid model of each object (nuclei). The optical aberrations and elongations described in the introduction to this chapter play a major role in determining the success or otherwise of any 3D rendering and subsequent segmentation.

Data volumes (z-series of a rabbit isolated perfused cutaneous resistance artery) were transferred to SiliconGraphics workstations for rendering by Microvision and Imaris. Figure 2.19a shows a maximum intensity (analogous to the EF model) projection produced by Microvision. In this method the dark voxels (which carry no valuable information) prevent efficient visualisation. Figure 2.19b shows a back-to-front (BTF) rendering of the same data with the dark voxels made transparent. This then allows lighting and textures to be mapped to the remaining objects to further enhance visualisation. The circle drawn on the volume denotes an area where the nuclei appear to fuse together (optical aberration). After iterative multi level thresholding (IMTS) the same group of nuclei are still fused (figure 2.19c). This is more apparent when the object analysis routine measures the segmented volume and draws a vector along the longest cord of each individual object (i.e. the software sees the group of fused nuclei as one object (figure 2.19d)).

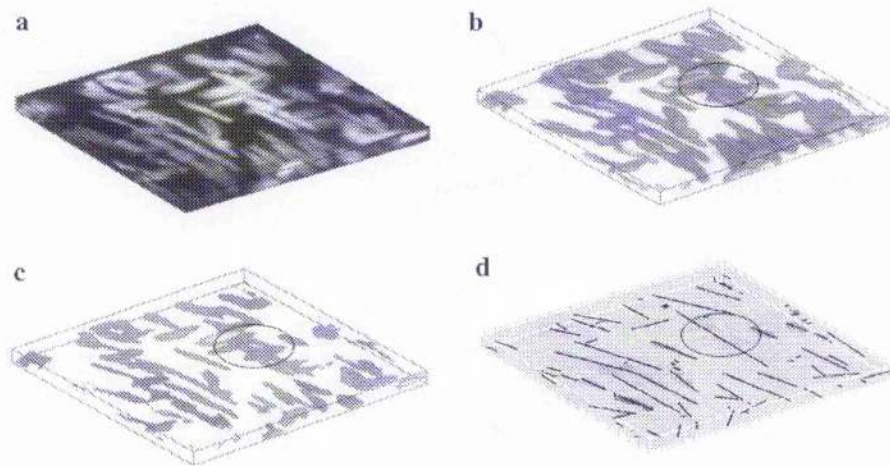


Figure 2.19. 3-dimensional reconstruction of raw and processed data from a segment of myograph mounted (pressurised) rabbit cutaneous resistance artery. The figure shows identical views of the same data set after different rendering and analysis processes. a) extended focus view of the nuclei within the wall of the vessel. Note that some nuclei are brighter than others (*object intensity heterogeneity*). b) The volume has been rendered using a back-to-front (BTF) algorithm which allows for the control of opacity of individual voxels. In this case the background (i.e. darkest) voxels have been made transparent. This method is effective for volume examination and identification of potential problems. One particular group of nuclei were found to be touching (*object fusion*) and have been circled in the figure. c) The data volume was then processed using the IMTS routine (without object classifiers) which segmented the objects. Some individual nuclei were clearly segmented while some others were not. Some degree of object fracturing and fusion was observed. d) The segmented volume was then passed for automated analysis. Only the longest cord of each object is shown. These cords are 3D-vectors which describe the length and orientation of the object. It is clear that the software has failed to identify certain 'individual' objects (circled).

Testing the IMTS segmentation method.

In choosing data sets with which to test the segmenter, I have kept in mind the major problems associated with object extraction from CLSM data volumes. These "real" data sets have been chosen as representative examples.

Confocal set-up

Serial optical sections were collected using either an Argon Ion laser (Ex. 488 nm; Em 610 nm; Data set 1) or a UV Argon ion laser (Ex. 364 nm; Em 400 nm; Data set 2 & 3). Individual volumes consist of serial images each of which represents a 64 frame average to reduce noise and improve image quality. Data set 1 was collected using a x40 water (NA 0.75 long working distance) immersion objective and as such represents a relatively poor quality (in terms of confocality) data set. Data sets 2 & 3 were collected using a x40 water (NA 1.13 short working distance) immersion objective and represent good "confocal" data sets. Deconvolution methods to account for blurring caused by the point spread function were not employed in this study.

Data set 1 (figure 2.20a)

The data volume is made up of 54 confocal serial sections of a segment of pressurised resistance artery, shown in figure 2.12. Sections were acquired at steps of 1 μm in the axial plane and are 512x512 pixels (102 μm) in x-y. The volume contains objects (cell nuclei stained with dihydroethidium) which define the number (i.e. one object/nucleus per cell) and type of cell (i.e. determined by shape, position and orientation). For further details see reference (Daly et al. 1992).

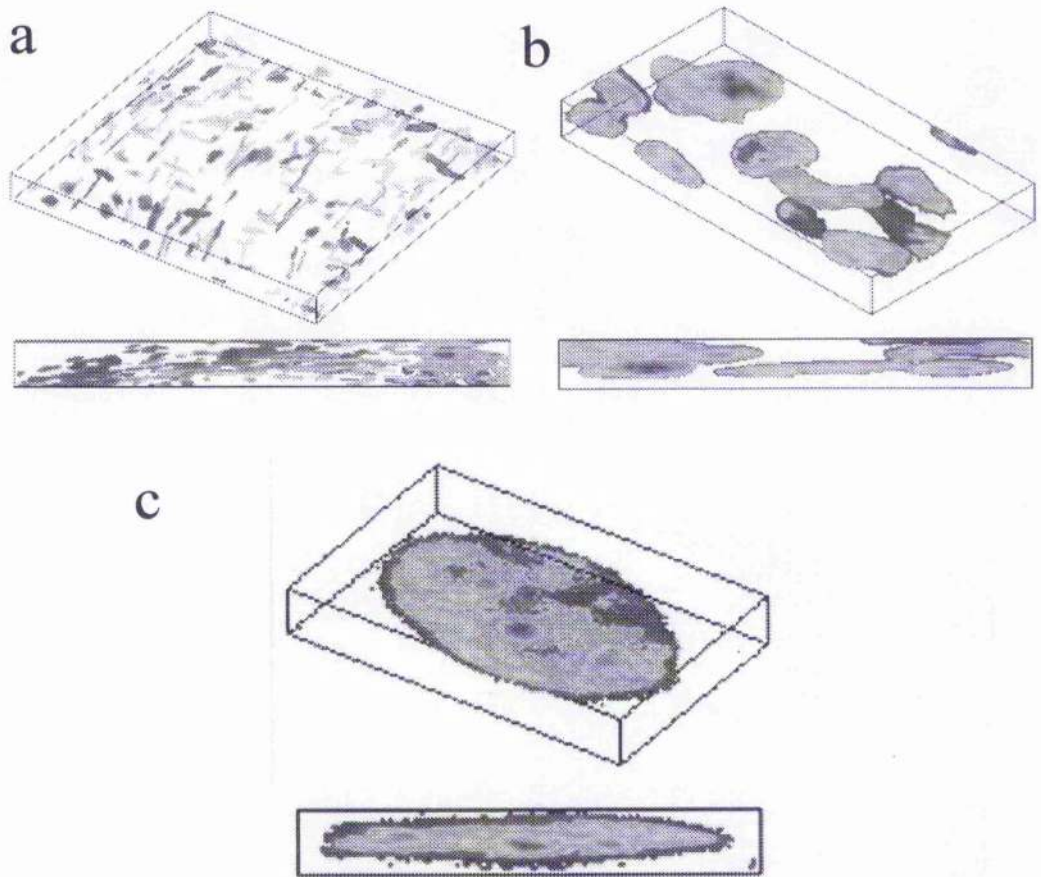


Figure 2.20 The figure shows top and end elevation views of three different confocal data sets. a) Segmented volume of a pressurised resistance artery (figure 11). The volume contains objects (cell nuclei) which define the number (i.e. one object/nucleus per cell) and type of cell (i.e. determined by shape, position and orientation). b) Confocal volume of endothelial cell nuclei on the inner surface or an isolated segment of pulmonary artery. These nuclei are characterised by their heterogeneity of intensities (indicative of DNA concentration). In particular some nuclei have a bright perimeter. c) A single endothelial cell nucleus.

Data set 2 (figure 2.20b)

The data volume consists of confocal serial sections of endothelial cell nuclei on the inner surface or an isolated segment of rat pulmonary artery. Sections are 332x174 pixels and axial spacing is 0.5 μm . These Hoechst 33342 stained nuclei are characterised by their heterogeneity of intensities (indicative of DNA concentration). In particular some nuclei have a bright perimeter.

Data set 3 (figure 2.20c)

A single endothelial cell nucleus. The bright spots are characteristic of some nuclei which may be about to die (apoptosis). The image size is 130x83 pixels (xy) and 18 μm (z).

IMTS Segmentation of Data Set 1

The relatively wide intensity distribution histogram (not shown) indicates that data set 1 is comprised of a wide range of voxel intensities, most of which were black (i.e. background / non-nuclear cellular material). The 3D rendered volume shows the range of intensities of individual nuclei (objects) within the volume. IMTS segmentation parameters (Table 2.5) extracted 188 objects which were identified as nuclei according to the pre-set classifiers (Table 2.5; Figure 2.20 (a)). An end elevation view of the 3D model reveals the curvature of the data set and demonstrates the efficient segmentation and separation of individual objects (Figure 2.20 (a); bottom panel).

Table 2.5.

Analysis of Multi-segmented vascular wall

Parameters

	<i>all nuclei</i>	<i>round nuclei</i>	<i>long nuclei</i>
Classifier vol.	> 10 μm^3 vol.	> 10 μm^3 vol. w / l > 0.49	> 10 μm^3 w / l < 0.49
No. of Objects	188	132	52
volume (μm^3)	47.06 \pm 2.39	48.10 \pm 2.93	43.48 \pm 4.25
length (μm)	8.93 \pm 0.27	7.78 \pm 0.22	11.65 \pm 0.67
width (μm)	4.96 \pm 0.13	5.19 \pm 0.15	4.34 \pm 0.22
width / length (μm)	0.59 \pm 0.01	0.67 \pm 0.01	0.39 \pm 0.01
thick / length (μm)	0.29 \pm 0.01	0.33 \pm 0.01	0.18 \pm 0.01

IMTS Segmentation of Data Set 2

The intensity histogram of data set 2 (not shown) indicated that this data set does not contain a wide range of intensity values and that the majority of voxel values represent the 'background' voxels. The 3D rendered volume reveals several nuclei with bright perimeters which appear to fuse with neighbouring nuclei (figure 2.20b). IMTS segmentation parameters successfully extracted 14 separate objects with 2 joined pairs.

IMTS Segmentation of Data Set 3

The intensity histogram of data set 3 (not shown) indicated that this data set does not contain a large range of intensity. However, a smaller peak representing the bright spots in the nucleus was apparent (figure 2.20c). The 3D-rendered volume shows that the single nucleus does not have a uniform intensity. IMTS segmentation parameters successfully segmented the nuclei into 1 separate object.

Discussion.

The Vascular Wall.

There are many reports describing the orientation of smooth muscle cells in the vascular wall. The general consensus is that the smooth muscle cells of arteries are orientated circumferentially and spiral around the vessel lumen (Garvin 1965; Rhodin (1982; Pease & Paule; 1960; Aalkjaer and Mulvany 1983). Few (if any) studies have focussed on the detailed arrangement of cells in the vascular wall. This is surprising given the intense research into the mechanisms of vascular remodelling which occurs in hypertension (Baumbach & Heistad 1989; Haegerty et al., 1993; Mulvany et al., 1996). The debate over remodelling in the literature tends to centre around the cause of the increased media thickness. However, no attempts have been made to describe the organisation of smooth muscle cells in normal vessels. Perhaps due to a lack of suitable methodology

Confocal (fluorescence) microscopy.

The aim of this part of the study was to investigate the use of confocal microscopy as a method for answering the primary question of the project; do selective agonists activate all cells equally? Secondly, can the reported asymmetry of responsiveness be visualised using CLSM methods. There are many technical advantages and disadvantages to using confocal based approaches (see Introduction) and so it was important to evaluate CLSM as an appropriate method for studying vascular structure (and possibly function).

The initial work with BCECF provided some of the most stunning images on smooth muscle cells in-situ. These particular images have been particularly useful as a

teaching aid for they provide an insight into the architecture of the vessel wall. If only the nuclei are visible the observer may be fooled into thinking that there is a considerable amount of extracellular space. However, the smooth muscle cells are packed very tightly leaving very little extracellular space. Unfortunately, the sheer amount of fluorescence caused by BCECF staining precludes imaging of deep layers of SMCs. However, 2-photon systems which have greater depth resolution may provide a solution here.

Nuclear Staining.

Nuclear stains were considered to be the best option for studying cell number, orientation and (perhaps) activation. The previous chapter had already provided data to suggest that nuclear stains were non-toxic and fairly stable under fluorescence excitation (Daly et al., 1992).

Visualising a full Z-series as an EF model provided spatial information on the distribution (and number) of adventitial, smooth muscle and endothelial cells. The adventitial cells do not appear to conform to any specific pattern. However, without any detailed analysis of spatial self-organisation it is difficult to be certain that there is indeed no pattern. The smooth muscle cells on the other hand have a specific orientation (perpendicular to the axis of flow) and appear to be diagonally offset (helical) with a pitch of between 45-55°. The diagonal arrangement of SMCs in the vascular wall is currently being studied as part of a Wellcome Project Grant recently awarded to Prof. McGrath. The aim of the project is to mathematically model the arrangement of cells in the vascular wall. This project is a direct result of the development work documented in this thesis. One of the interesting findings of this

study was the location of endothelial cells within the invaginating grooves of the internal elastic lamina under conditions of low pressure. Figures 2.9 (wistar RMA) & 2.10 (WKY RMA) show endothelial nuclei appearing to run in lines. However, when the pressure is increased the endothelial cells appear to be more evenly distributed within the lumen. It would be of interest to determine if the altered arrangement of endothelial cells has any differential effects on the overlying (inner layers) of smooth muscle.

Overall, the experiments on nuclear stained pressurised vessels confirmed that this is an excellent method for the study of vascular structure if detailed information on 3D spatial organisation of cells is required. Furthermore nuclei morphology can be conveniently analysed using routine image analysis on a slice by slice basis (i.e. 2D analysis). Morphometric and automated analysis of 3D volumes is discussed later.

Activation of pressurised segments of RMA was assessed using KCl. The contraction caused more nuclei to come into the field of view. However, the contraction was not sufficient to cause a significant change in the nuclear morphology (Table 2.2). These experiments show that it is possible to maintain function of a pressure mounted segment under laser scanning excitation. Furthermore it is possible to construct models of cellular position before and during contraction.

Application of the CLSM method to studies of vascular remodelling.

The techniques developed in the course of this project seemed ideal for investigating the nature of 'remodelling' in hypertensive arterial segments. Since the stroke prone spontaneously hypertensive rat model was available to our group it was decided to

investigate the structure of the isolated basilar artery using confocal microscopy. In normal (WKY) basilar arteries the cells, in all layers, were regularly arranged and deviated by no more than 7.2° from an axis perpendicular to the direction of flow (Figure 2.15). However, in the SPSHR basilar arteries several disorganised regions were found and these deviated by as much as 25° in the outer layers (Figure 2.16). The data is presented in Table 2.3.

It is interesting that the greatest differences were observed near the adventitia since a significant increase in the number of adventitial cells was also observed (Arribas et al., 1996). Adventitial-like cell nuclei were also observed in the medial layers of the basilar artery. In all of the hypertensive arterial segments of rat mesenteric artery examined in this study, a noticeable increase in adventitial cell density was observed. The importance of the adventitia is slowly being realised and it will be interesting to follow the research in this area since a more intimate relationship between adventitial and smooth muscle cells (with respect to remodelling) may be revealed.

Human Resistance Arteries.

The study of human vessels taken from cases of critical limb ischaemia demonstrated the power of the confocal method to quickly identify a structural difference in proximal and distal arterial segments following ischaemia. In general the distal portions of artery contained fewer cells and had a reduced wall thickness (see Table 2.4). This may be the reverse of the phenomenon observed in remodelled 'hypertensive' vessels and may point to a common mechanism of remodelling of arterial vessels. A more detailed study of Human limb arteries and an investigation of

common remodelling mechanisms will be undertaken during the forthcoming EU programme grant (VASCAN 2000).

CLSM methods can therefore reveal aspects of cellular organisation and morphology that are not obtainable by other methods. The foci of disorganised cells in SPSHR basilar arteries had not previously been described, perhaps due to the more aggressive nature of conventional histology where shrinkage artefacts and 'plane of section' can combine to give false impressions of structure (to an inexperienced observer). On the other hand, CLSM methods enable structural studies to be made on living and fixed tissue. The throughput is greater and the ability to build 3D-models adds another dimension to the possible analysis. Combining different stains in living tissues and studying function simultaneously will allow vascular scientists to tackle problems that would not have been possible without the development of confocal methods.

Ideally, it would be possible to pass a complete data volume (i.e. image stack) to a software routine that could identify discrete objects, count and classify them and then report the findings to the user. However, any computerised measurement system requires a set of classifiers that first tell the software within which parameters to operate. For a nuclei stained volume this could consist of a set of arguments that define the limits of individual nuclear dimension (e.g. minimum and maximum length and width). In this respect the measurement algorithm will be semi-automated in that it requires the user to set the classifiers at the beginning and then perhaps alter the classification depending on the output (results). If a given tissue and staining protocol yielded uniform staining each and every time then it may be possible to fully automate the process. However, in my experience, tissue variability makes it almost impossible

to predict for different vessels what the classifier values should be, particularly where intensity of staining is a factor. For this reason, and because of the problems described below, we have yet to find an algorithm that can fully automate this process. Furthermore, even our own semi-automated method is not 100% accurate.

Automated 3D-analysis.

The quantitative advantage of imaging modalities can only be fully realised once suitable analysis software is available. Unfortunately, the current state-of-the-art in rendering and segmentation is not equipped to cope with the variability of many biological tissues. The previous sections have dealt solely with 2-dimensional imaging. The extended focus models shown in this chapter are only pseudo-3D projections on which measurement is not permitted. Although structural studies were not the primary goal of the project it seemed necessary to investigate the power of 3D-rendering. I was particularly interested in investigating the possibilities for quantifying 3D volumetric data of vascular objects (i.e. nuclei). If vascular reactivity could be monitored in 2D, perhaps it could be quantified in 3D. This proved to be (and still is) an enormous task. It is not within the scope of this thesis to describe the development work and experiments in deconvolution and rendering that led to the final algorithms that were developed by Dr. Daisheng Luo. However, I will describe here the general problems that need to be overcome in studying blood vessel walls in 3D.

Thresholding and segmentation routines are at the heart of many image based measurements. I define 'thresholding' as being the process of selecting intensity ranges; 'segmentation' is defined as the process of extracting an object from a volume.

Nuclei stained blood vessels present a particular challenge to the thresholding and segmentation routines. Essentially, the vascular wall can be treated as a 3D volume containing several objects (in this case nuclei) which have different sizes, shapes, orientations and intensities. The challenge is to accurately segment each nucleus from the volume with the minimum input from the user. Several segmentation methods have been suggested. In biomedical image processing, Ong et al. (1996) give a review of four categories for the segmentation of tissue section images: thresholding, region growing, edge detection, and pattern matching. Most methods deal only with 2-D images and although some can be extended to 3D, it is far more complicated. Specific routines for confocal derived data are particularly difficult to find. The need for such routines has prompted us to develop our own methods designed to handle volumetric data from vascular segments.

Problems associated with CLSM.

The data of this chapter have identified a series of segmentation problems associated with studying nuclear stained vascular segments. For example, (1) objects (i.e. nuclei) can be as little as a few microns apart and may appear to fuse together in the segmented volume. (2) Neighbouring objects can have different intensities and individual objects can themselves have a wide range of intensity values. (3) Intensity will be lower deep within the specimen due to diffraction of light. (4) Even in CLSM data sets, some objects will be out-of-focus. The problems described above are general and will be relevant to most biological applications employing thick 'live' tissue. Now consider each problem with respect to the confocal study of blood vessels.

Object Fusion. With the exception of cells undergoing mitosis, there will be no cases where two nuclei occupy the same cell and therefore be touching. In general, cell nuclei must be separated by, at least, the thickness of two cell membranes. In this extreme case it will probably not be possible to resolve the distance between the nuclei, particularly in the optical (z) axis. Fortunately, the architecture of the vessel wall is such that cells are generally offset and are not stacked along the optical axis. Therefore, it is a reasonable assumption that where two nuclei appear to fuse it is probably the result of some optical aberration which may or may not be corrected. If the objects cannot be separated then the user must ensure that classifier parameters are stringent enough to eliminate objects whose volume is greater than the average by a factor of two (i.e. is it a double nuclei?).

Object intensity heterogeneity. This creates the greatest problem for efficient thresholding. Vital nuclear stains report the concentration of DNA. Therefore, if a nucleus has regions of high or low DNA concentration (i.e. an apoptotic nuclei) the resulting image of that nucleus will have a range of intensities. Selecting a fixed range of intensities for thresholding will undoubtedly result in fracturing of the object where only the brightest (or dimmest) regions will be segmented. One solution would be to broaden the thresholding range. However, this will increase the incidence of *object fusion*. In addition, two nuclei occupying the same optical plane can have completely different intensity ranges. This means that efficient segmentation of one nuclei in a plane does not guarantee segmentation of all other nuclei in that plane.

Intensity attenuation with depth. This is a more general problem which has a significant effect on our ability to image the complete vascular wall. As the focal

plane is increased along the z-axis the intensity of the fluorescent signal drops. This is mainly due to the diffraction of light and the efficiency of penetration of the laser. Practically, it means that nuclei deep within the wall (near the lumen) are more difficult to resolve cleanly. Moreover, it makes visualisation of the endothelial cells particularly difficult. One solution is to simply increase the PMT gain or laser power slightly with each increase in z-axis position during stack acquisition. This solution is only valid if intensity data *per se* is not meaningful or required.

Diffraction of light. Even in the best confocal system there will be some out-of-focus glare from fluorescent structures above and below the plane of focus. In vascular samples this is not a major problem since the relative size of the objects is greater than the actual diffraction from the point light source. Much has been written about the use of deconvolution methods to correct for this (Van Der Voort & Strasters 1995; Shaw 1995). I have tested several methods of deconvolution on vascular samples and have found the Iterative Constrained Tikhonov Miller and Maximum Likelihood methods to produce the best results for vascular tissues.

Multi-level thresholding and segmentation (IMTS).

To overcome the problems described above a specialised semi-automated algorithm for thresholding and segmenting objects from confocal volumes of vascular structure was developed in collaboration with Dr. Daisheng Luo.

The iterative multilevel thresholding and splitting (IMTS) method segments 3D images into volumes iteratively by increasing the threshold value and splitting larger volumes into smaller volumes. The volumes are extracted by the *slice merging*

method. The object segmentation is controlled by *intensity homogeneity* and *volume size* criterion.

Unlike the automatic multilevel thresholding (Chang, 1995) where threshold values are found from the global histogram and different objects are segmented in different threshold bands, IMTS segments different objects at different threshold values which match the object themselves. This method is particularly effective for segmenting nuclei in vascular segments. Operation of IMTS is simple. The routines have been built into an existing 3D-rendering package (Microvision; Fairfield Imaging). The software runs on SiliconGraphics hardware and has a friendly windows like interface. Once the volume has been loaded the user selects the thresholding range and the incremental step size. The software then segments the volume interactively and displays the segmented volume in the render window. the user can then examine the volume visually and can view the object data text file. If the results are not satisfactory, the thresholding step size and range is altered and the process is repeated.

Object Classification and measurement.

As stated earlier (and shown in the figures), cell type can be identified by nuclei position, shape and orientation. Therefore, segmented objects can be used to report the number, position and orientation of the different cell types. Once a data volume has been analysed by the IMTS segmenter the object data is output to a simple text file. Objects can then be ordered by size, shape factor orientation etc. If only smooth muscle cells are to be examined then classifiers which are unique to these cells can be defined (i.e. ratio of length to width; shape factor; orientation with respect to a fixed axis etc. Table 2.5).

In summary, the data within this chapter have helped clarify exactly what is possible in terms of studying vascular structure and function using confocal microscopy. Stains for the extracellular matrix, cytoplasm and nucleus have been validated and their respective limitations identified. It has been shown that nuclear stains can provide information on the spatial organisation of vascular cells. Furthermore, the cellular arrangement can be examined at different perfusion pressures or degrees of activation. The method is sensitive enough for detection of vascular abnormalities resulting from at least two cardiovascular disorders.

The process of thresholding and segmentation of 3D volumes has been tackled and was largely successful. A major conclusion to be drawn from these experiments is that structural analysis using the stains described here is unlikely to be useful in the study of vascular asymmetry. An alternative approach (studying receptor distribution) is described in the next chapter.

Focussing on the positive aspects of the results it should be noted we are now able to clearly define the way in which our studies of vascular structure and function will continue in the future. In the course of examining several hundred arterial segments, 2 questions are constantly raised in my mind.

1. Are there groups of cells which act as functional 'pacemaker' units for initiation of contraction? I firmly believe that we will find repeating patterns of cell arrangements which may or may not be functional units.
2. Is there a relationship between the adventitial nerve plexus and the arrangement of smooth muscle cells on the outermost layers of the tunica media? Do nerves follow the pattern of cell arrangement?

3. Is there a simple mathematical formulae to describe the arrangement of cells mapped to a tubular structure which could be used to build models of vascular cell arrangement. Furthermore, alteration of which variables of the formulae would cause reorganisation akin to remodelling.

The methods described in this chapter make it possible to address the questions outlined above. Answering these questions will form a major focus of my work in the coming years.

References.

- Aalkjaer C. and Mulvany M.J. (1983) Human and rat resistance vessels: A comparison of their morphological and pharmacological characteristics. *Gen. Pharmac.* Vol. **14**, 85-87.
- Amos WB, White J.G. & Fordham M (1987). Use of confocal imaging in the study of biological structures. *Appl. Opt.* **26**:3239-3243.
- Arribas S.M., Gordon J.F., Daly C.J., Davidson A., Dominiczak A.F. & McGrath J.C. (1994). Smooth muscle cell rearrangement and impaired contractions in basilar artery of SHRSP. *Methods & Findings in Experimental & Clinical Pharmacology*, **16**, p47
- Arribas S.M., Gordon J.F., Daly C.J., Dominiczak A.F. & McGrath J.C. (1996). Confocal microscopic characterisation of a lesion in a cerebral vessel of the stroke-prone spontaneously hypertensive rat. *Stroke*, **27**; 1118-1123
- Baumbach, G.L. & Heistad, D.D. (1989) Remodelling of cerebral arterioles in chronic hypertension. *Hypertension*, Vol **13**, 968-972.
- Brakenhoff G.J., van der Voort H.T.M., van Spronsen E.A. & Nanninga N. (1989). Three-dimensional imaging in fluorescence by confocal scanning microscopy. *J. Microscopy* Vol **153**, pt2 p151-159.
- Carlsson K., Danielsson P., Lenz R., Liljeborg A., Majlof L. & Aslund N. (1985). Three-dimensional microscopy using a confocal laser scanning microscope. *Opt. Lett.*, **10**:53-55

- Carlsson K (1991). The influence of specimen refractive index, detector signal integration, and non-uniform scan speed on the imaging properties in confocal microscopy. *J. Microscopy*. Vol. **163**, pt2 p167-178
- Chang F.J., Yen J.C. and Chang S. (1995). A new criterion for automatic multilevel thresholding. *IEEE Trans. Image Process* Vol. **4**, pp. 370-378.
- Chen E.Q., Chan F, Lam & Periasamy A (1991). Effect of refraction on optical microscopic measurement of internal blood vessel diameter and its correction. *J. Microscopy* Vol. **164**, pt3 0239-245
- Chen H, Swedlow J.R., Grote M., Sedat J. and Agard D. (1995). The collection, processing and display of digital three dimensional images of biological specimens. In *Handbook of Biological Confocal Microscopy*. Ed. J. Pawley, Plenum Press NY p197-210.
- Daly, C.J., Gordon, J.F., Boyle, F.C., Gillespie, J.S., McGrath, J.C., Moss, V.A. & Spurway, N.C. (1990) Fluorescent myography: the analysis of isolated vascular smooth muscle cells of the rat labelled with bisbenzamide during vasoconstriction. *J. Physiol (Lond.)*. **429** 11P.
- Daly, C.J., Gordon, J.F. & McGrath, J.C. (1991a) A fluorescence image analysis method for the study of smooth muscle cell interaction within the vascular wall of small blood vessels. *Blood Vessels* **28** 281.
- Daly, C.J., Gordon, J.F. & McGrath, J.C. (1991b) Fluorescence image analysis methods for the study of smooth muscle cell interaction within the vascular wall of small blood vessels. In '*Resistance Arteries, Structure and Function.*' Ed. M.J. Mulvany et al., The Netherlands: Elsevier. pp. 339-343. [ISBN 0 444 89193 5]

- Daly, C.J., Gordon, J.F. & McGrath, J.C. (1992) The use of fluorescent nuclear dyes for the study of blood vessel structure and function: novel applications of existing techniques. *J. Vasc. Res.* **29** 41-48.
- Daly C.J., Gordon J.F. & McGrath J.C. (1993a). 3-Dimensional analysis of smooth muscle cell reactivity within the rat resistance artery using confocal microscopy. Proceedings of the XXXII Congress of IUPS p249.47
- Daly C.J., Gordon J.F. & McGrath J.C. (1993b). Observation of vasodilatation in small arteries with confocal microscopy. Proceedings of the XXXII Congress of IUPS O73.12
- Gahn T & Witte S (1986). Measurement of the optical thickness of transparent tissue layers. *J. Microscopy* Vol. **141** pt1 p101-110.
- Garvin, H.S.D. (1965) *A Student's histology* (2nd Edition). Pub. E & S Livingstone Ltd.
- Halpern W, Osol G & Coy GS (1984). Mechanical behavior of pressurized in vitro prearteriolar vessels determined with a video system. *Ann Biomed Eng*; **12**(5):463-79.
- Haegerty, A.M., Aalkjaer, C. Bund, S.J., Korsgaard, N & Mulvany, M.J. (1993). Small artery structure in hypertension: dual process of remodeling and growth. *Hypertension* Vol **21**, 391-397.
- Hell S, Reiner G, Cremer C & Stelzer H.K. (1993). Aberrations in confocal fluorescence microscopy induced by mismatches in refractive index. *J. Microscopy* Vol. **169**, pt3, 391-405.

- Mulvany, M.J., Baumbach, G.L., Aalkjaer, C. & Heagerty, A.M. (1996). Vascular remodelling. *Hypertension*, Vol 28, 505-506.
- Ong SH., Jin XC, Jayasooriah, and Sinniah R (1996). Image analysis of tissue section. *Computers in Biology and Medicine* Vol. 26, No. 3, pp. 269-279.
- Pawley, J. B., (1995). *Handbook of biological confocal microscopy*. Second Edition, Plenum Press, London, pp. 200-201, 238-239, 373-402.
- Pease, D.C. & Paule, W.J. (1960). Electron microscopy of elastic arteries; the thoracic aorta of the rat. *J. Ultrastruc. Res.* Vol 3, 469.
- Rhodin. Vascular smooth muscle : metabolic, ionic, and contractile mechanisms. ed. by M.F. Crass and C.D. Barnes Pub. New York London : Academic Press, 1982
- Rigaut JP and Vassy J (1991). High resolution three-dimensional images from confocal scanning laser microscopy; quantitative study and mathematical correction of the effects from bleaching and fluorescence attenuation in depth. *Analytical and Quantitative Cytology and Histology*. Vol 13 No. 4 223-232
- Russ JC. (1995). *The Image Processing Handbook*. CRC Press Ann Arbor. Second edition. ISBN 0-8493-2516-1.
- Shaw PJ (1995). Comparison of wide-field deconvolution and confocal microscopy for 3D-imaging. In *Handbook of Biological Confocal Microscopy*. Ed. J. Pawley. Plenum Press New York and London
- Van der Voort HTM. and Strasters KC (1995). Restoration of confocal images for quantitative image analysis. *Journal of Microscopy*, Vol. 178, pp. 165-181.

White JG, Amos WB & Fordham M (1987). An evaluation of confocal versus conventional imaging of biological structures by fluorescence light microscopy.

J. Cell Biol., **105**: 41-48

Visser TD, Oud JL & brakenhoff GJ (1992). Refractive index and axial distance measurements in 3-D microscopy. *Optik*, Vol **90**, No. 1 p17-19

Chapter 3

The use of fluorescent ligands and the development of methods for fluorescent ligand-binding in isolated cells and tissues.

Introduction.

The previous chapters have dealt with fluorescence based methods for identifying cells and cell types. Much of the previous work was focused on developing a means of visualising cells during vasomotion at different depths within the vascular wall in response to agonists and other stimuli. In many respects the fluorescence based approach was largely successful, proving that it is indeed possible to stain living (pressurised) vessels, to identify cell type, to build 3D models of vascular structure and to monitor the change in position/arrangement of cells during contraction and changes in transmural pressure. In addition, several other interesting features of vascular structure and possible avenues for investigation became apparent and are currently being followed by members of Professor McGrath's research group (i.e. confocal studies of hypertension induced remodelling, confocal analysis of vessels from organoid culture, mathematical descriptions of vascular cell arrangement, automated analysis of 3D volumes etc.). However, with respect to the main aim of this project, which is the determination of sensitivity of individual cells and cell layers to selective agonists, it appears that the organelle staining approach might not be sensitive enough. Moreover, it is not exactly clear how much freedom of movement an individual cell might have. Even if one cell in a group is rich in adrenoceptors and is activated first, contraction of this cell may be constrained by other physical factors like anchorage to elastin and collagen or the presence of surrounding cells. This is indicated by careful examination of the movies of KCl and noradrenaline contraction of pressurised vessels where there is no evidence for initial activation of sub-populations of cells.

One possible line of attack would be to study Ca^{2+} activation in the cells of the vascular wall. α_1 -adrenergic receptor activation causes a rise in intracellular Ca^{2+} which leads to contraction of vascular smooth muscle (McGrath 1982). There are now many forms of fluorescent Ca^{2+} indicator which will increase or decrease their fluorescence in proportion to the amount of free cytosolic Ca^{2+} (Minta et al., 1989). This creates the possibility of using confocal microscopy to examine Ca^{2+} signalling in vascular smooth muscle at different depths within the media in response to selective agonists. However, while I believe that this particular approach will provide very important information in the future, I did not feel that it would fully address the real pharmacological question relating to receptor distribution and its relationship to the observed asymmetry of responsiveness. Nevertheless this approach is being strongly considered for future developments by professor McGrath's research group. A very recent paper described Ca^{2+} activation in renal arterioles using confocal microscopy (Miriel et al., 1999). Unfortunately, the image quality in the study was relatively poor and suggests work with thicker walled arteries may be problematic and difficult to interpret. My preliminary experiments (not shown here) of loading fura-red into blood vessels showed that it was possible to obtain reasonable resolution of smooth muscle cells in the region just underneath the adventitia. It will be interesting to watch the developments in this area.

At the same time as I was considering which direction to follow next (to go with Ca^{2+} , to stick with the fluorescent nuclear stains, or move to arterioles and try to establish the mechanics of contraction), Molecular Probes announced the synthesis and commercial availability of BODIPY FL-prazosin. Prazosin is a high affinity α_1 -adrenoceptor antagonist and has been used to distinguish α_1 and α_2 adrenoceptors pre-

and postjunctionally (McGrath 1982). BODIPY (borate-dipyrromethene) is a more stable (pH insensitive) fluorophore than FITC (FITC bleaches quickly under laser illumination and is sensitive to intracellular pH). Therefore BODIPY is a more suitable fluorophore for conjugating to a ligand.

The development of this compound raised the possibility of mapping the location of α_1 -ARs rather than inferring their presence indirectly based on cellular activation. Furthermore, since prazosin is not selective for the three α_1 -subtypes (see below) it may be possible to use the non-selective fluorescent drug in combination with subtype selective compounds in order to determine the distribution of individual receptor subtypes. It was thus decided to follow a program of work investigating the functional pharmacology and ligand-binding characteristics of BODIPY FL-prazosin in single transfected cells, in freshly dissociated cells and in living tissue sections. The experiments in this chapter describe the preliminary work leading up to the development of the method of fluorescent ligand binding. Data from some recent publications will also be presented (McGrath & Daly 1995; McGrath et al., 1996; Daly et al., 1998).

Current Classification of α_1 -adrenoceptor subtypes.

Classical pharmacological methods and theory dictate that identification of a receptor subtype requires proof of the existence of the endogenous ligand. In addition, an antagonist that binds to the receptor with high (nanomolar) affinity must be available. In recent years this approach has been radically changed. It is now possible to identify the genes which code for receptor subtypes. These genes (cDNA) can now be transfected into cells which will then transcribe the DNA and manufacture the

recombinant receptors. Therefore the classical requirements for identification of a receptor subtype have changed. The original requirements for an antagonist and endogenous ligand still stand, unless you have the gene! This situation has resulted in the discovery of receptor subtypes for which, in many cases, there is either no endogenous ligand or recognised physiological role. This situation now exists to a certain extent for the α_1 -ARs.

There are currently three recognised subtypes (known genes) of α_1 -ARs; α_{1A} , α_{1B} and α_{1D} (Hieble et al, 1995). The α_{1C} nomenclature has been abandoned to avoid confusion (see Hieble et al for details). A further important classification (α_{1L}) is recognised functionally but not 'officially accepted' due to the absence of a known cDNA sequence which can transcribe the functional receptor in recombinant systems. Nevertheless the α_{1L} -AR, which is characterised by its low affinity for prazosin, has been demonstrated functionally in many tissues including, most recently, those of the lower urinary tract (Ford et al., 1996). The wide range of observed pA_2 values for prazosin was highlighted by Drew (1985) at a workshop on α -adrenoceptors hosted by Prof. J.C. McGrath and later published in *Clinical Science*. Drew's observations led others to suggest that the low affinity prazosin site may represent a new α -AR subtype (Flavahan & Vanhoutte 1986; Murumatsu 1990). Some authors have suggested that the α_{1L} -AR is a low affinity state of the α_{1A} -AR (Ford et al., 1996). If this is the predominant AR on prostatic SMCs it may explain why prazosin is not used therapeutically since relatively high doses would need to be administered and the resulting hypotension caused by non-selective vasodilation would be an unacceptable side-effect.

Selectivity of Antagonist drugs and new compounds.

The quinazoline family of compounds (which includes prazosin, doxazosin, alfuzosin etc. Figure 3.1) are not selective among the three α_1 -AR subtypes. Tamsulosin (YM12617) has high affinity for α_{1A} -ARs but also has affinity for α_{1D} ARs. While the current group of pharmacological tools for subdivision of the α_1 -ARs are not ideal there are several compounds which do possess relatively high selectivity for individual subtypes (i.e. BMY7378 for α_{1D} ; 5-methylurapidil for α_{1A} ; L765,314 for α_{1B} etc.). Although many different compounds are used for the classification of subtypes it seems that the relatively 'non-selective' ones are used clinically, probably due to the mix of receptor subtypes that are generally present on native tissues. It should also be noted the the quinazolines are lipophilic and will therefore have access to any intracellular receptors which may contribute to their observed potency.

Receptor distribution and location

It is now apparent from biochemical and molecular studies that receptor desensitisation and downregulation is probably associated with the mechanism of receptor internalisation which occurs by an endocytotic process and which is reviewed extensively elsewhere (von Zastrow & Kobilka 1994).

It has been shown in recombinant systems that α_{1A} -ARs are expressed as intracellular receptors whereas α_{1B} -ARs are more readily translocated to the plasma membrane (Hirisawa et al., 1997). Presently, nothing is known about receptor turnover in blood vessels at the cellular level. It is also not known if cell surface ARs are distributed evenly through the medial smooth muscle cells of the vessel wall. It was therefore of

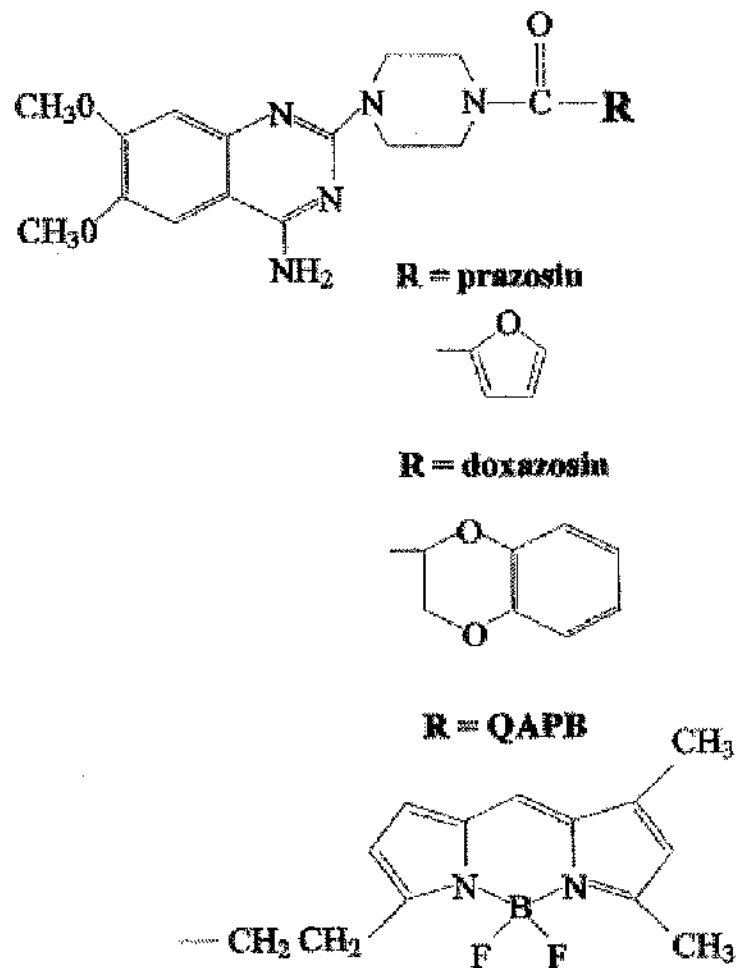


Figure 3.1. The structure of quinazolinyl piperazine (top) and the various substituents (R) that distinguish prazosin, doxazosin and QAPB. This particular form of BODIPY is excited at 488nm and emits above 515nm. The compound was obtained from Molecular Probes and is listed in their catalogue as "BODIPY FL-prazosin" but since it lacks the furan group which defines prazosin, as opposed to other compounds which share the quinazolinyl piperazine group, such as doxazosin, we refer to it by an acronym, "QAPB", derived from its chemical name (quinazolinyl piperazine borate-dipyrromethene).

interest to determine whether fluorescent ligands could be usefully applied to tackling these issues.

Until recently fluorescently labelled receptor ligands were used more or less as irreversible histological "stains". The long duration of the ligand-receptor association was considered as akin to a covalent bond. Unlabelled competitors were merely a means of occluding the association and validating the receptor type. However, some compounds are now available which have the ability to report the "amount" of ligand-receptor complex at equilibrium: these compounds fluoresce when bound to the receptor but have low background fluorescence in the aqueous phase giving a high signal to noise ratio. This opens up the possibility of assessing the affinity of the receptors for the fluorescent ligand and, further, of assessing the affinity of other ligands by competition. The big advantage is that quantitative ligand binding can be carried out with very high spatial resolution which is ideal for dealing with heterogeneous tissue, but many other advantages follow (table 3.1).

History of fluorescent "drug" ligands.

Many attempts have been made at conjugating fluorescent molecules to receptor ligands in the hope of identifying their binding sites. This was aimed mainly at the localisation of the receptors rather than studying their properties. The objective was to produce a fluorescent compound which would remain fluorescent when bound to the receptor and would remain bound when the free drug was washed away. This actually makes the experiment more demanding since washing is likely to cause the

Table 3.1 Fluorescent-ligands vs Radio-ligands

Advantages

- Fluorescence is relatively safe and inexpensive compared with tritiated or iodinated compounds.
- Spatial resolution is greatly enhanced: compared with autoradiography or cell fractionation.
- Experiments can be performed at true equilibrium.
- Fluorescent ligands can be displaced from their binding sites by non-fluorescent ligands. Using image subtraction it is thus possible to identify the sites recognised by the non-fluorescent ligand.
- Bleaching of certain fluorescent molecules (i.e. those which are only fluorescent when bound) can be used for FRAP type experiments. Once an area has been bleached the rate of recovery of fluorescence provides information on the association of the fluorescent ligand.
- Signal does not degrade. Although photobleaching of individual molecules can occur, the kinetic nature of binding replenishes the site with an intact ligand. This also allows signal averaging c.f. radioligand decay.
- Different fluorophores are available to suit particular experimental set-ups. This enables the use of multiple fluorescent ligands or the co-localisation of ligands and antibodies.
- Live or fixed tissue can be used.
- Small amounts of tissue or single cells can be studied.
- Immediate results are obtained.

Disadvantages

- The large fluorescent group can affect the affinity of some (but not all) ligands.
- The yield of a single fluorescent molecule may be different for different fluorophores and may be affected by the binding conditions. This complicates the calculation of a Bmax.
- Very sensitive detectors are required for the low concentrations of fluorescent ligands which are required to maintain specificity.
- Bleaching will occur if the excitation source is too great or the ligand concentration too low. In some cases it may be difficult to find the right balance if the source light is not tuneable.
- Tissue autofluorescence can cause significant problems in some samples. Elastin is particularly problematic.
- If fluorescent ligands are internalised in live tissue or cells they may be subject to degradation.

ligand to dissociate and diffuse away, unless it has very high affinity (or a slow off-rate). Increased fluorescence on binding was not an objective. Early studies were also limited by the insensitivity of detectors. However the greatest obstacle was the lack of suitable probes, necessitating the ad hoc development of the fluorescent ligands. In reviewing the limited critical acceptance of some early examples, it is worth noting whether the pharmacological properties of the ligands were examined or whether the assumption was made that they possessed similar properties to the parent compound. The contemporary situation is simpler since the development of fluorescent biochemicals has become important in molecular biology and the tools for rapid pharmacological screening are available.

Examples of fluorescent ligands for various receptors

Nicotinic: α -Bungarotoxin was one of the first drugs to be exploited as a fluorescent ligand (Anderson & Cohen 1974). It was used to label acetylcholine (ACh) receptors of *Xenopus sartorius* muscle fibres. Fluorescent α -bungarotoxin binding could be inhibited by carbachol or unlabelled α -bungarotoxin. This early report is significant in taking account of both the selectivity and affinity of the fluorescent ligand, noting that the fluorescent conjugate exhibited lower potency than the native toxin. Fluorescent α -bungarotoxin is still in use: one study combined this probe with 4-Di-2-ASP to visualise simultaneously the dynamic architecture of nerve terminals and their associated postjunctional receptors during development (Balice-Gordon & Lichtman 1993). High affinity toxins whose binding is virtually irreversible are ideal for these "localisation" studies and carry the additional advantage that they can be translocated inside the cell with receptors.

β -Adrenoceptors: Atlas and co-workers synthesised a fluorescent analogue of propranolol (9-AAP) and used this probe in an attempt to localise β -adrenoceptors in rat cerebellum (Atlas et al., 1976). They found 'spots' of fluorescence, consistent with binding to presynaptic sites, which were reduced in both number and intensity in the

presence of unlabeled propranolol. Similar results were obtained with a dansyl analogue of propranolol (DAPN) which prompted the authors to suggest that fluorescent β -adrenoceptor antagonists could be used in vivo to study β -adrenoceptors in the CNS (Atlas & Melamed 1978). However, the use of fluorescent β -antagonists did not find widespread use. There are two possible reasons for this. Firstly, the qualitative nature of the technique may have limited its appeal and, secondly, there was criticism that the fluorescent spots observed may be autofluorescent granules (Hess 1979). A later development in this field was the use of fluorescent labelled CGP12177. Heithier et al, (1994) showed that a BODIPY derivative of CGP12177 had similar binding properties to native CGP12177 on human β_2 -adrenoceptor transfected Sf9 cells and were able to demonstrate punctate fluorescence on lightly fixed cells which was abolished in the presence of non-fluorescent CGP.

Opioid: The understanding of opiate-induced desensitisation of receptors was advanced following the synthesis of a fluorescently labeled enkephalin which was used to study opiate receptors in neuroblastoma cells (Hazum et al., 1979). Using this probe it was found that opiate receptors normally exist in a diffuse state and that both agonists and antagonists can induce receptor clustering (Hazum et al., 1980).

Histamine: Petty & Francis(1986) synthesised and studied fluorescein-histamine. They identified clusters of mobile receptors on the cell surface of polymorphonuclear leukocytes. Furthermore, fluorescein-histamine binding was inhibited in the presence of histamine and cimetidine confirming that conjugation of the fluorophore does not markedly alter its selectivity.

Neurotensin: Faure et al., (1994) synthesized a fluorescent derivative of neurotensin, N α -FITC-[Glu¹]NT (fluo-NT). Using (i) flow cytometry, (ii) ligand binding and (iii) confocal microscopy the authors demonstrated that fluo-NT, over the concentration range tested (0.16-16nM), exhibits (i) 85% specific binding, (ii) a pK_i (0.67nM) against [¹²⁵I]-NT similar to non fluorescent NT (0.55nM) and (iii) granular hot spots within nerve cell bodies on rat brain sections. Fluo-NT binding to SN17 cells (septal

neuron-neuroblastoma hybrid cells, which express high affinity NT-binding sites) produced hot spots which were predominantly on the cell surface although a population of intracellular hot spots was identified using confocal microscopy.

α -adrenoceptors: The experiments of this chapter have employed a BODIPY-labelled fluorescent quinazoline, QAPB (figure 3.1) which is related to the α_1 adrenoceptor antagonists doxazosin, prazosin and terazosin (Ruffolo et al., 1995) to visualise α -adrenoceptors on live cells and intact pieces of tissue. The punctate fluorescence found is visually similar to that found with other receptor antibodies and confirms the punctate nature of α -adrenoceptor distribution found by Uhlen et al., (1995) in MDCK cells.

Cell surface G-protein-coupled receptors are notoriously difficult to localise accurately, even in fixed tissue using antibodies, due to the non-specificity caused by the high degree of conservation of sequence, or using radioligands due to the inherent low resolution of autoradiography. However, high affinity fluorescent ligands based on "antagonist" drugs/ligands could be used in a manner analogous to radioligands, but with much higher spatial resolution and in real-time on live tissue, if their concentration can be measured photometrically.

The data which follow document the validation of the compound BODIPY FL-prazosin (or QAPB). Firstly, the pharmacology of the ligand is established in a variety of tissue types using functional, binding and biochemical assays. Secondly, by using a transgenic cell line, the concentration-fluorescence characteristics of the compound are investigated in an attempt to produce data similar to that obtained in conventional radioligand binding. In addition, the fluo-ligand is tested on dissociated cells and tissue sections harbouring known α_1 -AR subtype populations. Finally, the use of image analysis methods for studying receptor binding induced fluorescence and spatial distribution is also considered.

Methods

Reagents

Reagents used were of the highest analytical grade. The following compounds were used: DMEM (GIBCO UK); [³H]-prazosin (86Ci mmol⁻¹) and *myo*-[2-³H]inositol were obtained from Amersham; BODIFY FL-prazosin 'QAPB'(Molecular Probes Inc); prazosin HCl and doxazosin (Pfizer); phentolamine mesylate (Ciba); phenylephrine HCl & phenoxybenzamine (Sigma); YM12617 (Chinoïn).

Cell culture.

Rat 1 fibroblasts stably expressing the α_{1D} -adrenoceptor (see Wise et al., 1995) were maintained in DMEM containing 5% (v/v) new-born calf serum, glutamine, penicillin, streptomycin and geneticin (G418) in a humidified atmosphere at 37°C containing 5% CO₂.

Inositol phosphate studies.

Cells were seeded in 24-well plates and labelled close to isotopic equilibrium by incubation with 1 μ Ci/ml *myo*-[2-³H]inositol in 0.5 ml of inositol-free DMEM containing 1% (v/v) dialysed newborn calf serum for 36 h. On the day of the experiments the labelling medium was removed and cells were washed twice with HBG buffer [0.5 ml Hanks buffered saline, pH 7.4, containing 1% (w/v) BSA and 10 mM glucose]. Cells were then washed twice for 10 min with HBG/LiCl buffer (HBG supplemented with 10 mM LiCl) and subsequently stimulated with agonist in HBG/LiCl for 20 min. All incubations were conducted at 37 °C. Reactions were terminated by the addition of 0.5 ml of ice-cold methanol. Cells were then scraped, transferred to vials and chloroform was added to a CHCl₃/MeOH ratio of 1:2 (v/v). Total inositol phosphates were extracted for 30 min before the addition of chloroform and water to a final ratio of 1:1:0.9 (CHCl₃/MeOH/H₂O, by vol). The upper phase

was taken and total inositol phosphates were analysed by batch chromatography on Dowex-1 formate as previously described (MacNulty *et al.*, 1992).

Membrane preparation.

Cells were grown to confluence and harvested using a rubber policeman followed by centrifugation at 600xg for 5mins. The cell pellet was resuspended in 5mls of Tris-HCl assay buffer (150mM NaCl, 50mM Tris-HCl, 10mM MgCl₂, 5mM EDTA, 1ug/ml leupeptin, 10mM benzamidine, 500ug/ml soya bean trypsin inhibitor, pH 7.4) and homogenised at setting 6 for 3x5secs using an ultrapolytron. Following centrifugation (600g, 10mins, 4⁰C) the supernatant was retained on ice while the pellet was resuspended, rehomogenised and recentrifuged. The supernatants were pooled and centrifuged at 56,000g for 30mins at 4⁰C. The resulting membrane pellet was resuspended in 1ml of ice-cold Tris-HCl assay buffer and homogenised with a 5ml teflon-in-glass homogeniser. The homogenate was processed for protein estimation using a Pierce protein assay kit and adjusted to 0.5 mg/ml. Aliquots which were not used immediately for ligand binding were stored frozen at -80⁰C.

Radioligand binding studies.

Saturation studies were performed with rat α_1 d fibroblast membranes (0.05mg/ml) which were incubated in triplicate with [³H]-prazosin (0.05-10nM) in a total volume of 0.5ml of 150mM NaCl, 50mM Tris-HCl, 10mM MgCl₂, 5mM EDTA, pH 7.4. Competition binding assays were performed by incubating membranes with 0.2nM [³H]-prazosin in the presence or absence of a range of 12 concentrations of the competing ligands. Non-specific binding was defined as the concentration of bound ligand in the presence of 10 μ M phentolamine. Following equilibrium (30mins at 25⁰C) bound ligand was separated from free by vacuum filtration over GF/C filters on a Brandell cell harvester. Inhibition of specific binding of [³H]-prazosin by ligands

was analysed to estimate the IC₅₀ (concentration of the ligand displacing 50% of specific binding). The inhibitory constant (K_i) was calculated from the IC₅₀ by the equation of Cheng and Prusoff (1973). Binding isotherms from displacement studies were analysed by a non-linear least square parametric curve fitting programme GRAPHPAD Prism, capable of iterative curve fitting to a single or two-site model.

Analysis of functional antagonism by QAPB.

Preparations of rabbit saphenous artery or rat aorta were cut transversely into 3-4mm rings and suspended between thick wire supports. Each ring was suspended horizontally by means of two stainless-steel L-shaped hooks carefully passed through the lumen. The upper support was connected by cotton to an isometric transducer while the lower support was connected to a glass tissue holder. The arterial rings were mounted in 10ml isolated organ bath, bathed in Krebs maintained at 37°C and gassed with 95% O₂ plus 5% CO₂. The rings were then placed under resting tension at 1.5-2g for each group of arterial rings, which was determined from active tension development curves and found to be optimal. Segments of rat (epididimal) vas deferens were isolated and mounted longitudinally (under 1g tension) in a 10 ml organ bath. Isometric contractions were measured by a Grass FT03 transducer connected to a Linseis (TYP 7208) pen recorder. In all experiments, tissues were left to equilibrate for a 60 min period, during which time the tension was re-adjusted to a set value which was maintained constant throughout the rest of the experiment. Each preparation was then exposed to NA (1µM) and allowed to contract for 5-10 min. This first contraction to an agonist minimised changes in the sensitivity of preparations to further addition of agonists. The presence of the endothelium (on vascular segments) was confirmed pharmacologically by a relaxant response to acetylcholine (1µM). Following

complete washout, an additional one hour equilibration period was allowed before commencement of any other experimental procedure.

Assessment of antagonist potency versus agonist concentration response curves

Cumulative concentration response curves to noradrenaline or phenylephrine (0.1nM to 30 μ M in increments of a half of a log unit) were constructed. When QAPB was used, the preparations were incubated at least for 45 minutes with the antagonist drug prior to the onset of a second cumulative concentration response curve. Only two consecutive curves were tested on each preparation.

The potency of agonist was determined as the pD₂, which is the negative logarithm of the concentration causing half the maximal response.

In examining the effects of the antagonist versus concentration response curves to agonists, agonist concentration ratio values were determined from the concentrations producing 50% of the maximum response (EC₅₀) in the absence and presence of each concentration of antagonist. The EC₅₀ value of the agonist was expressed as the pD₂ value which was calculated as the negative logarithm of the EC₅₀ value (pD₂ = -log EC₅₀).

Confocal Microscopy.

A Noran Odyssey real-time confocal laser scanning microscope (CLSM) was used in conjunction with an Nikon Diaphot (inverted) microscope. The 488nm line (515 band pass) of an argon-ion laser was used throughout. In order to maximise the signal detection at very low concentrations of the fluorescent ligand a 100 μ m slit was used in all experiments. While not giving the optimum 'confocality' required for 3D-reconstruction work, this slit width nevertheless gave a significant increase in axial resolution compared with a conventional fluorescence microscope. A Nikon 40x oil

immersion objective (NA 1.3) was used throughout. Krebs solution is identical to that given in chapter 1.

Whole cell image analysis.

Images were collected and analysed using Universal Imaging's 'MetaMorph' software. Cells were grown on coverslips for 24 hours prior to use. Coverslips were mounted in a flow chamber (WPI) and placed on the stage of an invert (Nikon Diaphot) microscope fitted with a Noran Odyssey Laser Scanning Confocal Module. Using cell autofluorescence a suitable group of cells was selected and the focal plane fixed by locking the focus motor. The system was then set to acquire images (64 frame averages; 2.56 seconds exposure) at 1 minute intervals. After a 'run in' period of 5-6 minutes the first concentration of fluorescent ligand was added and allowed to equilibrate for at least 5 minutes. After equilibration the next concentration of fluorescent ligand is added, without washing, and given at least 5 minutes to reach equilibrium (i.e. no further increase in fluorescence). Once saturation has been reached the individual cells are outlined using MetaMorph's define-region tool and the whole time series is plotted as intensity vs time for each cell. Non-specific binding was defined as fluorescent binding in the presence of 10 μ M phentolamine. The composition of the HEPES buffer for cellular studies was as follows: (mM) NaCl 130, KCl 5.0, HEPES 20, Glucose 10, MgCl 1, CaCl 1.

Ligand binding to tissue slices.

Rat mesenteric artery segments were isolated and cleared of connective tissue. The segments (5-10mm in length) were placed in a mixture of molten glycerine and gelatine (37 $^{\circ}$) and allowed to cool to room temperature when the gelatine would set firmly. Segments were then cut transversely using a Sorvall TC-2 tissue chopper. Cut

ring segments (75-100um thickness) were then suspended in fresh HEPES for 10-15 minutes. Ring segments were then placed on coverslips coated with Cel-Tak tissue adhesive (3.5ug/cm²). The coverslips were then mounted in a flow chamber for microscopy studies identical to those used for isolated and cultured cells.

Iso-Surface Modelling.

Using the depth analysis module of the Imaris image analysis suite, a suitable iso-value was selected for construction of an iso-surface model. The iso-value represents and intensity value (or range). The full data volume is inspected for comparable values. The co-ordinates of the iso-values are plotted and connecting vectors are drawn between the points to create simple geometric shapes (i.e. triangles). This creates a wire-frame model upon which a surface can be mapped. The surface colour, texture and opacity can be user defined to enable visualisation of multi-layered surfaces. The surface area of each 'layer' can be quantified. Unfortunately, current software versions do not permit accurate calibration to provide quantification to be expressed in microns or some other suitable unitary measure.

Simulated Fluorescence Projection.

SFP is another rendering method offered by the Imaris suite (Messerli et al., 1993). The software treats the data volume as a block of absorbent material. If a light ray passes through the volume at a given point it will be adsorbed and cast a shadow. In a fluorescent stained volume areas of heavy staining (fluorescence) will tend to cast shadows on the background. This method is ideal in certain situations for showing a 2D image of a 3D volume.

Results.

Ligand affinity.

In Rat-1 fibroblasts expressing the rat α_{1d} -adrenoceptor, co-incubation of the cells with increasing concentrations of QAPB resulted in a progressive, parallel rightward shift in the concentration-effect curve for the generation of inositol phosphate induced by the α_1 -adrenoceptor agonist phenylephrine (Wise *et al.*, 1995) without alteration in the maximal effect (Figure 3.2a), demonstrating QAPB to act as a competitive, functional antagonist at this receptor. Transformation of this data to produce a Schild plot resulted in an estimated pA_2 for QAPB at the rat α_{1d} -adrenoceptor of 7.78 which was not significantly different from its antagonism of phenylephrine in rat aorta (pA_2 8.25, figure 3.3a).

3H -prazosin binding to fractionated cell membranes is the common method used to determine α_1 -adrenoceptor number and affinity (Kenny *et al.*, 1996). Inhibition of 3H -prazosin binding to α_{1d} -membranes by unlabelled competitors resulted in K_i (pK_i ; antagonist) values of 1.04 (9; prazosin), 1.24 (8.9; QAPB) and 17.8nM (7.5; doxazosin) (figure 3.2b). Inhibition curves were analysed using GraphPad PRISM and were statistically best fit by a single site model, confirming binding-site homogeneity.

QAPB acted as a competitive antagonist versus phenylephrine in rat aorta (pA_2 8.25 slope 0.9; figure 3.3a) and against noradrenaline in rabbit saphenous artery (pA_2 7.6 slope 0.75; figure 3.3b)

QAPB (0.1 μ M) caused a rightward shift in the concentration response curve to noradrenaline in isolated rat vas deferens (figure 3.4a). Versus acetylcholine in the same preparation QAPB (0.1 μ M) caused no shift in the CRC, confirming that there is no non-specific effect (or toxicity; figure 3.4b).

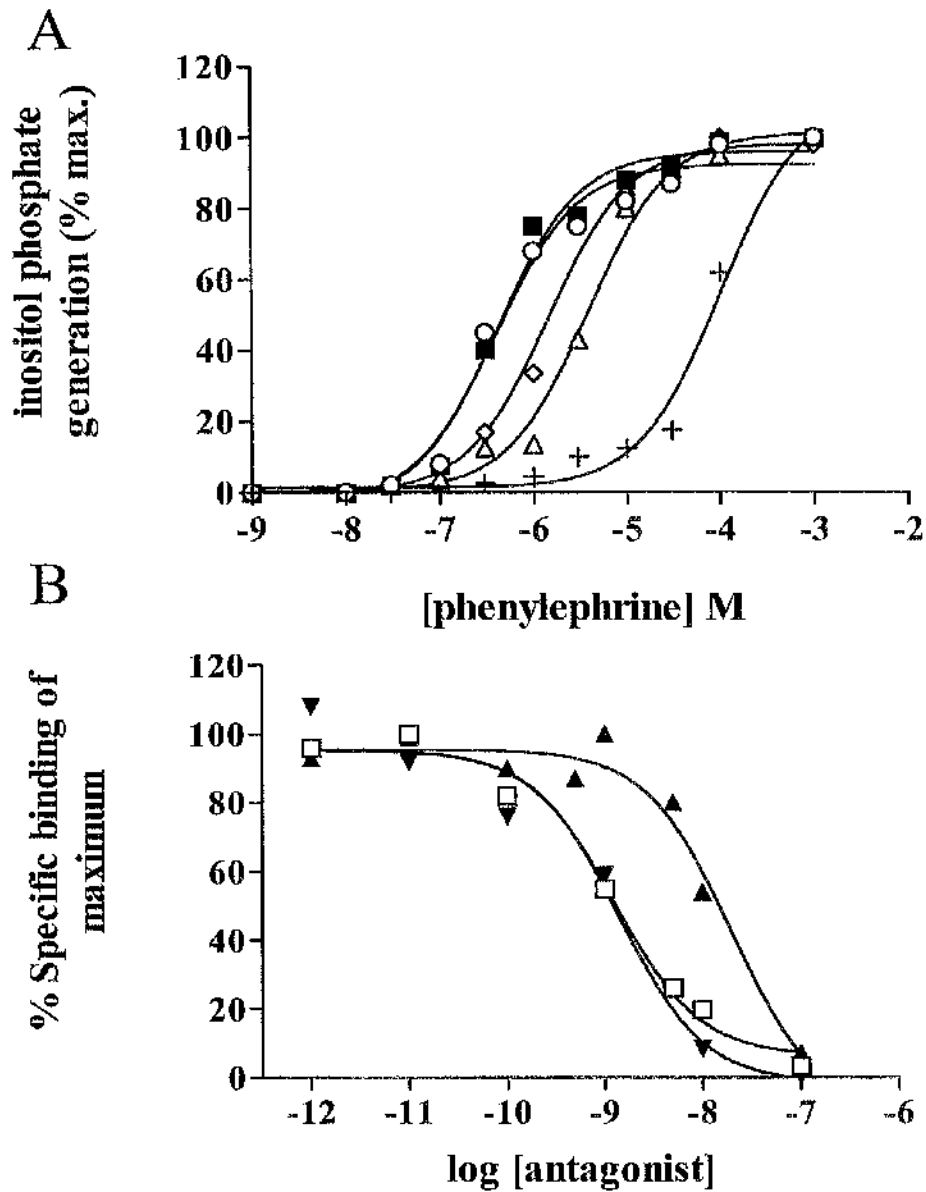
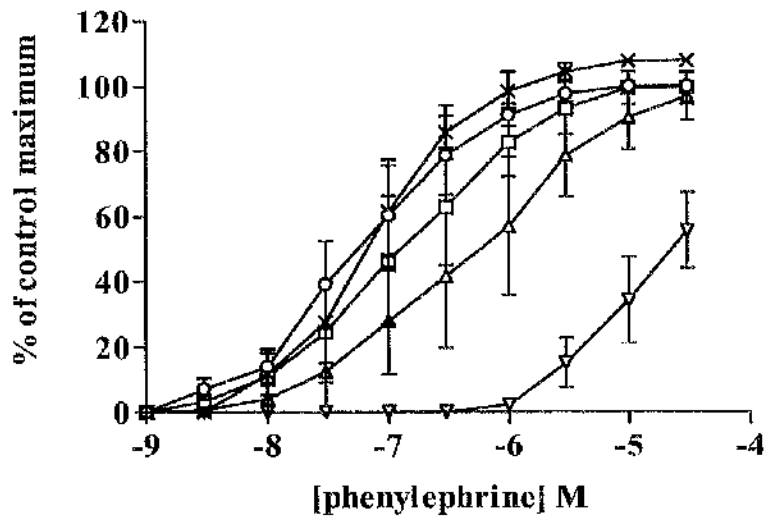


Figure 3.2. The graphs show two different assays in which QAPB has been tested for its functional antagonism at α_{1dD} -adrenoceptors. A) Inositol phosphate generation in response to varying concentrations of phenylephrine was measured in the presence of a range of concentrations of QAPB (control ■; 10nM ○; 30nM ◇; 100nM △; 1µM +) in cells of the α_{1d} -adrenoceptor expressing clone. B) Inhibition of 0.2nM ^3H -prazosin from α_{1d} -membranes by prazosin ▼, QAPB □ and doxazosin ▲.

A



B

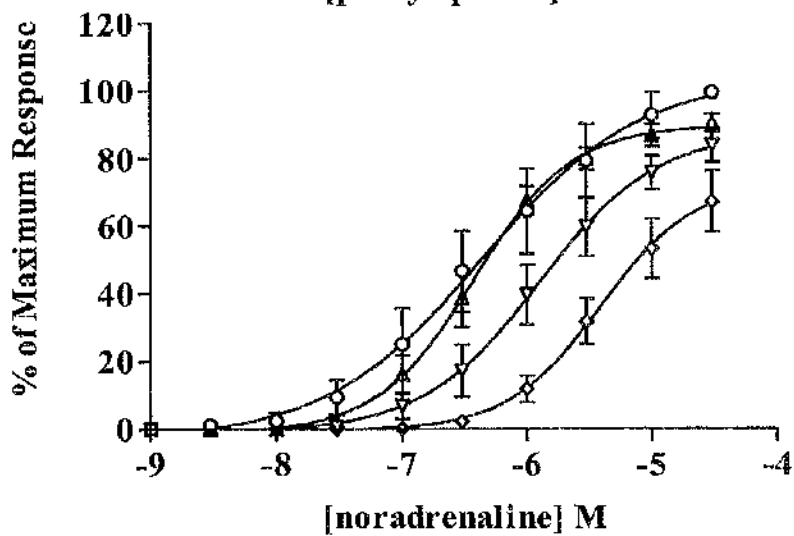


Figure 3.3. QAPB antagonism of phenylephrine (A; rat aorta) and noradrenaline (B; rabbit saphenous artery). Control (○); time control (X); 1nM (□); 10nM (△); 100nM (▽); 1uM (◇). All data points represent the mean \pm s.e.m. of n=4-6 experiments.

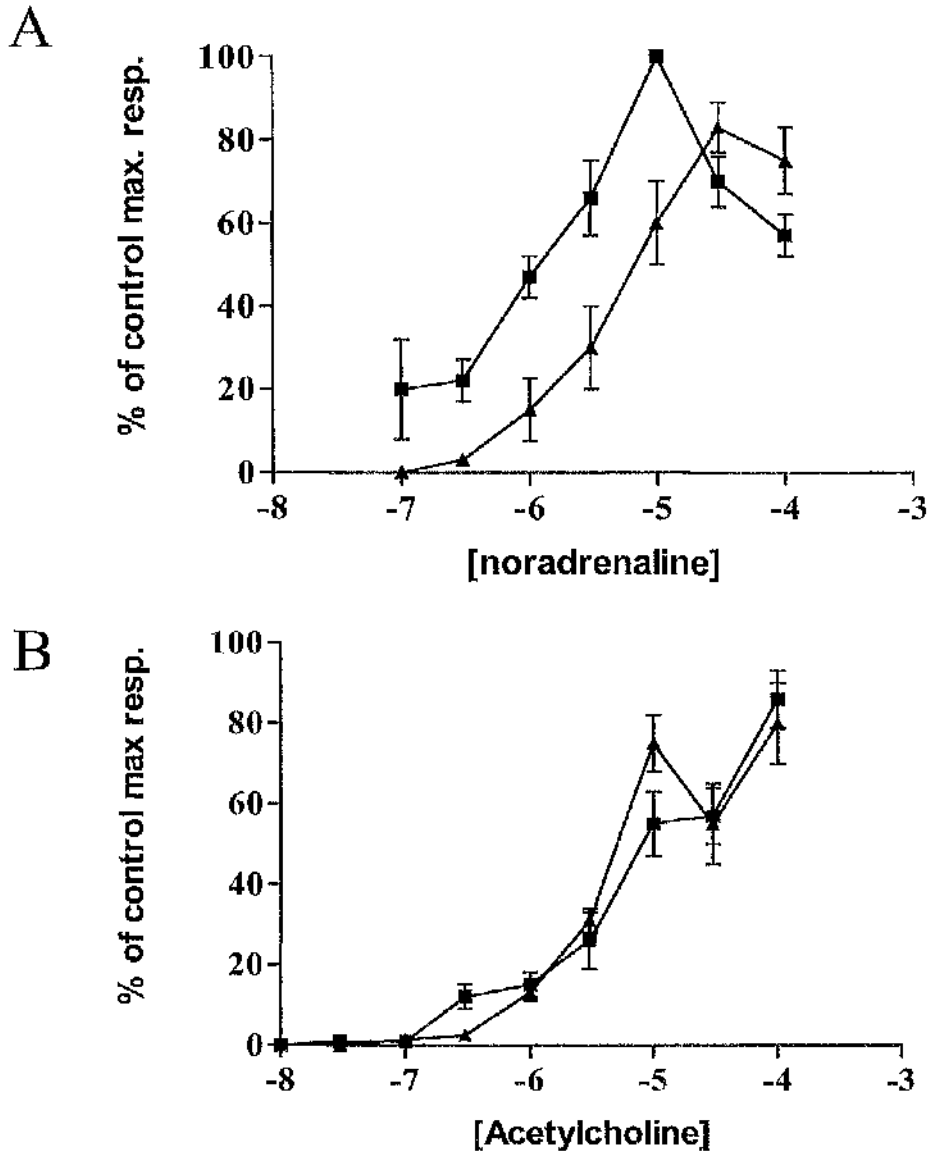


Figure 3.4. The antagonism of QAPB (0.1 μ M) versus noradrenaline (A) and acetylcholine (B) in the rat isolated vas deferens. Control CRC (■). Agonist in the presence of QAPB (▲). Each data point represents the mean \pm s.e.m of 4 experiments.

Concentration dependent fluorescence.

Initial experiments examined the binding of QAPB to fibroblasts transfected with the rat α_{1d} adrenoceptor. Using a 15 μ m slit and an oil immersion objective (x40 NA 1.13) produced a faint image of the unstained cells (autofluorescence) which was used to fix the focal plane. The CLSM system was then set to collect images (64 frame averages) every minute. QAPB was increased from 10 – 160nM in steps of 10nM every minute. Figure 3.5 shows the development of fluorescence with increasing concentrations. The development of clusters (hot spots) can be seen from frame 11 onwards. Fluorescence developed in clusters and in a diffuse manner with regions of high and low intensity.

The image produced by incubating with 100nM QAPB was selected for the construction of image masks. By selecting (thresholding, see chapter 2) a range of low (33-64), intermediate (65-96) and high (97-128) intensities it was possible to make masks of the regions which achieved the designated intensity (Figure 3.6). These masks were then used to measure the fluorescence development in only those regions through the course of the entire experiment. As can be seen from the graph in figure 3.5, the high intensity fluorescence is last to develop (at 90nM) while the low intensity fluorescence develops from 50nM.

To demonstrate the specific nature of the binding, experiments were performed in the presence and absence of the non-fluorescent α_1 -antagonist prazosin. Prazosin (100nM) inhibited the development of QAPB-induced fluorescence (figure 3.7). By measuring the average fluorescence in each image it is possible to plot a concentration fluorescence curve (CFC). Figure 3.8 shows the CFC in the presence and absence of non-fluorescent prazosin. As expected, the control CFC was shifted to the left.

The experiments thus far have shown that it is possible to inhibit the development of binding-induced fluorescence. I then considered the possibility of reversing the

fluorescence by adding a high concentration of non-fluorescent ligand in the presence of QAPB (at equilibrium). Figure 3.9 shows the effect of applying 10 μ M of prazosin and phentolamine in the presence of QAPB-induced fluorescence. 3 sample traces are shown in figure 3.9 which accurately represent the overall conclusion of many attempts to 'reverse' QAPB fluorescence, namely that it is not possible to completely reverse the binding of 5-10nM QAPB. These results led to the assumption that either QAPB has a slow dissociation rate, there is a population of receptors unavailable to the competitor or the concentration of QAPB is too high and thus has a non-specific component.

There followed a period of experimentation in which the sensitivity of the CLSM method was increased to enable visualisation of binding at lower (i.e. < 5nM) concentrations. Increasing CLSM sensitivity was achieved by

1. opening the pinhole aperture
2. increasing the gain of the PMT
3. Allowing longer incubation periods.
4. removing the secondary dichroic block from the system.

Point 4 is a technical consideration and has no effect on image quality (only system flexibility). However, point 1 & 2 have serious implications for image quality. Point 1 reduces confocality to almost non-confocal condition. Point 2 introduces PMT noise into the image. Point 3 allows more time for equilibrium to be achieved and for fluorescence to develop.

Figure 3.10 shows the results using the new parameters of 100 μ m slit, increased gain, 5 minute incubations. QAPB was applied every 5 minute (or longer if required) from 0.4nM – 10nM. Figure 3.10a shows the individual data (average intensities) measured at each point in a fluorescence saturation experiment on live cells, fixed cells and fixed cells + prazosin (1 μ M). By plotting the maximum point (intensity measure) of

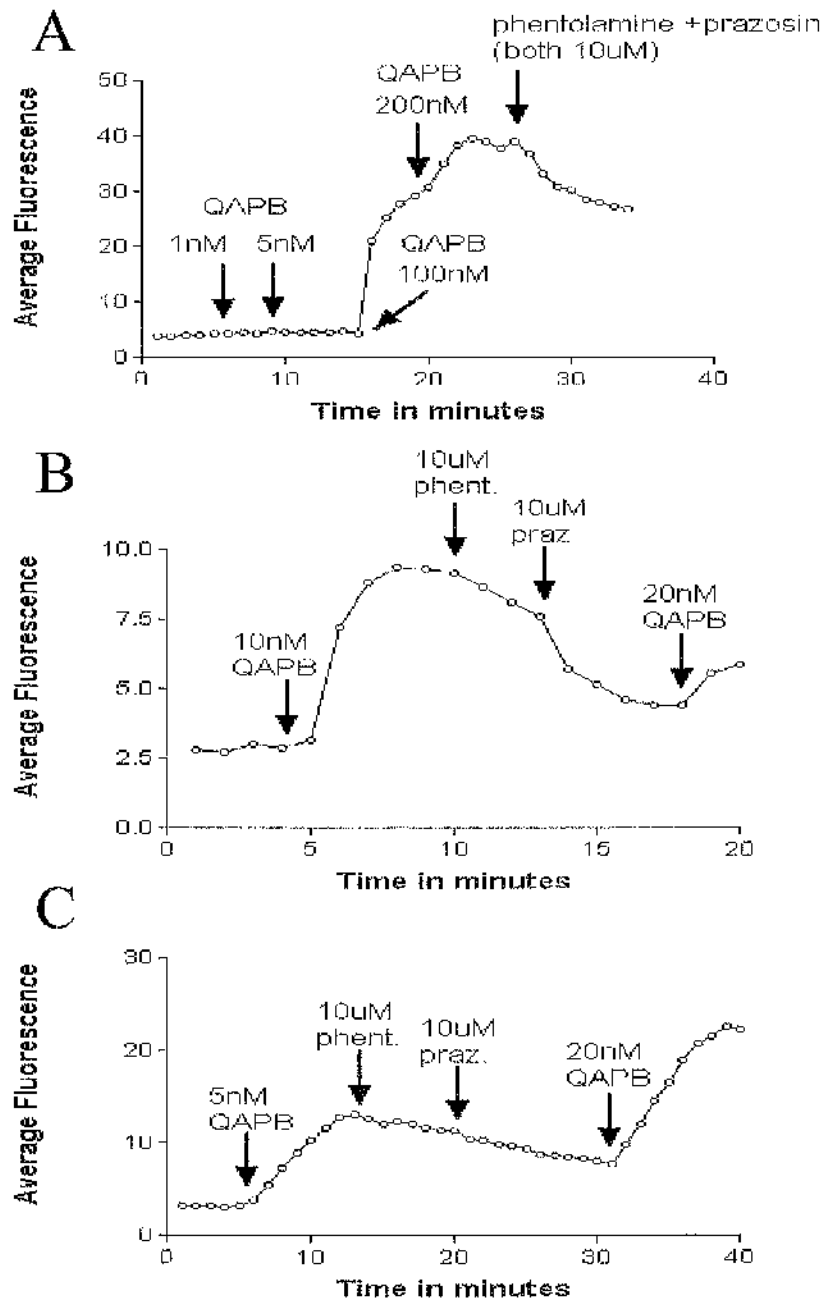


Figure 3.9. Experiments showing the effect of non-fluorescent ligands on QAPB fluorescence development in rat α_{1D} -adrenoceptor transfected fibroblasts.. A) The effect of phentolamine versus 200nM QAPB. B) Phentolamine + prazosin (10uM) vs 10nM QAPB. C) phentolamine + prazosin (10uM) vs 20nM QAPB.

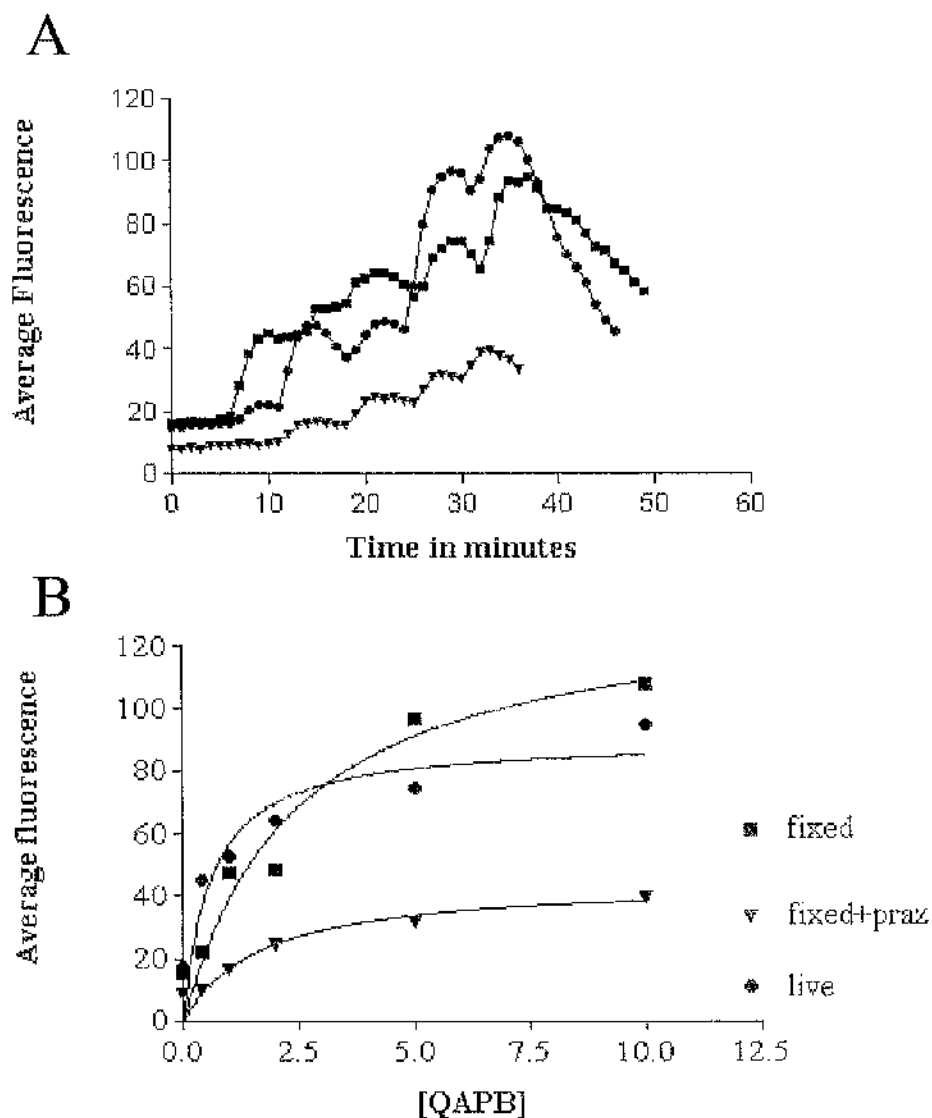


Figure 3.10. Concentration fluorescence curves (A) and saturation curves (B) for QAPB (0.4 - 10nM) versus fixed cells, fixed in the presence of 1μM prazosin and live cells. A) Average fluorescence measured at 1 minute intervals and plotted versus time; live cells (■), fixed (●) fixed + prazosin (▲). B) Peak fluorescence measured at each concentration of QAPB and plotted versus QAPB concentration; live cells (●), fixed (■) fixed + prazosin (▲). Non-linear regression was used to estimate fluorescence KD (FKD) values (see results). Data points represent the mean fluorescence value obtained from a patch of cells comprising 10-15 cells expressing rat α_{1d} -adrenoceptors.

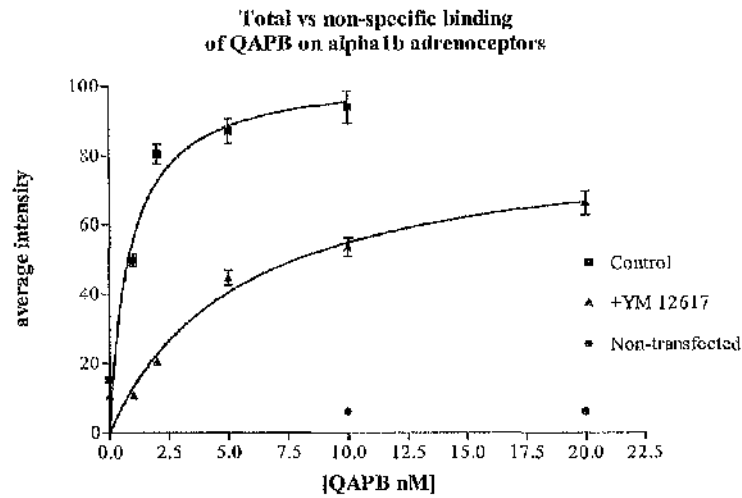
each concentration and performing a non-linear regression analysis, saturation curves similar to those of a radioligand binding study were produced. K_D values were as follows; live cells 0.6nM, fixed cells 2.4nM, fixed + prazosin 1.6nM. These curves represented the first time a saturation binding curve has been constructed (at equilibrium) for a living or fixed single cell. Radioligand binding is a non-equilibrium method. Having proved the principal with prazosin as the competitor it was important to try other α_1 -adrenoceptor antagonists.

YM12617 (also known as tamsulosin) is a high affinity α_1 -antagonist which is structurally unrelated to the quinazoline family of compounds (shown in figure 3.1). YM12617 caused a decrease in the maximum fluorescence and a rightward shift in the saturation curve (FK_D 5.5nM) compared with control experiments (FK_D 0.8nM; n=9; figure 3.11a). The non-transfected control cells displayed no fluorescence at 10 – 20nM QAPB.

The prazosin-related compound (doxazosin 0.1 - 1uM; see figure 3.1) also inhibited QAPB induced fluorescence (figure 3.11b). Control FK_D =1.6nM; + doxazosin 0.1uM = 1.7nM; + doxazosin 1uM = 1.4nM.

So far the saturation curves shown have been of total binding in either the presence or absence of competitor. The next stage of development was to examine the saturation of diffuse (low intensity) and clustered (high intensity) binding and to determine the specific binding using fluorescence. This was tested on the cells expressing the recombinant α_{1D} -adrenoceptor. Incubation with QAPB produced concentration-related fluorescence on the cells. There was virtually no background fluorescence from QAPB in solution and minimal fluorescence from non-transfected fibroblasts demonstrating a high specificity of fluorescence for the presence of the receptors. This enabled capture of a fluorescent image of the α_{1D} -adrenoceptor expressing cells in the presence of the fluorescent ligand which is virtually an image of the receptor distribution (Figures 3.12a-h).

A



B

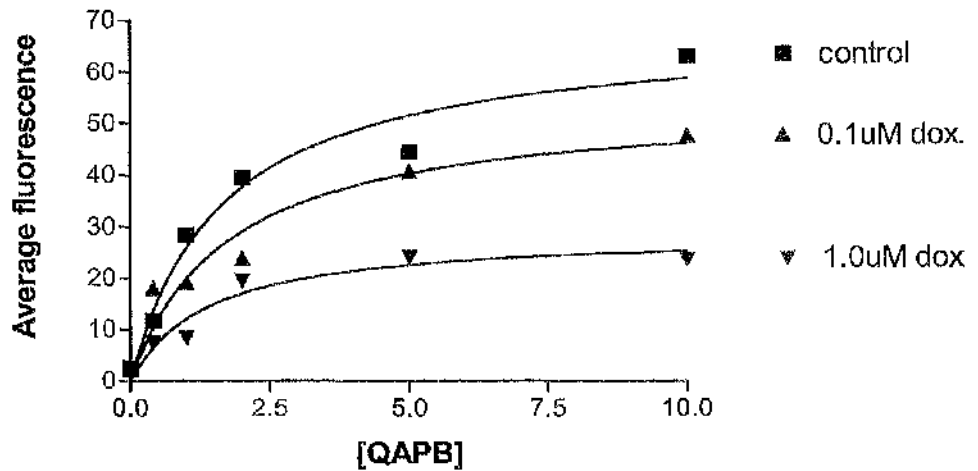


Figure 3.11. Fluorescence saturation curves for control 'live' cells (α_{1b} -adrenoreceptors) in the presence of (A) YM12617 or (B) doxazosin. A) QAPB (0.4-10nM) versus human α_{1b} -adrenoreceptors in the presence (\blacktriangle) and absence (\blacksquare) of YM12617. B) QAPB (0.4-10nM) + doxazosin (\blacktriangle 0.1uM; \blacktriangledown 1uM) versus rat α_{1d} -adrenoreceptors. Estimated FKD values are given in the results section. Data points represent the average of 9 individual cells (a) or average fluorescence from a patch of cells (b).

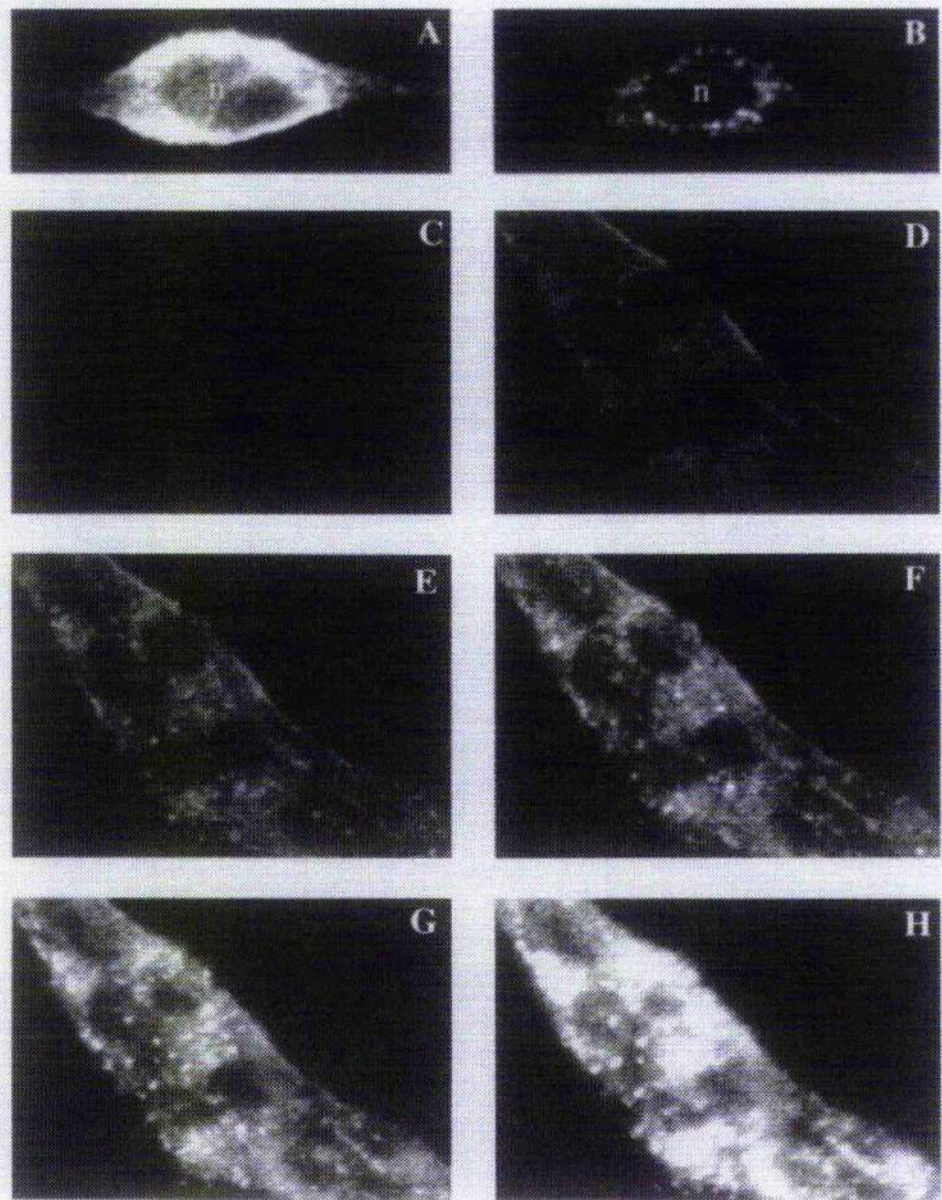


Figure 3.12. QAPB binding-induced fluorescence on α_{1d} -adrenoceptor transfected cells. Patches of cells grown on coverslips were examined by confocal microscopy. A) single cell plus 1nM QAPB. B) 1nM QAPB in the presence of phenoxybenzamine (10uM). C-H) timelapse photography of a patch of 7 fibroblasts. Increasing concentrations (0.4 - 10nM) were added cumulatively and images were collected at 1 minute intervals. C-H) show images collected at equilibrium point for each concentration (C, control - autofluorescence; D, 0.4; E, 1; F, 2; G, 5; H, 10 nM). Images are in greyscale where black indicates no staining and white indicates maximal concentration (saturation) of the fluorophore.

A single cell stained with 1nM QAPB exhibits binding on the cell membrane (figure 3.12a). The presence of phenoxybenzamine (10uM) markedly inhibited the binding of 1nM QAPB leaving only the intracellular sites available. The nucleus (n) contains no binding sites for QAPB. The diffuse fluorescence over the nucleus in (figure 3.12a) is probably the result of light diffraction from the overlying membrane.

For saturation experiments images were taken at 1 minute intervals and each concentration was given time to reach equilibrium, typically 3-6 minutes. Two patterns of fluorescence were visible over a cumulatively increasing concentration range (0.4-10nM). At the lowest concentration (0.4nM) binding sites appeared to be diffuse and tended to be concentrated at the cell membrane/boundaries (figure 3.12d). At 1nM diffuse staining became stronger and clusters of binding sites became visible (figure 3.12d). As the concentration increased to 10nM (figure 3.12e-h) the clusters became visibly more distinct from the diffuse staining.

Image analysis.

The digital image contains considerable information on the concentration as well as localisation of the fluorescent ligand-receptor complex. The image was segmented into three regions of interest, i. the high intensity 'clusters', ii the mid-range intensities and iii. lower intensity 'diffuse' fluorescence, to compare how much of the total receptor population each represented and to assess whether their affinities differed (figure 3.4a-d). The regions were set according to the images obtained at 5nM QAPB (figure 3.3e). This shows that the majority of the total fluorescence emanates from the diffuse and mid-range regions (41.2 and 43.2% respectively), even though the average fluorescence intensity of the clusters is greater. The clusters cover 9.4% of the cell area and contain 15.5% of the total fluorescence and hence receptors. The diffuse staining covers 54.9% of the total cell area providing 41.2% of the total fluorescence. This data is summarised in table 3.2

	Total Intensity (%)	Cell Coverage (%)	Average Intensity
Red (65-128)	41.2	54.9	96.7 ± 17.6
Green (129-191)	43.2	35.6	156.5 ± 17.5
Blue (192-255)	15.5	9.4	212.4 ± 16.8

Table 3.2. Analysis of the image obtained after incubation with 5nM QAPB (figure 3.12 & 3.13). Red represents the low level (diffuse) staining. Green and blue represent the mid-range and clustered staining respectively, numbers in parentheses show the actual range of pixel intensities analysed in each range. Values between 0 and 64 are considered as background noise in this example.

The data can be scattered and fit by a non-linear regression to give a fluorescence half maximum (FHM) value in nM (Figure 3.13c&d). The mid range intensities (green) produced a value of 1.6, slightly higher than the low (diffuse; red) and high (clustered; blue) ranges which produced identical values of 1.3nM, consistent with the K_i (1.04nM) calculated from displacement of ^3H -prazosin with QAPB. This is of course total binding, although the very low fluorescence from non-transfected cells suggests that the amount of non-specific binding at the concentrations employed is negligible.

Specificity of binding was further defined in a separate series of experiments in which absolute values of fluorescence intensity were measured over a range of concentrations under identical conditions in separate sets of cells. Data was collected from experiments in the absence (total binding; example cell shown in figure 3.13e) or presence (non-specific binding; example shown in figure 3.13f) of 10 μM phentolamine and used to construct a specific binding curve (Figure 3.13g; $K_D = 3.9 \pm 0.74$ nM). Scatchard analysis of the specific binding curve for ^3H -prazosin binding

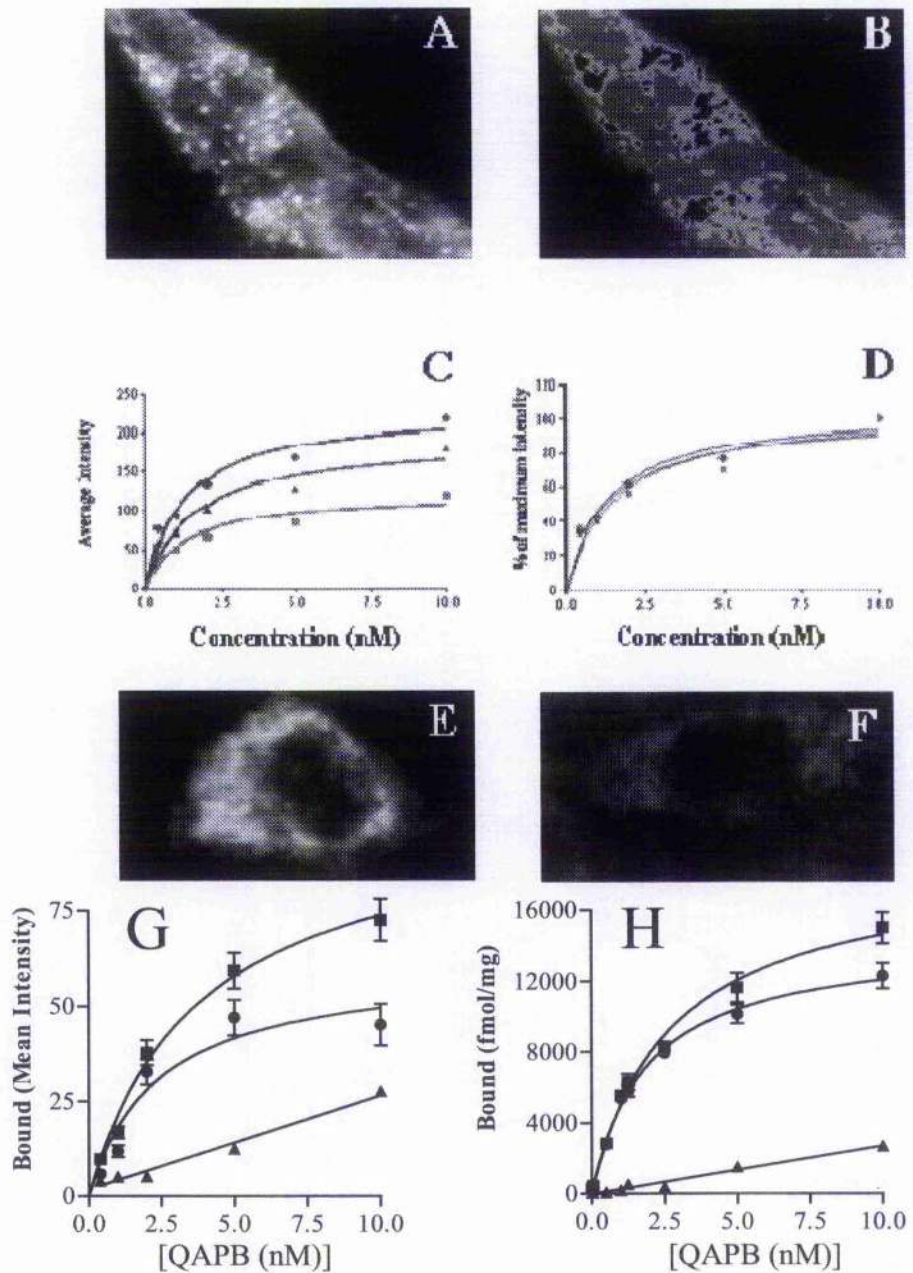


Figure 3.13. A-D) Image analysis of the data set shown in figure 3.12. A) 5nM QAPB staining (taken from fig 3.12e). B) The diffuse, mid-range and clustered areas were separately analysed. The image of the receptors was split into low intensity (65-128; red) "diffuse" areas, mid-range intensity (129-191; green) and high intensity (192-255; blue) "clustered" areas, prepared from figure 3.12e. C) The "masks" were then used to construct saturation curves. D) The data from figure c as percentage of maximum fluorescence. E) control cell (1nM QAPB). F) 1nM QAPB + phentolamine 10uM. G&H) Total (■), Specific (●) and non-specific (▲) binding of radiolabelled (H) and fluorescent-labelled 'prazosin' (G) to α_{1d} -adrenoceptors. Non-specific binding was determined in the presence of 10uM phentolamine.

to α_{1d} -membranes produced a K_D of 1.89 ± 0.15 nM. Thus the binding characteristics of fluorescent QAPB on living cells and radioactive prazosin on membrane fractions are very similar as shown by their dissociation constants and saturation binding curves (figure 3.13g & 3.13h).

3-dimensional visualisation and localisation of QAPB (30nM) binding to α_{1d} -adrenoceptor transfected fibroblasts.

Cells were grown on coverslips and visualised on an inverted CLSM. QAPB (30nM) was added to the cells and allowed to achieve equilibrium (15 minutes). This relatively high concentration was required in order to optimise the confocality (in the absence of any deconvolution) by using a 15 μ m slit. Without washing, individual cells were selected for serial sectioning and reconstruction. 30 serial sections (0.3 μ m apart) were collected along the z-axis of the cell. The data set was then reconstructed as a simulated fluorescence projection (sfp; figure 3.14a). In the presence of phenylephrine (10 μ M) the fluorescence was significantly reduced (figure 3.14b). Z-sectioning was used to determine the degree of intracellular fluorescence. Figure 3.14c shows a single xy-section, indicating the presence of fluorescence inside the cell. The xz and yz-sections also indicate intracellular fluorescence at the planes studied. The presence of intracellular sites was confirmed in all experiments. Figure 3.15 shows z-sectioning on two representative experiments (QAPB 10nM). In both panels (figure 3.15a & b) the xz and yz-sections show clear intracellular staining. However, the cells have regions where the fluorescence is largely confined to the cell membrane (figure 3.15a, figure 3.16). Examples of visualisation methods are shown in figure 3.16. The z-sectioning method is useful for determining spatial distribution at a single plane/section. Figure 3.16a shows a more detailed z-section of the intense membrane binding shown in figure 3.15a. The z-sections show strong binding within the membrane. The SFP reconstruction of the full data set (of figure 3.16a) confirms the membrane binding (figure 3.16b). To visualise the membrane binding from any angle

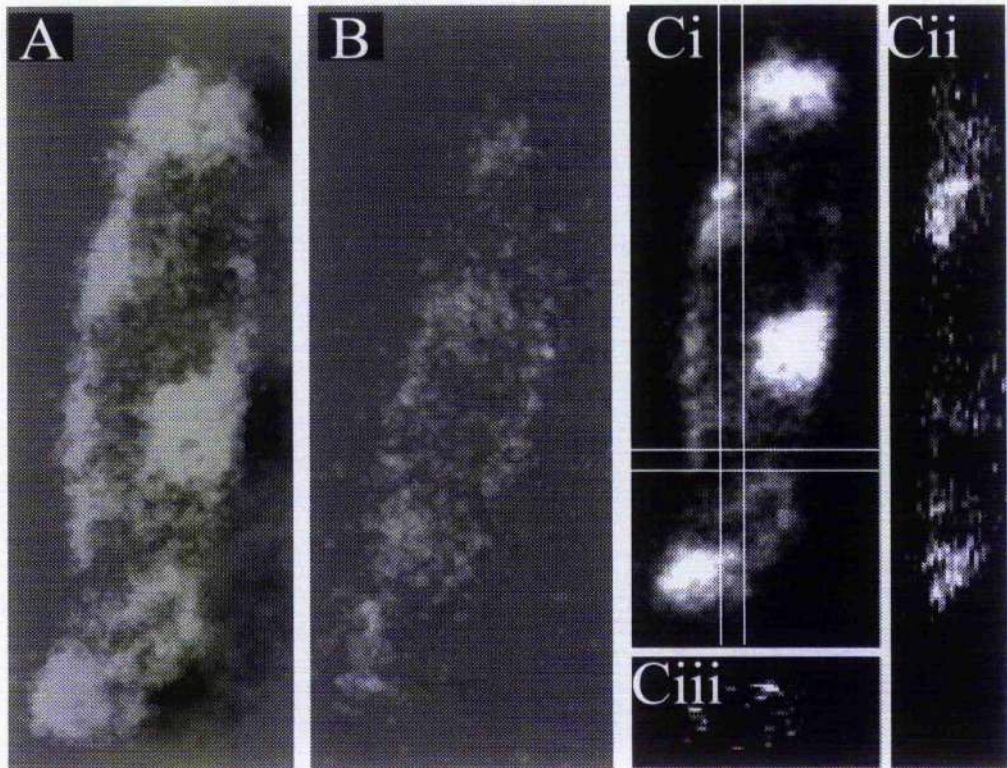
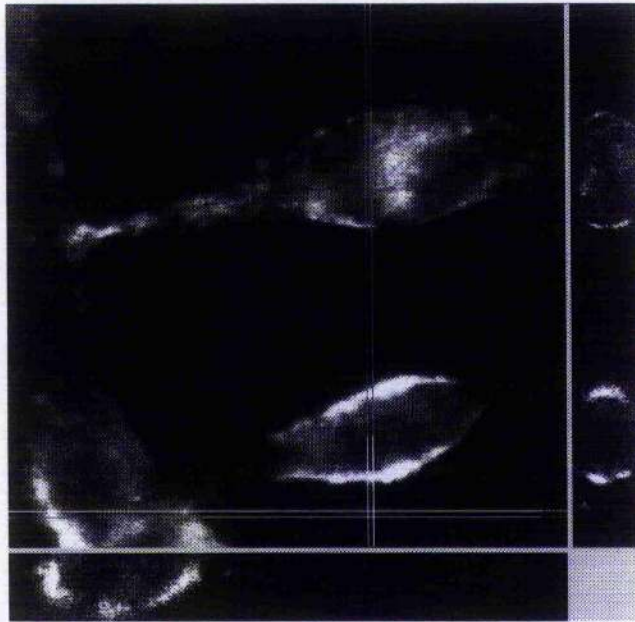


Figure 3.14 A. and B. QAP-B-induced fluorescence is shown on two similar cells, one in the absence (A), the other in the presence (B), of the α_1 -adrenoceptor agonist phenylephrine ($10\mu\text{M}$). This view shows the overall reduction in fluorescence produced by phenylephrine. Measuring the "total" fluorescence the cell exposed to phenylephrine had 30% of that on the other cell. This difference is likely to be due to competition between the two ligands rather than down regulation of receptors since the time of exposure was short (20 min). C. The sub-cellular location of QAP-B (30nM) binding is shown. (Ci) shows a single optical section (x-y plane) through the middle of the cell. The bright areas indicate regions of intense binding at the cell edges. An impression of the three dimensional distribution can be obtained by resectioning the cell. y-z (Cii) and x-z (Ciii) sections are shown: these are taken from between the vertical or horizontal lines, respectively. These views suggest that both membrane located and intracellular binding sites exist for QAPB.

A



B

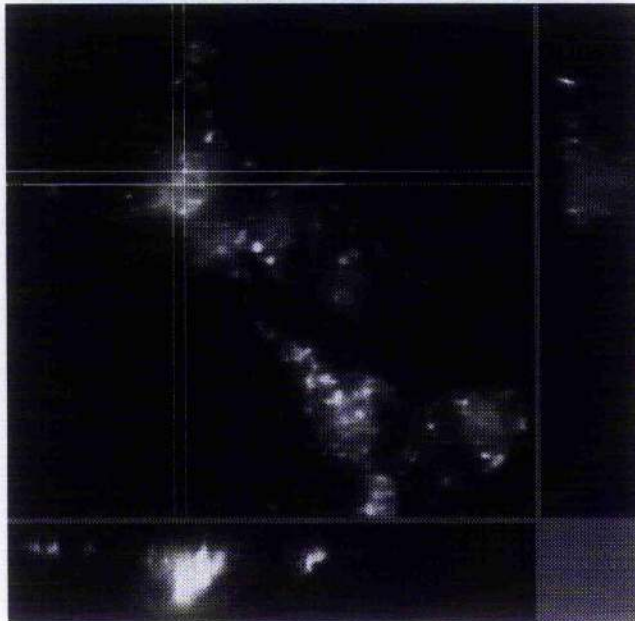


Figure 3.15. Z-sectioning of two groups of fibroblasts. QAPB (10nM) binding to α_{1d} -transfected fibroblasts. A) 3 fibroblasts showing strong membrane binding. B) A group of fibroblasts showing diffuse and clustered intracellular binding. Both groups of cells are obtained from the same cell line and represent the heterogeneity of cells in culture with respect to receptor distribution.

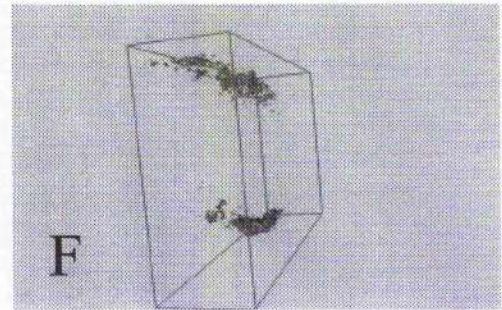
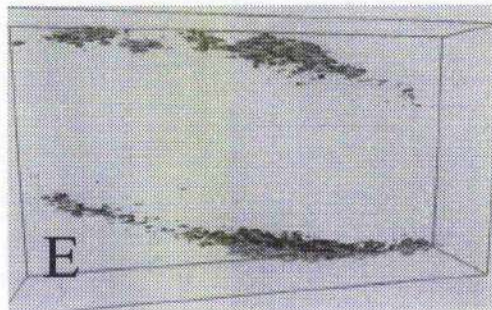
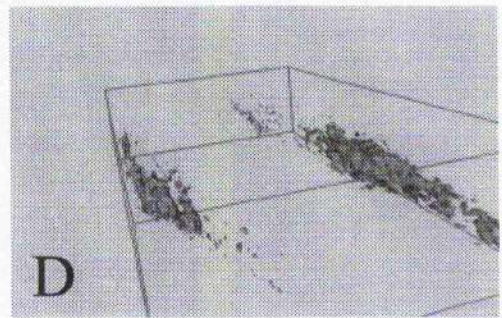
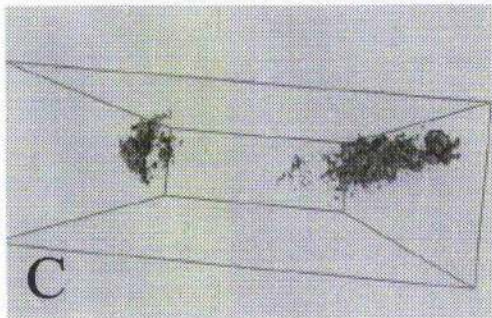
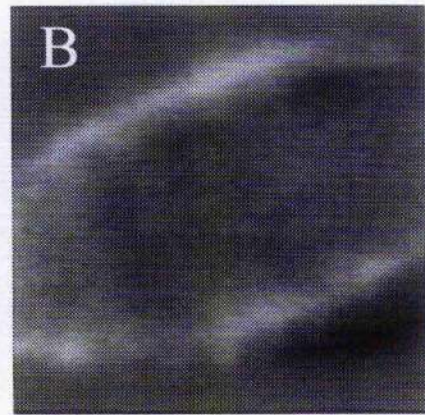
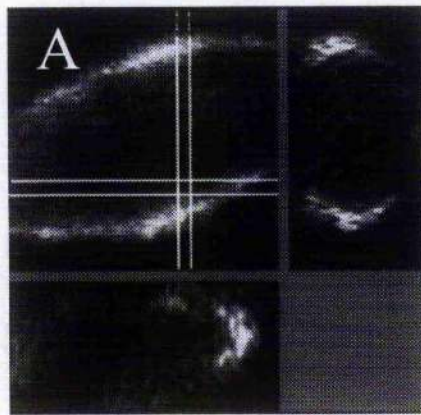


Figure 3.16. Three different methods of visualising the same data set. The data is a subset of data taken from fig 3.15a. A) Z-sectioning the subset using the same method shown in fig 3.15. B) the simulated fluorescence projection (SFP) mode. C-F) Different views of the fully interactive iso-surface model. All methods are supplied as part of the Imaris visualisation software suite.

or magnification it is possible to build a 'virtual' iso-surface model (see methods). Four views of the data set are shown in figures 3.16c-f. The flat images do not fully convey the flexibility offered to the viewer by using this method. It is possible to fly through the data and even position the viewer in the middle of the data set.

This iso-surface analysis was further developed by combining multiple channels of data. Figure 3.17 shows a variety of views of a single cell (α_{1d} -transfected) which is displayed as 3 channels of data comprising the nucleus, diffuse membrane binding and clustered (intracellular) binding.

QAPB (0.1 μ M) binding to whole tissue.

Using the CLSM optical sections from the media of rat mesenteric artery and basilar artery were examined. The rat mesenteric artery (RMA) was incubated in 0.1 μ M of QAPB (a concentration which is at the upper limit of its selectivity) for 30 minutes. Optical sections were collected along the optical axis. Selected optical planes are shown in figure 3.18. Staining in the mesenteric artery was greatest in the medial smooth muscle layers (figure 3.18b). The adventitia showed clustered staining (figure 3.18a) while there was little visual evidence of staining in the intima (figure 3.18c).

Rat isolated basilar artery was studied under identical conditions to those described above for RMA. Figure 3.19a shows the same image from figure 3.18b for reference. Figure 3.19b shows a medial optical section of the basilar artery. The relatively poorer staining of the basilar artery is consistent with the lack of contractile responsiveness to noradrenaline in this vessel. In both plates the out-of focus autofluorescent internal elastic lamina in a lower plane can be seen running perpendicular to the smooth muscle orientation.

QAPB binding to non-vascular smooth muscle cells of the rat anococcygeus was also examined. Once again an image of RMA is shown for reference (figure 3.20a). Figure

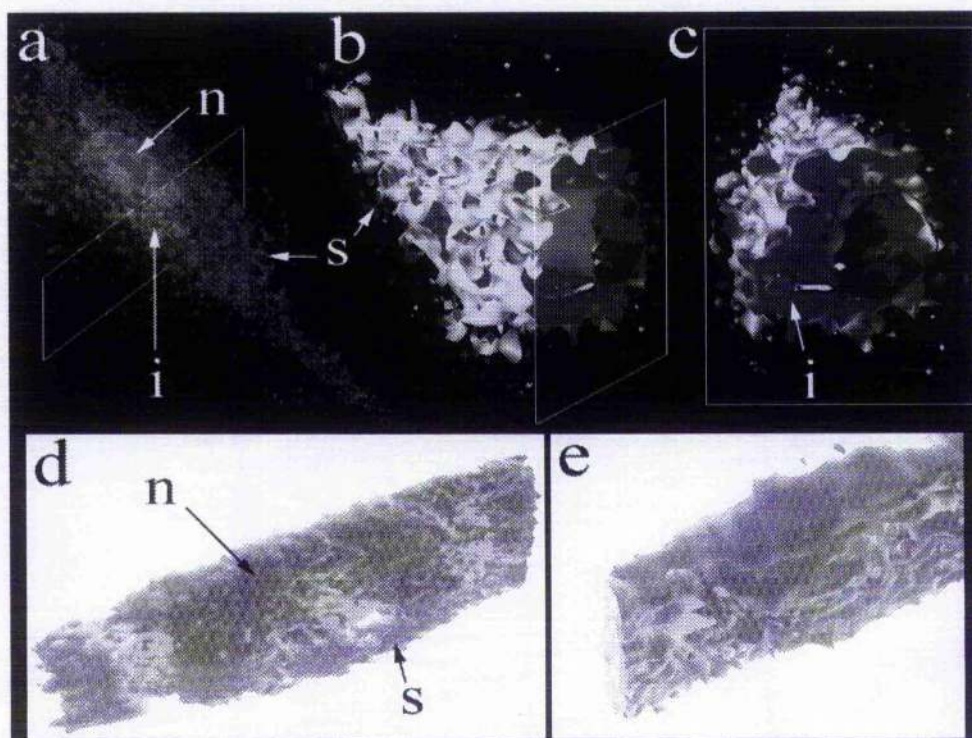
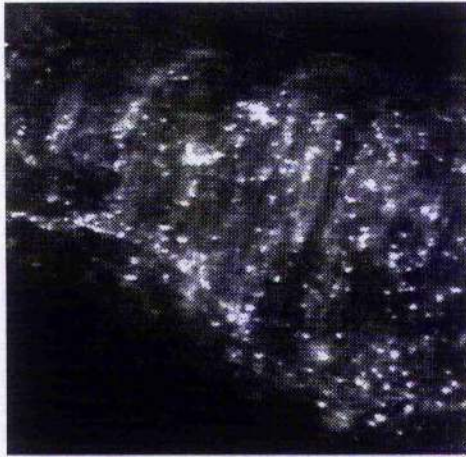
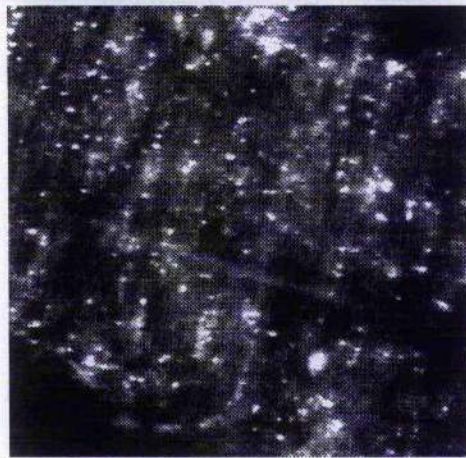


Figure 3.17. Images a-c show 3D localisation of QAPB-associated fluorescence (100nM) on the cell membrane (yellow) and in the cytosol (blue) of rat-1-fibroblasts transfected with α_{1d} -adrenoceptors. 3D images were constructed using the ISO-surface module of IMARIS on a SGI workstation. Two ISO values were selected, one for the surface (s) and another for the intracellular (i) QAPB signal. A separate ISO value was selected for the nucleus (red) using a nuclear stain (Syto13). Images b and c are cut to show the location of intracellular QAPB-associated fluorescence. Images d and e show 3D localisation of QAPB-associated fluorescence (0.4nM) on the membrane (blue) and the nucleus (yellow) of a freshly dissociated human prostatic smooth muscle cell. (see chapter 4 for cell dissociation method).

A



B



C

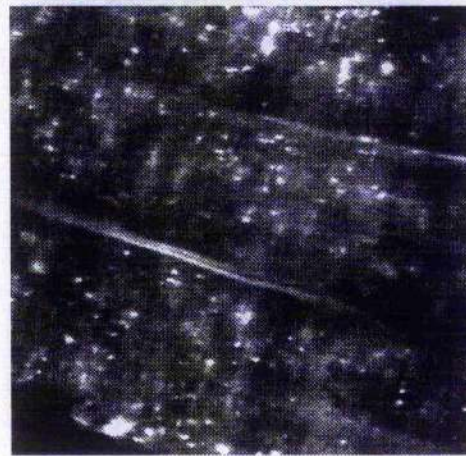
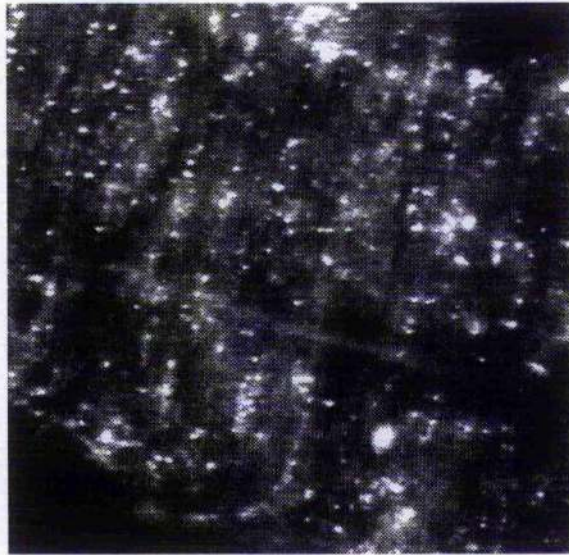


Figure 3.18. QAPB (100nM) binding to whole mount (slide mounted) segments of rat mesenteric artery. Bright spots represent regions of high intensity binding. A) adventitial optical section. B) medial optical section showing binding consistent with SMC orientation. C) luminal section showing less binding and internal elastic lamina gooves. x40 objective (0.57 optical zoom); field size 200um square.

A



B



Figure 3.19. Comparison of QAPB (100nM) binding to rat mesenteric artery medial smooth muscle cells (A) and rat isolated basilar artery smooth muscle cells (B). x40 objective (0.57 optical zoom); field size 200um square.

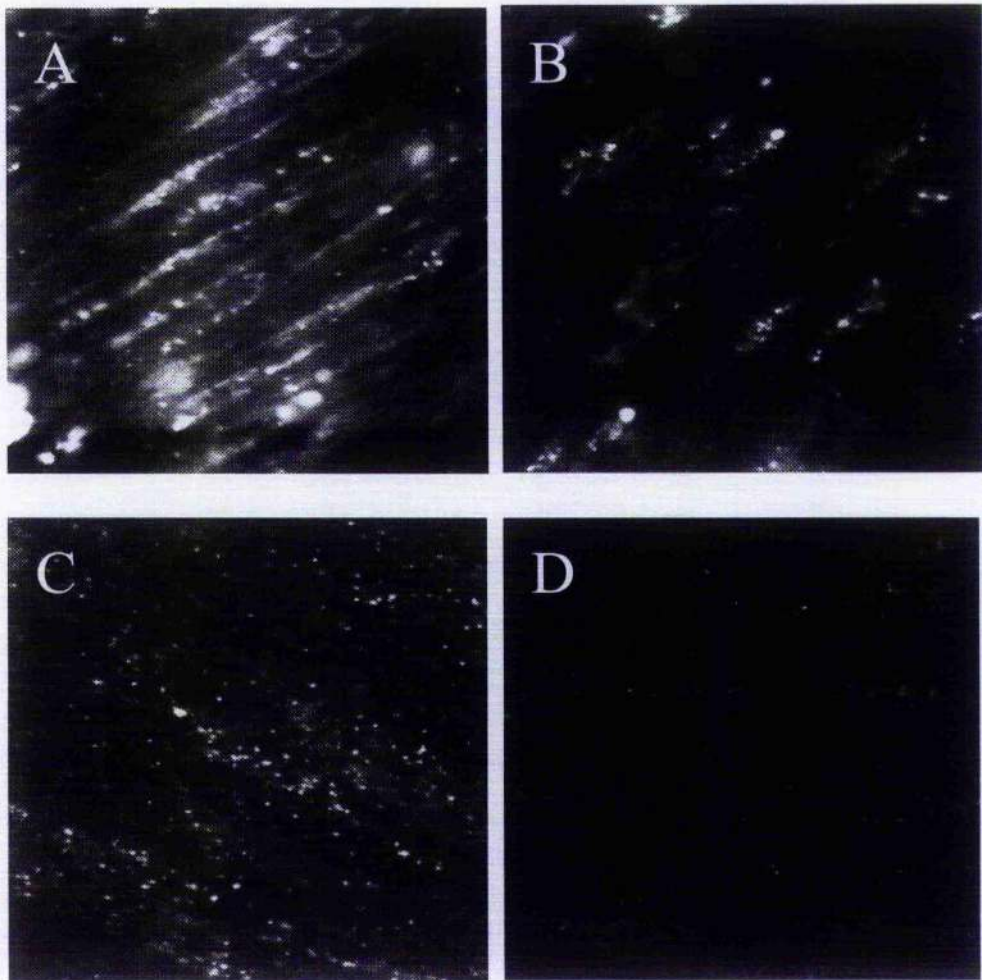


Figure 3.20. Comparison of QAPB (100nM) binding to rat mesenteric artery medial smooth muscle (A) and rat anococcygeus smooth muscle (C). Binding was also examined in the presence of 10uM phenoxybenzamine for mesenteric artery (B) and in the presence of 10uM YM12617 for anococcygeus (D).

(A&B) x60 oil immersion objective; field size 70um square.

(C&D) x40 water objective; field size 100um square.

3.20b shows the effect of preincubating RMA with 10uM phenoxybenzamine prior to application of QAPB (0.1uM). Figure 3.20c&d shows QAPB binding to anococcygeus smooth muscle prior to (3.20c) and following preincubation with YM12617 (10uM) (3.20d). QAPB binding to anococcygeus smooth muscle was consistent with the orientation of the cells. This is similar to the observations made for QAPB binding in the media of RMA (figures 3.19a & 3.20a).

QAPB binding to transverse sections of rat mesenteric artery.

Figure 3.21 shows a diagram of the method used to study binding to transverse sections of RMA (see methods section for details). QAPB bound to transverse sections to produce a strong fluorescence signal at 5-10nM. Binding was most notable in the regions of internal and external elastic lamina (figure 3.22b & 3.22c). Use of the low (more specific) concentration of QAPB required use of a wide confocal slit (i.e. 100um). Reducing the slit to 15um for the 10nM QAPB response confirmed binding in the external lamina. The time course of binding in both lamina and media was examined using a 'region brightness over time' function. The average data is plotted in figure 3.23a. The time course graph indicates that fluorescence developed more quickly in the lamina than in the medial smooth muscle. These findings are discussed in the next section.

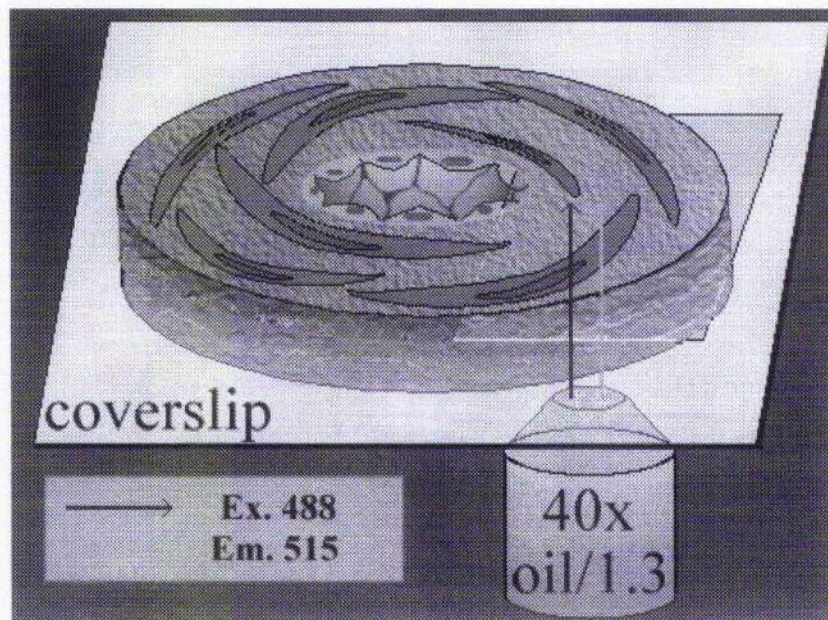


Figure 3.21. Schematic diagram of the method used to study QAPB binding on transverse sections of blood vessels (details in methods section). This setup enables the use of high NA oil immersion objectives and thus optimal confocality can be achieved if the fluorescence signal is great enough. More importantly the method enables visualisation of inner and outer layers of smooth muscle simultaneously.

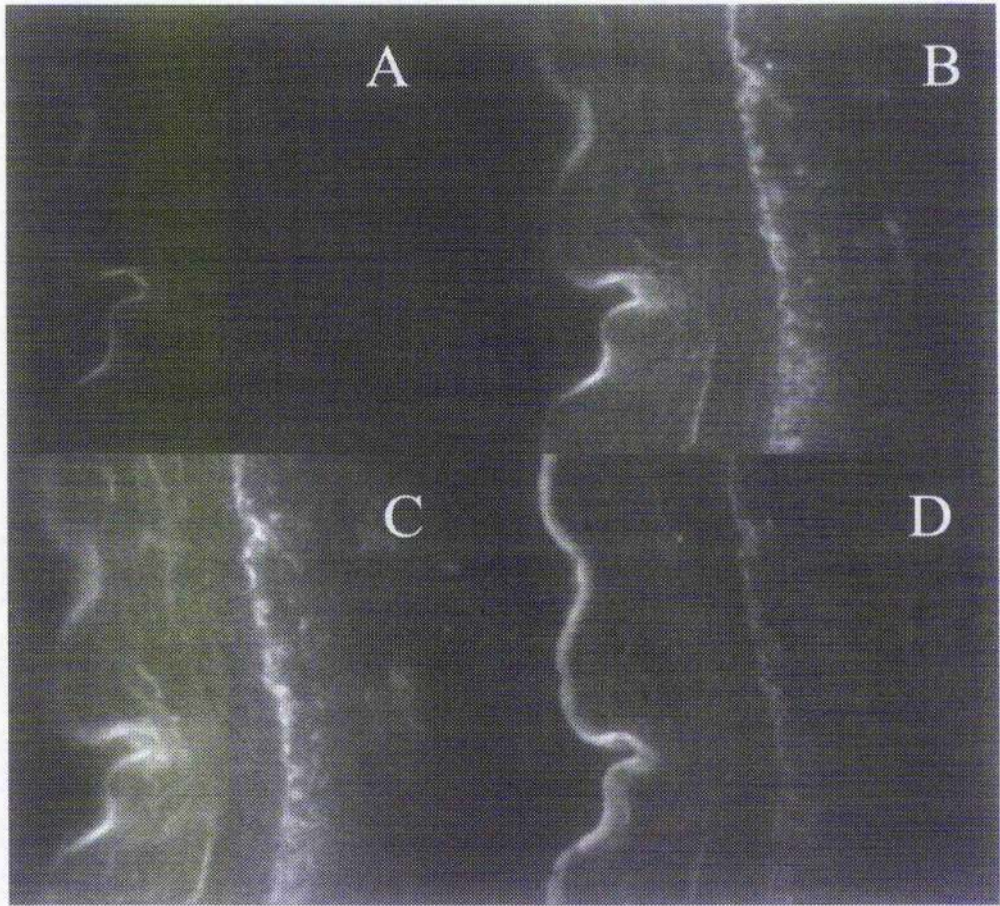


Figure 3.22 . CLSM optical images (extended focus models, 100um slit) of rat mesenteric artery transverse sections mounted as shown in figure 21. A) autofluorescence from unstained tissue. (B). Binding of QAPB 5nM. (C) QAPB 10nM binding. (D) The section in (C) imaged using a 15um slit to increase confocality (BUT reduce the fluorescence). x40 oil immersion objective; field size 102um.

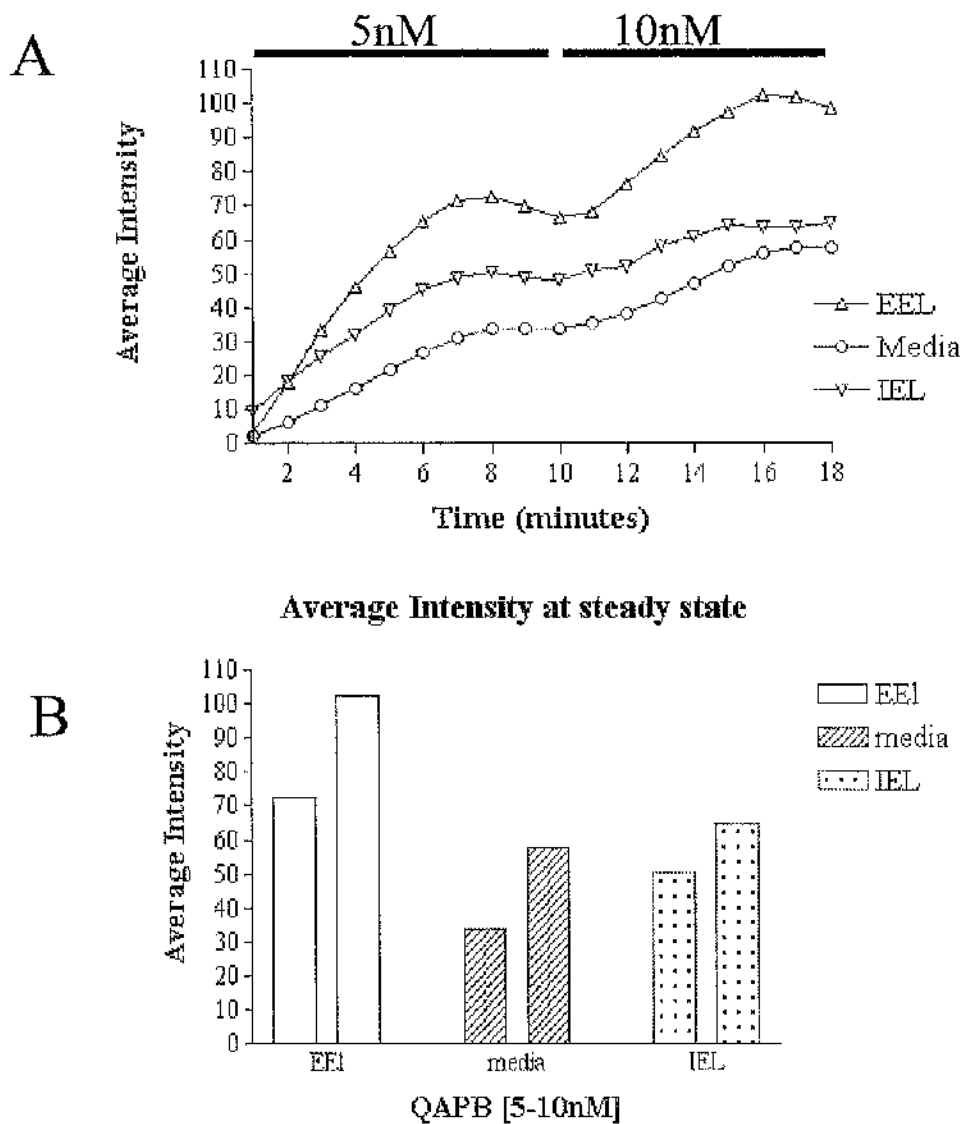


Figure 3.23. The graphs show the fluorescence development of QAPB (5-10nM) on the transverse sections shown in figure 3.22. A) Fluorescence development plotted versus time. B) Average data plotted as a bar chart showing maximum intensity in three regions of the vascular wall. The data were collected by defining a region outlining the two lamina and media and then following the development of fluorescence at 1 minute intervals.

Discussion.

The results of this chapter have produced the only available characterisation of the fluorescent ligand QAPB (BODIPY FL-prazosin). The model presented here could be applied to the validation of any new fluorescent ligand which may be developed. There is a growing list of fluorescent peptides which are currently available (eg fluo-endothelin, fluo-angiotensin & fluo-NPY; Advanced Bioconcepts, Canada). In addition, a current collaboration with Prof. D. Robins (Chemistry Dept., Glasgow University) has resulted in the production of two novel fluorescent compounds, FITC-QAPB (α_1 -AR ligand) and rhodamine-yohimbine (α_2 -AR ligand). Both compounds are currently being evaluated by Professor McGrath's group.

A recent collaboration with Advanced Bioconcepts provided positive results in the study of NPY receptors in rat anococcygeus. The validation methods outlined here were perfectly suited to testing of a fluo-peptide on living tissues.

Many of the advantages of confocal microscopy (table 3.1) could have been identified based on technical theory alone. In practice, many other key issues emerged which on one hand caused delay but on the other provided fascinating new avenues to explore.

Following the routine pharmacological analysis, it was necessary to consider some aspects of what is expected of 'membrane bound' receptors. Interpretation of image data is a considerable departure from reading averaged data presented in graphical form. Ironically, it became clear at an early stage that in order to quickly convey image data it is necessary to have a means of graphing it.

Since the image data to be generated represented ligand-binding processes it seemed reasonable to apply known pharmacological methods (and theories) to the image analysis process.

The most demanding part of image analysis is in not seeing. This was perfectly demonstrated in chapter 2 where efficient image segmentation is the barrier. In receptor imaging we see total (specific and non-specific) binding. We are also blinded by our prejudices concerning what we 'know' to be true from non-image based functional studies.

Aside from the technical construction of the fluo-ligand (discussed later), the experiment can be made simpler by staying within the specific concentration range of the fluo-ligand. Knowledge of the native ligand pharmacology cannot be relied on. The first (and most important) question to be asked of any ligand must be affinity at the receptor. Fluorescent characteristics are secondary.

Affinity and Selectivity.

The most important characteristic of any fluorescent ligand should be that it retains as much as possible of the affinity and selectivity of the related un-labelled compound for the receptors of interest.

Borate-dipyrrromethene (BODIPY) has become one of the most popular fluorophores in recent years and a variety of receptor and ion-channel ligands have been synthesised (table 3.3). BODIPY iodoacetamides have very high fluorescent yields,

Table 3.3 Receptor selective fluorescent probes.

Ligand	Site of action
BODIPY FL-prazosin (green)	α -adrenoceptors ¹
BODIPY FL-prazosin (red)	α -adrenoceptors ²
BODIPY CGP 12177A	β_2 -adrenoceptors ³
BODIPY FL-ABT	muscarinic receptors ⁴
BODIPY pirenzepine	muscarinic (M1) receptors ⁵
BODIPY α -bungarotoxin	nicotinic receptors ⁶
BODIPY FL-NAPS	D2-receptors ⁷
BODIPY FL-SCH 23390	D1-receptors ⁸
BODIPY Ro-1986	benzodiazepine ⁹
BODIPY dihydropyridine	Ca ⁺⁺ Channels ¹⁰

The table shows a selection of site selective BODIPY ligands which are currently available. This is by no means an exhaustive list. The purpose of this table is to emphasise the growing popularity of BODIPY as a fluorescent conjugate. The site of action is that claimed by the manufacturer or from studies undertaken by the cited authors. Many of the probes listed are available in both red and green versions as shown for prazosin.

1. McGrath, J.C. and Daly, C.J. (1995) *Pharm. Comm.*, 6(1-3), 269-279
2. Spence, T.Z. (1993). *Bio Probes 18* . Molecular Probes, Inc.
3. Heithier, II., *et.al.*, (1994). *Biochemistry*, 33, 9126-9134
4. Spence, T.Z. (1994). *Bio Probes 22* . Molecular Probes, Inc.
5. Wang, Y., Gu, Q., Mao, F., Haugland, R.P. and Cynader, M.S. (1994) *J.Neurosci.*, 14, 4147-4158
6. Robitaille, R., Adler, E.M. and Charlton, M.P. (1990) *Neuron*. 5, 773-779
7. Aboud, R., Shafiq, M. and Docherty, J.R. (1993). *Br.J. Pharmacol.*, 109, 80-87.
8. Ariano, M.A. *et. al.* , (1989) *Proc. Natl. Acad. Sci.* 86 (21), p8570-8574
9. Velazquez, J.L., Thompson, C.L., Barnes, E.M. Jr and Angelides, K.J. (1989) *J. Neurosci.* , 9, 2163-2169
10. Goligorsky, M.S., Colflesh, D., Gordienko, D and Moore, J.C. (1995) *Am J Physiol.* , 268, F251-F257.

are relatively pH insensitive and long wavelength versions are also available (Haugland 1992). A crucial issue is whether the addition of the fluorescent moiety affects ligand affinity. A comparative study of BODIPY and another fluorescein derivative (FITC) of CGP 12177 demonstrated that the BODIPY conjugate exhibited 10 fold higher affinity for the recombinant human β_2 -receptor than did the FITC conjugate (Heithier et al., 1994).

QAPB was validated as a competitive antagonist versus phenylephrine's production of inositol phosphates and as a competitive ligand versus ^3H -prazosin, confirming that it is a ligand for functional α_{1D} -adrenoceptors. The binding and functional antagonism data shows that despite the modification of the molecule to incorporate the fluorescent tag, it retains the properties required of a high affinity pharmacological "antagonist" ligand. The affinity for QAPB versus ^3H -prazosin (-Log $K_i = 8.9$) is slightly higher than the derived pA_2 values of 8.25 (in rat aorta) and 7.78 (vs IP₃ generation in transfected cells) and is consistent with other comparisons of binding and functional antagonism which tend to imply higher affinity in radioligand binding studies.

Functional studies with QAPB suggest that this compound has an approximately ten fold lower affinity for α_1 -adrenoceptors than prazosin (QAPB pA_2 8.25 vs phenylephrine in rat aorta; 7.9 vs phenylephrine in rat anococcygeus; 7.6 vs noradrenaline in rabbit saphenous artery). A reduction in affinity caused by conjugation of the BODIPY in place of the furan ring in prazosin might be expected given the large size of the BODIPY ring structure (Mole wt. prazosin HCl 419.9;

QAPB 563.41). The good retention of affinity probably derives from the placement of the substituent away from the parts of the molecule involved in binding.

Anderson and Cohen (1974) attributed the reduced affinity of α -bungarotoxin (conjugated to either fluorescein isothiocyanate or tetramethylrhodamine isothiocyanate) to the fact that the dyes react with amino acid residues which alter their charge. Faure *et.al.* (1994) report identical K_i values for fluo-NT and unlabeled NT. Heithier *et.al.*, have reported similar K_D values for both BODIPY CGP 12177 and native CGP 12177. It is possible therefore to add a fluorescent molecule to a ligand with minimal alteration to its affinity although this will depend largely on the structure of the native ligand. Choice of "substrate" drug therefore becomes an important factor in the synthesis of any putative fluo-ligand.

Visualisation and construction of concentration / fluorescence curves and competition binding studies on live cells.

With QAPB it is not necessary to remove the unbound ligand by washing the tissues before visualisation. The lack of any significant background fluorescence makes it possible to measure fluorescence at equilibrium and to record the development of fluorescence/binding with time. The binding over time can be performed by time-lapse recording at a fixed focal plane. Fluorescence measured in this way is both time and concentration dependent (figures 3.5 & 3.7). Analogous to ligand binding studies, pre-incubation of cells in a high concentration of a 'cold' competitor shifts the fluorescence curve to the right revealing the extent of non-specific binding (figure 3.8, 3.10 & 3.11). Cultured cells show low non-specific binding and a ready visualisation

of the recombinant receptors which gives some confidence that the ligand might allow visualisation of receptors in native tissue.

Initial experiments were designed to produce good quality images under optimal confocal conditions (figure 3.5). The high quality images permitted image analysis using masks which could be used to investigate the fluorescence development in different regions of the cell. However, further work demonstrated that use of such high concentrations (i.e. >10nM) caused a degree of non-specific binding which was difficult to displace with non-fluorescent competitor ligands (figure 3.9). Nevertheless, even very high concentrations of QAPB (10 -- 100nM) could be inhibited by preincubation with prazosin (figure 3.8). The difficulty in displacing QAPB from its binding sites awaits clarification. Current work in Professor McGrath's laboratory suggests that QAPB may dissociate very slowly from its receptor. Furthermore, the competitor ligand may not have access to QAPB-bound intracellular receptors.

In order to reduce the concentration of QAPB required to produce a detectable signal it was necessary to compromise the image quality by increasing the PMT gain and opening the confocal slit. Compare figure 3.12h (10nM QAPB; 100um slit) with figure 3.5 (plate 20; 150nM QAPB; 15um slit). If a 100um slit had been used for the 10-160nM curve the signal would have saturated resulting in a useless image for quantification purposes. If a 15um slit had been used for the 0.4-10nM curve there would have been no detectable signal since around 90% of the light is rejected by the slit. Experiments on live and fixed cells in the presence and absence of high affinity

α_1 -antagonists proved that it is possible to construct saturation binding curves for individual cells which exhibit similar characteristics to the binding of the native ligand in conventional radioligand binding studies (figures 3.10 & 3.11).

If the interpretation is correct, then the fluorescence binding characteristics should correspond quantitatively to the other pharmacological measures. The binding characteristics of QAPB's fluorescence (FK_D between 1-5nM) lay between its functional competitive antagonism at the α_{1d} -adrenoceptor ($A_2 = 12nM$) and its displacement of 3H -prazosin ($K_D = 2nM$). A further corollary confirming that fluorescence indicates the ligand-receptor complex is the reduction of fluorescence by other competitive ligands for the site. Experiments performed in the presence of phentolamine (figure 3.13g) allow the quantification of "specific" binding. In fact this is an extremely useful feature of fluorescence binding because image subtraction can remove the non-specific binding leaving only the image of the receptors which have been "removed", i.e. competitively antagonised by the competitor.

A requirement for efficient ligand binding is the ability to use the ligand at concentrations which are low in relation to its binding affinity. To represent receptor binding, the concentration of unlabelled ligand displacing 50% of the labelled ligand should be similar to the K_D . It proved possible to use the fluorescent antagonist QAPB on live cells at similar concentrations to those of 3H -prazosin on membrane preparations in radioactive binding experiments. A study of α_{1b} -adrenoceptors using flow cytometry (Hirasawa *et.al.*, 1996) examined QAPB binding at $1\mu M$, a concentration which is almost certain to have significant non-specific effects. Similarly, Wang *et.al.*, (1997) employed 50-500nM

of QAPB to study α_1 -adrenoceptors in rat cultured cortical neurons. Interestingly, the same group also reported an apparent K_i for QAPB of 64nM (vs 10nM [3 H]-prazosin). This is in contrast to our estimation of 1.24nM (vs 0.2nM [3 H]-prazosin). It is clear from the present work and other studies with QAPB that great caution should be taken in the interpretation of fluorescence-derived images. It is crucial that for any given tissue and receptor subtype the degree of non-specific binding at the concentrations used should be determined. In this study I have sacrificed a certain degree of confocality (i.e. by using a wide, 100 μ m, slit) thus retaining ligand specificity in the low nM range (0.4-10).

Since the detection is by microscopy, analysis can be made on the subcellular level and under physiological conditions, both of which are advances on radioligands. New information on both of these aspects was found in relation to "clusters" of receptors, which have previously been demonstrated by immunohistochemistry in fixed tissue for several receptor types. For example, Uhlen *et al.*,(1995) using antibodies for epitope tagged receptors, reported that α_{2a} -adrenoceptors exist as two populations of diffuse and clustered receptors which is in accord with the known clustering of G proteins.

This study demonstrates for the first time the existence of diffuse and clustered populations of α_1 -adrenoceptor binding sites in live cells. The results indicate that the affinity of both populations for the ligand is identical. This shows that the environment of the clustered domain leaves the binding site accessible to ligands. I then estimated the relative distribution of receptors between these two domains. This quantitative analysis showed that although the clusters are visually striking they represent a relatively small proportion of the receptor population which is accessible to ligand. This emphasises that

subjective visual assessment can exaggerate the relative proportion of receptors which appears to be present in the clusters. It is also possible to be misled by quantification of processed photographic images since alteration of 'contrast' can change the linearity of the signal, thus underestimating the diffuse signal or in other circumstances underestimating intense 'out-of-range' peaks. In immunohistochemistry a similar bias against low level diffuse staining is found since this can be dismissed as background noise.

Spatial distribution of α_1 -adrenoceptor subtypes.

There is currently much interest in identifying the mechanisms of receptor internalisation and sequestration. The development of GFP and flag-tagged receptors has enabled new ways of localising receptors in single cells. Biochemical methods are now being replaced by more visual methods which have the advantage of being performed on living cells. It has been suggested that α_{1b} -adrenoceptors are primarily located on the cell membrane whereas α_{1a} -adrenoceptors are largely confined to the cytoplasm (Hirisawa et al., 1996). It also been shown that stimulation of NPY receptors in the membrane can inhibit the recycling of α_{1a} -adrenoceptors back into the membrane following stimulation with phenylephrine (Holtback et al., 1999). Many receptor systems have now been shown to internalise following agonist stimulation and it is now accepted that intracellular receptors do exist in most cells (Hall et al., 1999.).

The results of this study confirm the presence of intracellular binding sites for QAPB. When discussing α_1 -adrenoceptors I prefer to reserve the term 'receptor' for a binding site which is known to couple to a G-protein and initiate a 2nd messenger cascade. Presently we can not be certain of the function of these intracellular sites and it is not known if they are functionally coupled or are merely primitive proteins which are pre-cursors of the

membrane bound receptors. Intense staining was often observed around the nucleus and this may represent sites in the Golgi apparatus. However, no counter-staining was used to confirm this.

The Z-sectioning module of IMARIS permitted the visualisation of 3D volumes from any plane or angle. Figures 3.14 – 3.16 show representative examples of the type of receptor distribution seen in transfected fibroblasts. Figure 3.14 shows a fibroblast with strong binding on the cell surface although some faint intracellular fluorescence was observed. Figure 3.15 (top panel) shows very clear membrane binding in a group of 3 fibroblasts. The bottom panel (figure 3.15) shows diffuse and clustered intracellular binding. In general the findings suggest that in transfected cell systems there is a considerable proportion of intracellular binding sites. It will be extremely interesting to study freshly dissociated cells to determine whether they have the same proportions of intracellular and membrane bound binding sites. Initial studies of dissociated prostate smooth muscle cells indicates that both exist in real tissues (McGrath et al., 1999).

Iso-surface modelling.

Alternatives to Z-sectioning are the various rendering and visualisation methods made available by the IMARIS and Microvision software programs. The iso-surface modelling method appears to be the best when multiple data sets are to be visualised simultaneously.

Figure 3.16 shows a region of a fibroblast (shown in figure 3.15) following deconvolution using the iterative constrained Tikhonov Miller algorithm (supplied as a HuygensII module). It can be seen that the fluorescence is largely confined to the cell membrane. A simulated fluorescence projection of the sub-volume also shows strong membrane

binding (figure 3.16b). By constructing an iso-surface model it is possible to view the data from any angle, four examples are shown in figure 3.16c-f. The power of the iso-surface modelling procedure lies in its ability to combine channels of data. Figure 3.17 shows different views of a 3 channel iso-model. The raw data has been segmented into three distinct volumes for the nucleus, diffuse staining and clustered (high intensity) staining. It can be clearly seen that the clusters are located inside the cell in close proximity to the nucleus and are probably located in the Golgi-apparatus. Figure 3.17 also shows the iso-model of a dissociated human prostatic smooth muscle cell indicating that this technique will be applicable to native cells even where the receptor expression level may not be as high as is found in recombinant systems.

Analysis of receptor binding intensity in thick biological specimens.

In cell culture monolayers it is possible to visualise and measure receptor-activated fluorescence with conventional fluorescence microscopy since the cell membranes are directly visible. With intact pieces of tissue this is impractical due to "bleed through" from out-of-focus planes. This problem can be addressed by the use of either confocal microscopy or wide field/deconvolution. One technical problem in attempting to measure receptor distribution, at different depths, is that concentration of the fluorescent ligand may vary according to the rate of diffusion and time of incubation. However, if the incubation time needed for full functional antagonism is known then analysis at that time point should indicate which receptors are involved in the response. Depending on the composition of the tissue, it is practicable to "see through" tissue to a depth of between 20 and 50 μm . Small resistance vessels and other thin preparations are therefore ideal. Unfortunately, thick preparations

containing large amounts of elastin (i.e. aorta, carotid artery etc.) exhibit autofluorescence in the same spectrum as many of the available fluorescent probes.

Rat mesenteric arteries (RMA) and basilar arteries (RBA) are particularly well suited to optical methods of studying their structure (see chapter 2). In this chapter I have examined the binding of QAPB to whole mount (unfixed) samples of RMA and RBA. To enable the capture of high quality confocal sections it was necessary to use a concentration of QAPB (0.1 μ M) which was higher than its anticipated dissociation constant and therefore may display some non-specific binding. However, this is an acceptable concentration of QAPB to use as an antagonist on blood vessels since it is expected to have approximately 10 fold lower affinity than prazosin which would commonly be used in functional studies at around 10nM. Furthermore, QAPB binding (100nM) was significantly reduced in the presence of phenoxybenzamine and YM12617. In all of the RMA sections studied the QAPB binding was found to be both diffuse and clustered. In addition the binding was consistent with the orientation of the smooth muscle cells. Figure 3.18a shows a significant degree of binding in the adventitia. The presence of α_1 -adrenoceptors in the adventitia has yet to be described and this binding may simply reflect non-specific binding to prejunctional α_2 -adrenoceptors. However, the affinity of QAPB at α_{2D} -adrenoceptor subtypes (the expected subtype on rat sympathetic varicosities) is unknown and this is merely speculation.

Further confirmation of the relative selectivity of QAPB on blood vessels comes from the observation that 100nM produced less binding in the media of the rat basilar artery

(a tissue which responds poorly to noradrenaline). When compared with the RMA media it appears that the RBA does not exhibit the diffuse binding which I believe represents the membrane bound 'specific' binding sites.

Non-vascular smooth muscle also exhibits diffuse and clustered binding. The rat isolated anococcygeus muscle is richly innervated with sympathetic nerves (Gillespie & Maxwell 1971) and produces a powerful (α_1 -adrenoceptor mediated) contraction in response to noradrenaline (Docherty et al., 1979). In this tissue QAPB binding was associated with the orientation of smooth muscle cells and was inhibited in the presence of the high affinity α_1 -antagonist YM12617.

Having proved that fluorescent-ligand binding could provide information on the spatial distribution of α_1 -adrenoceptors it was decided that a method of visualising binding to inner and outer layers of vascular smooth muscle simultaneously would be advantageous. Figure 3.21 shows such a method where the blood vessel is cut into transverse sections (TS), mounted on cover slips and visualised using the method developed for single cells. Interestingly, the results of QAPB binding to TS rings of RMA were almost identical to the results obtained by using tritiated prazosin binding to rat aortic sections (Dashwood & Jacobs 1985). These authors claimed their data showed the presence of high concentrations of α_1 -adrenoceptors in the inner layers of smooth muscle. However, it is also possible that they were observing binding of prazosin to the internal elastic lamina. In the present study, binding of QAPB was found to be strongly associated with the internal and external elastic lamina (figure 3.23). It is not clear if the binding is to the laminae per se or if the binding is to cells

which are lining the laminae. Nevertheless, the binding of QAPB is almost identical to that observed with radio-labelled prazosin which further confirms the similarity between both compounds.

In conclusion, fluorescent ligands combined with confocal microscopy can provide new methods for studying receptors and receptor-mediated mechanisms in living tissues. QAPB is an interesting example with which to explore the potential of the method since it fluoresces more brightly when bound to the receptors. It is possible, using such a fluorescent ligand, to determine the presence and distribution of receptors within a multi-cellular preparation and to localise the binding on or within single cells at a given time point. It is also possible to measure concentration-dependent binding in the presence and absence of non-labelled competitors to further determine receptor profiles in order to locate subtypes.

Using confocal microscopy or similar techniques, the study of receptors can be extended beyond the approaches described here. Receptor populations within intact live tissue can be localised and analysed at the cellular and sub-cellular level. There are possibilities to study the spontaneous or induced relocation and cycling of receptors.

A further important advantage of having developed the method using confocal microscopy is that important questions such as the localisation of the signal to the membrane phase and the extent of penetration of the probe into the cell can be characterised. This validates the technique and sets the scene for the development of

simpler, less expensive and, potentially, automated analytical systems based on the same principle.

The technology can thus be extended in the hi-tech or lo-tech directions.

References.

- Anderson, M.J. and Cohen, M.W. Fluorescent staining of acetylcholine receptors in vertebrate skeletal muscle. *J. Physiol.*, **237**, 385-400, 1974
- Atlas D, Melamed E & Lahav M (1976). Direct localisation of β -adrenoceptor sites in rat cerebellum by a new fluorescent analogue of propranolol. *Nature*, **261**; 420-421
- Atlas D & Melamed, E. (1978) Direct mapping of β -adrenergic receptors in the rat central nervous system by a novel fluorescent β -blocker *Brain Res.*, **150**, 377-385
- Balice-Gordon, R.J. and Lichtman, J.W. (1993) In Vivo observations of pre- and postsynaptic changes during the transition from multiple to single innervation at developing neuromuscular junctions. *J. Neuroscience*, **13**(2), 834-855
- Cheng, Y.C. & Prusoff, W.H. (1973) Relationship between the inhibition constant (K_i) and the concentration of inhibitor which causes 50% inhibition (IC₅₀) of an enzymatic reaction. *Biochem. Pharmacol.*, **22**, 3099-3108
- Daly CJ, Milligan CM, Milligan G, Mackenzie JF & McGrath JC (1998) Cellular localisation and pharmacological characterisation of functioning α 1-adrenoceptors by fluorescent ligand binding and image analysis reveals identical binding properties of clustered and diffuse populations of receptors. *J. Pharmacol. Exp. Ther.* **286** 984-990.
- Dashwood M, Jacobs M (1985). Autoradiographic study of the alpha-adrenoceptors of rat aorta and tail artery. *Eur J Pharmacol* Sep **10**;115(1):129-30

- Docherty, J.R., MacDonald, A. & McGrath, J.C. (1979) Further sub-classification of α -adrenoceptors in the cardiovascular system, vas deferens and anococcygeus of the rat. *Br. J. Pharmacol.* **67** 421-422P.
- Drew GM (1985) What do antagonists tell us about α -adrenoceptors. *Clin Sci.*, **68**, (Suppl 10), 15s-19s
- Faure, M-P., Gaudreau, P., Shaw, I. Cashman N. and Beaudet A. (1994). Synthesis of a biologically active fluorescent probe for labeling neurotensin receptors. *J. Histochem and Cytochem*, **46**(6), 755-763,
- Flavahan NA & Vanhoutte PM (1986) α_1 -adrenoceptor subclassification in vascular smooth muscle. *TIPS* **7**, 347-349.
- Ford AP, Arredondo NF, Blue DR Jr, Bonhaus DW, Jasper J, Kava MS, Lesnick J, Pfister JR, Shieh IA, Vimont RL, Williams TJ, McNeal JE, Stamey TA & Clarke DE. (1996) RS-17053 (N-[2-(2-cyclopropylmethoxyphenoxy)ethyl]-5-chloro-alpha, alpha-dimethyl-1H-indole-3-ethanamine hydrochloride), a selective alpha 1A-adrenoceptor antagonist, displays low affinity for functional alpha 1-adrenoceptors in human prostate: implications for adrenoceptor classification. *Mol Pharmacol* Feb;**49**(2):209-15
- Gillespie JS & Maxwell JD (1971). Adrenergic innervation of sphincteric and nonsphincteric muscle in the rat intestine. *Journal of Histochemistry and Cytochemistry* **19**, 676-681.
- Hall R.A., Premont R.T., and R. J. Lefkowitz. (1999). Heptahelical Receptor Signaling: Beyond the G Protein Paradigm. *J. Cell Biol.* **145**: 927-932.
- Haugland, R.P. (1992), Molecular Probes Handbook, set 1, 9

- Hazum, E., Chang, K-J. and Cuatrecasas, P. (1979) Role of disulphide and sulphhydryl groups in clustering of enkephalin receptors in neuroblastoma cells. *Nature*, **282**, 626-628
- Hazum, E., Chang, K-J. and Cuatrecasas, P. (1980) Cluster formation of opiate (enkephalin) receptors in neuroblastoma cells: Differences between agonists and antagonists and possible relationships to biological functions. *Proc. Natl. Acad. Sci.* **77**(5), 3038-3041
- Heithier H, Hallmann D, Boege F, Reilander H, Dees C, Jaeggi KA, Arndt-Jovin D, Jovin TM & Helmreich EJ (1994). Synthesis and properties of fluorescent beta-adrenoceptor ligands. *Biochemistry*, **33**, 9126-9134
- Hess, A. (1979) Visualisation of beta-adrenergic receptor sites with fluorescent beta-adrenergic blocker probes – or autofluorescent granules? *Brain Res.*, **160**, 533-538
- Hieble, J.P., Bylund, D.B., Clarke, D.E., Eikenburg, D.C., Langer, S.Z., Lefkowitz, R.J., Minneman, K.P. and Ruffolo, R.R. International union of pharmacology X. Recommendation to nomenclature of α_1 -adrenoceptors; consensus update. *Pharmacological Reviews*, **47**, No.2, 255-266, 1995.
- Hirasawa, A. Tsumaya, K., Awaji, T., Shibata, K., Homma, N., Shinomiya, T. & Tsujimoto, G. Flow cytometry analysis of α_1 -adrenoceptor subtypes. *FEBS letters* **386**; 141-148, 1996.

- Hirasawa A, Sugawara T, Awaji T, Tsumaya K, Ito H, & Tsujimoto G (1997) Subtype-Specific Differences in Subcellular Localization of α_1 -Adrenoceptors: Chlorethylclonidine Preferentially Alkylates the Accessible Cell Surface α_1 -Adrenoceptors Irrespective of the Subtype. *Mole. Pharmacol.* **52**, Issue 5, 764-770
- Holtback U., Brismar H., DiBona G.F., Fu W., Greengard P. & Aperia A (1999). Receptor recruitment: A mechanism for interactions between G protein-coupled receptors. *Proc. Nat. Acad. Sci.*, **96**; 7271-7275.
- Miriell VA, Mauban JR, Blaustein MP, Wier WG. (1999) Local and cellular Ca^{2+} transients in smooth muscle of pressurized rat resistance arteries during myogenic and agonist stimulation. *J Physiol (Lond)* Aug 1; **518**(Pt 3):815-824
- Kenny, B.A., Miller, A.M., Williamson, I.J.R., O'Connell, J., Chalmers, D.H. and Naylor, A.M. Evaluation of the pharmacological selectivity profile α_1 -adrenoceptor antagonists at prostatic α_1 -adrenoceptors: binding, functional and in-vivo studies. *Br. J. Pharmac.* **118**, 871-878, 1996.
- MacNulty, E. E., McClue, S. J., Carr, I. C., Jess, T., Wakelam, M. J. O. and Milligan, G. Alpha 2-C10 adrenergic receptors expressed in rat 1 fibroblasts can regulate both adenylylcyclase and phospholipase D-mediated hydrolysis of phosphatidylcholine by interacting with pertussis toxin-sensitive guanine nucleotide-binding proteins. *J. Biol. Chem.* **267**, 2149-2156, 1992.
- McGrath, J.C. (1982) Commentary: Evidence for more than one type of post-junctional α -adrenoceptor. *Biochem. Pharmacol.* **31**: 467-484.

- McGrath, J.C., Arribas, S.M. and Daly, C.J. Fluorescent ligands for the study of receptors. *TIPS*, **17** (11), 393-399, 1996.
- McGrath, J.C. and Daly, C.J. (1995) Viewing adrenoceptors; past, present, and future; commentary and a new technique. *Pharmacology Communications* Vol **6** 269-279,.
- McGrath, J.C., Nagadeh, M.A., Pediani, J.D., Mackenzie, J.F. & Daly, C.J. (1999) Importance of agonists in α -adrenoceptor classification and localisation of α_1 -adrenoceptors in human prostate. *Eur. Urol.* **36** Suppl 1 80-88
- Messerli JM, Van Der Voort HTM, Rungger-Brandle & Perriard JC. (1993). Three-dimensional visualisation of multi-channel volume data: The amSFP algorithm. *Cytometry*, **14**: 725-735.
- Muramatsu I, Ohmura T, Kigoshi S, Hashimoto S & Oshita M (1990). Pharmacological subclassification of α_1 -adrenoceptors in vascular smooth muscle. *Br. J. Pharmacol.*, **99**, 197-201
- Petty, I.R. and Francis, J.W. Polymorphonuclear leukocyte histamine receptors: Occurrence in cell surface clusters and their redistribution during locomotion. *Proc. Natl. Acad. Sci.*, **83**, 4332-4335, 1986.
- Von Zastrow M & Kobilka BK. (1994). Antagonist-dependent and -independent steps in the mechanism of adrenergic receptor internalisation. *J. Biol. Chem.*, **269** No. 28, pp18448-18452.
- Minta A, Kao JP, Tsien RY (1989). Fluorescent indicators for cytosolic calcium based on rhodamine and fluorescein chromophores. *J Biol Chem* **1989** May 15;264(14):8171-8

- Ruffolo, R.R., Bondinell, W. , and Hieble, J.P. α - and β -adrenoceptors: From gene to the clinic. 2. Structure-activity relationships and therapeutic applications. *J. Med. Chem.*, **38** (19), 3681-3716, 1995.
- Uhlén, S., Axelrod, D., Keefer, J., Limbird, L. and Neubig, R. Membrane organisation and mobility of α_2 -adrenergic receptors in MDCK cells. *Pharmacology Communications* Vol 6 155-167, 1995.
- Wang, Y, Gu, Q., Mao, F. & Cynader, M.S. (1997) Developmental expression and regulation of α_1 adrenergic receptors in cultured cortical neurons. *Dev. Brain Res.*, **102**, 35-46,.
- Wise, A. Lee, T.W. MacEwan,D.J. and Milligan, G. Degradation of G11 alpha/Gq alpha is accelerated by agonist occupancy of alpha1A/D, alpha1B and alpha1C adrenergic receptors. *J. Biol. Chem.* **270**, 17196-17203, 1995.

Chapter 4

Pharmacological and CLSM study of the mouse tail artery; a case study bringing together the methods developed in the previous chapters.

Introduction.

In the previous chapters confocal-based methods for the study of vascular structure and receptor distribution were developed. This chapter is a case study of one particular artery and aims to show how CLSM methods can complement the conventional pharmacological (functional) studies that are normally employed.

The pharmacology of the mouse vasculature is relatively unknown since most studies of blood vessels have tended to focus on higher animals due to their ease of study and due to the technical limitation of studying such small diameter vessels. In addition, many workers have attempted to study human vessels due to their clinical relevance. However, genomic research has resulted in a proliferation of transgenic animal models harbouring various mutated genes or lacking in specific genes. The mouse has become a favourite for reasons other than an existing comprehensive knowledge of murine physiology. This may not be important from a molecular point of view but it leaves physiologist and pharmacologists with a significant amount of ground work to do prior to studying the effect of any gene defects. Fortunately, the methods of confocal myography described in this thesis are ideal for studying mouse blood vessels. The myographs are tailor made for small vessels and the microscopy permits the visualisation of structure and receptor distribution.

Wild type and KO mice

Cavalli et al., (1997) have engineered an α_{1B} -knockout mouse using targeted gene disruption and have shown that pressor responses to phenylephrine are reduced and that binding sites in both liver and brain are reduced. This type of approach to

determining adrenergic receptor (AR) subtype function is essential since the current collection of subtype-selective antagonists and agonists do not display sufficient selectivity for the α_{1B} -AR over α_{1A} - and α_{1D} . The original definition of the α_{1B} -AR was that it showed high affinity for the alkylating agent chloroethylclonidine (CEC) and relatively low affinity for WB4101 (Morrow & Creese 1986; Han et al., 1987). However, later studies have shown that CEC is an unreliable compound that is relatively non-selective between α_1 -AR and α_2 -AR subtypes, its action is dependent on the protocol used (Michel et al., 1993). Studies with transfected cells have suggested that the α_{1B} -AR is confined mainly to the cell membrane while the α_{1A} -AR is mainly intracellular (Hirisawa et al 1997). Functionally, the α_{1B} -AR has been suggested to be involved in growth regulation (Chen et al., 1995.) and is thought to be present on rabbit cutaneous resistance arteries (Smith et al., 1997) and rat carotid artery (Stassen et al., 1998). More recently, a new compound L765,314 has been reported to display 100 fold higher affinity for α_{1B} -AR over α_{1A} or α_{1D} (Patane et al., 1998) although this compound appears to have been tested in only one published report and its acceptance as a highly selective compound awaits further study by other investigators. Preliminary work from Professor J.C. McGrath's research group suggests that L765,314 does not show the same degree of selectivity (i.e. 100 fold higher) for α_{1B} - over α_{1A} - & α_{1D} .

Overall, the role of the α_{1B} -AR in vascular function awaits clarification. Since there are no reports of a vessel which expresses α_{1B} - alone it is likely that it plays a synergistic role with other receptor subtypes. The advantage of using tissues (vessels) from an α_{1B} -KO mouse is that the loss of such an interaction may cause a change in

expression or coupling efficiency of the remaining receptors. If the change can be identified then the functional role of the missing receptor can be inferred indirectly. Until such times as the pharmaceutical companies can produce high affinity receptor ligands at the same speed with which molecular biologists identify and express gene products, we will have to rely on transgenic models to provide less complicated functional tissues. Even if such high affinity compounds were available the ability to remove one subtype completely (as opposed to a pharmacological blockade) from a multi-receptor system would prove invaluable.

Colonies of α_{1B} -KO and wild-type (WT) C57-black mice have been raised from breeding pairs kindly supplied by Prof. Susanna Coteccia (University of Lausanne; Switzerland). The lack of any literature concerning murine vasculature required a preliminary study of selected vessels to determine which would give strong and reproducible contraction to adrenergic agonists. A comparison of mouse carotid, mesenteric and tail artery showed the latter to be a strong candidate. The rat tail artery has already been widely studied and shown to possess a rich adrenergic innervation along with postjunctional α_1 - and α_2 -ARs (Redfern et al., 1995). The subtype of α -AR has been suggested to be mainly α_{1A} . Therefore if the mouse tail artery exhibits a similar adrenergic system it may provide information on the possible interactions between α_{1A} - and α_{1B} -AR.

Mouse tail artery segments taken from WT and KO mice were studied on the wire myograph to determine the major postjunctional receptor subtype and to establish a functional role (if any) for the α_{1B} -subtype. Following the suggestion that α_{1B} -AR is

involved in growth a structural study was undertaken using CLSM. In addition a short study of receptor distribution in isolated cells and tissue sections was attempted to show the distribution of native receptors.

It is not within the scope of this chapter to present a full and comprehensive description of the pharmacology, structure and receptor distribution of the mouse tail artery. The aim of the chapter is merely to give a flavour of what is now possible following the development of the CLSM and fluorescence based methods and to show how these types of studies can be combined with the more conventional studies.

Methods.

C-57 black (Wild Type and Knockout) mice weighing between 25-35g were killed by stunning. The tail was marked on its underside before being removed and placed in a Petri dish containing normal Krebs' solution. A mid section (1-2cm) of tail artery was removed for staining, cell dissociation or myograph mounting. Preliminary studies employed the normalisation technique of Mulvany & Halpern (1977; see chapter 1). In order to obtain vessel internal diameter and normalised resting tension. Thereafter, vessel segments were set at 200mg resting tension prior to construction of concentration response curves (CRCs).

Functional Studies.

CRCs to noradrenaline (NA; 1nM - 10uM), phenylephrine (phe; 1nM - 10uM) and the selective α_{1A} -adrenoceptor agonists A86641 (0.01nM - 0.1uM) were constructed in the presence and absence of α_1 -adrenoceptor subtype selective antagonists. After an initial sighting concentration to NA (10uM) tissues were washed and allowed 40 minutes before beginning the first CRC. Antagonists were allowed at least 45 minutes to reach equilibrium prior to the beginning of a second or third CRC.

Analysis of functional data.

The potency of the agonists was determined by comparing EC_{50} (concentration required to produce 50% of maximum response) values obtained for each agonist. This value is sometimes referred to as the pD_2 (see methods section of Chapter 3). Antagonist affinity was determined by calculating the pK_B where a single antagonist concentration was used.

Confocal Study of Structure.

Vessel segments were stained with 10ug/ml of H33342 as described in chapters 1 & 2. For studies of adventitial cell density, vessels were slide mounted. For pressurised structural studies, segments were mounted in a specialised pressure myograph system (JP Trading).

Using an upright Noran Instruments Odyssey CLSM, optical sections of vessels were obtained as single images (adventitial study) or as z-series (structural study). For z-series capture a step size of 1um was maintained.

Dissociation of Smooth Muscle cells.

Cells were dissociated by the method of Kamishima *et al.*, 1997. Briefly, tail artery segments are immediately placed in buffer 1 (147mM NaCl, 5mM KCl, 1mM MgCl₂, 1.8mM CaCl₂, 10mM HEPES, 0.1% BSA, pH7.4). Segments are washed once in buffer 1, resuspended in buffer 2 (80mM sodium glutamate, 54mM NaCl, 5mM KCl, 1mM MgCl₂, 0.1mM CaCl₂, 10mM HEPES, 10mM glucose, 0.2mM EDTA, 0.1% BSA, pH7.3) with 1.7mM papain, 0.7mM dithioerythritol and incubated at 35°C for 30mins. Segments were centrifuged at 1200g for 2mins and supernatant discarded. Segments were resuspended in buffer 2 with 1.0mM collagenase II, 1.0mM hyaluronidase and SMC were dispersed immediately with a fire polished pasteur pipette. Cells were plated onto coverslips.

Drugs and Solutions.

The composition of the modified Krebs solution was as follows: (in mM): NaCl 118.4, NaHCO₃ 25, KCl 4.7, KH₂PO₄ 1.2, MgSO₄ 1.2, CaCl₂ 2.5 and glucose 11.

Na₂EDTA (23μM) was also included in the Krebs in all experiments to prevent degradative oxidation of NA.

Noradrenaline, phenylephrine (Sigma Chemical Co.); A86441 (Dr Hancock, Abbott laboratories); BMY7378, YM12617, chloroethylclonidine (Research Biochemical International, RBI); delequamine (low affinity isomer; Roche pharmaceuticals); QAPB (BODIPY-FL prazosin), H33342 (Molecular Probes).

Results.

Antagonist profile

In wire mounted segments of mouse tail artery, the high affinity α_1 -adrenoceptor antagonist YM12617 (tamsulosin; 1nM) caused a rightward shift in the CRC to NA with a pK_B of 9.41 (Figure 4.1a). YM12617 also caused a reduction in maximum response. The α_2 -antagonists delequamine (1uM, pK_B 6.02; figure 4.1b) and rauwolscine (1uM, pK_B 6.33; figure 4.1c) displayed low potency versus NA in the tail artery.

Chloroethylclonidine (CEC; 10uM) caused a small rightward shift in the CRC to NA in normal (wild type) mouse tail artery (figure 4.2b). In tail arteries taken from knockout (KO) mice devoid of α_{1B} -adrenoceptors CEC was less effective (figure 4.2c). BMY7378 displayed no antagonism at concentrations up to and including 0.1uM. At 1uM BMY7378 exhibited slight rightward shift versus the α_{1A} -agonist A86441 (figure 4.3).

Agonist potency

The α_{1A} -agonist 86641 was approximately 100 fold more potent than phenylephrine (which was equipotent with noradrenaline). (Figure 4.3).

Electrical field stimulation.

Stimulus parameters of 4-64Hz (of 1 second duration) produced frequency dependent responses which were transient in nature, having a fast initial component with a slower declining phase to the response. Maximum size of response, time to reach maximum amplitude and the slope of the initial fast phase was calculated for

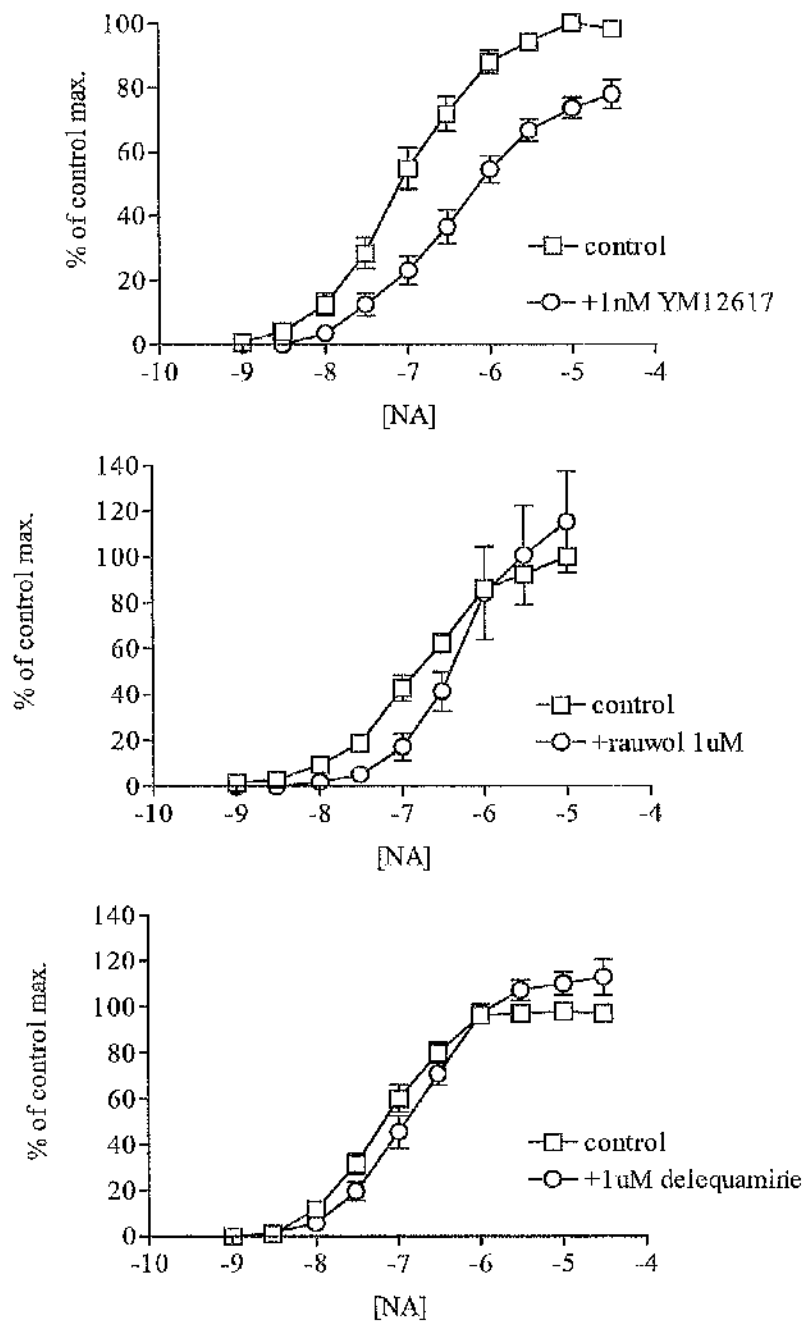


Figure 4.1. The effect of α -adrenoceptor antagonists versus noradrenaline (NA) on the mouse isolated tail artery. (n=5)

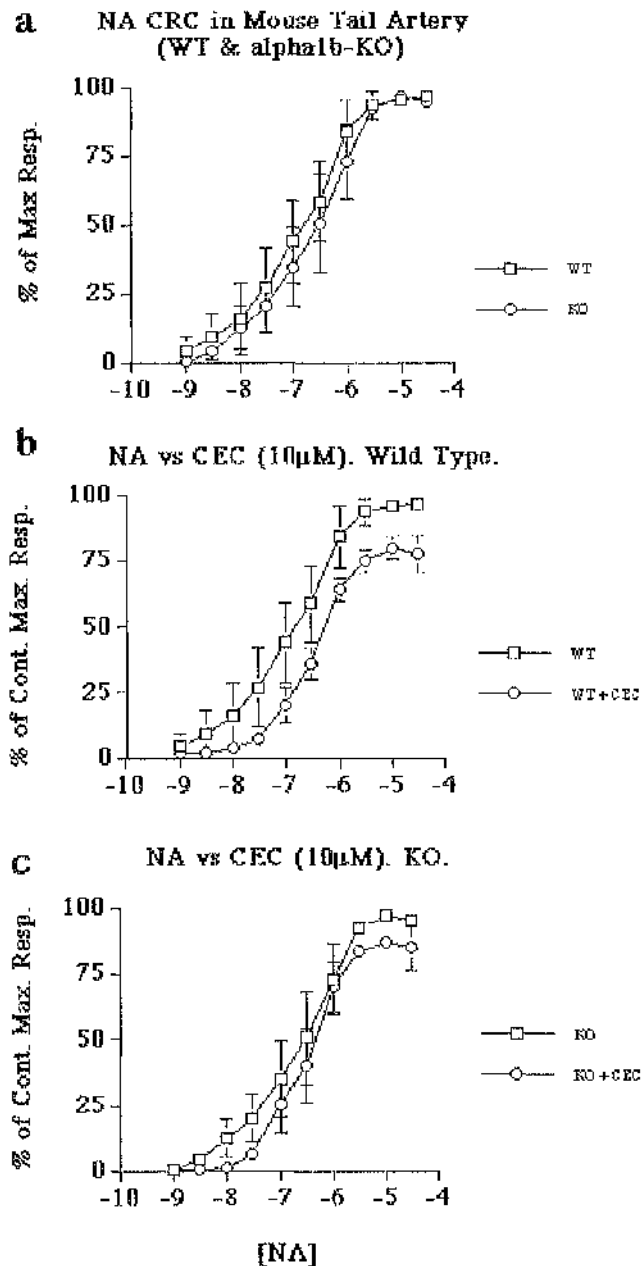


Figure 4.2. The role of α_{1B} -adrenoceptors in the mouse isolated tail artery in response to noradrenaline induced contraction. a) NA CRC in both normal (WT) and α_{1B} -knockout (KO) mouse tail artery. b) the effect of the α_{1B} -adrenoceptor blocker chloroethylclonidine (CEC) in WT tail artery. c) the effect of CEC on KO tail artery. Data points represent the mean of 4 experiments \pm S.E.M. Shifts with CEC were non-significant (WT $p=0.2$; KO $p=0.18$; paired t-test)

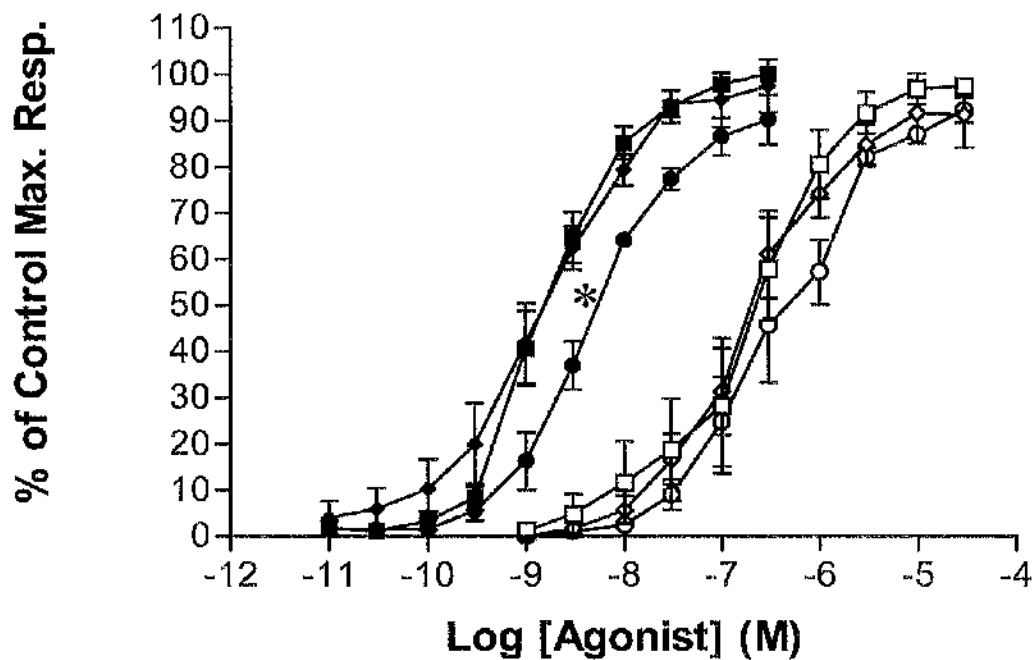


Figure 4.3 The effect of the α_{1D} -adrenoceptor antagonist BMY7378 versus contractile responses induced by A86641 (filled symbols) or phenylephrine (empty symbols) in the mouse isolated tail artery. Control (squares), 0.1 μ M BMY (diamonds), 1 μ M BMY (circles). The data points represent the mean of 4 experiment \pm S.E.M. * $p = 0.018$ (paired t-test).

each frequency. Low frequency responses (4-16Hz) were significantly greater in magnitude in the WT compared with the KO ($p < 0.05$; figure 4.4a). In addition the time to maximum for low frequency response was also greater (Figure 4.4b) and this is accounted for by the reduction in slope (expressed in mV/sec.) (Figure 4.4c).

Confocal analysis of structure.

Arterial segments from WT and KO mice were taken from 4 animals of each type (representative images are shown in figure 4.5). Nuclear (and thus cell) density (number per unit volume) was found to be $59.2 \pm 17\%$ lower in the KO adventitia. In addition, more autofluorescent extracellular material, perhaps elastin or collagen, was observed.

Analysis of pressure-mounted segments of WT tail artery revealed a characteristic punctate staining of the nucleus, by H33342, which was also observed in the KO tail artery. The orientation of the smooth muscle cells indicate that at least two orientations (or bands) of smooth muscle exist in the tail artery of WT mice (figure 4.6).

Fluorescent ligand binding.

QAPB binding to dissociated cells was time and concentration dependent and was inhibited in the presence of 10 μ M phentolamine. The binding sites were found to be associated with the membrane but also with intracellular sites (figure 4.7). Clusters of intracellular binding sites were also apparent. the calculated F_{KD} was 2.0 μ M which is consistent with the expected affinity of QAPB at α_{1A} -adrenoceptor subtypes.

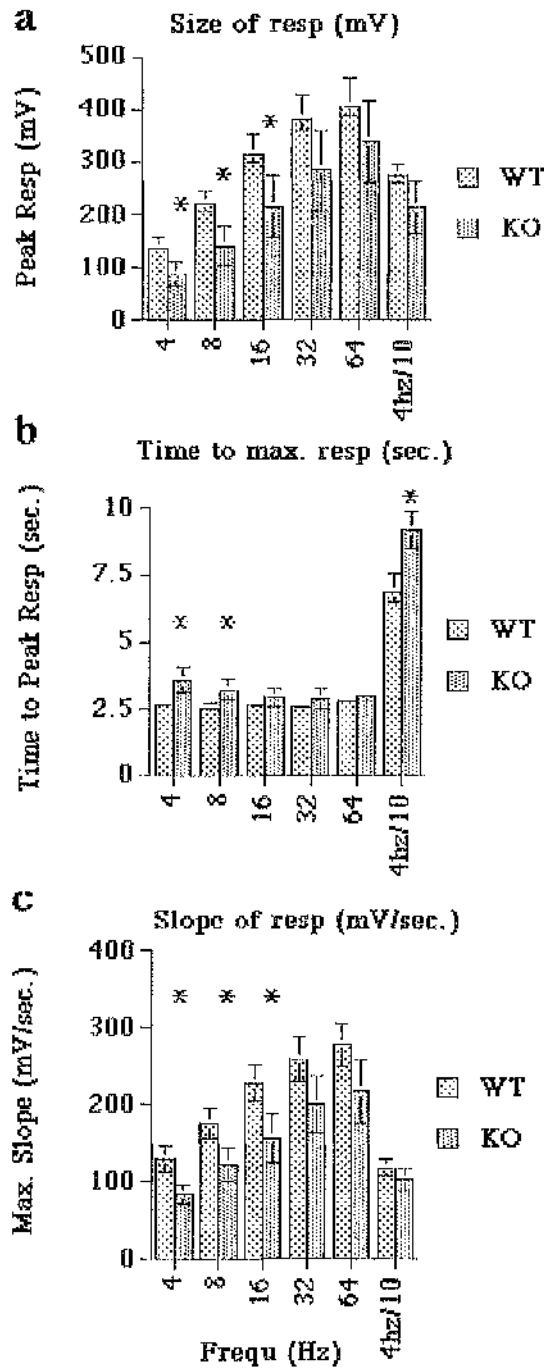


Figure 4.4 Analysis of the responses in mouse isolated tail artery elicited by electrical field stimulation. a) Size of the response. b) Time taken to reach maximum peak. c) The rate of rise of the initial component of the response. All data represent the mean of 4 experiments \pm S.E.M. (* $p < 0.05$).

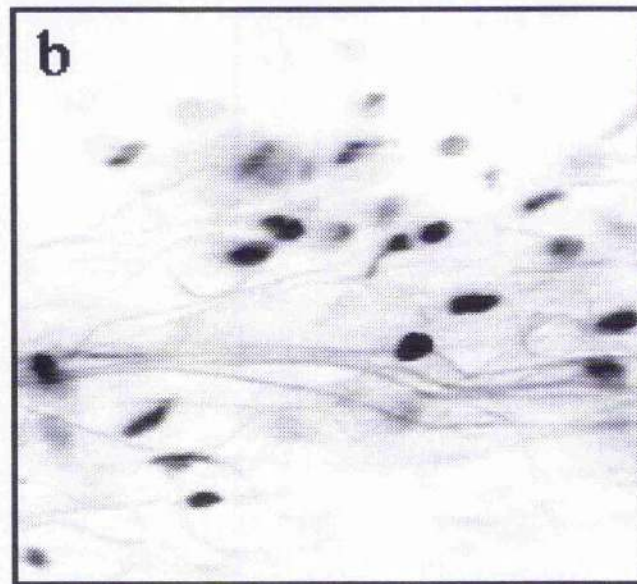
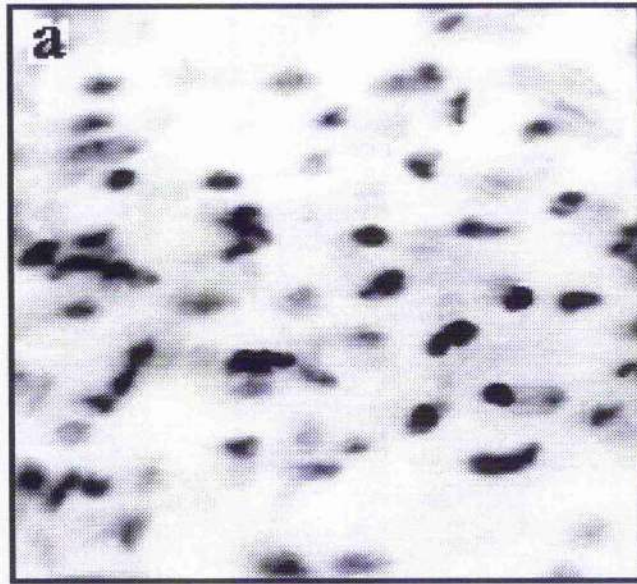


Figure 4.5. Representative images of the adventitial cell nuclei in the normal (WT) and knockout (KO) isolated mouse tail artery. The black spots represent individual nuclei. Each image is 102 μ m square.

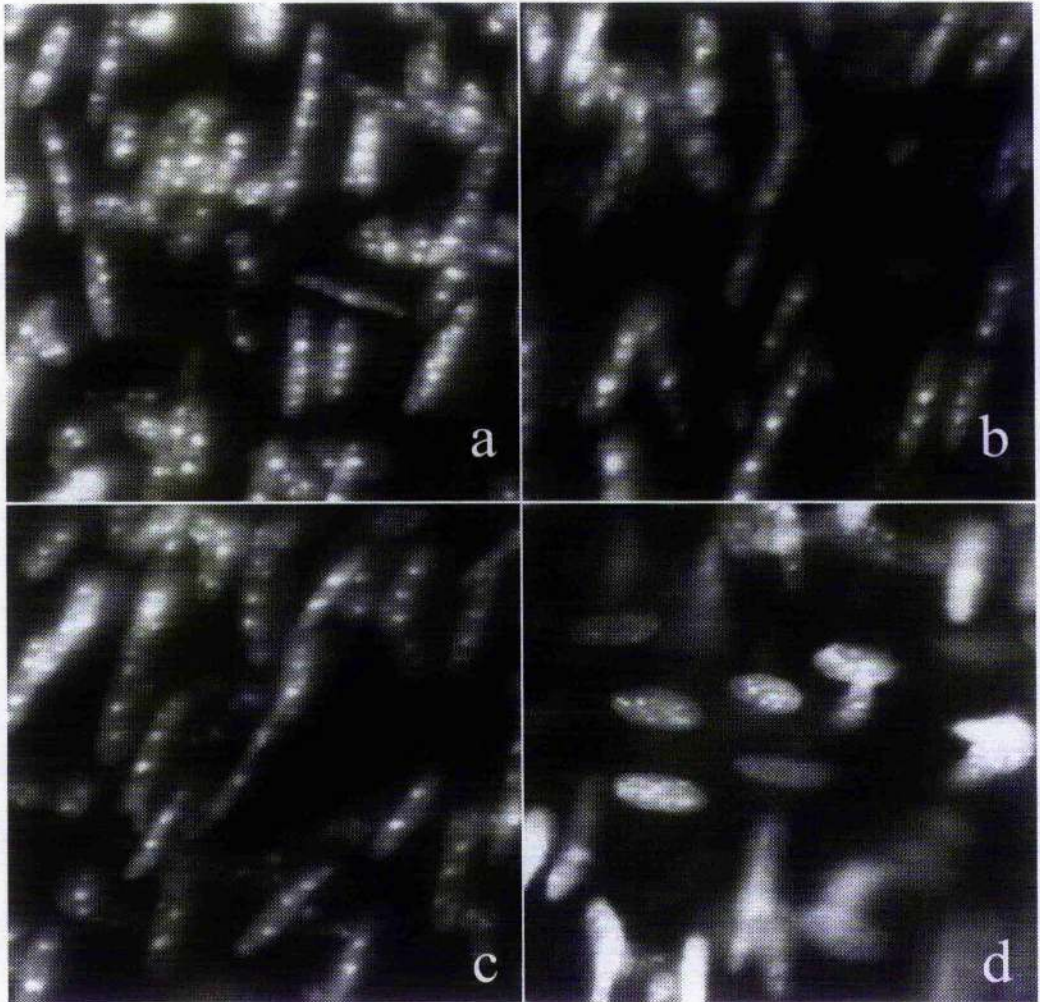


Figure 4.6. Extended focus images of a mouse tail artery segment mounted on a perfusion myograph at 100mmHg and stained with H33342 (10ug/ml). a-c) Show different regions of the same vessel. d) endothelial cell nuclei on the luminal surface. Images were collected using ax40 water objective (NA1.13). Field (image) size 97um square.

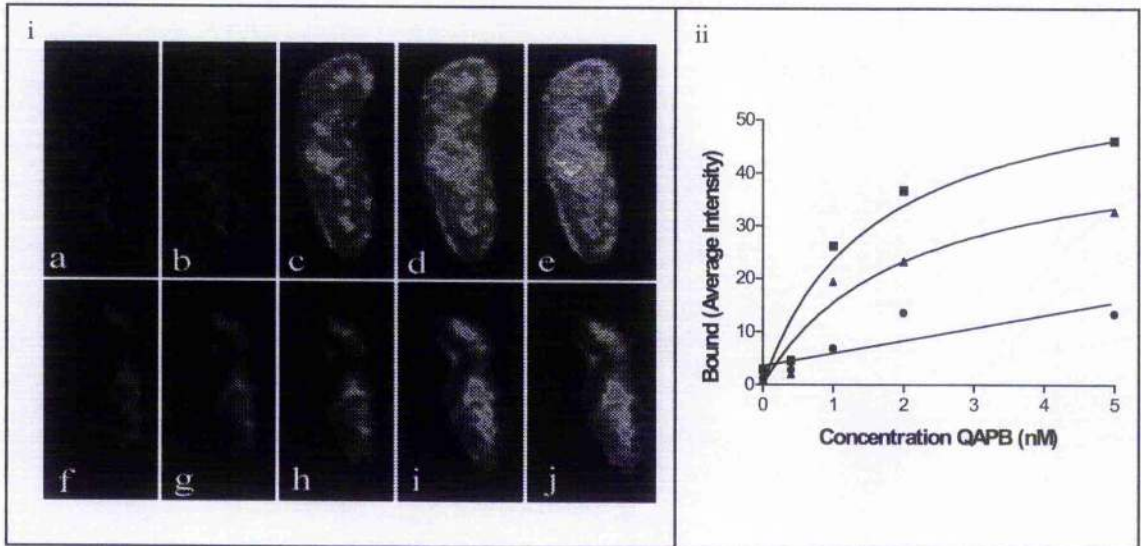


Figure 4.7. i. Smooth muscle cells freshly dissociated from murine tail artery, were plated on coverslips and examined by confocal microscopy and time-lapse photography at 1min intervals with increasing concentrations of QAPB (0, 0.4, 1, 2, 5nM) in the absence (a-e) and presence (f-j) of 10 μ M Phentolamine. Representative images of cells are shown in pseudocolour, where black indicates no staining and blue, green, and yellow indicate increasing levels of saturation of QAPB. ii. QAPB-associated fluorescence intensity was calculated by MetaMorph software and plotted against increasing concentrations of QAPB to demonstrate the levels of total (■), non-specific (●) and specific (▲) binding. The specific affinity (FK_D) of QAPB for murine tail artery smooth muscle cells was estimated as 2.0nM.

Discussion.

The purpose of this chapter was to demonstrate how the confocal approach can compliment the pharmacological study of an unknown vessel. The idea was to use some of the methods developed in the previous chapters and apply them to the study of a new vessel. The mouse represents a relatively unknown species with respect to its pharmacology. It is reasonable to assume that it will be similar to the rat and other rodents and indeed this assumption would suffice if only a general knowledge of function was required. However, now that molecular biology has delivered a multitude of transgenic models (mainly mice) it has become important to fully understand the 'lower' animals that have previously been ignored in favour of studying the physiology of 'higher' animals and humans where possible.

The mouse brings other advantages for microscopy and myography. Previously, it was not feasible to study large thick walled vessels (of larger rodents) under the microscope without first fixing and sectioning. The mouse gives us the chance to study intact segments of conduit vessels on the myograph and under the confocal microscope. One such line of study (the mouse carotid artery) is presently being followed by a member of Prof. McGraths research group.

For this chapter I have chosen to study the mouse tail artery. This vessel has a rich adrenergic innervation, has relatively few branches and contracts powerfully to noradrenaline. Until the present study, the relative contribution of α -adrenoceptor subtypes to contraction was unknown. The receptor distribution in murine smooth muscle cells and the 3D architecture of the vessel wall were also unknowns.

Antagonist potency.

The first question I would ask of any new vascular preparation is; what is the ratio of α_1 - to α_2 -adrenoceptors. The low potency of delequamine and rauwolscine suggest that in the isolated tail artery α_2 -adrenoceptors do not play a major functional role. The potency of YM12617 confirms the involvement of α_1 -adrenoceptors. However, the apparent non-competitive action of YM (i.e. reducing the maximum) may indicate an unusual property of the murine adrenoceptor.

CEC is reported to be an alkylating agent at α_{1B} -adrenoceptors and therefore should reduce the response to NA if α_{1B} -adrenoceptors play a significant role. In the present study CEC (10 μ M) caused only a slight reduction in maximum and rightward shift in normal mice. In the α_{1B} -KO mice CEC was even less effective. This points to only a minor role (if any) for α_{1B} -adrenoceptors in the response to NA in the mouse tail artery.

A comprehensive study of α_{1B} -AR distribution in 7 rat arteries found that α_{1B} -immunoreactivity was widely distributed in all arteries but that α_{1B} - functionality could only be attributed to the mesenteric resistance arteries (Piascik et al., 1997)

The α_{1D} -selective antagonist BMY7378 exhibited low potency against A86441 and phenylephrine, in mouse tail artery, which precludes any involvement of the α_{1D} -adrenoceptor.

Agonist potency.

The selective α_{1A} -agonist A86441 was approximately 100 fold more potent than phenylephrine which is consistent with a functional population of α_{1A} -adrenoceptors (Knepper et al., 1995). This is similar to the rat tail artery which has also been reported to be mainly α_{1A} (Lachnit et al., 1997).

Electrical field stimulation.

Since the tail artery is expected to be richly innervated (from knowledge of the rat) I decided to investigate the nature of the neuroeffector response in both wildtype and knockout mice. If a functional difference could be identified then perhaps a structural alteration may also exist since the α_{1B} -adrenoceptor has been implicated in mediating a growth response (Chen et al., 1995).

The sensitivity to exogenous agonists was no different in the WT and KO mice. However, responses to electrical field stimulation were smaller in the KO mouse, particularly at low frequencies. A detailed analysis of the shape of the responses indicated that the initial rapid response to EFS was slowed in the KO mouse tail artery. This was the first evidence of a difference in the small (resistance?) vessels of the mouse.

The postganglionic sympathetic nerves are located in the adventitia/medial border. Therefore it was of interest to examine the adventitia of the WT and KO mice.

Confocal Studies of Structure.

WT and KO mice (4 of each) were selected at random and a mid section of tail artery was removed from each and stained with H33342 and mounted on slides. In all cases the cell density (indicated using nuclear staining) was lower in the adventitia of the KO mice. This supports the previously reported suggestion that the α_{1B} -adrenoceptors play a role in growth.

Further experiments using pressure (100mmHg) mounted 'living' vessels showed an arrangement of smooth muscle cells which was apparently more complex than that observed in the rat mesenteric resistance arteries. At least two orientations of SMCs were observed. It is possible that this arrangement may play a role in the rhythmic activity which often develops in response to low concentrations of α -AR agonists. A characteristic of the mouse tail artery vascular cells was the punctate staining obtained with the nuclear stain H33342. The spots of fluorescence within the nucleus are similar to those observed in apoptotic nuclei. However, it is unlikely that all cells in the wall are in this state. Nevertheless, this staining pattern was observed in 3 WT arteries and 1 KO artery and certainly warrants further study.

α -adrenoceptor distribution.

It has previously been shown that recombinant adrenoceptor subtypes can have differential localities. Hirisawa et al. (1997) found that α_{1b} -adrenoceptors are confined to the cell membrane whereas α_{1a} -adrenoceptors are mainly intracellular. The pharmacological data of this chapter indicates that the α_{1A} -adrenoceptor subtype is functionally expressed in the tail artery smooth muscle cells. However, the

presence of α_{1B} -ARs cannot be discounted.. To distinguish clearly subcellular receptor location it is necessary to first dissociate cells. QAPB binding to dissociated cells was found to be both intracellular and membrane bound. Presumably these receptors represent the previously identified functional sites. However, it is not possible to say from these experiments what the proportion of α_{1A} - and α_{1B} -adrenoceptors is. Further experiments with non-fluorescent antagonists used in competition studies, followed by image processing and subtraction, are necessary to establish the proportions of each receptor type in different locations.

In conclusion, the main functional α -adrenoceptor subtype is the α_{1A} -subtype. The functional role of α_{1B} -adrenoceptors appears to be confined to the initial phase of the neuroeffector response and may be involved in growth. Since the major structural alterations were observed within the adventitia, it is interesting to speculate that the role of α_{1B} -ARs in neurotransmission and the location of the sympathetic nerves in the adventitia may be a significant factor in the growth and structure of the adventitia.

Confocal studies have revealed an alteration in the adventitial structure and have confirmed the existence of two spatially distributed populations of adrenoceptor subtypes which may correlate with the expected locations of α_{1A} - and α_{1B} -adrenoceptors.

References.

- Cavalli, A., Lattion, A., Hummler, E., Nenniger, M., Pedrazzini, T., Aubert, J.F., Michel, M.C., Yang, M., Lembo, G., Vecchione, C., Mostardini, M., Schmidt, A., Beerman, F. and Cotecchia, S. (1997). Decreased Blood Pressure Response in Mice Deficient of the α_{1B} -Adrenergic Receptor. *Proc. Natl. Acad. Sci. USA* **94**, 11589-11594.
- Chen L, Xin X, Eckhart AD, Yang N, Faber JE. (1995) Regulation of vascular smooth muscle growth by alpha 1-adrenoreceptor subtypes in vitro and in situ. *J Biol Chem.* Dec 29;**270**(52):30980-8
- Han, C., Abel, P.W. & Minneman, K.P. (1987b). α_1 -adrenoceptors linked to different mechanisms for increasing intracellular calcium in smooth muscle. *Nature*, **329**, 333-5
- Hirasawa A, Sugawara T, Awaji T, Tsumaya K, Ito H, & Tsujimoto G (1997) Subtype-Specific Differences in Subcellular Localization of α_1 -Adrenoceptors: Chlorethylelonidine Preferentially Alkylates the Accessible Cell Surface α_1 -Adrenoceptors Irrespective of the Subtype. *Mole. Pharmacol.* **52**, Issue 5, 764-770.
- Kamishima, T & McCarron, J.G. 1997. Regulation of the cytosolic Ca^{2+} concentration by Ca^{2+} stores in single smooth muscle cells from rat cerebral arteries. *J. Physiol.* **501**; 497-508.
- Knepper, S.M., Buckner, S.A., Brune, M.E., Debernardis, J.F., Meyer, M.D. & Hancock A.A. (1995). A-66103, a potent α_1 -adrenergic receptor agonist, selective for the α_{1A} receptor subtype. *J. Pharmacol. Exp. Ther.*, **274**, 97-103

- Lachnit WG, Tran AM, Clarke DE & Ford APDW (1997). Pharmacological characterisation of an α_{1A} -adrenoceptor mediated contractile responses to noradrenaline in isolated caudal artery of rat. *Br. J. Pharmacol.*, **120**, 819-826.
- Michel MC, Kerker J, Branchek TA & Forray C. (1993). Selective irreversible binding of chloroethylelonidine at α_1 - and α_2 -adrenoceptor subtypes. *Mol Pharmacol.*, **44**, 1165-1170.
- Morrow AL. & Creese I. (1986). Characterization of alpha1-adrenergic receptor subtypes in rat brain: A reevaluation of [3H]WB4101 and [3H]prazosin binding. *Molecular Pharmacology*. Vol **29**(4)(pp 321-330)
- Patane, M. A., Scott, A. L., Broten, T.P., Chang, R.S.L., Ransom, R. W., Disalvo, J. Forray, C. & Bock, M.G. (1998). 4-Amino-2-[4-[1-(benzyloxycarbonyl)-2(S)-[[[(1,1-dimethyl)amino]carbonyl]-piperaziny]-6,7-dimethoxyquinazoline (L-765, 314): A Potent and Selective α_{1B} Adrenergic Receptor Antagonist. *J. Med. Chem.*, **41**; 1205-1208.
- Piasecik MI, Frometz SL, Edelmann SE, Guarino RD, Hadley RW & Brown RD. (1997). Immunocytochemical localisation of the alpha1B- adrenergic receptor and the contribution of this and other subtypes to vascular smooth muscle contraction: Analysis with selective ligands and antisense oligonucleotides. *J. Pharmacol. Exp. Ther.* **283**: 854-868.
- Redfern, W.S., MacLean, M.R., Clague, R.U. & McGrath, J.C. (1995) The role of α_2 -adrenoceptors in the vasculature of the rat tail. *Br. J. Pharmacol.* **114** 1724-1730.

Smith, K.M., Macmillan, J.B. & McGrath, J.C. (1997) Investigation of α_1 -adrenoceptor subtypes mediating vasoconstriction in rabbit cutaneous resistance arteries. *Br. J. Pharmacol.* **122** 825-832.

Stassen, F.R.M., Maas, R.G.H.T., Schiffers, P.M.H., Janssen, G.M.J. and DeMey, J.G.R. (1998) A Positive and Reversible Relationship Between Adrenergic Nerves and Alpha-1A Adrenoceptors in Rat Arteries. *J. Pharm. Exp. Ther.* **284**, 399-405

General Discussion and Future Research.

The original aim of this study was to investigate the phenomenon known as vascular asymmetry whereby the inner layers of smooth muscle are more sensitive to activation by noradrenaline than the outer layers. This characteristic of many blood vessels has been known about for almost 30 years and yet we still do not fully understand the underlying mechanism. A major goal was to investigate the nature of asymmetry and to try to determine its basis. Initially it was thought that this would simply involve mounting a small vessel under a microscope and focusing on the different layers while monitoring the activation caused by a range of α -adrenoceptor subtype selective and non-selective agonists. In practice it became clear that this would not be a simple task.

The first problem to overcome was that of contrast within the living vessels. Studies with brightfield illumination confirmed that vascular contraction was a complex (multi-cellular) process. However, it was not possible to identify individual cells at varying depths within the wall. This led to the development of methods employing fluorescent nuclear stains. These stains proved to be non-toxic and enabled the identification of cell type, position, orientation and viability within a living (unfixed) vascular wall.

The work with fluorescent nuclear stains led to the realisation that activation of cells within a 3D matrix would require a more sophisticated method of analysis. This led to the evaluation and eventual purchase of a laser scanning confocal microscope (CLSM) which provided a means of collecting 3D volumes of vascular cell

arrangement. While this alone provided interesting insights into the structure of the resistance artery wall, it also created a requirement to use image analysis and processing methods which previously had not been used within our research group. A variety of fluorescent stains were evaluated along with a large number of image processing and analysis methods. The outcome of the work presented here is that we are now in a position to define the next set of problems which must be solved in order to fully automate the process of quantifying 3D volumes of vascular structure. In support of this, a multi-centre European partnership to study vascular structure using CLSM methods has recently been funded which Professor McGrath's group will co-ordinate.

The methods I have developed have already been used for the study of cellular rearrangements within SPSHR basilar arteries, mouse tail artery, rat mesenteric arteries and human subcutaneous resistance arteries. Furthermore, Professor McGrath's research group have recently been awarded a Wellcome Trust project grant to construct mathematical models of vascular structure based on the CLSM data which we have collected. Briefly, I believe that there may be a simple mathematical formula that will describe the arrangement of smooth muscle cells in the vascular wall. This model may contain repeating patterns of cells which may or may not represent groups of pacemaker cells. The project is a combination of pattern recognition and mathematical modelling. It will be very interesting if we can find a simple formula to describe the arrangement of cells mapped to a cylindrical structure. Even more interesting will be to alter the variables in the formula to cause cellular rearrangement. The question then would be; what physiological factors do these variables relate to? In many respects this is 'blue skies' research but the ideas within

the project outline are the result of studying structure from a 3D point of view. The Wellcome project and VASCAN-2000 (EU programme grant) will form a major part of my research in the next 2-3 years.

Segmentation of objects within 3D volumes of biological data is currently the focus of much attention within the computer imaging field. Presently there is not one well defined (or accepted) method of segmenting biological data. Much of the research centres around MRI and High Resolution ultrasound scanning. While the spatial resolution of these imaging modes is far lower than that of CLSM, the same problems apply. In fact, efficient segmentation/thresholding will continue to be a problem for my confocal studies in the years to come. It will be important therefore to keep up to date with the current methods and wherever possible identify collaborators who are working in this field.

Fluorescent ligands provided an interesting avenue of research at a point where the structural studies had reached a major hurdle to be overcome in the form of segmentation. It seemed an altogether simpler approach to map the receptor distribution within the vascular wall. However, as now expected with this project, there were many problems to overcome first.

Historically, fluorescent ligands were used like dyes and were not employed by pharmacologists. It took many months of studying the binding characteristics of BODIPY FL-prazosin (QAPB) before I would be convinced that any observed fluorescence was the result of the formation of a receptor-ligand complex. Once again I had to employ methods that I was not previously familiar with, namely cell culture

and the use of recombinant cell lines. There followed many more months of study with cloned cell lines which eventually resulted in the development of a fully quantitative method of ligand binding that could be performed at equilibrium on a single cell. This is perhaps the single biggest scientific achievement of the project (and the one which brought the most personal satisfaction). The method is now in regular use and we have recently published binding curves derived from a single human prostatic smooth muscle cell. The work is now being applied to whole sections of blood vessels and I believe that here we will find some answers to the question of asymmetry.

The work with fluorescent ligands is timely. Almost every month a new fluorescent peptide is synthesised by Advanced Bioconcepts or Molecular probes. There are now fluo-peptides for angiotensin II, endothelin, bradykinin, CGRP, substance P and a host of other molecules that are important to the cardiovascular system. The British Pharmacological Society awarded last year's AJ Clark scholarship to Professor McGrath to develop new fluorescent compounds for the study of α -adrenoceptors. This was a direct result of our work and publications in this area. We are currently evaluating an FITC-prazosin and a FITC-yohimbine which have been synthesised by our collaborators in the Dept of Chemistry (University of Glasgow). In the next two years it is hoped that we will be able to synthesise subtype-selective fluorescent probes for the known subtypes of α_1 - and α_2 -adrenoceptors.

In conclusion, the central question of vascular asymmetry remains unanswered and may remain so for a few years to come. However, in the course of working on this project I feel that I have more clearly defined some of the problems which must first

be solved if we are get closer to an understanding of the mechanisms of vascular cell interactions. The confocal methods described here will go a long way in helping to define vascular structure and receptor distribution. Much of the hard work has now been done and I believe that this now sets the scene for new approaches to the interesting problems of vascular biology.

